A theoretical study on the nature of organometallic carbene bonding in Titanium Schrock carbene complexes

by

Shane de Beer[a]

Supervisor: Doctor Jurgens H. de Lange[b]

Co-supervisor: Professor Ignacy Cukrowski[c]

Department of Chemistry

University of Pretoria

Submitted in partial fulfilment of the requirements for the degree

Master of Science

in the Faculty of Natural and Agricultural Sciences,

University of Pretoria

Pretoria, South Africa

November, 2020

E-mails: [a] shane.debeer@tuks.co.za

[b] jurgens.delange@up.ac.za

[c] ignacy.cukrowski@up.ac.za

Declaration

I, Shane de Beer, declare that the dissertation, which I hereby submit for the degree Master of Science at the University of Pretoria, is my own work and has not previously been submitted by me for a degree at this or any other tertiary institution.

_____

(Signature of Candidate)

___ day of _____ 2020

Outputs from this work

Journal publication

de Beer, S.; Cukrowski, I.; de Lange, J. H. Journal of Computational Chemistry 2020, https://doi.org/10.1002/jcc.26423.

Conference presentation

S. de Beer, J.H. de Lange, I. Cukrowski. "Teoretiese benadering tot die studie van chemiese verbinding in karbeen komplekse". *Suid-Afrikaanse Akademie vir Wetenskap en Kuns, Studentesimposium in die Natuurwetenskappe* **2019**, Bloemfontein, South Africa. (*oral*)

S. de Beer, J.H. de Lange, I. Cukrowski. "The Investigation of Long-Range Ligand-Ligand Interactions in Organometallic Carbene Complexes: A Fragment-Based Approach". *4th International Symposium on Halogen Bonding* **2020**, Stellenbosch, South Africa. (*poster*)

Abstract

Although various organometallic carbene complexes have found use in industry or research, they still lack some fundamental footing in theory. These complexes have found significant use in catalysis. This is especially true for Schrock carbene complexes in olefination reactions. A few such titanium-based olefination catalyst examples are the Tebbe reagent, Petasis reagent and the Ziegler-Natta catalyst.

The nature of organometallic carbene bonding is still not well defined theoretically. Schrock carbenes are expected to have a covalent bonding nature, but multiconfigurational studies have shown this to not be the best description of the bonding. Furthermore, expected Schrock carbenes have been shown to be Fischer carbenes due to the electronic structure.

This work investigates the nature of the carbene bond in titanium Schrock carbene complexes by utilising DFT and further application of MO, NBO, QTAIM and FALDI methods. This allows for a modernised description of the nature of this bond as well as the identification of an important long-range ligand-ligand interaction that has not been reported on previously.

The research aims to define the nature of titanium Schrock carbene bonding on a theoretical basis by the use of integrated cross-sections on the electron and orbital densities to determine the σ- and π-character of the interaction. These cross-sections provided the means to determine the major components of the bonding interaction.

This is further investigated by defining FALDI fragment-based delocalisation indices which revealed the presence of long-range ligand-ligand interactions. The FALDI fragment approach also provided the means to quantify the inter-fragment delocalisation along with intra-fragment localisation and delocalisation which would prove useful for further investigation into the characteristics or various chemical interactions. The fragment-based description should prove to be more intuitive to the chemist than diatomic interactions between atoms where a chemical bond or interaction is not classically expected.

This study was followed by a decomposition of the molecular orbitals into localised and delocalised components from atomic contributions which provides a novel approach to determining the bond order in compounds. This provided a quantitative means to describe which atoms contribute to the formation of each molecular orbital as well as providing a measure of the degree to which these atoms are contributing localised as well as delocalised electrons to the molecular orbital.

Keywords: Theoretical Chemistry, Organometallic, Schrock Carbene, Titanium, DFT, MO, NBO, QTAIM, FALDI

Acknowledgements

I would like to thank the following individuals and/or bodies for their respective contributions:

My supervisor, Dr Jurgens H. de Lange, and my co-supervisor, Prof Igancy Cukrowski, for their role in my development as an academic.

The Department of Science and Technology and the Council for Scientific and Industrial Research for financial support as well as support in developing my research skills as a future academic.

The University of Pretoria for financial support and access to resources.

Finally, I want to extend a warm thanks to my parents, Gert and Drieka de Beer, family and friends for the emotional support they had given me during the research process and especially at the write up stage.

Table of Contents Page

List of Figures

Page

Appendix A. Supplementary Information for Chapter Three

Appendix B. Supplementary Information for Chapter Four

List of Tables

Page

Appendix B. Supplementary Information for Chapter Four

Appendix C. Supplementary Information for Chapter Five

Appendix D. Supplementary Information for Chapter Six

List of Abbreviations

a.u.	atomic units
AOM	Atomic Overlap Matrix
BCP	Bond Critical Point
CCP	Cage Critical Point
CP	Critical Point
Cp	Cyclopentadienyl
DAFH	Domain Averaged Fermi Hole
deloc-ED	Delocalised electron density
DFT	Density Functional Theory
DI	Delocalisation index
DMAT	Delocalisation Matrix
ED	Electron density
EDA	Energy Decomposition Analysis
ETS-NOCV	Extended Transition State coupled with Natural Orbitals for Chemical Valence
FALDI	Fragment, Atomic, Localised, Delocalised and Interatomic
HOMO	Highest Occupied Molecular Orbital
HP	Hartree product
LDO	Localised-Delocalised Overlap
LI	Localisation index
LMAT	Localisation Matrix
LO	Localised Overlap
loc-ED	Localised electron density
LSDA	Local spin density approximation
MO	Molecular Orbital
NAO	Natural Atomic Orbital
NBO	Natural Bond Orbital
NCP	Nuclear Critical Point
NDF	Natural Density Function
QCT	Quantum Chemical Topology
QTAIM	Quantum Theory of Atoms in Molecules

RCP	Ring Critical Point
Rem	Remaining
SALC	Symmetry Adapted Linear Combination
SD	Slater determinant

Chapter One

Introduction

Background

The Tebbe reagent is one of the oldest known titanium-based olefination catalysts.[1] It was shown that the carbene complex acts as the active intermediate in the methylidene transfer process (a Wittig-type transformation).[2] Schemes of the preparation of this compound have been developed and crystallographic data has been collected on it since its discovery[3] even though the characterisation of this complex has been quite a challenge due to its reactive nature. Limits exist on this reagent only being useful in methylidene transfers,[4] thus other catalysts have succeeded it.

The Ziegler-Natta catalyst is another example of an aluminium supported titanium-based olefination catalyst.[5] Developments on the original aluminium support showed that other metals, such as magnesium and zinc, increased the activity of the catalyst.[6] A similar structure to the Tebbe reagent can be used to perform near identical methylidene transfers. This complex is called the Petasis reagent and is an aluminium-free option to the Tebbe reagent.[7] This reagent is especially effective in the olefination of carbonyl containing compounds and is itself much more stable compared to the Tebbe reagent.[4]

Two bonding models (Figure 1) have been suggested for transition metal carbene complexes.[8] One model suggests electrophilic transition metal carbene complexes where the carbene bond is formed by combining a singlet metal fragment with a singlet carbene fragment, also called Fischer carbene complexes. The alternative model suggests nucleophilic carbene complexes formed by combining a triplet metal fragment with a triplet carbene fragment, also called Schrock carbene complexes.[9]

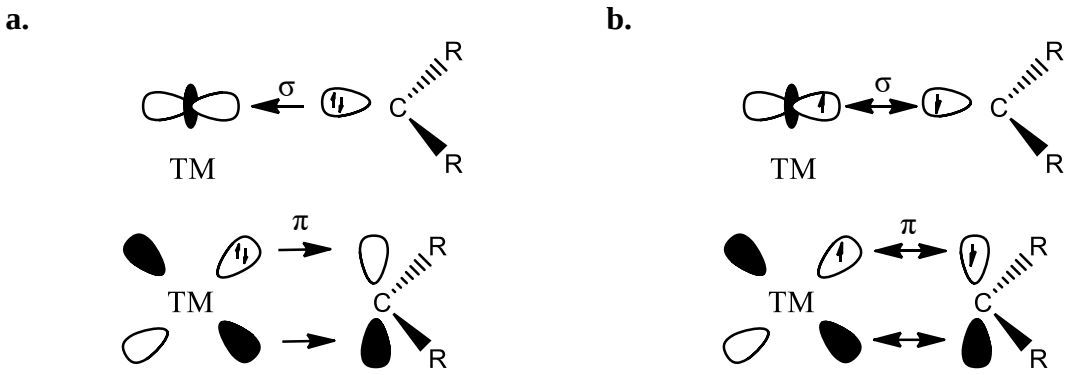

Figure 1. Representations of the current models on carbene bonding where a. represents the Fischer-type carbene and b. represents the Schrock-type carbene.

An additional group, called the N-heterocyclic carbene complexes, are a special case of Fischer carbene complexes where the carbene ligand is relatively stable and can exist as an independent species.

These models have been quite successful in describing the nature of organometallic carbene bonding and have been adopted as an important aspect in organometallic chemistry courses.[10] Fischer carbene complexes have many applications in organic synthesis[11] while Schrock carbene complexes are important as catalysts in olefin metathesis.[12] Common properties of Fischer type carbene complexes are that they contain lower oxidation state transition metals of the middle to late transition metals (such as W, Mo or Cr in a zero oxidation state) with ligands that are π-acceptor type ligands and often π-donor substituents (e.g. alkoxy or amine groups) on the carbene carbon.[12] Contrary to this common properties of Schrock carbene complexes are that they contain high oxidation state transition metals of early transition metals (such as Ti or Ta in oxidation states IV or V, respectively) with little or no π-effects from ancillary ligands and carbene substituents.[12]

The donor-acceptor model, also called the Dewar-Chatt-Duncanson model, dates back to the middle of the twentieth century.[13,14] The donor-acceptor model is similar to Lewis acid-base chemistry descriptors where the Lewis base would donate an electron pair to the Lewis acid.[15] Similarly, the donor group in the donor-acceptor model donates electrons towards the acceptor group. The covalent model of chemical bonding is based on the idea that the exchange and correlation effects lower the molecular energy of a complex when electrons are shared between atoms in the complex.[16] For covalent bonds the consensus is that two electrons are shared per bond with each atom donating one electron towards the bonding.[17]

Work from the early ‘90s suggested an alternative view on carbene bonding in transition metal Schrock carbene complexes where multiconfigurational wavefunctions were used on the electrons of the M—C σ and π orbitals to determine contributing resonance structures.[18] It was found that those resonance structures where the negative charge resides on the carbon atom contribute 50% of the ground-state wavefunction, those where the carbon is neutral contribute 45% and the last 5% are structures where the carbon has a positive charge (indicating a deficiency of electrons). Until the publication of this work[18] a third of the resonance structures identified had not been reported on in previous literature. These structures suggested a dative carbon-to-metal σ bond and a covalent M—C π bond.

Work by the same researchers showed important considerations which influenced the

electronic structures of organometallic carbene complexes.[19] Three aspects were identified as key role players in the determining the electronic structure: first, the presence of highly electropositive substituents, second, the identity of the central metal atom and thirdly, the presence of substituents with good π-donating ability. More studies have begun to surface which focus on the holistic design of complexes for specific applications including considerations of ancillary ligands.[20,21]

Problems still exist with functionalisation of carbonyls by titanium-based reagents, such as functionalised Petasis reagent, if the reagent can undergo β-elimination.[4] There is great use in the development of models which can be used to investigate the bonding characteristics in carbene complexes when the structures are modified.

Research statement

The use of density functional theory (DFT) and recent developments in Quantum Chemical Topology (QCT) allows for the study of the electron density in the interatomic region where bonding components can be determined. Schrock carbenes are hypothesised to have a covalent bonding nature and should thus show this distribution or sharing of electrons between atoms partaking in the bonding, i.e. M—C, as well as the effect of long-range ligand-ligand interactions.

Research aims and objectives

This work seeks to provide useful insights to the nature of organometallic carbene bonding in Schrock carbenes using DFT studies by determining the degree of σ- and π-bonding in Schrock carbenes, the effects of delocalisation on complexes and bonding, and the role of metal core densities on the electronic structure. The work then seeks to provide a novel measure by which the bond order can be determined in order to differentiate donor-acceptor character and covalent character in Schrock carbenes.

Significance of research

Schrock carbenes are used as catalysts in processes such as olefination. There is a gap in what is known on the bonding in these complexes which prevents developments in the field of

catalysis where these complexes are employed. Much focus has been placed on a related class of organometallic carbene complexes, namely Fischer carbene complexes. Recent studies have shown suspected Schrock carbenes to have the nature of typical Fischer carbenes. It would add value to existing knowledge to better explore the nature of Schrock carbenes to give insights to their nature and also to clarify the observation that Schrock carbenes and Fischer carbenes may not be as different as initially proposed.

Scope and limitations

The research focusses on titanium Schrock carbenes for their industrial value as catalysts – such as the Tebbe reagent, Ziegler-Natta catalyst, Petasis reagent. The complexes studied here can also be prepared and tested experimentally to criticize the validity of findings given by this research, such validation against experimental data is outside the scope of the current work.

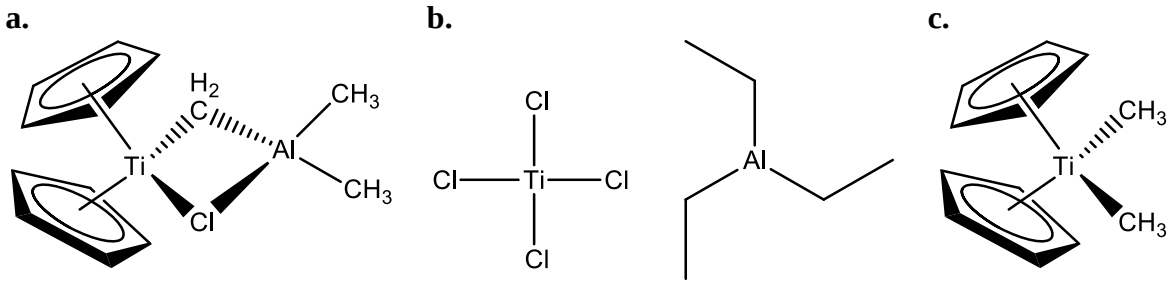

Figure 2. Three catalysts used to motivate the complexes studied in the following chapters with a. being the Tebbe reagent, b. the Ziegler-Natta catalyst and c. the Petasis reagent.

DFT is used as a framework as it has good computational scaling while still maintaining good accuracy, especially for transition metal complexes. It is taken as an assumption that the ground state wavefunction can sufficiently describe the system as to draw conclusions on the nature of bonding to be expected in experimental work. This assumption is made as the study of excited states is outside the scope of this research, but may be included in future work. Further it is hoped to find an approach that is not computationally expensive nor intellectually exhausting.

Outline of this work

This work contains seven chapters followed by four appendices. Chapter two gives the theoretical background to theories and methodologies used in this work. Chapter three presents a publication on the study by cross-sections of electron and orbital densities as a means to determine the degree of σ- and π-character of orbitals and densities relative to specific interactions or bonds. Chapter four applies the methodology from chapter three on various systems in order to gain generalised insights on transition metal organometallic carbene bonding in titanium Schrock carbene complexes when structural changes are applied. Chapter five investigates the delocalisation index of fragments and contrasts these results to those obtained from diatomic studies to illustrate multicentric natures in chemical bonding. Chapter six proposes a method to decompose the molecular orbital densities into localised and delocalised indices based on atomic basins to obtain more insightful bond orders per atomic interaction which also provides insight on the degree of covalency of an orbital and the donor-acceptor character of an orbital. Lastly, chapter seven draws final conclusions on the nature of organometallic carbene bonding and makes suggestions for future work.

References

1. Tebbe, F. N.; Parshall, G. W.; Reddy, G. S. *J. Am. Chem. Soc.* **1978**, 100(11), 3611-3613.

2. Meinhart, J. D.; Anslyn, E. V.; Grubbs, R. H. *Organometallics* **1989**, 8(3), 583-589.

3. Thompson, R.; Nakamaru-Ogiso, E.; Chen, C.-H.; Pink, M.; Mindiola, D. J. *Organometallics* **2014**, 33(1), 429-432.

4. Hartley, R. C.; Li, J.; Main, C. A.; McKiernan, G. J. *Tetrahedron* **2007**, 63, 4825-4864.

5. Cecchin, G.; Morini, G.; Piemontesi, F. *Kirk-Othmer Encyclopedia of Chemical Technology* **2000**, 502-554.

6. Mayr, A.; Galli, P.; Susa, E.; Di Drusco, G.; Giachetti, E.; *Google Patents*, **1981**.

7. Petasis, N. A.; Bzowej, E. I. *J. Am. Chem. Soc.* **1990**, 112(17), 6392-6394.

8. Taylor, T. E.; Hall, M. B. *J. Am. Chem. Soc.* **1984**, 106(6), 1576-1584.

9. Frenking, G.; Solà, M.; Vyboishchikov, S. F. *J. Organomet. Chem.* **2005**, 690(24-25), 6178-6204.

10. Montgomery, C. D. *J. Chem. Educ.* **2015**, 92(10), 1653-1660.

11. Doetz, K. H.; Stendel Jr, J. *Chem. Rev.* **2009**, 109(8), 3227-3274.

12. Kotha, S.; Dipak, M. K. *Tetrahedron* **2012**, 68(2).

13. Dewar, J. S. *Bull. Soc. Chim. Fr.* **1951**, 18(3-4), C71-C79.

14. Chatt, J.; Duncanson, L. A. *J. Chem. Soc.* **1953**, 2939-2947.
15. Haaland, A. *Angew. Chem. Int.* **1989**, 28(8), 992-1007.
16. Kurth, S.; Perdew, J. P. *Int. J. Quantum Chem.* **2000**, 77(5), 814-818.
17. Frenking, G.; Pidun, U. *J. Chem. Soc., Dalton Trans.* **1997**, 10, 1653-1662.
18. Cundari, T. R.; Gordon, M. S. *J. Am. Chem. Soc.* **1991**, 113(14), 5231-5243.
19. Cundari, T. R.; Gordon, M. S. *J. Am. Chem. Soc.* **1992**, 114(2), 539-548.
20. Cundari, T. R.; Gordon, M. S. *Organometallics* **1992**, 11(1), 55-63.
21. Munz, D. *Organometallics* **2018**, 37(3), 275-289.

Chapter Two

Theoretical Background

Introduction

Theoretical chemistry gives an elegant mathematical description of the chemical processes that drive our everyday existence. Since the development of quantum mechanics in the 1900s the mathematical rigour with which chemistry can be described has increased tremendously.

Recent years have seen computational methodologies become commonplace in many research projects due to the advantageous insights it provides. Much of this is due once again to the mathematical rigour in chemical models developed by chemists and physicists in the fields of quantum physics and quantum chemistry.

This chapter aims to give the theoretical framework used in the remainder of this work, although some sections will be highlighted again in later parts. The first section will cover the fundamental quantum mechanics required in this work. After that follows the Hartree-Fock approximation, then the density function theory framework which forms the backbone of this work. After this follows sections on the quantum theory of atoms in molecules (QTAIM), natural bond orbitals (NBOs) and the fragment, atomic, (de)localised, and interatomic (FALDI) electron density (ED) decomposition which serves as the basis of the analysis in consecutive chapter. Finally, there follows some sections on ED analysis by cross section and bond order analysis based on delocalised indices. This chapter then ends off with a conclusion giving some perspective on how it all fits together.

The majority of the rest of this chapter is summarised from the books by Cramer,[1] Jensen,[2] Szabo and Ostlund[3] and Atkins and Friedman[4] which provides a good introduction to the fundamentals of computational chemistry. Where relevant additional sources will be provided.

Molecular Quantum Mechanics

In order to gain useful theoretical insight into the chemistry one can expect from a system it is needed to describe such a system using quantum mechanics. This description is obtained by constructing a wavefunction which encodes all properties of the system. The wavefunction of a chemical system can be obtained by solving the Schrödinger equation defined as:

$$\hat{\mathrm{H}}\Psi(\mathbf{r}) = \hat{\mathrm{T}}\Psi(\mathbf{r}) + \hat{\mathrm{V}}\Psi(\mathbf{r}) = \mathrm{E}\Psi(\mathbf{r}) \qquad (1)$$

where $\hat{\mathrm{H}}$ is the Hamiltonian operator, $\hat{\mathrm{T}}$ is the kinetic energy operator and $\hat{\mathrm{V}}$ the potential energy operator which gives the energy E from which all properties of the system can be determined

by applying the appropriate operator over the wavefunction $\Psi(\mathbf{r})$.

The Schrödinger equation (eq. 1) is fairly straight forward in concept, but finding the analytical solutions to the differential equation is impossible for systems with more than a single electron. The solutions can be obtained numerically by setting up an approximate wavefunction and optimizing the required parameters until the lowest energy wavefunction is obtained. The energy of the system can be calculated by applying the following Hamiltonian operator over the wavefunction:

$$\hat{H} = -\frac{1}{2}\sum_{i=1}^{N}\nabla_i^2 - \frac{1}{2}\sum_{A=1}^{M}\frac{1}{M_A}\nabla_A^2 - \sum_{i=1}^{N}\sum_{A=1}^{M}\frac{Z_A}{r_{iA}} + \sum_{i=1}^{N}\sum_{j>i}^{N}\frac{1}{r_{ij}} + \sum_{A=1}^{M}\sum_{B>A}^{M}\frac{Z_A Z_B}{R_{AB}} \qquad (2)$$

where N is the total number of electrons in the system, M is all the nuclei in the system, Z_A is the nuclear charge of nucleus A, R_{AB} is the distance between nuclei A and B, r_{iA} is the distance between electron i and nucleus A, r_{ij} is the distance between electrons i and j and ∇_i^2 is the Laplacian operator defined as:

$$\nabla_q^2 = \frac{\partial^2}{\partial x_q^2} + \frac{\partial^2}{\partial y_q^2} + \frac{\partial^2}{\partial z_q^2} \qquad (3)$$

The Hamiltonian can be more simply written as:

$$\hat{H} = \hat{T}_e + \hat{T}_N + \hat{V}_{eN} + \hat{V}_{ee} + \hat{V}_{NN} \qquad (4)$$

where $\hat{T}_e$ and $\hat{T}_N$ is the electronic and nuclear kinetic energy operators, respectively, and $\hat{V}_{eN}$, $\hat{V}_{ee}$ and $\hat{V}_{NN}$ are the electron-nucleus, electron-electron and nucleus-nucleus potential energy operators, respectively.

The mass of the nucleus is much greater than the mass of the electron, thus the electrons will move at a much greater speed. It is therefore useful in approximating the nuclei as static point charges and deriving a new Hamiltonian for the electronic wavefunction, known as the Born-Oppenheimer approximation:

$$\hat{H}_{elec} = \hat{T}_e + \hat{V}_{eN} + \hat{V}_{ee} \qquad (5)$$

where the kinetic term for the nuclei is taken to be zero and the nucleus-nucleus potential term is a constant which can be added to the electronic Hamiltonian in order to obtain the total energy of the geometry, i.e.

$$\hat{H}_{total} = \hat{H}_{elec} + \hat{V}_{NN} \quad (6)$$

Giving the total energy for the specific nuclear geometry,

$$E_{total} = E_{elec} + E_{nuc} \quad (7)$$

From quantum mechanics, electrons cannot be distinguished and this must be reflected in the nature of the wavefunction used to describe their behaviour. There is a requirement that the wavefunction must not change when the positions of electrons are shifted around, i.e.

$$\left|\Psi(\mathbf{x}_1, \mathbf{x}_2, \dots, \mathbf{x}_i, \mathbf{x}_j, \dots, \mathbf{x}_N)\right|^2 = \left|\Psi(\mathbf{x}_1, \mathbf{x}_2, \dots, \mathbf{x}_j, \mathbf{x}_i, \dots, \mathbf{x}_N)\right|^2 \quad (8)$$

Furthermore, electrons are fermions (spin-half particles) and thus the wavefunction must change sign if the spatial and spin coordinates of two electrons are interchanged, i.e.

$$\Psi(\mathbf{x}_1, \mathbf{x}_2, \dots, \mathbf{x}_i, \mathbf{x}_j, \dots, \mathbf{x}_N) = -\Psi(\mathbf{x}_1, \mathbf{x}_2, \dots, \mathbf{x}_j, \mathbf{x}_i, \dots, \mathbf{x}_N) \quad (9)$$

Lastly, the wavefunction must describe all the electrons in the system, no more and no less. This imposes the criteria that the wavefunction describing the electrons in the system must be normalised, i.e.

$$\int \dots \int |\Psi(\mathbf{x}_1, \mathbf{x}_2, \dots, \mathbf{x}_N)|^2 \, d\mathbf{x}_1 d\mathbf{x}_2 \dots d\mathbf{x}_N = 1 \quad (10)$$

Only a wavefunction which adheres to the criteria given by equations 8-10 can be used to describe the electrons in a chemical system and can consequently be used to study the chemistry in such a system.

Since the Schrödinger equation (1) can only be solved analytically for a few select cases it is required that it be solved numerically in most chemically interesting cases. This iterative approach to calculating the wavefunction of the lowest energy is called the variational principle and is implemented in most quantum chemical software. This process involves setting up a trial wavefunction Ψ^{trial} with approximate values and then optimizing the parameters of the wavefunction until an energy minimum is obtained. By the variation principle the energy calculated by this iterative process cannot drop below the true minimum of the system.

$$E_0 \leq E_{trial} = \int \Psi^{trial^*} \hat{H} \Psi^{trial} d\boldsymbol{\tau} \quad (11)$$

The basis set in a computational chemistry problem describes a set of mathematical functions (often gaussian functions) used to define the quantum mechanical wavefunction in an approximate manner. These sets can be constructed as linear combinations of functions to better define the wavefunction.

The Pople basis sets are used in this work, although others do exist. However, since the systems studied in this work only contain main group elements and at most one additional titanium atom the Pople basis sets provide sufficient variability on the wavefunction to give a good numerical approximation to the true wavefunction. The basis set used in this work follows the notation,

$$6-311++\mathrm{G}(\mathrm{d},\mathrm{p}) \tag{12}$$

where the 6 indicates that six primitive gaussian functions were used for core electrons, valence electrons were described by three basis set functions with the first being a linear combination of three gaussian primitives the second and third are single primitive functions indicating an overall triple-zeta split-valence basis function. The ++ indicates that diffuse function were added to all atoms with an additional s orbital function being added to hydrogen atoms and an additional s orbital function with three addition p orbital functions on heavy atoms. The (d,p) indicates additional polarization functions were added as follows; three p orbital functions on hydrogen atoms, and five d orbital functions on heavy atoms.

Unless otherwise indicated atomic units (a.u.) were used throughout this work. Atomic units are set up such that the constants in the Schrödinger equation, when written in SI units, will drop out of the equation (or rather equal one, as any value multiplied by one is that value). This makes computations easier since there is no need to keep track of constants which need only be added later as a conversion factor.

Hartree-Fock Approximation

A detailed description of the Hartree-Fock approximation can be found in chapter three of Szabo and Ostlund[3] and the reader is encouraged to consult this source.

Under the assumption that electrons are noninteracting particles we can define a Hamiltonian which is the sum of all one electron Hamiltonians of a system of noninteracting electrons,

$$\hat{H} = \sum_{i=1}^{N} h(i) \tag{13}$$

where h(i) is the one electron Hamiltonian for a noninteracting electron, describing the kinetic and potential energy of electron i in orbital χ_j. The energy of a single orbital can then be obtained by applying this Hamiltonian over the function of the orbital,

$$h(i)\chi_j(\mathbf{x_i}) = \varepsilon_j \chi_j(\mathbf{x_i}) \tag{14}$$

where the energy of orbital j is given as the ε_j eigenvalue of the equation. It can then be stated that the energy of the system is given by the sum of all noninteracting orbital energies,

$$E = \sum_{i=1}^{N} \varepsilon_i \tag{15}$$

where N is the total number of noninteracting electrons in the system. The respective wavefunction is written as the product of all spin orbital functions,

$$\Psi^{\mathrm{HP}}(\mathbf{x_1}, \mathbf{x_2}, \dots, \mathbf{x_N}) = \chi_i(\mathbf{x_1})\chi_j(\mathbf{x_2}) \dots \chi_k(\mathbf{x_N}) \tag{16}$$

From the noninteraction of electrons it can be stated that the Hartree product (HP) wavefunction is uncorrelated as the total probability of all electrons in the system is equal to the product of their individual probabilities,

$$|\Psi^{\mathrm{HP}}(\mathbf{x_1}, \dots, \mathbf{x_N})|^2 \mathrm{d}\mathbf{x_1} \dots \mathrm{d}\mathbf{x_N} = |\chi_i(\mathbf{x_1})|^2 \mathrm{d}\mathbf{x_1} \left|\chi_j(\mathbf{x_2})\right|^2 \mathrm{d}\mathbf{x_2} \dots |\chi_k(\mathbf{x_N})|^2 \mathrm{d}\mathbf{x_N} \tag{17}$$

However, this HP wave function does not satisfy the anti-symmetry condition given in the section on molecular quantum mechanics above since it distinguishes between electrons which is physically not possible.

The failure of the HP wavefunction under the anti-symmetry condition is corrected by taking the linear combination of all arrangements of electrons in respective spin orbitals. It can be shown that the HP wavefunction distinguishes between electrons by determining the wavefunction for two electrons and then interchanging their positions to see if the same wavefunction is yielded in both cases, i.e.

$$\Psi_{12}^{\mathrm{HP}}(\mathbf{x_1}, \mathbf{x_2}) = \chi_{\mathrm{i}}(\mathbf{x_1})\chi_{\mathrm{j}}(\mathbf{x_2}) \neq \Psi_{21}^{\mathrm{HP}}(\mathbf{x_2}, \mathbf{x_1}) = \chi_{\mathrm{i}}(\mathbf{x_2})\chi_{\mathrm{j}}(\mathbf{x_1}) \tag{18}$$

Both of these HP wavefunctions represent some degree of the real-world case and therefore it is possible to obtain a better description of the true wavefunction by taking a linear combination of these HP wavefunctions where electrons are interchanged, thus yielding the Slater determinant (SD) wavefunction, i.e.

$$\Psi^{\mathrm{SD}}(\mathbf{x_1}, \mathbf{x_2}) = 2^{-1/2}\left(\chi_{\mathrm{i}}(\mathbf{x_1})\chi_{\mathrm{j}}(\mathbf{x_2}) - \chi_{\mathrm{i}}(\mathbf{x_2})\chi_{\mathrm{j}}(\mathbf{x_1})\right) \tag{19}$$

This can be generalised to a system of any number of electrons by the equation,

$$\Psi^{\mathrm{SD}}(\mathbf{x_1}, \mathbf{x_2}, \ldots, \mathbf{x_N}) = \mathrm{N}!^{-1/2} \begin{vmatrix} \chi_{\mathrm{i}}(\mathbf{x_1}) & \chi_{\mathrm{j}}(\mathbf{x_1}) & \cdots & \chi_{\mathrm{k}}(\mathbf{x_1}) \\ \chi_{\mathrm{i}}(\mathbf{x_2}) & \chi_{\mathrm{j}}(\mathbf{x_2}) & \cdots & \chi_{\mathrm{k}}(\mathbf{x_2}) \\ \vdots & \vdots & \ddots & \vdots \\ \chi_{\mathrm{i}}(\mathbf{x_N}) & \chi_{\mathrm{j}}(\mathbf{x_N}) & \ldots & \chi_{\mathrm{k}}(\mathbf{x_N}) \end{vmatrix} \tag{20}$$

By the mathematical laws of determinants, it can be show that interchanging any two rows of the SD changes its sign (anti-symmetry principle), having two columns equal will yield a determinant equal to zero (Pauli exclusion principle). Since the SD is a linear combination of all HP wavefunctions it can be shown that electrons are indistinguishable.

Chemists can use quantum mechanical descriptions of a system to obtain useful information on the properties of a chemical system. However, solving Schrödinger's equation for many particle systems has not been achieved analytically and instead it must be solved numerically with additional approximations on how to treat the system. One approximation is to solve the equation for each individual electron in the system using the one-electron Hamiltonian,

$$h(i) = -\frac{1}{2}\nabla_i^2 - \sum_{A=1}^{M}\frac{Z_A}{r_{iA}} \tag{21}$$

To incorporate electron-electron interactions, the one-electron Hamiltonian is extended as the Fock operator by adding a term which describes the Coulomb interaction as well as the exchange interaction between electrons in an averaged manner,

$$f(i) = h(i) + v^{HF}(i) \tag{22}$$

The Coulomb and exchange interactions represent the correlated motion of electrons, with

$$v^{HF}(i) = \sum_{b} \mathcal{J}_b(i) - \mathcal{K}_b(i) \tag{23}$$

Where $\mathcal{J}_b(i)$ represents the Coulomb interaction of electrons i and b, and $\mathcal{K}_b(i)$ represents the exchange interaction of electrons i and b if they are of the same spin, the exchange interaction is null for opposite spin electrons.

Density Functional Theory

Density functional theory (DFT) is a theory based on the electron gas model that uses the ED as opposed to a quantum mechanical wavefunction over which operators can be applied to obtain properties of the system. An excellent introduction can be found in the book by Koch and Holthausen[5].

DFT has good scaling while maintaining good chemical accuracy. This reduces the time taken for calculations although the limitations are still on the functionals used in these calculations where only specific functionals can be used based on the expected interactions in the system. Hybrid functionals are being developed to circumvent this problem by introducing semi-empirical parameters into the functionals.

Hohenberg and Kohn developed modern day DFT by defining a Hamiltonian operator that works on the ED,

$$\mathrm{E_0[\rho_0]} = \int \rho_0(\vec{r}) \mathrm{V_{Ne}} \mathrm{d}\vec{r} + \mathrm{F_{HK}[\rho_0]} \tag{24}$$

where the first term defines the nuclei-electron attraction which is dependent on the system (nuclear coordinates and nuclear charges) under study and the $\mathrm{F_{HK}}$ functional is the Hohenberg-Kohn potential functional, defined as

$$\mathrm{F_{HK}[\rho]} = \mathrm{T[\rho]} + \mathrm{E_{ee}[\rho]} = \langle \Psi | \hat{\mathrm{T}} + \hat{\mathrm{V}}_{\mathrm{ee}} | \Psi \rangle \tag{25}$$

where $\mathrm{T[\rho]}$ is the kinetic energy functional and $\mathrm{E_{ee}[\rho]}$ is the electron-electron interaction functional, both of which are independent of the system (nuclear coordinates and nuclear charges). The exact forms of both of these functionals are unknown, but the electron-electron interaction can be decomposed into the known classical Coulomb part $\mathrm{J[\rho]}$ and an unknown non-classical part $\mathrm{E_{ncl}[\rho]}$, describing all sorts of quantum effects.

$$E_{ee}[\rho] = \frac{1}{2}\int\int \frac{\rho(\vec{r_1})\rho(\vec{r_2})}{r_{12}} d\vec{r_1} d\vec{r_2} + E_{ncl}[\rho] = J[\rho] + E_{ncl}[\rho] \quad (26)$$

This non-classical electron-electron interaction term is defined in DFT using the functionals develop for various specific systems.

Kohn and Sham developed on the work of Hohenberg and Kohn by introducing the concept of non-interacting one-electron functions. This neglects the electron-electron interaction, giving only the kinetic energy is an effective potential field. They defined the one-electron Hamiltonian in DFT as

$$\hat{f}^{KS}\varphi_i = \varepsilon_i \varphi_i \quad (27)$$

with the Kohn-Sham operator defined as

$$\hat{f}^{KS} = -\frac{1}{2}\nabla^2 + V_s(\vec{r}) \quad (28)$$

This operator then yields one electron orbitals defined as Kohn-Sham orbitals, from which the total ED is then given by

$$\rho_s(\vec{r}) = \sum_i^N \sum_s |\varphi_i(\vec{r}, s)|^2 = \rho_0(\vec{r}) \quad (29)$$

What remains to be solved then is a functional describing the energy of the system. The nucleus-electrons interaction V_{Ne} can be calculated, Hohenberg-Kohn gave a functional for Coulombic interaction $J[\rho]$ and Kohn-Sham gave a functional for an approximate kinetic energy $T_s[\rho]$. A non-classical term is added E_{XC} to describe self-interaction corrections, exchange, correlation and some part of the kinetic energy.

Hybrid functionals are used to describe the exchange-correlation E_{XC} in this work. This calculates the exchange energy from the Hartree-Fock model and then adds the correlation in an approximate manner. The B3LYP functional[6] used employs other functionals derived from the BLYP functional[7]

$$E_{xc}^{B3LYP} = (1 - a_0)E_x^{LSDA} + a_0 E_x^{HF} + a_x \Delta E_x^{B88} + a_c E_c^{LYP} + (1 - a_c)E_c^{VWN} \quad (30)$$

The functionals referred to were described in other literature and the details of these are not discussed here. Here LSDA refers to the local spin density approximation[8], HF to Hartree-

Fock, B88 to Becke 1988[9], LYP to Lee, Yang and Parr[10] and VWN to Vosko, Wilk and Nusair[11].

Natural Bond Orbitals

The "natural" bond orbitals approach seeks the simplest expression of the underlying quantum mechanics to give chemically meaningful interpretations thereof to the chemist. It therefore also relies on the natural Lewis-structure model of chemistry as is commonly taught at schools and universities for students in the sciences to understand the basics of chemical structure. The details for the approach can be found in the book by Weinhold and Landis[12] but the core aspects used in this work are summarised in this section.

Orbitals in chemistry refer to the one-electron function which describes the probability of an electron being present in a particular special region. These orbitals are expressed using quantum number *n* (principal), *l* (azimuthal) and *m* (magnetic) which gives the size, shape and orientation of the respective orbital. The energy of such an orbital is determined by the principal quantum number. There are a number of such orbitals which make up a chemical system and some of these are filled while other are unfilled. The unfilled orbitals give the variability of the electronic structure of the system when undergoing physical and chemical processes, such as photoexcitation or a chemical reaction.

The number of electrons in a specific orbital may thus change depending on the environment in which the system is placed. The electron occupation of orbitals is used to express the total ED giving the equation,

$$\rho(\mathbf{r}) = \sum_i n_i |\phi_i(\mathbf{r})|^2 \tag{31}$$

where n_i is the electron occupation of orbital ϕ_i and is some value greater than or equal to zero and less than or equal to two.

The first-order reduced density operator can be expressed as its kernel function, i.e.

$$\gamma(\mathbf{r_1}|\mathbf{r_1'}) = N \int \psi(\mathbf{r_1}, \mathbf{r_2}, \dots, \mathbf{r_N}) \psi^*(\mathbf{r_1'}, \mathbf{r_2}, \dots, \mathbf{r_N}) d^3\mathbf{r_2} \dots d^3\mathbf{r_N} \tag{32}$$

for an N electron wavefunction $\psi(\mathbf{r_1}, \mathbf{r_2}, \dots, \mathbf{r_N})$ where this kernel function generally operates on a one-particle function according to;

$$\hat{\gamma} f(\mathbf{r}) = g(\mathbf{r}) = \int \gamma(\mathbf{r}|\,\mathbf{r}') f(\mathbf{r}') d^3\mathbf{r}' \tag{33}$$

A complete, orthonormal basis set $\gamma(\mathbf{r}|\mathbf{r})$ can be expanded as

$$\gamma(\mathbf{r}|\mathbf{r}') = \sum_{ij} \gamma_{ij} \chi_i(\mathbf{r}) \chi_j^*(\mathbf{r}') \tag{34}$$

where $\gamma_{ij} = (\mathbf{D})_{ij}$ which is the density matrix.

The diagonalization of the kernel function gives the eigenorbitals and their corresponding eigenvalues as,

$$\hat{\gamma}\theta_i = n_i \theta_i \tag{35}$$

which gives the occupations n_i and the natural orbitals θ_i.The search for the maximum occupation n_i^A in a localized region of atom A yields the natural atomic orbitals θ_i^A (NAOs) or alternatively searching for the maximum occupation n_i^{AB} in a diatomic, bonding region for atoms A—B yields the natural bond orbitals θ_i^{AB} (NBOs). The NBOs obtained are representative of the Lewis structures that can be determined using classical chemistry thinking, except that these NBOs are quantitative and derived from quantum mechanics to allow for the determination of other properties from the orbital functions.

Quantum Theory of Atoms in Molecules

The quantum theory of atoms in molecules (QTAIM) stems from the topology of the ED of a chemical system where atoms are described by the zero-flux surface. This gives a means to transform quantum mechanical wavefunctions into a description that is more intuitive to the chemist. Such an atomistic approach is justified as it is known that the behaviours of molecules can be related to the functional groups present and consequently such wavefunctions must have some degree of similarity between them. For more in-depth descriptions of QTAIM see the works by Matta and Boyd[13], Popelier[14] or the book by Bader[15].

The atomic basin in QTAIM is defined by the zero-flux surface which is obtained by taking the gradient of the ED:

$$\nabla\rho = \mathbf{i}\frac{\partial\rho}{\partial x} + \mathbf{j}\frac{\partial\rho}{\partial y} + \mathbf{k}\frac{\partial\rho}{\partial z} \rightarrow \begin{cases} = \vec{\mathbf{0}} \text{ (at critical points and } \infty) \\ \neq \vec{\mathbf{0}} \quad \text{(all other points)} \end{cases} \tag{36}$$

where ρ is the ED. The critical points of the ED are special points in the cartesian space where the curvature of the ED is extremised (each partial spatial derivative equals zero at a critical point). The critical points are classified by a rank (ω) and a signature (σ) using the symbolism (ω, σ). The values for the rank and signature depend on the eigenvalues of the Hessian matrix which gives the curvature of the ED in real-space:

$$\mathbf{A}(\mathbf{r_c}) = \begin{pmatrix} \frac{\partial^2\rho}{\partial x^2} & \frac{\partial^2\rho}{\partial x\partial y} & \frac{\partial^2\rho}{\partial x\partial z} \\ \frac{\partial^2\rho}{\partial y\partial x} & \frac{\partial^2\rho}{\partial y^2} & \frac{\partial^2\rho}{\partial y\partial z} \\ \frac{\partial^2\rho}{\partial z\partial x} & \frac{\partial^2\rho}{\partial z\partial y} & \frac{\partial^2\rho}{\partial z^2} \end{pmatrix}_{\mathbf{r}=\mathbf{r_c}} \tag{37}$$

Diagonalization of the Hessian matrix gives the eigenvectors. Alternatively, these eigenvectors can also be recovered from the Laplacian applied at the critical point:

$$\nabla^2\rho(\mathbf{r}) = \frac{\partial^2\rho(\mathbf{r})}{\partial x^2} + \frac{\partial^2\rho(\mathbf{r})}{\partial y^2} + \frac{\partial^2\rho(\mathbf{r})}{\partial z^2} = \lambda_1 + \lambda_2 + \lambda_3 \tag{38}$$

The rank is determined by the number of non-zero curvatures of the ED. Generally, critical points with $\omega < 3$ are unstable and not found for equilibrium structures (as in this work). The signature is the algebraic sum of the signs of the curvatures, $\sigma = \sum_i^{\omega} \lambda_i / \|\lambda_i\|$ which then leaves four possible combinations of rank and signature, i.e. nuclear critical point (NCP) (3,-3); bond critical point (BCP) (3, -1); ring critical point (RCP) (3,+1); and cage critical point (CCP) (3,+3).

As mentioned before, QTAIM used the topology of the ED to define the atomic subspace within the molecular space by determining the zero-flux surface of the atoms:

$$\nabla\rho(\mathbf{r}) \cdot \mathbf{n}(\mathbf{r}) = 0; \text{for } \mathbf{r} \in \Omega \tag{39}$$

where Ω is the atomic basin. By defining such an atomic basin and the inter-basin (inter-atomic) surface it becomes possible to find atomic properties from the ED by integrating over these atomic basins. The expectation value of an operator gives the mathematical means to determine atomic properties either from the wavefunction or by using atomic basins:

$$\langle \hat{O} \rangle_{molecule} = \sum_{i}^{all\ atoms} \left(N \int_{\Omega_i} \left\{ \int \frac{1}{2} [\Psi^* \hat{O} \Psi + (\hat{O}\Psi)^* \Psi] d\tau' \right\} d\mathbf{r} \right) = \sum_{i}^{all\ atoms} \left(\int_{\Omega_i} \rho_O d\mathbf{r} \right) = \sum_{i}^{all\ atoms} O(\Omega_i) \tag{40}$$

The total electron population for a specific atomic basin is given by integrating the ED over that atomic basin:

$$N(\Omega_i) = \int_{\Omega_i} \rho(\mathbf{r}) d\mathbf{r} \tag{41}$$

The total electron count for an atom can be decomposed into a localised index (electrons that are only found within the specific atomic basin) and a delocalised index (electrons that are also found outside the atomic basin):

$$N(A) = \lambda(A) + \frac{1}{2} \sum_{B \neq A} \delta(A, B) \tag{42}$$

Although the localised and delocalised indices can be calculated as an integration of the correlation function[16], in this work it will be expressed in matrix notation to emphasise the developments in latter sections. Therefore, a matrix can be defined which gives the overlap of the atomic basins (called the atomic overlap matrix, AOM):

$$S_{ij}^{A} = \int_{A} \chi_i^*(\mathbf{r}) \chi_j(\mathbf{r}) d\mathbf{r} \tag{43}$$

where S_{ij}^{A} represents the elements of the AOM for atomic basin A.

The localised and delocalised indices can then be expressed as:

$$\lambda(A) = \sum_{i} \sum_{j} \sqrt{n_i n_j} S_{ij}^{A} S_{ji}^{A} \tag{44}$$

for the localised index and

$$\delta(A, B) = \sum_{i} \sum_{j} \sqrt{n_i n_j} (S_{ij}^{A} S_{ji}^{B} + S_{ij}^{B} S_{ji}^{A}) \tag{45}$$

for the delocalised index, where n_k indicates the occupation of orbital k.

QTAIM allows for an atomistic view on quantum mechanics which allows for a chemically intuitive interpretation of the often complex systems found in chemistry. Classical chemistry is based on atoms and bonds for which QTAIM provides a bridge between this classical description and modern quantum mechanics.

Fragment, Atomic, (De)Localised, and Interatomic ED Decomposition

For readers interested in the details of the fragment, atomic, localised, delocalised and interatomic (FALDI) density decomposition see the works by de Lange[17-21] and Cukrowski[22]. The approach followed hereafter to explain the decomposition will first give a condensed introduction to domain averaged fermi holes (DAFH), then the FALDI decomposition up to the generation of natural density functions after using the orthodox (QTAIM) localisation and delocalisation indices, then will follow a description of how localised overlap (LO) free and localised-delocalised overlap (LDO) free electron distributions are obtained. The FALDI analysis in this work makes use of LDO free electron distributions.

In most cases where an ED decomposition is used a partitioning of the density is done such that the components describe parts of the total density, in equation form it can be written as

$$\rho(\mathbf{r}) = \sum_{i}^{M} \rho_i(\mathbf{r}) \tag{46}$$

where M is the fragments or atoms used as the partitions, this could be QTAIM defined atomic basins where the electron density then yields the following

$$\rho_i(\mathbf{r}) = \begin{cases} \rho(\mathbf{r}), & \mathbf{r} \in \Omega_i \\ 0, & \mathbf{r} \notin \Omega_i \end{cases} \tag{47}$$

where Ω_i is the ith atomic basin.

DAFH[23,24] suggest the use of an electron correlation function instead leading to the equation for the total ED as

$$\rho(\mathbf{r}) = \sum_{i}^{M} g_i(\mathbf{r}) \tag{48}$$

where M is then the domain of the electron. The $g_i(\mathbf{r})$ function is the correlation function integrated over the atomic basin Ω_i, such that

$$g_i(\mathbf{r_1}) = -\int_{\Omega_i} C(\mathbf{r_1}, \mathbf{r_2})\, d\mathbf{r_2} \tag{49}$$

with

$$\begin{aligned} C(\mathbf{r_1}, \mathbf{r_2}) &= 2\rho_2(\mathbf{r_1}, \mathbf{r_2}) - \rho(\mathbf{r_1})\rho(\mathbf{r_2}) \\ &= \rho_2(\mathbf{r_1}, \mathbf{r_2}) - \rho^{\text{Hole}}(\mathbf{r_1}, \mathbf{r_2})\rho(\mathbf{r_2}) \end{aligned} \tag{50}$$

where $\rho_2(\mathbf{r_1}, \mathbf{r_2})$ is the pair density describing the probability of finding an electron at one coordinate if another is known to be at another coordinate. In matrix form this can be written

$$g_i(\mathbf{r_1}) = -\sum_{\sigma\lambda}^{N} \chi_\lambda(\mathbf{r_1})\chi_\sigma(\mathbf{r_1})S^{\Omega}_{\sigma\lambda} \tag{51}$$

where $S^{\Omega}_{\sigma\lambda}$ is an element of the atomic overlap matrix which can be calculated by

$$S^{\Omega}_{\sigma\lambda} = \langle\chi_\sigma|\chi_\lambda\rangle = \int_{\Omega_i} \chi_\sigma(\mathbf{r_1})\chi_\lambda(\mathbf{r_1})d\mathbf{r_1} \tag{52}$$

The total atomic electron population can be obtained by integrating the ED over the atomic basin or by integrating the $g_i(\mathbf{r})$ function over all space

$$N(\Omega_i) = \int_{\Omega_i} \rho(\mathbf{r})d\mathbf{r} = \int_{-\infty}^{\infty} g_i(\mathbf{r})d\mathbf{r} \tag{53}$$

The total atomic electron population can be decomposed into localised ED and delocalised ED

$$N(\Omega_i) = \lambda_i(\Omega_i) + \frac{1}{2}\sum_{X\neq i}^{M} \delta(\Omega_i, \Omega_X) \tag{54}$$

where

$$\lambda(\Omega_i) = \int_{\Omega_i} g_i(\mathbf{r})d\mathbf{r} \tag{55}$$

and

$$\delta(\Omega_i, \Omega_j) = \int_{\Omega_j} g_i(\mathbf{r_1})\, d\mathbf{r_1} + \int_{\Omega_i} g_i(\mathbf{r_2}) d\mathbf{r_2} = 2\int_{\Omega_j} g_i(\mathbf{r_1}) d\mathbf{r_1} \tag{56}$$

From here onwards this section will cover the FALDI density decomposition.

The correlation function from DAFH (eq. 51) can be expressed as localised and delocalised electron densities,

$$g_i(\mathbf{r}) = \mathcal{L}_i(\mathbf{r}) + \frac{1}{2}\sum_{j\neq i}^{M} \mathcal{D}_{ij}(\mathbf{r}) \tag{57}$$

where *loc*-ED is given by

$$\mathcal{L}_A(\mathbf{r}) = \sum_{ij} \chi_i^*(\mathbf{r})\chi_j(\mathbf{r})\left(\mathbf{S}^{\mathrm{A}}\mathbf{S}^{\mathrm{A}}\right)_{ji} \tag{58}$$

and *deloc*-ED is given by

$$\mathcal{D}_{A,B}(\mathbf{r}) = \sum_{ij} \chi_i^*(\mathbf{r})\chi_j(\mathbf{r})\left(\mathbf{S}^{\mathrm{A}}\mathbf{S}^{\mathrm{B}}\right)_{ji} \tag{59}$$

noting that $\mathbf{S}^{\mathrm{A}}\mathbf{S}^{\mathrm{B}}$ is taken here to mean $\mathbf{S}^{\mathrm{A}}\mathbf{S}^{\mathrm{B}} + \mathbf{S}^{\mathrm{B}}\mathbf{S}^{\mathrm{A}}$.

Diagonalization is performed for the *loc*-ED and the *deloc*-ED to afford orthogonal functions which are called natural density functions (NDFs). This diagonalization is achieved by diagonalizing $\mathbf{S}^{\mathrm{A}}\mathbf{S}^{\mathrm{X}}$, where X represents every atom with which A can be combined

$$\mathbf{S}^{\mathrm{A}}\mathbf{S}^{\mathrm{X}}\mathbf{U}^{\mathrm{AX}} = n^{\mathrm{AX}}\mathbf{U}^{\mathrm{AX}} \tag{60}$$

where n^{AX} gives the eigenvalues representing occupations and $\mathbf{U}^{\mathrm{AX}}$ gives the associated eigenvectors representing the NDFs. The occupation and parameters of a specific NDF can be obtained by

$$n_i^{AX} = \sum_{jk}^{N_{MO}} U_{ji}^{AX}\left(\mathbf{S}^{\mathrm{A}}\mathbf{S}^{\mathrm{X}}\right)_{kj} U_{ki}^{AX} \tag{61}$$

The *loc*-ED can then be expressed as a linear combination of NDFs with their associated occupations as

$$\mathcal{L}_A(\mathbf{r}) = \sum_i^{N_{MO}} n_i^{AA}\left[\phi_i^{AA}(\mathbf{r})\right]^2 \tag{62}$$

where the NDF is calculated as

$$\phi_i^{AA}(\mathbf{r}) = \sum_j^{N_{MO}} \chi_j(\mathbf{r}) U_{ji}^{AA} \tag{63}$$

This approach lends an alternative manner in which QTAIM localised and delocalised indices can be calculated as the sum of occupations of the NDFs, thus the localisation index can be calculated as

$$\lambda_{\mathrm{QTAIM}}(A) = \sum_i n_i^{AA} \tag{64}$$

and similarly, for the delocalisation index

$$\delta_{\mathrm{QTAIM}}(A,B) = \sum_i n_i^{AB} \tag{65}$$

This final part of the discussion on FALDI will give the localised overlap (LO) and localised-delocalised overlap (LDO) methods which improves upon the orthodox descriptions of λ_{QTAIM} and δ_{QTAIM} where no such overlap is calculated. The LO-method will be discussed in detail whereas for the LDO method only the relevant parts will be discussed as needed to understand the difference. Both methods do however follow a similar logic.

The overlap between *loc*-ED NDFs is calculated by

$$\boldsymbol{s}\left(\mathcal{L}_A^i; \mathcal{L}_B^j\right) = \sqrt{n_i^{AA} n_j^{BB}}\left[(\mathbf{U}^{\mathrm{AA}})^{\dagger}\mathbf{U}^{\mathrm{BB}}\right]_{ij} \tag{66}$$

The total *loc*-ED overlap of the ith NDF of atomic basin A with all other *loc*-ED NDFs of all other atomic basins is then given by

$$\mathrm{LO}(\mathcal{L}_A^i) = \sum_{X \neq A}^{N_{Atoms}} \sum_j^{N_{MO}} \boldsymbol{s}(\mathcal{L}_A^i; \mathcal{L}_X^j) \tag{67}$$

The occupations are then adjusted to remove this density from the *loc*-ED. The overlap is

normalised to the square root of the product of occupations and thus if the $\mathrm{LO}(\mathcal{L}_A^i)$ is less than the occupation n_i^{AA} of the NDF $\mathcal{L}_A^i$ then the orbital is fully delocalised and its *loc*-ED is set to zero. The adjustment can be written as the following rule

$$n_i'^{AA} = \begin{cases} n_i^{AA} - \mathrm{LO}(\mathcal{L}_A^i), & n_i^{AA} > \mathrm{LO}(\mathcal{L}_A^i) \\ 0, & n_i^{AA} \leq \mathrm{LO}(\mathcal{L}_A^i) \end{cases} \tag{68}$$

where the prime indicates that the occupation is LO-free and it is then used to calculate an LO-free *loc*-ED distribution,

$$\mathcal{L}_A'(\mathbf{r}) = \sum_i^{N_{MO}} n_i'^{AA} \left[\phi_i^{AA}(\mathbf{r})\right]^2 \tag{69}$$

When integrated over all space a localisation index is calculated which is itself LO-free,

$$\lambda_{\mathrm{LO-free}}(A) = \int_{-\infty}^{\infty} \mathcal{L}_A'(\mathbf{r}) d\mathbf{r} \tag{70}$$

The density that was removed from the *loc*-ED must be added back to recover the total ED. This is achieved by adding weighted parts of the removed *loc*-ED to the relevant *deloc*-ED,

$$n'\left(\mathcal{L}_A^i \to \mathcal{D}_{A,B}^j\right) = w'(\mathcal{L}_A^i; \mathcal{D}_{A,B}^j)(n_i^{AA} - n_i'^{AA}) \tag{71}$$

where the weighting is given by

$$w'\left(\mathcal{L}_A^i; \mathcal{D}_{A,B}^j\right) = \frac{\boldsymbol{s}(\mathcal{L}_A^i; \mathcal{D}_{A,B}^j)}{\sum_j \boldsymbol{s}(\mathcal{L}_A^i; \mathcal{D}_{A,B}^j)} \cdot \frac{\sum_k \boldsymbol{s}(\mathcal{L}_A^i; \mathcal{L}_B^k)}{\mathrm{LO}(\mathcal{L}_A^i)} \tag{72}$$

From this an LO-free *deloc*-ED can then be calculated,

$$\begin{aligned} \mathcal{D}_{A,B}'(\mathbf{r}) = &\sum_j^{N_{MO}} n_j^{AB} \left[\phi_j^{AB}(\mathbf{r})\right]^2 \\ &+ \sum_j^{N_{MO}} \sum_i^{N_{MO}} \left(n'\left(\mathcal{L}_A^i \to \mathcal{D}_{A,B}^j\right)\left[\phi_i^{AA}(\mathbf{r})\right]^2 + n'\left(\mathcal{L}_B^i \to \mathcal{D}_{A,B}^j\right)\left[\phi_j^{BB}(\mathbf{r})\right]^2\right) \end{aligned} \tag{73}$$

Again, integration of the LO-free *deloc*-ED gives the LO-free delocalisation index,

$$\delta_{\mathrm{LO-free}}(A,B) = \int_{-\infty}^{\infty} \mathcal{D}'_{A,B}(\mathbf{r})d\mathbf{r} \tag{74}$$

The LDO-method follows the same logic with the total *loc*-ED overlap of the ith NDF of atomic basin A with all other NDFs of all other atomic basins being given by

$$\mathrm{LDO}(\mathcal{L}_A^i) = \sum_{X\neq A}^{M_{Atoms}} \sum_{j}^{N_{MO}} \boldsymbol{s}\left(\mathcal{L}_A^i; \mathcal{L}_X^j\right) + \sum_{X}^{M_{Atoms}} \sum_{Y\neq A}^{M_{Atoms}} \sum_{j}^{N_{MO}} \boldsymbol{s}(\mathcal{L}_A^i; \mathcal{D}_{X,Y}^j) \tag{75}$$

The same rule as for LO is applied (eq 68) is applied, substituting $\mathrm{LDO}\left(\mathcal{L}_A^i\right)$ for $\mathrm{LO}(\mathcal{L}_A^i)$ and using double primes to indicate LDO-free occupations. Just as with LO the LDO-free *loc*-ED and LDO-free *deloc*-ED can be calculated and subsequently integrated over all space to give the LDO-free localisation $\lambda_{\mathrm{LDO-free}}(A)$ and delocalisation $\delta_{\mathrm{LDO-free}}(A,B)$ indices .

It is found that $\lambda_{\mathrm{LO-free}}$ describes the electrons that are not found in the *loc*-ED of another atomic basin, generally regarded as core and non-bonded (lone-pair) electrons. However, $\lambda_{\mathrm{LDO-free}}$ describes electrons exclusively found in a single atomic basin, what chemists call the core electrons.

A note on FALDI notation:

The localisation index is written as λ_{QTAIM}, $\lambda_{\mathrm{LO-free}}$, and $\lambda_{\mathrm{LDO-free}}$ which indicates the unadjusted, LO-free and LDO-free localisation indices, respectively. The delocalisation index is written as δ_{QTAIM}, $\delta_{\mathrm{LO-free}}$, and $\delta_{\mathrm{LDO-free}}$ which indicates the unadjusted, LO-free and LDO-free delocalisation indices, respectively. Lastly, when referring to a specific NDF it is written, for example, as $\lambda^3_{\mathrm{LO-free}}(\mathrm{A})$ which refers to the third NDF of the LO-free localisation index of atomic basin A.

Cross-section of electron and orbital densities

Cross-sections of the ED are calculated as the density along the λ-eigenvectors of the Hessian matrix[25]. By performing an integration along the λ-eigenvectors such that relative contributions of density functions or orbital densities to the bonding nature can be determined along with the symmetry of these interactions.

The BCP is identified by analysis of the Hessian eigenvectors, where the BCP has eigenvalues that are minima in two directions and a maximum in one. The λ-eigenvector, as

used in this work, is defined as the vector which extends from this bond critical point in the direction pointed in by the λ-eigenvector of the Hessian matrix. The vector is followed along both the positive and negative directions for a set distance. To simplify the calculation of this vector it was approximated as a linear vector with a gradient determined by the Hessian vector at the BCP. The use of the BCP is not critical, but does provide the most insightful data. A similar λ-eigenvector drawn at any arbitrary location does not necessarily provide any useful insights.

The orbital and electron densities are calculated as numerical approximations using points uniformly distributed along the eigenvector. The densities are calculated for each coordinate point using a similar decomposition with $\chi_i(\mathbf{r})$ here denoting any orbital and n_i denoting the occupation of that orbital,

$$\rho(\mathbf{r}) = \sum_{i}^{N} n_i |\chi_i(\mathbf{r})|^2 \tag{76}$$

A special note should be added on the newer FALDI decomposition of the ED which is given as localised and *deloc*-ED, but since the analysis is along the interatomic surface the localised component makes no contribution by definition, thus the equation is simplified to only the *deloc*-ED given by the equation

$$^{FALDI}\rho(\mathbf{r}) = \sum_{A}^{M} \mathcal{L}_A(\mathbf{r}) + \sum_{A}^{M}\sum_{B\neq A}^{M} \mathcal{D}_{A,B}(\mathbf{r}) \cong \sum_{A}^{M}\sum_{B\neq A}^{M} \mathcal{D}_{A,B}(\mathbf{r}) \tag{77}$$

The NDF decomposition for the *deloc*-ED of each atom pair is given by

$$^{NDF}\rho(\mathbf{r}) = \sum_{j}^{N_{MO}} \sum_{i}^{N_{MO}} n_i^{AB} \left|\phi_j^{AB}(\mathbf{r})\right|^2 \tag{78}$$

In all cases the integration is performed numerically, however, the concept of integration remains conceptually the same for all applications, thus it can be represented as

$$\int_{\lambda} \rho(\mathbf{r}) d\mathbf{r} \cong \sum_{i}^{\mathrm{N}} \rho(\mathbf{r}_i) \Delta\mathbf{r} \tag{79}$$

where $\Delta\mathbf{r}$ represents the step-size used in the calculation, also given by $\Delta\mathbf{r} = \|\lambda\|/N$, and N is the number of steps used in the approximation.

The integrated densities carried no physical meaning and normalisation against the total integrated total density yields a percentage contribution of each orbital or density component to the total bonding interaction,

$$\%contribution = \frac{\int_{\mathbf{r}} \rho_i(\mathbf{r}) d\mathbf{r}}{\int_{\mathbf{r}} \rho_{total}(\mathbf{r}) d\mathbf{r}} \tag{80}$$

This method provides insights on the considerations towards the important aspects in the picture of chemical bonding. It lends insights regardless of the methodological approach (MO, NBO, FALDI) and regardless of the topology or symmetry of the system. It is meant to serve as a guide to the chemist by identifying important components in a chemical bond or interaction.

Delocalisation index decomposition

The final method presented attempts to decompose the orbital densities into localised and delocalised atomistic contributions. Atomic basins Ω are defined using the descriptors from QTAIM[13,15]. Atomic overlap matrices can then be calculated for each atomic basin by

$$S_{ij}^{\Omega} = \int_{\Omega} \chi_i(\mathbf{r}) \chi_j(\mathbf{r}) d\mathbf{r} = \langle \chi_i | \chi_j \rangle_{\Omega} \tag{81}$$

where χ_i and χ_j are the molecular orbitals (MOs) which are integrated over the volume of the atomic basin to obtain the contribution of those orbitals to the atom described by that particular basin.

In order to calculate atomistic MO occupations correctly it is required to set up an occupation matrix. This work only uses double occupied closed shell and single determinant wavefunctions within the Hartree-Fock approximation and thus the occupation matrix can be constructed as an (N × N)-matrix with all diagonal elements equal to 2 and all off-diagonal elements zero with N as the number of occupied MOs.

Two sets of matrices are then calculated representing the localised occupations

$$LMAT_{ij}^{A} = \sum_{i}^{N} \sum_{j}^{N} \sqrt{n_i n_j} S_{ij}^{A} S_{ji}^{A} \tag{82}$$

and the delocalised occupations

$$DMAT_{ij}^{A,B} = \sum_{i}^{N}\sum_{j}^{N}\sqrt{n_i n_j}(S_{ij}^{A}S_{ji}^{B} + S_{ij}^{B}S_{ji}^{A}) \quad (83)$$

The diagonals of these matrices for each atom or atom pair are collected together in a separate table to gain an overview of the occupations per atom for each MO. This gives insight into the mode of bonding (covalent or donor-acceptor) while providing quantitative occupations for the bonding, anti-bonding or non-bonding nature of MOs with respect to individual interactions.

References

1. Cramer, C. J. Essentials of Computational Chemistry: Theories and Models; Wiley, **2004**, 1-16; 105-130.

2. Jensen, F. Introduction to Computational Chemistry; Wiley, **2007**, 1-21; 80-231.

3. Szabo, A.; Ostlund, N. S. Modern Quantum Chemistry : Introduction to Advanced Electronic Structure Theory; Dover Publications: Mineola, N.Y., **2006**, 39-230.

4. Atkins, P. W.; Friedman, R. S. Molecular Quantum Mechanics; Oxford University Press: Oxford, **2004**, 249-341.

5. Koch, W.; Holthausen, M. C. A Chemist's Guide to Density Functional Theory; Wiley, **2015**, 1-116.

6. Stephens, P. J.; Devlin, F. J.; Chabalowski, C. F.; Frisch, M. J. *J. Phys. Chem.* **1994**, 98(45), 11623-11627.

7. Becke, A. D. *J. Chem. Phys.* **1993**, 98(2), 1372-1377.

8. Salahub, D. R.; Zerner, M. C. *Chemical Congress of North America* **1988**: Toronto, Ont), 1989.

9. Becke, A. D. *J. Chem. Phys.* **1988**, 88(2), 1053-1062.

10. Lee, C.; Yang, W.; Parr, R. G. *Phys. Rev. B* **1988**, 37(2), 785.

11. Vosko, S. H.; Wilk, L.; Nusair, M. *Can. J. Phys.* **1980**, 58(8), 1200-1211.

12. Weinhold, F.; Landis, C. R.; Press, C. U. Valency and Bonding: A Natural Bond Orbital Donor-Acceptor Perspective; Cambridge University Press, **2005**, 1-41.

13. Matta, C. F.; Boyd, R. J.; Becke, A. The Quantum Theory of Atoms in Molecules: From Solid State to DNA and Drug Design; Wiley, **2007**, 1-30.

14. Popelier, P. Atoms in Molecules: An Introduction; Prentice Hall, **2000**.

15. Bader, R. F. W. Atoms in Molecules : a Quantum Theory; Clarendon Press: Oxford, **1990**.

16. Bader, R. F. W.; Stephens, M. E. *J. Am. Chem. Soc.* **1975**, 97(26), 7391-7399.

17. de Lange, J. H. Fundamental nature of chemical bonding from the novel Fragment, Atomic, Localised, Delocalised and Interatomic (FALDI) electron density decomposition scheme. A theoretical study. In Chemistry; University of Pretoria: Pretoria, South Africa, **2018**, 17-52.

18. De Lange, J. H.; Cukrowski, I. *J. Comp. Chem.* **2017**, 38(13), 981-997.

19. de Lange, J. H.; van Niekerk, D. M.; Cukrowski, I. *J. Comp. Chem.* **2018**, 39(16), 973-985.

20. de Lange, J. H.; Cukrowski, I. *J. Comp. Chem.* **2018**, 39(20), 1517-1530.

21. de Lange, J. H.; van Niekerk, D. M.; Cukrowski, I. *J. Comp. Chem.* **2018**, 39(27), 2283-2299.

22. Cukrowski, I.; van Niekerk, D. M.; de Lange, J. H. *J. Struct. Chem.* **2017**, 28(5), 1429-1444.

23. Ponec, R. *J. Math. Chem.* **1997**, 21(3), 323-333.

24. Ponec, R. *J. Math. Chem.* **1998**, 23(1-2), 85-103.

25. Cukrowski, I.; de Lange, J. H.; Adeyinka, A. S.; Mangondo, P. *Comput. Theor. Chem.* **2015**, 1053, 60-76.

Chapter Three

Characterization of Bonding Modes in Metal Complexes through Electron Density Cross-Sections

For this publication the work was produced as:

Shane de Beer: data collection, processing, writing and editing.

Jurgens H. de Lange: writing and editing.

Ignacy Cukrowski: writing and editing.

The publication is presented here exactly as it was published in the Journal of Computational Chemistry.

Received: 21 July 2020 | Revised: 8 September 2020 | Accepted: 11 September 2020

DOI: 10.1002/jcc.26423

FULL PAPER

Journal of COMPUTATIONAL CHEMISTRY WILEY

Characterization of bonding modes in metal complexes through electron density cross-sections

Shane de Beer | Ignacy Cukrowski | Jurgens H. de Lange

Department of Chemistry, Faculty of Natural and Agricultural Sciences, University of Pretoria, Pretoria, South Africa

Correspondence
Jurgens H. de Lange, Department of Chemistry, Faculty of Natural and Agricultural Sciences, University of Pretoria, Lynnwood Road, Hatfield, Pretoria 0002, South Africa.
Email: jurgens.delange@up.ac.za

Funding information
Council for Scientific and Industrial Research, South Africa; University of Pretoria; National Research Foundation of South Africa, Grant/Award Number: 105855

Abstract

Qualitative inspection of molecular orbitals (MOs) remains one of the most popular analysis tools used to describe the electronic structure and bonding properties of transition metal complexes. In symmetric coordination complexes, the use of group theory and the symmetry-adapted linear combination (SALC) of fragment orbitals allows for a very accurate and informative interpretation of MOs, but the same procedure cannot be performed for asymmetric complexes, such as Schrock and Fischer carbenes. In this work, we present a straight-forward approach for classifying and quantifying MO contributions to a particular metal–ligand interaction. Our approach utilizes the topology of MO density contributions to a cross-section of an internuclear region, and is computationally inexpensive and applicable to symmetric and asymmetric complexes alike. We also apply the same approach with similar decompositions using Natural Bond Orbitals (NBO) and the recently developed Fragment, Atomic, Localized, Delocalized and Interatomic (FALDI) density decomposition scheme. In particular, FALDI analysis provides additional insights regarding the multicentric nature of metal-carbene bonds without resorting to expensive multireference calculations.

KEYWORDS

bonding, FALDI, molecular orbitals, organometallic

1 | INTRODUCTION

The modes of bonding in transition metal carbene complexes have been a puzzle since their discovery by Fischer and Maasböl in 1964.[1,2] The classes of transition metal carbene complexes discovered have been expanded by Schrock,[3] Öfele,[4,5] and Wanzlick,[6–9] and modern day classification of transition metal carbene complexes generally falls within three categories, Fischer-, Schrock- and *N*,*N*-heterocyclic carbene complexes.

Each class of transition metal carbene complexes shows different bonding characteristics and models to describe each class's electronic structure have been developed. Works by Taylor and Hall[10] and by Rappé, Carter and Goddard[11–15] showed the bonding of Schrock carbene complexes to be due to the combination of a triplet metal fragment with a triplet carbene fragment forming covalent bonds. This has become the accepted model for bonding in Schrock carbene complexes, with the Dewar–Chatt–Duncanson donor–acceptor model[16,17] explaining the bonding in Fischer carbene complexes.

Interpretation of bonding through these models generally requires fragmentation of the complex into multiple atoms and/or ligands. Qualitative interpretations can then be made, usually through the construction of MOs through symmetry-adapted linear combinations (SALCs) of fragment orbitals, and additional quantitative insights can be gained with approaches such as Energy Decomposition Analysis (EDA)[18,19] or the Extended Transition State coupled with Natural Orbitals for Chemical Valence (ETS-NOCV).[20] Unfortunately, approaches requiring fragmentation provide interpretations that are highly dependent on the fragmentation scheme used—a problem that is particularly apparent when analyzing a single metal–ligand bond in biscarbene or chelate complexes.

An alternative to the use of fragmentation schemes is to analyze the wavefunction directly, usually in terms of MOs or valence bond resonance states. A wealth of chemical and physical information, ranging from atomic properties and reactivities to photophysical behavior, can be obtained from fully characterized MOs; however, characterization generally requires (i) the use of fragmentation in the form of SALCs, and (ii) a high degree of symmetry to be present. To illustrate the benefit that can be gained from an in-depth MO analysis, however, consider the conceptual MO diagram of $TiCl_3^+$—a model complex studied in this work—in Figure 1. SALCs of $3p_{Cl}$ atomic orbitals form fragment orbitals with symmetries a_1', a_2', a_2'', e' and e'' whereas Ti^{IV} atomic orbitals have symmetries a_1', a_2'', e' and e''. SALCs and metal atomic orbitals with the same symmetries can overlap to form bonding and antibonding MO pairs: MOs with a_1' and e' symmetries form σ-bonds, MOs with a_2'' and e'' form $\pi_\perp$ bonds and MOs with e' can also form in-plane $\pi_{//}$ bonds.

The highest occupied molecular orbital (HOMO) of $TiCl_3^+$ is expected to be fully nonbonding and ligand-centered, as no metal atomic orbital has a_2' symmetry. Three sets each of bonding σ- and $\pi_\perp$-MOs are occupied, as well as two $\pi_{//}$-MOs, which gives each Ti—Cl bond a formal bond order slightly greater than two. The expectation that all ligand orbitals but none of the metal atomic orbitals will be

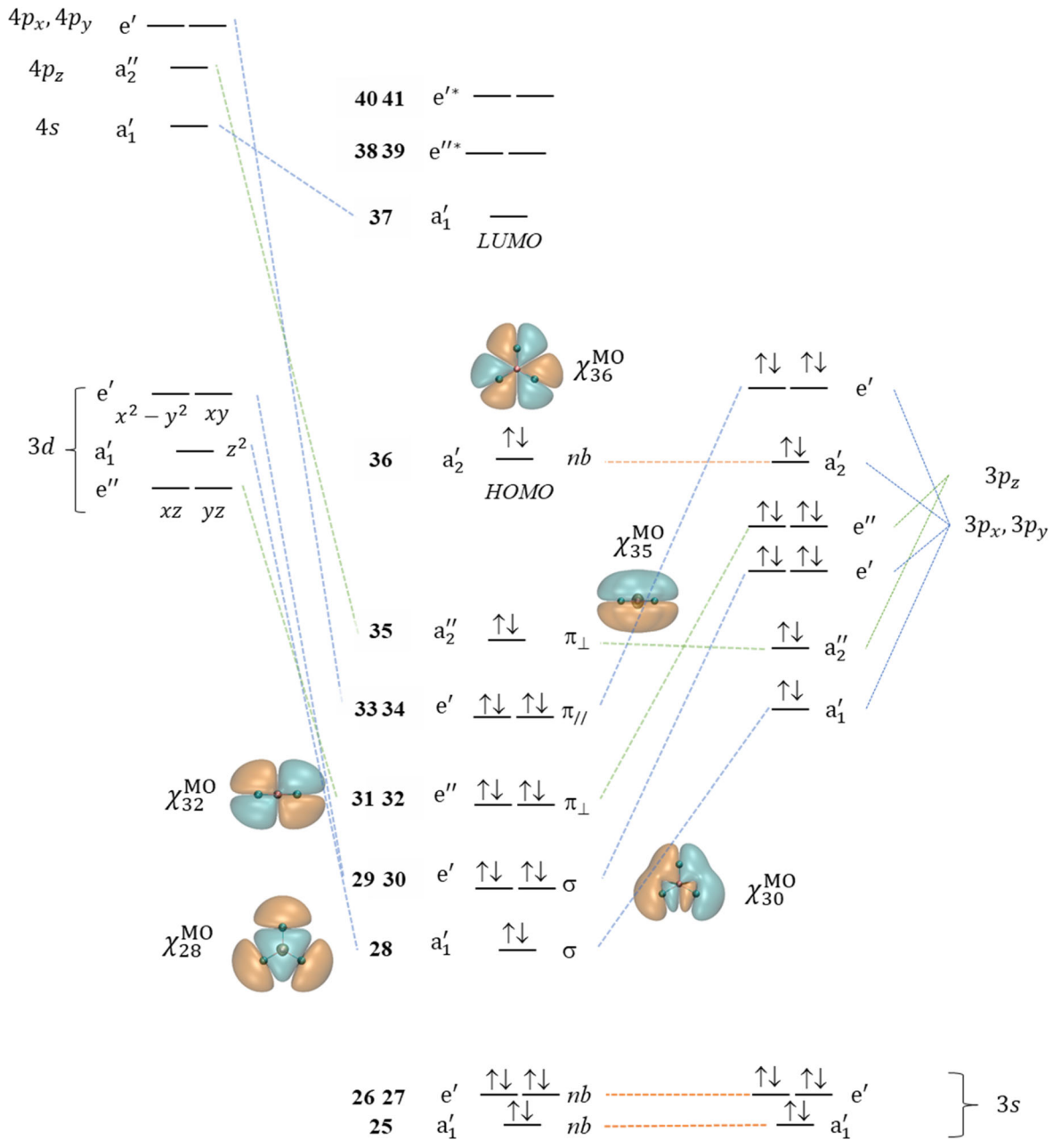

FIGURE 1 Conceptual MO diagram of $TiCl_3^+$, constructed using SALCs of the ligand orbitals (right) and metal atomic orbitals in a trigonal ligand field (left). Dashed blue, green, and red lines indicate σ-, π- and nonbonding modes, respectively. Computed isosurfaces of selected MOs are shown, at an isovalue of 0.001 au

occupied suggests that the σ- and π-bonding modes will be ligand-centered with a strong donating character and that the metal will be cationic. The strong π-donating character of Cl (as implied by Figure 1 and in correspondence with Cl's position on the spectrochemical spectrum) suggests that the axial valence orbitals on the metal ($3p_z$ and $4p_z$) will be quite reactive and electrophilic. Finally, the symmetries of the MOs can be used to analyze the photophysical properties of the complex, suggesting a weak, symmetry-forbidden HOMO→LUMO transition but intense, high energy $\pi \rightarrow \pi^*$ ($e'' \rightarrow e''^*$) transitions. It should also be noted that such a MO diagram can be constructed using knowledge from graduate-level textbooks (e.g., References 21,22, with no computational modeling required.

Unfortunately, an equivalent MO diagram cannot be generated for an asymmetrical carbene complex, as no meaningful SALCs can be generated due to the lack of symmetry. Accordingly, MO-analysis becomes much more complicated than for a symmetrical complex, with MO characteristics usually inferred from similar, symmetrical structures. Alternatively, advanced computational techniques can be used to investigate the bonding modes of metal complexes without the use of fragmentation schemes. Cundari and Gordon[23,24] illustrated the multi-centric nature of a metal-carbene interaction by using multi-configurational wavefunctions and finding multiple resonance structures, of which the accepted model is only a single possibility. Other post-SCF, orbital-based analysis techniques, such as Natural Bonding Orbitals (NBOs),[25] have also shed significant insight on the various bonding modes accessible to organometallic compounds.[26–28] Finally, density-based methods have also been used to study both Fischer and Schrock carbenes[27,29] and have reached many of the same insights as multi-configurational wavefunction approaches.

While all of the approaches detailed above provide useful insights to the problem of organometallic bonding in asymmetric complexes, basic inspection and analysis of computed MO eigenvalues and isosurfaces still seem to be preferred by many chemists. Unfortunately, the exact interpretation of frontier MOs (as well as the remainder of canonical MOs) becomes increasingly more difficult with larger, less symmetric and more conjugated metal complexes. In fact, and as we shall demonstrate in this work, MO interpretation of even the smallest carbene complexes is considerably more complex than symmetric coordination complexes. It, therefore, becomes desirable to develop an approach that (i) extends MO-analysis to yield more accurate interpretations for any metal complex, (ii) can provide comparable results to other post-SCF analyses and (iii) does not sacrifice the ease of interpretation and low computational cost that MO-analysis offers.

This work presents a method of decomposing, classifying and quantifying MO contributions to the density in the internuclear region of a metal–ligand bond using density cross-sections.[30] Similar approaches have proven useful in identifying (anti)bonding and non-bonding orbitals in chemical systems,[31] as well as investigate multi-centric interactions.[32] The same method is also used here to investigate the contributions from two other decompositions, the orbital-based NBO analysis and density-based Fragment, Atomic, Localized, Delocalized and Interatomic (FALDI) charge decomposition scheme.[33,34]

2 | THEORETICAL BACKGROUND

2.1 | Cross-section analysis

Cross-sections of the electron density (ED)[30] are generated by first calculating the Hessian matrix and associated principle eigenvectors at a (3,–1) critical point (CP, also known as a bond critical point) of an interaction of interest, as defined by the Quantum Theory of Atoms in Molecules (QTAIM).[35] The eigenvector associated with the λ_2 eigenvalue is then followed in both directions to a maximum distance of 3.00 Bohr. The path generated in this manner will henceforth be referred to as the λ_2–eigenvector. Note that any of the three principle axes can be followed (generating λ_1-, λ_2- or λ_3-eigenvectors), but the λ_2-eigenvector generally provides the most information regarding the interaction of interest.[36] Regardless, once the cross-section coordinates are generated, the ED at each point can be decomposed into more informative contributions. In this work, we will apply three independent ED decomposition schemes: (i) canonical MO, (ii) NBO and (iii) FALDI density decompositions. Since NBO analysis is quite well established, we will only provide some theoretical background on relatively recently developed FALDI scheme; readers interested in more information on NBOs are encouraged to consult Reference 25.

2.2 | Orbital decomposition

The total ED at any given coordinate **r** can be decomposed in terms of MO densities by,

$$^{\mathrm{MO}}\rho(\mathbf{r}) = \sum_{i}^{N_{\mathrm{MO}}} \upsilon_i \left|\chi_i^{\mathrm{MO}}(\mathbf{r})\right|^2 \tag{1}$$

where χ_i^{MO} is an MO with occupation υ_i. In this work, we are only considering restricted, single-determinant wavefunctions, thus υ_i = 2 for all MOs.

Similarly, the electron density can also be decomposed in terms of NBO density contributions, after an NBO transformation is completed,

$$^{\mathrm{NBO}}\rho(\mathbf{r}) = \sum_{i}^{N_{\mathrm{NBO}}} \upsilon_i \left|\chi_i^{\mathrm{NBO}}(\mathbf{r})\right|^2 \tag{2}$$

where χ_i^{NBO} is an NBO with occupation υ_i. Unlike decomposition into canonical MOs (Equation (1)), the NBOs generally have variable occupations.

Each MO or NBO contribution can be further classified based on the sign of their directional, partial second derivative (henceforth referred to as only 2nd derivative). Specifically, if the 2nd derivative of an MO or NBO density contribution is negative at **r**, the orbital

concentrates ED at **r**,[35] as its value is larger than the average of its contribution at neighboring coordinates. Similarly, if the 2nd derivative is positive at **r**, the orbital *depletes* ED at **r**. Note that an MO or NBO can contribute zero at **r**, yet still be classified as *concentrating* or *depleting* based on its 2nd derivative at **r** (such as when **r** is located at a node of a π-orbital). For this reason, we also report the integrations along the λ_2-eigenvector in order to quantify the relative contributions of each decomposition product.

2.3 | FALDI decomposition

The FALDI density decomposition scheme expands on concepts introduced by the Domain Averaged Fermi Hole (DAFH) analysis,[37,38] and provides an effective mapping of the electron-pair density distribution over atomic volumes defined in real space. Typically, as for DAFH analysis, QTAIM-defined atomic basins are used as domains, but most atoms-in-molecule schemes can be employed. FALDI decomposition then results in a set of pseudo-second order functions that can decompose the total electron density at any coordinate **r** into contributions from molecular fragments, atoms, intra-atomic localized electrons and inter-atomic delocalized electrons.

In this work, we are primarily interested in the decomposition into intra-atomic localized (*loc*–ED) and inter-atomic delocalized (*deloc*–ED) density distributions, which can be given by:

$$^{\mathrm{FALDI}}\rho(\mathbf{r}) = \sum_{A}^{M} \mathcal{L}_A(\mathbf{r}) + \sum_{A}^{M-1} \sum_{B=A+1}^{M} \mathcal{D}_{A,B}(\mathbf{r}) \tag{3}$$

where M is the number of QTAIM-defined atomic basins. $L_A(\mathbf{r})$ describes the contribution to **r** made by electrons localized to a single atomic basin Ω_A, whereas $D_{A,B}(\mathbf{r})$ describes the contribution to **r** made by electrons delocalized over two atomic basins Ω_A and Ω_B. Notably, $L_A(\mathbf{r})$ and $D_{A,B}(\mathbf{r})$ can be measured anywhere in the molecule, and in particular, $D_{A,B}(\mathbf{r})$ tends to be non-zero even when $\mathbf{r} \notin \Omega_A, \Omega_B$. FALDI analysis, therefore, provides a holistic, molecular-wide description of atomic electron distributions. A brief description is given below for the calculation of these terms; for more information, please consult Reference 33.

In order to calculate $L_A(\mathbf{r})$ and $D_{A,B}(\mathbf{r})$, an atomic overlap matrix (AOM) first needs to be defined. An AOM for atom A, $\mathbf{S}^A$, has elements:

$$S_{ij}^{A} = \sum_{ij} \int_{A} \sqrt{\nu_i}\sqrt{\nu_j}\chi_i^*(\mathbf{r})\chi_j(\mathbf{r})d\mathbf{r} \tag{4}$$

where integration is over the atomic basin Ω_A. Equation (4) satisfies the relation $tr(\mathbf{S}^A) = N(A)$—the total electronic population of the atom. Matrix multiplication of $\mathbf{S}^A$ with itself then leads to a *localized* matrix, $\mathbf{S}^A\mathbf{S}^A$, which satisfies $tr(\mathbf{S}^A\mathbf{S}^A) = \lambda(A)$—the QTAIM-defined localization index (LI).[39] Similarly, AOMs of two different atoms can be combined as $\mathbf{S}^A\mathbf{S}^B + \mathbf{S}^B\mathbf{S}^A$ to define a *delocalized* matrix, with $tr(\mathbf{S}^A\mathbf{S}^B + \mathbf{S}^B\mathbf{S}^A) = \delta(A,B)$—the QTAIM-defined delocalization index (DI).[39] Note that $N(A) = \lambda(A) + \frac{1}{2}\sum_{B\neq A}\delta(A,B)$, and accordingly, $\mathbf{S}^A = \mathbf{S}^A\mathbf{S}^A + \frac{1}{2}\sum_{B\neq A}\left(\mathbf{S}^A\mathbf{S}^B + \mathbf{S}^B\mathbf{S}^A\right)$. In addition, we note that these definitions only hold exactly for restricted, Hartree-Fock or Density Functional Theory wavefunctions.

Once localized and delocalized matrices have been obtained, *loc*–ED and *deloc*–ED distributions can be calculated by considering the overlap of each MO contribution at a given coordinate **r** with the relevant matrix:

$$\mathcal{L}_A(\mathbf{r}) = \sum_{ij}^{N} \chi_i^*(\mathbf{r})\chi_j(\mathbf{r})\left(\mathbf{S}^A\mathbf{S}^A\right)_{ji} \tag{5}$$

for *loc*–ED distributions, and

$$\mathcal{D}_{A,B}(\mathbf{r}) = \sum_{ij}^{N} \chi_i^*(\mathbf{r})\chi_j(\mathbf{r})\left(\mathbf{S}^A\mathbf{S}^B + \mathbf{S}^B\mathbf{S}^A\right)_{ji} \tag{6}$$

for *deloc*–ED distributions. In accordance with the above interpretation of these fields, $\mathcal{L}_A(\mathbf{r})$ and $\mathcal{D}_{A,B}(\mathbf{r})$, when integrated over *all* molecular space, yield the QTAIM-defined localization and delocalization indices, $\lambda(A)$ and $\delta(A,B)$, respectively. *loc*–ED and *deloc*–ED distributions, therefore, provide a very useful tool to quantify or visually inspect how electrons are distributed or shared among atoms, whether through rendering as a 3D isosurface or scanning along a 1D vector.

Each $\mathcal{D}_{A,B}(\mathbf{r})$ can be further decomposed into sets of orthogonal natural density functions (NDFs), through diagonalization of the delocalized matrix $\mathbf{S}^A\mathbf{S}^B + \mathbf{S}^B\mathbf{S}^A$. Each $\mathcal{D}_{A,B}(\mathbf{r})$ decomposes into N number of NDFs (where N is the number of occupied MOs) with decreasing occupation numbers:

$$\mathcal{D}_{A,B}(\mathbf{r}) = \sum_{i}^{N_{MO}} n_i^{AB}\left[\phi_i^{AB}(\mathbf{r})\right]^2 = \sum_{i}^{N} \mathcal{D}_{A,B}^{i}(\mathbf{r}) \tag{7}$$

NDFs provide chemically-intuitive descriptions of the various modes through which electrons can be shared by two atoms, and the occupation number of each NDF is its contribution to $\delta(A,B)$. For instance, for a covalent interaction, the largest occupied NDFs usually resemble σ- and π-bonding modes.

Some of us have previously shown[33] that QTAIM's $\lambda(A)$ and $\delta(A,B)$, while useful and exact within quantum mechanics, provide a somewhat chemically unintuitive picture of electron distributions within a molecule, especially when considering lone-pairs. Specifically, QTAIM's LIs describe core and non-bonded electrons, as well as a portion of bonded valence electrons. We proposed the Localized-Delocalized Overlap (LDO) algorithm, which ensures that $\mathcal{L}_A(\mathbf{r}) \cong 0$ when **r** is outside of Ω_A. Specifically, the LDO algorithm takes the overlap, in an MO basis, between localized NDFs (*loc*–NDFs) of different atoms as well as the overlap between *loc*– and *deloc*–NDFs into account. If the *i*th *loc*–NDF of atom A overlaps with the *j*th *loc*–NDF of atom B, then the degree of overlap can be considered as electron

delocalization between the atom-pair unaccounted by orthodox DI values. The LDO algorithm then reduces the occupation values of the two *loc*–NDFs, and increases the occupation value of the relevant *deloc*–NDF.

All LIs and DIs reported in this work have been subjected to the LDO algorithm, and consequently, will differ from QTAIM-reported values. $\lambda_{LDO}(A)$ will generally be smaller than $\lambda_{QTAIM}(A)$, whereas $\delta_{LDO}(A,B)$ will generally be larger than $\delta_{QTAIM}(A,B)$. For instance, in the N_2 molecule, $\lambda_{QTAIM}(N) \approx 5.5\ e^-$ and $\delta_{QTAIM}(N,N) \approx 3.0\ e^-$; on the other hand, $\lambda_{LDO}(N) \approx 4.0\ e^-$ (reflecting the core 1 *s* electrons and a non-bonded lone-pair) and $\delta_{LDO}(N,N) = 6.0\ e^-$ (reflecting 3 electron-pairs shared between the triple-bonded N-atoms).[33] In molecules with a large degree of multicenter and long-range delocalized characters, LDO DIs tend to be considerably larger than their QTAIM counterparts and LDO DIs should be seen as the *maximum possible* electron delocalization that can occur among an atom-pair. In addition, in this work we will always focus on electron density distributions at (3,–1) CPs, which can only occur on inter-nuclear surfaces. Consequently, with the LDO algorithm, $\mathcal{L}_A(\mathbf{r}^*) \cong 0$ if $\mathbf{r}^*$ is at a CP, which then simplifies Equation (3) to

$$^{FALDI}\rho(\mathbf{r}^*) \cong \sum_{A}^{M-1} \sum_{B=A+1}^{M} \mathcal{D}_{A,B}(\mathbf{r}^*) \tag{8}$$

The same holds true, in this work, for all coordinates on the λ_2–eigenvector and, therefore, $\int_{\lambda_2} \mathcal{L}_A(\mathbf{r})d\mathbf{r} \cong 0$.

Finally, each FALDI component can also be classified based on the sign of its second derivative at $\mathbf{r}$ as *concentrating* or *depleting*, as noted above for NBO and MO decompositions.

3 | COMPUTATIONAL DETAILS

All structures were optimized in Gaussian 09, Rev. D.01,[40] using B3LYP with the 6–311++G(d,p) basis set in gas phase. The symmetry on the $TiCl_3^+$ optimisation was manually set to D_{3h} and the $TiCl_2CHCH_3$ optimisation was calculated with no symmetry specified. QTAIM molecular graph and atomic overlap matrices were calculated using AIMAll version 17.11.14.[41] NBO electronic structures were calculated in Gaussian 09, with NBO version 3.1.[42] FALDI data was calculated using in-house software with the LDO algorithm. All MO, NBO and FALDI isosurfaces were visualized using VMD version 1.9.3.[43]

Cross-section densities were calculated using in-house software, with the λ_2–eigenvector always originating from a Ti,X (3,–1) CP. λ_2–eigenvectors were calculated to a total length of 6.0 Bohr and evaluated at 0.01 Bohr increments. Integrations across λ_2–eigenvectors were performed numerically on a uniform grid.

4 | RESULTS AND DISCUSSION

$TiCl_3^+$ and $TiCl_2CHCH_3$ are discussed below as two model complexes; the former is a symmetric, coordination complex and the latter is an asymmetric Schrock carbene complex. Cross-section analyses using MO, NBO and FALDI decompositions are performed for each of these complexes and will be discussed first for $TiCl_3^+$.

4.1 | Analysis of bonding in a coordination complex

In the qualitative conceptual model, the chlorine atom in $TiCl_3^+$ acts as a strong σ-donor, π-donor type X-ligand in accordance with its position on the spectrochemical series. From an MO perspective, Cl forms both σ- and π-bonds to Ti through donation of ED from low-energy, occupied Cl atomic orbitals to higher energy, empty atomic orbitals on the titanium atom.

Due to the D_{3h} point group symmetry of the $TiCl_3^+$ system, group theory can be used without too much difficulty in order to gain insights regarding each MO describing a Ti—Cl bond. A set of SALCs can be derived with their symmetry labels by a linear combination of atomic orbitals (AOs) which would then give a guideline for how molecular bonding interactions are formed with the metal orbitals. A list of orbital isosurfaces can be found in the Supporting Information showing the titanium atomic orbitals (Figure S1), valence set of the SALCs (Figure S2), and the canonical molecular orbitals (Figure S3) for the $TiCl_3^+$ system. The valence MO diagram constructed in this manner is shown in Figure 1 in the Introduction.

A selection of significant MOs, together with their symmetry labels, is shown in Figure 1. MOs with a_1' symmetry only participate in σ-type overlap, such as for χ_{28}^{MO}, whereas orbitals with a_2'' or e'' symmetry only participate in π-type overlap; e.g., χ_{35}^{MO} and χ_{32}^{MO}. MOs with e' symmetry can form either σ- or π-bonds, for example, χ_{30}^{MO}, and seemingly make up the majority of interactions due to the large number of orbitals with this symmetry. All of the MOs shown in Figure 1 are formed by overlap of various Ti AOs and Cl 3*p* SALCs.

Importantly, group theory also predicts the presence of non-bonding orbitals. A SALC with a_2' symmetry can be found on the ligand system but not among the titanium AOs and, therefore, the resulting MO should be non-bonding and completely ligand centered. For the $TiCl_3^+$ system the HOMO is indeed such a non-bonding orbital, χ_{36}^{MO}. Inspection of the MO's isosurface alone (Figure 1), however, could easily and erroneously suggest that χ_{36}^{MO} is of bonding nature, since it seemingly covers both metal and ligand atomic domains. Such an interpretation shows how investigation of MO isosurfaces without the benefit of group theory can be very misleading.

The above observations, as well as the discussion regarding the MO diagram of $TiCl_3^+$ in the Introduction, clearly illustrate the power and simplicity of MO analysis using a SALC approach. However, such an approach is only valid *if* a high degree of symmetry is present. In addition, while the MO diagram reveals the presence of 2.6 occupied bonding orbitals per Ti—Cl bond (one σ, one $\pi_\perp$ and two-thirds of a $\pi_{//}$ orbital), it is difficult to quantify the relative contribution to the covalent and/or dative covalent character of each bond. We will now investigate the same set of MOs using the approaches discussed in

the Theoretical Background in order to recover and improve upon the SALC approach.

Selected MOs' contributions to the ED along the λ_2–eigenvector associated with a Ti—Cl bond are shown in Figure 2a; these MOs also contribute most to the total ED integrated along the λ_2–eigenvector, Figure 2b. The curves obtained for χ_{30}^{MO}, χ_{28}^{MO}, and χ_{24}^{MO} in Figure 2a are all bell-shaped, with a maximum at the Ti,Cl CP and represent a *concentration* of ED (second derivatives are all negative); these MOs are all of σ-character. χ_{32}^{MO} has a double-belled curve with a minimum at the Ti,Cl CP and this represents a *depletion* of ED (second derivative is positive); this MO is of π-character. The remaining ED (marked as χ_{Rem}^{MO} in Figure 2a) is also predominantly of σ-character, and it would, therefore, be expected that the Ti—Cl bond—in terms of the ED along the λ_2–eigenvector—is predominantly of σ-character.

The set of all MOs can also be grouped by their symmetry characters (as defined by the SALC approach above) and their contributions are plotted along the λ_2–eigenvector in Figure 3c. The expected bonding modes of each symmetry group are recovered: MOs with e' and a_1' symmetries show a maximum at the CP and are of σ-character, whereas MOs with e" and a_2" symmetries show a minimum at the CP and are of π-character. The non-bonding character of the HOMO (a_2') is perfectly captured (contributing zero to the ED along the λ_2–eigenvector and negligibly to the ED along the λ_1–eigenvector, Table S3). Our approach also provides a quantitative measure (Figure 3d), and the majority of the density integrated along the λ_2–eigenvector is contributed by MOs with e' symmetry. Therefore, the description of the ED associated with a Ti—Cl bond is exactly the same regardless of whether individual MOs (Figure 3a,b) or symmetry-grouped MOs (Figure 3c,d) are used. Our results, therefore, perfectly recover all of the predictions regarding bonding modes made by the qualitative SALC model and, in particular, in capturing the non-bonding nature of the HOMO. Interestingly, whereas the SALC model assumes that the $3s_{Cl}$ AOs are too low in energy to interact with metal AOs, results in Table S3 in the SI show that the resulting MOs (χ_{25}^{MO}, χ_{26}^{MO}, and χ_{27}^{MO}) contribute significantly to the ED associated with a Ti—Cl bond; in fact, all of the lower-energy MOs labeled as "nonbonding" by the SALC approach contribute 32.4% of the total ED integrated along the λ_2–eigenvector. Finally, unlike the SALC model, our approach is also fully applicable to asymmetric systems as well, as we will show later.

NBO-analysis is often used to characterize bonding in organometallic complexes. Localisation of the electron densities by the NBO method for a Ti—Cl bond in $TiCl_3^+$ leads to a σ- and a π-symmetry NBO (χ_{29}^{NBO} and χ_{32}^{NBO}, respectively—Figure 3). The two bonding NBOs are both almost doubly-occupied, leading to the interpretation that the Ti—Cl bond consists of equal σ- and π-character. Note also that

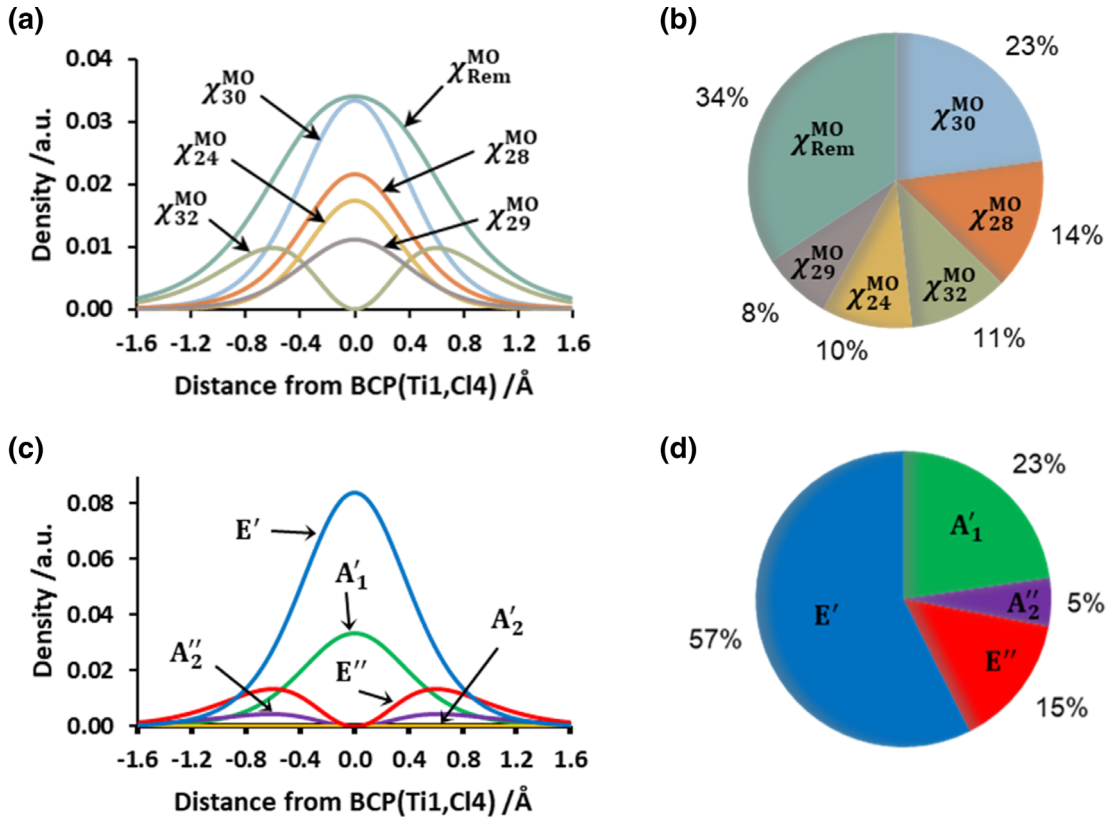

FIGURE 2 Cross-section of MO densities along the λ_2–eigenvector originating at a Ti,Cl (3,–1) CP in $TiCl_3^+$. Density contributions of selected MOs as (a) a function of the λ_2–eigenvector and (b) integrated along the λ_2–eigenvector. χ_{Rem}^{MO} collects the contributions from all remaining MOs. Density contributions of all MOs grouped by their symmetry characters as (c) a function of the λ_2–eigenvector and (d) integrated along the λ_2–eigenvector

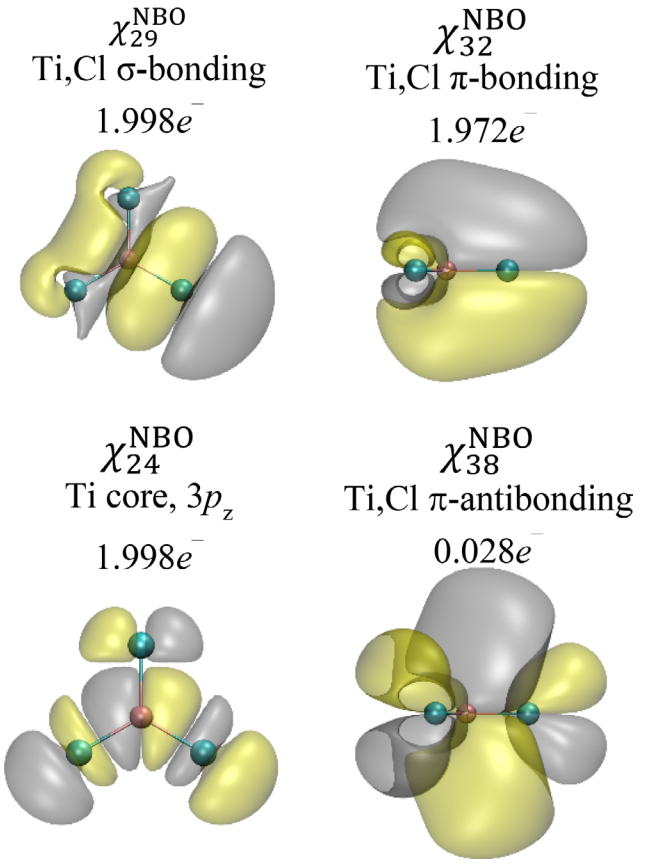

FIGURE 3 Isosurfaces of NBOs that contribute significantly to the ED of a Ti—Cl bond in $TiCl_3^+$, together with their occupations and NBO-defined classifications. All isovalues are at 0.001 au

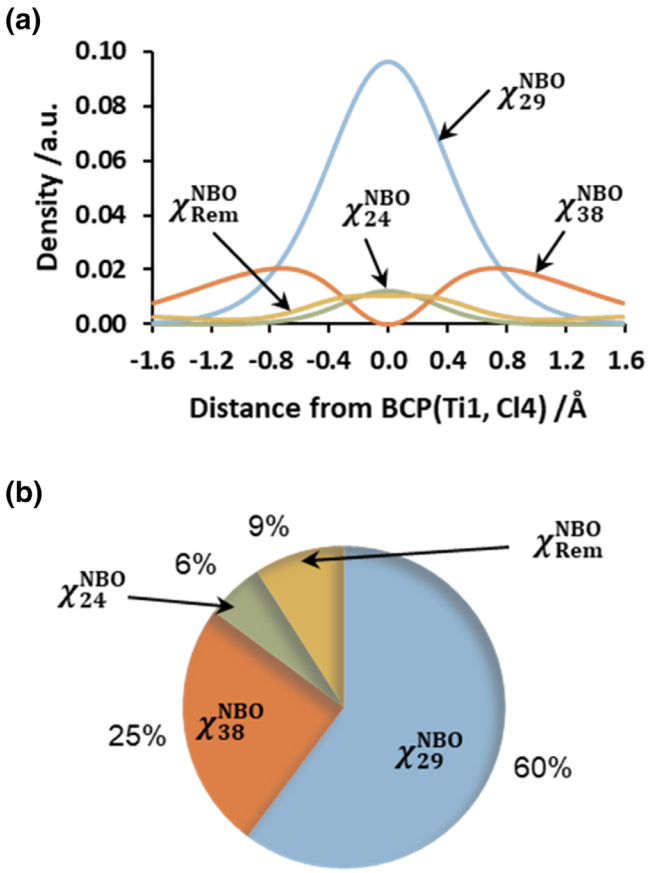

FIGURE 4 Density contributions of selected NBOs as (a) a function of the λ_2–eigenvector and (b) integrated along the λ_2–eigenvector originating at a Ti,Cl (3,−1) CP in $TiCl_3^+$. χ_{Rem}^{NBO} collects the contributions from all remaining NBOs

both NBOs are triply degenerate—one set for each Ti—Cl bond. Barring any energy and more in-depth NBO analysis, we traced the NBO contributions to the density along the same λ_2–eigenvector as we used in the MO decompositions above, Figure 4. The cross section analysis identifies the same two bonding NBOs as the major contributors to the density at the Ti,Cl CP as well as integrated along the λ_2–eigenvector (as expected), but also shows the relatively larger contribution by the σ-NBO—in agreement with our MO results. Interestingly, our analysis also identifies a formal Ti-core NBO (χ_{24}^{NBO}, Figure 3) as a small but significant contributor to the density, as well as a number of smaller contributions from various other NBOs (such as a non-Lewis NBO, χ_{38}^{NBO}, with π*-symmetry). This result is not surprising, since in order to achieve NBOs corresponding as closely to an idealized Lewis structure, orthogonal NBOs must necessarily be somewhat delocalized. This observation does, however, suggests a significant degree of non-Lewis interactions describing the Ti—Cl interaction.

We now turn to a similar analysis using FALDI. Since FALDI has never before been used to study metal complexes such as the ones investigated in this work, a brief overview of the FALDI description of bonding patterns in this complex are given below.

Selected atom-pair contributions to the molecular density are shown in Figure 5.The total number of electrons delocalized between Ti and a Cl atom, as defined by FALDI with the LDO algorithm, is δ_{LDO}(Ti,Cl) = 4.88 e^-. This suggests that almost two-and-a-half electron pairs are shared along the Ti—Cl interaction, in accordance with the slightly greater than double-bonded character predicted by the qualitative LCAO model. Interestingly, the QTAIM-defined DI for the same atom-pair is δ_{QTAIM}(Ti,Cl) = 1.23 e^--pairs, suggesting a bond order slightly above one. We note, however, that δ_{LDO} provides the maximum allowed delocalization, including contributions form dative-covalent modes and lone-pair delocalization. FALDI also allows for decomposition into orthogonal natural density functions (NDFs, Figure 6), which show three major bonding modes: a σ-NDF (contributing 1.43 e^-) and two perpendicular π-contributions (contributing 1.42 and 1.04 e^-).

FALDI can also provide and visualize delocalization indices for any atom-pair, whether regarded as bonded or not. In $TiCl_3^+$, each Cl···Cl pair shares 2.57 e^- as visualized in Figure 5. This non-classical result—which indicates that each Cl,Cl atom-pair shares at least an electron pair—cannot be predicted by either the SALC model nor the Lewis-centric NBOs. Interestingly, inspection of the corresponding

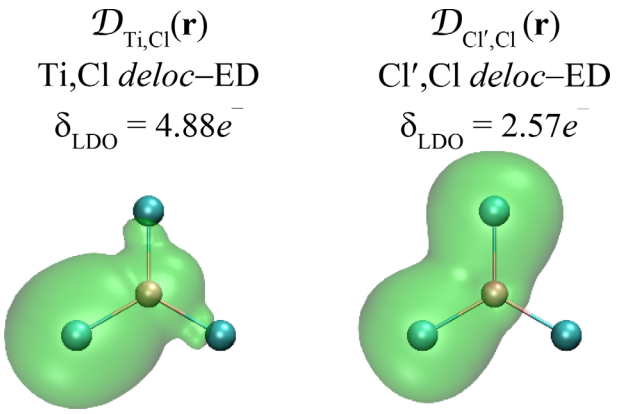

FIGURE 5 Isosurfaces of the dominant FALDI components that contribute to the ED of a Ti—Cl bond in $TiCl_3^+$. The FALDI-defined delocalization indices of each component are also shown. All isosurfaces are displayed at an isovalue of 0.001 au

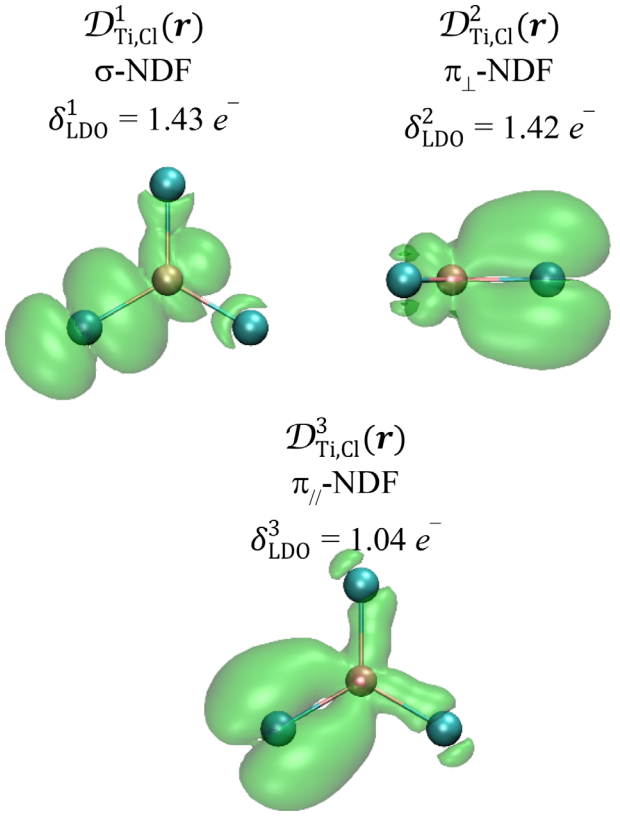

FIGURE 6 Isosurfaces of the highest occupied NDFs describing the electron delocalization among Ti and a Cl atom in $TiCl_3^+$. FALDI-defined occupation for each NDF is also shown. All isovalues are presented at 0.001 au

FALDI isosurface (Figure 5) shows that the non-covalent Cl···Cl electron sharing occurs *through bond* (through the existing Ti—Cl interaction) rather than *through space*, suggesting that the density describing the Ti—Cl bond is more multi-centric than would be expected from the MO or NBO descriptions.

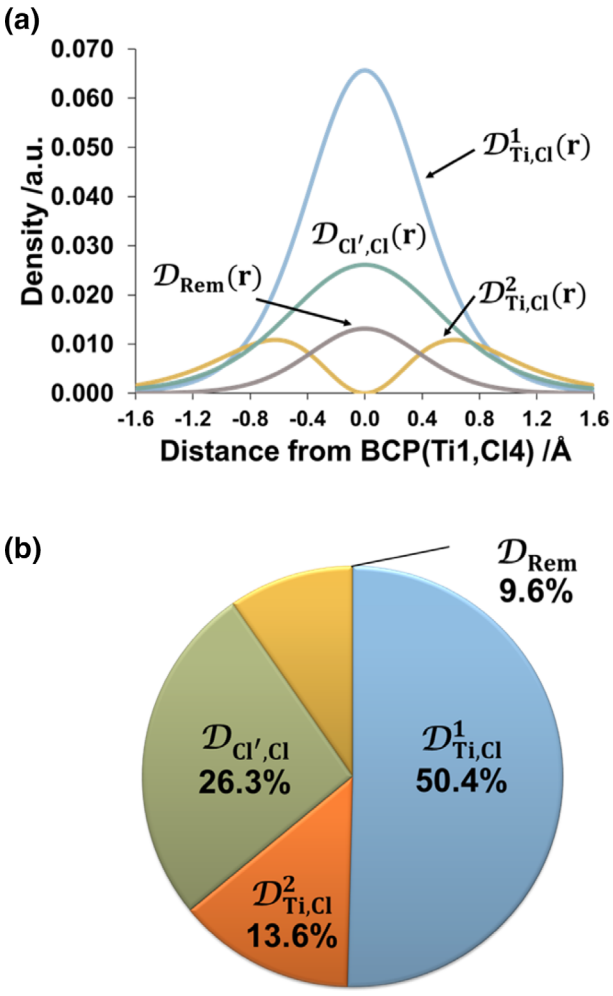

FIGURE 7 Density contributions of selected FALDI *deloc*–EDs and *deloc*–NDFs as (a) a function of the λ_2–eigenvector and (b) integrated along the λ_2–eigenvector originating at a Ti,Cl (3,–1) CP in $TiCl_3^+$. $D_{Cl',Cl}$ contains the *deloc*–ED of 2 Cl atoms with the third Cl atom, and D_{Rem} captures the remainder of the density contributions

Decomposing the density in FALDI components along the λ_2–eigenvector (Figure 7, as well as Figures S6 and S7) reveals the same trend as observed for both MO and NBO approaches: a majority σ-component ($D^1_{Ti,Cl}$, 50.4%) and minority π-component ($D^2_{Ti,Cl}$, 13.6%) accounts for density integrated along the λ_2–eigenvector. Therefore, all three decompositions along the λ_2–eigenvector were able to recover the predictions made by the qualitative, SALC model. Unlike the MO and NBO decompositions, however, FALDI clearly shows the contributions made by the various Cl···Cl interactions (accounting for a total 26% of the ED integrated along the λ_2–eigenvector)—an observation that the SALC model cannot easily predict. Interestingly, the Cl···Cl interactions result in a single-belled concentration of ED at the Ti,Cl CP, indicating that it predominantly delocalizes electrons in a σ rather than π fashion.

Summarizing the information from all three approaches above, a Ti—Cl bond in $TiCl_3^+$ can be described as: (i) a bonding interaction with a bond order slightly greater than 2, (ii) composed of a majority

σ-bonding mode, a strong $\pi_{\perp}$-bonding mode and a minor $\pi_{//}$–bonding mode, (iii) with significant involvement of lower energy and core AOs, including $3s_{Cl}$ and $3p_{Ti,z}$ AOs, and (iv) displaying a significant multicenter character arising from Cl···Cl electron sharing along the Ti—Cl bond. We now turn to an asymmetric, organometallic complex for which the classical SALC approach does not apply.

4.2 | Analysis of bonding in an asymmetric Schrock Carbene

The same set of cross-section analyses that were used above can be applied to a titanium carbene complex, $TiCl_2CHCH_3$. This carbene complex has a C_1 point group symmetry and it thus becomes difficult to gain useful insight to the bonding when using SALC analysis. Due to the lack of insight from group theory, chemists have used visual inspection to gain insight into the bonding interactions associated with molecular orbitals. While the nature of many MOs in an asymmetric system can be inferred through comparison to a similar symmetric system (in this case, $TiCl_3^+$), such an approach is notoriously unscientific and can lead to highly inaccurate interpretations. For instance, χ_{34}^{MO} (Figure S8) in the $TiCl_2CHCH_3$ system has a very similar appearance to the HOMO of $TiCl_3^+$ system (Figure 1), which might lead one to believe it would have the same non-bonding nature. The accuracy of such an interpretation is, however, very difficult to evaluate without extremely in-depth population analyses. Each individual MO's isosurface (Figure S8) can similarly be scrutinized, but ultimately the lack of insight from group theory makes such an endeavor mostly a guessing game. Subsequently, an MO diagram with the same level as insight as for $TiCl_3^+$ (Figure 1) cannot be generated and the various bonding modes in the complex remain unclear.

To alleviate such questions in a straightforward manner and without resorting to a fragmentation of the molecule, we now apply our same MO decomposition to the Ti—C bond in $TiCl_2CHCH_3$, Figure 8. The character of each MO, based on their second derivatives at the Ti,C CP, can easily be read from the cross-section along the λ_2–eigenvector. For instance, χ_{35}^{MO} and χ_{36}^{MO} have bell- and double-belled curves, respectively and can, therefore, be said to be of σ- and π-characters, respectively. These MOs also contribute most to the ED integrated along the λ_2–eigenvector. The majority of the remaining MOs that contribute to the ED do so in a σ-fashion, which leads to an overall σ-character of the Ti—C bond. Grouping all MOs with the same topology results in an overall contribution to the ED associated with the Ti—C interaction of 71.74% σ and 27.14% $\pi_{\perp}$ along the λ_2–eigenvector, and 93.42% σ and 6.58% $\pi_{//}$ along the λ_1–eigenvector. Notably, χ_{34}^{MO} —the MO that resembles the non-bonding HOMO of $TiCl_3^+$ – contributes in a small yet significant σ-fashion (accounting for

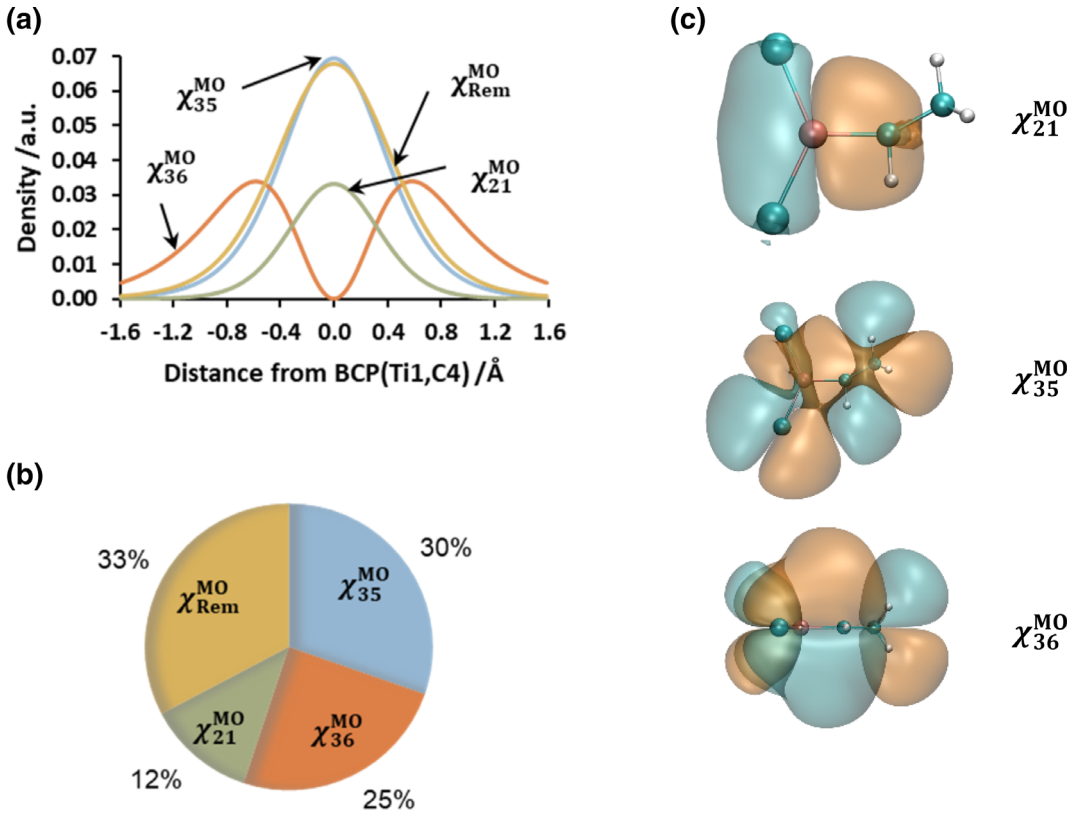

FIGURE 8 Density contributions of selected MOs as (a) a function of the λ_2–eigenvector and (b) integrated along the λ_2–eigenvector originating at a Ti,C (3,−1) CP in $TiCl_2CHCH_3$. (c) Selected MO isosurfaces, rendered at an isovalue of 0.01 a.u

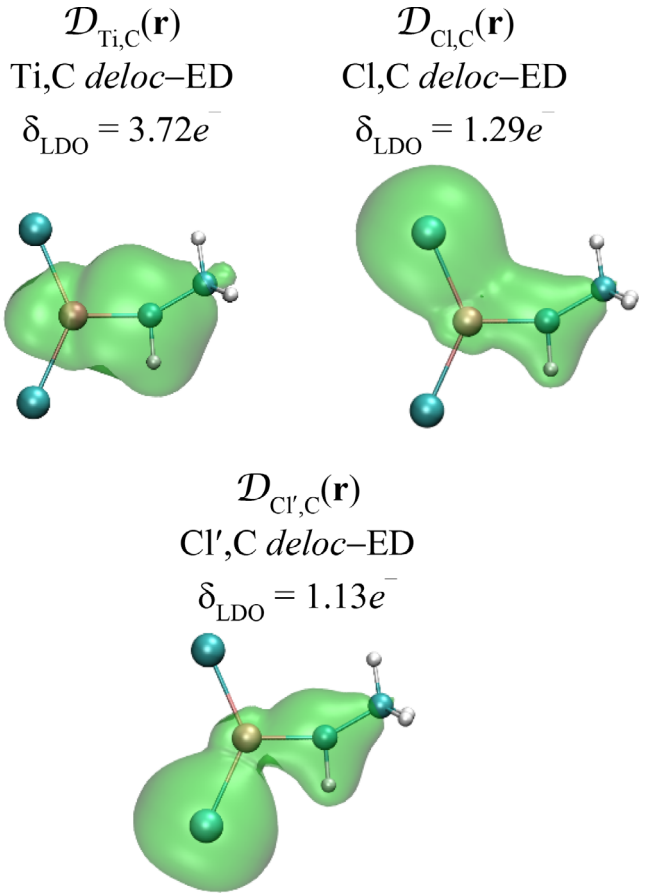

FIGURE 9 Isosurfaces of the dominant FALDI components that contribute to the ED of a Ti—C bond in $TiCl_2CHCH_3$. The FALDI-defined delocalization indices of each component are also shown. All isosurfaces are displayed at an isovalue of 0.001 au

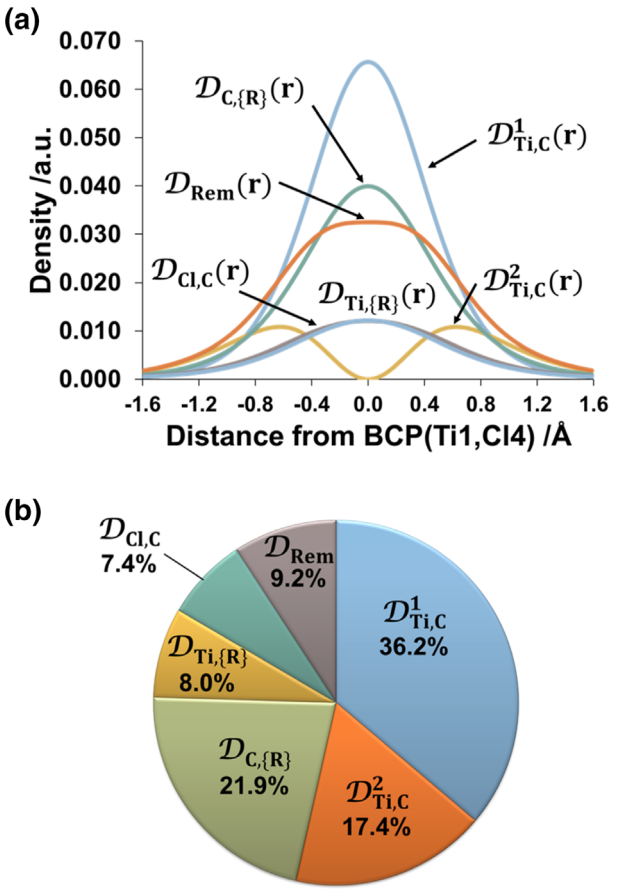

FIGURE 10 Density contributions of selected FALDI *deloc*–EDs and *deloc*–NDFs as (a) a function of the λ_2–eigenvector and (b) integrated along the λ_2–eigenvector originating at the Ti,C (3,–1) CP in $TiCl_2CHCH_3$. {*R*} refers to the combined R-groups attached to the carbene carbon, Cl to the combined Cl ligands and D_{Rem} captures the remainder of the density contributions

4.73% and 3.22% of the integrated ED along the λ_1– and λ_2–eigenvectors, respectively—Table S8). This result confirms that classification of χ^{MO}_{34} based on the HOMO of $TiCl_3^+$ as non-bonding is incorrect and shows that visual inspection of MOs in asymmetric carbene complexes can be very misleading. As for the Ti—C bond in $TiCl_3^+$, the lower energy MOs also contributes significantly (28.12%) to the total ED integrated along the λ_2–eigenvector of the Ti—C bond in $TiCl_2CHCH_3$. Importantly, our approach works just as well in asymmetric carbene complexes as in symmetric coordination complexes, and can recover the correct nature of each MO relative to a specific chemical interaction.

NBO-analysis for the Ti—C interaction reveals an σ- and π-NBO (Figure S10), and again with double occupations for both bonding modes. Cross-section analysis (Figure S11) confirms that these two NBOs are the greatest contributors; however, the σ-NBO makes a contribution to the total ED integrated along the λ_2–eigenvector more than double (60.65%) than that of the π-NBO (27.03%), in contrast to the NBO's occupations. Inspection of the isosurfaces of the σ-NBO also shows that it is quite delocalized across the entire carbene ligand as well as the Cl atoms. Again, as for the Ti—Cl interaction in $TiCl_3^+$, the remainder of the ED is made up of various core Ti electrons and non-Lewis NBOs.

FALDI analysis (Figure 9) reveals a total of 3.72 e^- shared among the Ti,C atom-pair—a value slightly less than the pure double bond estimated by classical models.[10–15] A π and a σ-NDF (Figure S14) describe the bonding modes with occupations of 1.31 and 1.28 e^-, respectively. As for $TiCl_3^+$, non-covalent interactions can also be quantified, and the Cl atoms each share an average of 1.21 electrons with the carbene carbon in a through-bond fashion (Figure 9)—similar to the Cl···Cl interactions in $TiCl_3^+$. For the current system, it also makes sense to analyze the delocalization between various fragments of the molecule; inter-fragment delocalization isosurfaces are shown in Figure S13. The Ti atom and entire carbene fragment (—$CHCH_3$) share 5.38 e^-, indicating that a large component of the overall metal–ligand bond is a result of the metal's interaction with the R groups (—CH_3 and —H) attached to the carbene carbon. Furthermore, each Cl atom shares 2.67 e^- with the carbene fragment. These results show the great degree of multi-centric and long-range effects that are

present in the interaction of the metal cluster with the carbene ligand. Notably, our FALDI results are in-line with the degree of multicenter bonding in carbene complexes that was recovered from expensive, multi-configurational calculations,[23,24] despite using a single-determinant wavefunction.

Analysis of the cross-section along the λ_2–eigenvector (Figure 10) the σ- and π-NDFs of the Ti—C bond makes up 36.2 and 17.4%, respectively, of the total ED integrated along the λ_2–eigenvector. The remaining 43.4% is composed of long-range, multicenter contributions that concentrates density in a σ-fashion, including Cl···C interactions (7.4%), Ti delocalization with the R-groups on the carbene carbon (8.0%) and a contribution from the C—CH_3 and C—H bonds of the ligand (21.9%). The latter contribution from C—R bonds, in particular, highlight the extent to which σ-delocalization stabilizes the Ti—Carbene bond.

Taking the above results from all three decompositions into account, we arrive to a very similar description of the Ti—C bond in $TiCl_2CHCH_3$ as for the Ti—Cl bond in $TiCl_3^+$: (i) a bonding interaction with a diatomic bond order slightly less than 2, (ii) composed of a majority σ- and minority $\pi_\perp$-bonding modes and a very small $\pi_{//}$–bonding mode, (iii) significant involvement of lower energy MOs and (iv) a large degree of multi-centric character due predominantly to C—R σ-delocalization, Ti···R interactions and Cl···carbene interactions. In comparison to the Ti—Cl bond in $TiCl_3^+$, however, we note that the density associated with the Ti—C bond contains a relatively larger σ-character (as established by all three decompositions). However, FALDI alone reveals that the Ti—C bond seems to be considerably more multi-centric than the Ti—Cl bond. As a result, a total of 10.72 e^- is delocalized between the metal cluster ($TiCl_2$) and the entire carbene ligand (—$CHCH_3$), and is much larger than the total of 7.45 e^- delocalized between $TiCl_2$ and the third Cl atom in $TiCl_3^+$.

5 | CONCLUSIONS

Group theory (in terms of the SALC approach) provides an extremely powerful conceptual tool to fully characterize and interpret MOs in symmetric coordination compounds; however, the same approach is generally unavailable in asymmetric metal complexes such as metal-carbene compounds. We have shown that inspection of MO isosurfaces in metal-carbene complexes can lead to mis-characterization of the MO natures, even in small and supposedly straight-forward Schrock carbenes.

We have shown that the use of cross-sections of MO densities along the λ_2–eigenvector of a metal–ligand bond (i) can accurately characterize and relatively quantify each MO's contribution, (ii) recovers contributions from non-frontier orbitals, (iii) is conceptually simple, (iv) carries very little computational cost and (v) can be used for symmetric and asymmetric complexes alike. In the symmetric coordination complex $TiCl_3^+$, our approach yields the exact same interpretations as that from group theory. We have also corroborated our results using different density decompositions (notably NBO and FALDI schemes) along the same λ_2–eigenvector and arrived to the same conclusions as with the MO decomposition. The same approach was also used for the asymmetric Schrock carbene complex, $TiCl_2CHCH_3$, where group theory cannot be effectively applied. Again, however, our MO decomposition characterized each MO in terms of various bonding modes, and corresponds accurately with NBO and FALDI decompositions. Therefore, the method described in this work represents a straightforward approach to classify as well as relatively quantify MOs' density contributions to specific bonds in asymmetric and larger organometallic complexes. In addition, the use of cross-sections can also provide additional insight toward the interpretation of other orbital isosurfaces and post-SCF analyses, such as NBOs or FALDI.

That said, FALDI analysis alone revealed the large influence of multi-centric character (such as long range ligand···ligand interactions) on the density of a M—ligand bond, as previously only revealed by expensive, multi-configurational calculations.[23,24] In particular, FALDI identified the strong influence of extensive σ-delocalization in the $TiCl_2CHCH_3$ Schrock carbene. In this regard, FALDI seems a promising candidate as a post-SCF tool to analyze organometallic bonds in a chemically intuitive and computationally inexpensive manner.

Finally, our decompositions along λ_2–eigenvectors can be easily automated and is well-suited for high-throughput screening and comparative analysis. We suggest our approach as an inexpensive but insightful addition to a computational chemist's toolbox for the characterization of bonding properties in metal complexes.

ACKNOWLEDGMENT

The authors gratefully acknowledge the Centre for High Performance Computing (CHPC), South Africa, for providing computational resources to this research project, the National Research Foundation of South Africa, Grant Number 105855, the University of Pretoria and the Council for Scientific and Industrial Research (DSI—CSIR Interbusary Support) for financial support.

ORCID

Shane de Beer https://orcid.org/0000-0002-8809-5029
Ignacy Cukrowski https://orcid.org/0000-0001-8007-5675
Jurgens H. de Lange https://orcid.org/0000-0003-2614-0151

REFERENCES

[1] E. O. Fischer, A. Maasböl, *Am. Ethnol.* **1964**, *76*, 645.
[2] E. O. Fischer, A. Maasböl, *Angew. Chem. Int. Ed. Engl.* **1964**, *3*, 580.
[3] R. R. Schrock, *J. Am. Chem. Soc.* **1974**, *96*, 6796.
[4] K. Öfele, *J. Organomet. Chem.* **1968**, *12*, 42.
[5] K. Öfele, E. Roos, M. Herberhold, *J. Nat. Res. B* **1976**, *31*, 1070.
[6] H.-W. Wanzlick, H.-J. Schönherr, *Am. Ethnol.* **1968**, *80*, 154.
[7] H.-W. Wanzlick, H.–. J. Schönherr, *Angew. Chem. Int. Ed. Engl.* **1968**, *7*, 141.
[8] W. A. Herrmann, C. Köcher, *Am. Ethnol.* **1997**, *109*, 2256.
[9] W. A. Herrmann, C. Köcher, *Angew. Chem. Int. Ed. Engl.* **1997**, *36*, 2162.
[10] T. E. Taylor, M. B. Hall, *J. Am. Chem. Soc.* **1984**, *106*, 1576.
[11] A. K. Rappé, W. A. Goddard, *J. Am. Chem. Soc.* **1977**, *99*, 3966.
[12] A. K. Rappé, W. A. Goddard, *J. Am. Chem. Soc.* **1982**, *104*, 448.
[13] E. A. Carter, W. A. Goddard, *J. Phys. Chem.* **1984**, *88*, 1485.
[14] E. A. Carter, W. A. Goddard, *J. Phys. Chem.* **1986**, *108*, 2180.

[15] E. A. Carter, W. A. Goddard, *J. Phys. Chem.* **1986**, *108*, 4746.
[16] M. J. S. Dewar, *Bull. Soc. Chem. Fr.* **1951**, *18*, C71.
[17] J. Chatt, L. A. Duncanson, *J. Chem. Soc. (Resumed)* **1953**, 2939.
[18] K. Kitaura, K. Morokuma, *Int. J. Quantum Chem.* **1976**, *10*, 325.
[19] M. von Hopffgarten, G. Frenking, *WIREs Comput. Mol. Sci.* **2012**, *2*, 43.
[20] M. P. Mitoraj, A. Michalak, T. Ziegler, *J. Comput. Chem. Theory* **2009**, *5*, 962.
[21] Y. Jean, *Molecular Orbitals of Transition Metal Complexes*, Oxford University Press, Oxford **2005**.
[22] T. A. Albright, J. K. Burdett, M. Whangbo, *Orbital interactions in Chemistry*, 2nd ed., John Wiley & Sons, Hoboken **2013**.
[23] T. R. Cundari, M. S. Gordon, *J. Am. Chem. Soc.* **1991**, *113*, 5231.
[24] T. R. Cundari, M. S. Gordon, *J. Am. Chem. Soc.* **1992**, *114*, 539.
[25] E. D. Glendening, R. L. Clark, F. Weinhold, *WIREs Comput. Mol. Sci.* **2012**, *2*, 1.
[26] C. C. Wang, Y. Wang, H. J. Liu, K. J. Lin, L. K. Chou, K. S. Chan, *J. Phys. Chem. A* **1997**, *101*, 8887.
[27] R. Fraser, P. H. van Rooyen, J. de Lange, I. Cukrowski, M. Landman, *J. Organomet. Chem.* **2017**, *840*, 11.
[28] G. Frenking, in *The Chemical Bond: Fundamental Aspects of Chemical Bonding* (Eds: G. Frenking, S. Shaik), Wiley-VCH, Weinheim **2014**, p. 175.
[29] K. Boguslawski, M. Reiher, in *The Chemical Bond: Fundamental Aspects of Chemical Bonding* (Eds: G. Frenking, S. Shaik), Wiley-VCH, Weinheim **2014**, p. 219.
[30] I. Cukrowski, J. H. de Lange, A. S. Adeyinka, P. Mangondo, *Comput. Theor. Chem.* **2015**, *1053*, 60.
[31] J. H. de Lange, D. M. E. van Niekerk, I. Cukrowski, *Phys. Chem. Chem. Phys.* **2019**, *21*, 20988.
[32] J. H. de Lange, D. M. E. van Niekerk, I. Cukrowski, *J. Comput. Chem.* **2018**, *39*, 973.
[33] J. H. de Lange, I. Cukrowski, *J. Comput. Chem.* **2018**, *39*, 1517.
[34] J. H. de Lange, I. Cukrowski, *J. Comput. Chem.* **2017**, *38*, 981.
[35] R. F. Bader, *Atoms in Molecules*, Clarendon Press, Oxford **1990**.
[36] J. H. de Lange, D. M. E. van Niekerk, I. Cukrowski, *J. Comput. Chem.* **2018**, *39*, 2283.
[37] R. Ponec, *J. Math. Chem.* **1997**, *21*, 323.
[38] R. Ponec, *J. Math. Chem.* **1998**, *23*, 85.
[39] R. F. Bader, M. E. Stephens, *J. Am. Chem. Soc.* **1975**, *97*, 7391.
[40] M. J. Frisch, G. W. Trucks, H. B. Schlegel, G. E. Scuseria, M. A. Robb, J. R. Cheeseman, G. Scalmani, V. Barone, B. Mennucci, G. A. Petersson, H. Nakatsuji, M. Caricato, X. Li, H. P. Hratchian, A. F. Izmaylov, J. Bloino, G. Zheng, J. L. Sonnenberg, M. Hada, M. Ehara, K. Toyota, R. Fukuda, J. Hasegawa, M. Ishida, T. Nakajima, Y. Honda, O. Kitao, H. Nakai, T. Vreven, J. A. Montgomery Jr., J. E. Peralta, F. Ogliaro, M. Bearpark, J. J. Heyd, E. Brothers, K. N. Kudin, V. N. Staroverov, T. Keith, R. Kobayashi, J. Normand, K. Raghavachari, A. Rendell, J. C. Burant, S. S. Iyengar, J. Tomasi, M. Cossi, N. Rega, J. M. Millam, M. Klene, J. E. Knox, J. B. Cross, V. Bakken, C. Adamo, J. Jaramillo, R. Gomperts, R. E. Stratmann, O. Yazyev, A. J. Austin, R. Cammi, C. Pomelli, J. W. Ochterski, R. L. Martin, K. Morokuma, V. G. Zakrzewski, G. A. Voth, P. Salvador, J. J. Dannenberg, S. Dapprich, A. D. Daniels, O. Farkas, J. B. Foresman, J. V. Ortiz, J. Cioslowski, D. J. Fox, *Gaussian 09*, *Revision D*, Vol. 01, Gaussian, Inc., Wallingford CT **2013**.
[41] T. A. Keith, *AIMAll (Version 17.11.14)*, TK Gristmill Software, Overland Park KS, USA **2016**. aim.tkgristmill.com.
[42] A. E. Reed, L. A. Curtiss, F. Weinhold, *Chem. Rev.* **1988**, *88*, 899.
[43] W. Humphrey, A. Dalke, K. Schulten, *J. Mol. Graphics* **1996**, *14*, 33.

SUPPORTING INFORMATION

Additional supporting information may be found online in the Supporting Information section at the end of this article.

How to cite this article: de Beer S, Cukrowski I, de Lange JH. Characterization of bonding modes in metal complexes through electron density cross-sections. *J Comput Chem*. 2020;41:2695–2706. https://doi.org/10.1002/jcc.26423

Chapter Four

Integrated Cross Section Analysis on Electron Density

Introduction

The publication in the previous chapter[1] illustrated a method for the classification and quantification of molecular orbital (MO) contributions to a particular metal-ligand interaction, with similar analyses being performed on natural bond orbital (NBO) and fragment, atomic, localised, delocalised and interatomic (FALDI) data. The approach integrated the density contributions to a cross-section based on the λ-eigenvectors of the Hessian matrix. This showed insights into the multicentric nature of the metal-carbon carbene bond that were otherwise only possible through multiconfigurational computations. However, this only considered a single carbene complex. The present chapter serves as an extension to this publication in order to apply the method to four related systems and study trends observed when changing the carbene ligand structure or changing the ancillary ligands.

Literature on carbene bonding provides examples of non-heteroatom stabilised carbene complexes.[2] It shows that current models of bonding in transition metal carbene are incomplete and do not provide sufficiently detailed descriptions of the reactivities observed for these complexes. Theoretical results are highly dependent on being proven applicable by experimental work which might not be feasible in all cases. Experimental work has shown how the structure of carbene complexes can greatly influence their reactivity and stability.[3] Ideally it is desirable to develop a model which can sufficiently describe the bonding in these complexes such that confirmation from experimental results is only rudimentary.

It has been proposed that organometallic carbene bonding can be explained by either the covalent model or by the donor-acceptor model.[4] Fischer carbene bonding is described by the donor-acceptor model whereas Schrock carbene bonding is described by the covalent model.[5] These models give the general trends observed for these complexes, but do not give quantitative insights unless they are accompanied by quantum chemical calculations. The dominant factor determining transition metal carbene stability is the occupation of the carbon p-orbital forming the π-symmetric interaction of the carbene bond.[6] To date these descriptions are still being used[7] with little adaptations even though the models are strained under these restrictions.[8,9] There is still great reliance on experimental data to confirm theoretical results on the electronic structures.

Based on observations from the previous chapter the results presented here should indicate that there are multiple orbitals contributing density to the M—C interatomic region and thus contributing to the bonding. It is further hoped to show that there exists a long-range ligand-

ligand interaction which has a great influence in determining the nature of the bonding interaction. This is achieved by studying cross-sections on the orbital and electron densities (EDs) in the interatomic region and integration of EDs to give relative σ- and π-symmetric contributions from these densities.

Theoretical Background

Cross-sections of the electron density (ED) have been reported in literature previously.[10] This work extends on the reported method by performing an integration over the λ-eigenvectors such that relative contributions of specific components (either orbitals or density functions) to the bonding nature can be determined along with the symmetry of these interactions.

The bond critical point (BCP) is identified by analysis of the Hessian eigenvectors, where the BCP has eigenvalues that are minima in two directions and a maximum in one. The λ-eigenvector, as used in this work, is defined as the vector which extends from this bond critical point in the direction pointed in by the λ-eigenvector of the Hessian matrix. The vector is followed along both the positive and negative directions for a set distance. To simplify the calculation, this vector it was approximated as a linear vector with a gradient determined by the Hessian vector at the BCP.

The orbital and electron densities are calculated at points uniformly distributed along the eigenvector. The decomposition of the MOs χ_i is given by the equation

$$^{MO}\rho(\mathbf{r}) = \sum_{i}^{N_{MO}} n_i |\chi_i(\mathbf{r})|^2 \qquad (1)$$

The NBO decomposition is given by a similar equation using the NBOs ϕ_i

$$^{NBO}\rho(\mathbf{r}) = \sum_{i}^{N_{NBO}} n_i |\phi_i(\mathbf{r})|^2 \qquad (2)$$

The FALDI decomposition of the electron density is given as localised and delocalised electron density. However, since the analysis is along the interatomic surface, the localised component makes no contribution by definition. Thus, the equation is simplified to only the delocalised electron density as given in equation 3 below.

$$^{FALDI}\rho(\mathbf{r}) = \sum_{A}^{M} \mathcal{L}_A(\mathbf{r}) + \sum_{A}^{M}\sum_{B\neq A}^{M} \mathcal{D}_{A,B}(\mathbf{r}) \cong \sum_{A}^{M}\sum_{B\neq A}^{M} \mathcal{D}_{A,B}(\mathbf{r}) \quad (3)$$

The natural density function (NDF) decomposition for the delocalised electron density of each atom pair is given by

$$^{NDF}\rho(\mathbf{r}) = \sum_{j}^{N_{MO}}\sum_{i}^{N_{MO}} n_i^{AB}\left|\phi_j^{AB}(\mathbf{r})\right|^2 \quad (4)$$

In all cases the integration is performed numerically

$$\int_{-a}^{a} \rho(\mathbf{r})d\mathbf{r} \cong \sum_{i}^{\mathrm{N}} \rho(\mathbf{r}_i)\Delta\mathbf{r} \quad (5)$$

where a is the length of the vector in either the positive or negative direction, $\Delta\mathbf{r}$ is the step size used in the calculation, also given by $\Delta\mathbf{r} = (a-(-a))/N$, and N is the number of steps used in the approximation.

The integrated densities carried no physical meaning and were normalised to the total integrated total density to obtain a percentage contribution of each orbital or density component to the total bonding interaction, given by the equation

$$\%contribution = \frac{\int_{\mathbf{r}} \rho_i(\mathbf{r})d\mathbf{r}}{\int_{\mathbf{r}} \rho_{total}(\mathbf{r})d\mathbf{r}} \quad (6)$$

The symmetries of orbitals or densities can be obtained by inspection of the cross-section densities. The relative percentage contributions (eq. 6) of these to the overall interaction are obtained from the integration.

Computational Details

The structures were optimized in Gaussian 09, Rev. D.01[11] using DFT with the B3LYP functional and a basis set 6-311++G(d,p) in the gas phase. NBO single point analysis was performed using NBO 3.1[12] as part of the Gaussian 09 software suite. QTAIM atomic basins and atomic overlap matrices were calculated with AIMAll version 17.11.14.[13] FALDI data was calculated using in-house software with the LDO algorithm specified.

Cross-sections on the densities were done using in-house software, with the λ-eigenvectors always originating from a Ti,X (3,-1) CP. The λ-eigenvectors were calculated to a total length of 6.0 Bohr and evaluated at 0.01 Bohr increments. Integrations across the λ-eigenvectors were performed numerically on a uniform grid.

Results and Discussion

The structures studied in this section (Figure 1) serve as a guide to the electronic structure changes that occur when i) the substituents on the carbene are changed (R = H to CH_3), and ii) the ancillary ligands are changed (L = Cl to Cp, with Cp = C_5H_5). This illustrates changes when the complex undergoes olefination reactions as well as electronic structures in related complexes. The structures were conceptually derived from the Tebbe reagent,[14] Petasis reagent[15] and Ziegler-Natta catalyst.[16] The proposed olefination mechanism does not include the ancillary ligands therefore no significant changes in the electronic structures are expected for these structural modifications.

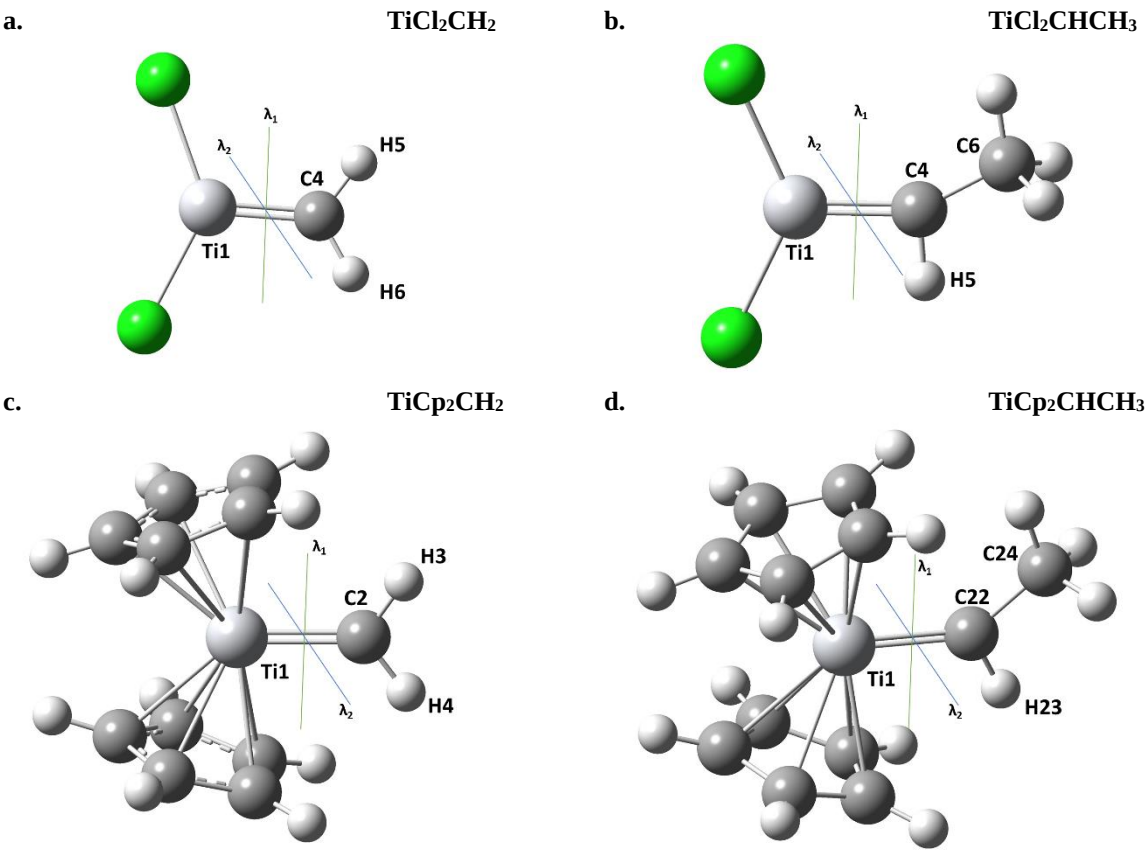

Figure 1. Structures studied in this chapter with indications of the λ-eigenvector with λ_1 always in the plane of the carbene and λ_2 always perpendicular to this plane.

MO Cross-Section Analysis

From a classical perspective it is expected that the carbene bonding is composed of σ- and π-symmetric orbitals. The π-symmetric orbital is seen as the highest occupied molecular orbital (HOMO) while the σ-symmetric orbital is often also one of the highest lying orbitals. Although, it cannot be established with certainty which orbital is the σ-symmetric orbital for the carbene bond as multiple orbitals show this symmetry (Figure B3-B6). It is suggested[1] that the two-orbital description is not sufficient to describe the carbene bond characteristics; hence, the cross-sections are employed here on various structures to gain a more inclusive description of the bonding in organotitanium carbene complexes.

Analysis of the MO cross-sections shows that more than two MOs are involved in the same M—C interaction for these structures (Figure 2 and Figure B1). Thus, the data in Figure 2 suggests that the larger carbene ligands led to more delocalisation of the electrons. The orbitals for all structures are symmetric along the λ_2-eigenvector, but this trend does not hold for the λ_1-eigenvector even when the structures are symmetric (Figure B1 a and b). The lost symmetry led to much polarisation of the orbitals along the λ_1-eigenvector. Changing to the Cp ligands does not change the number of MOs, but rather the contributions made by similar orbitals.

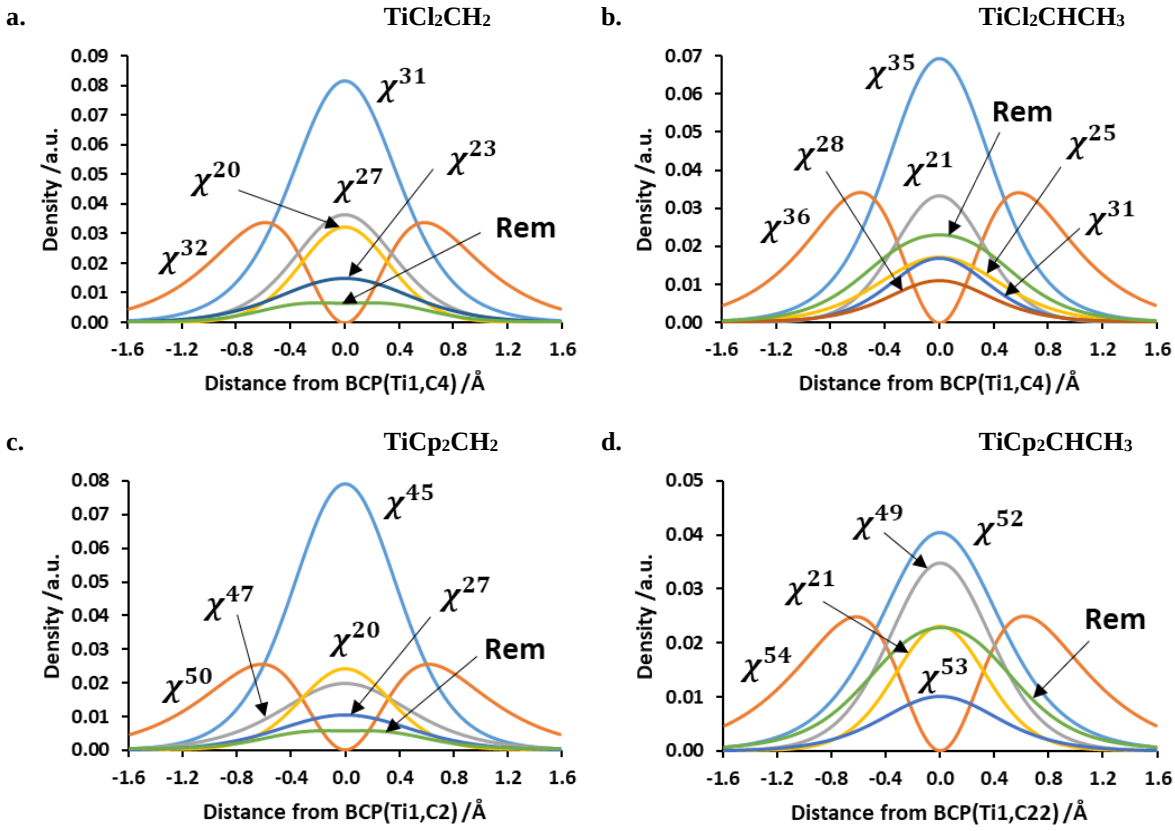

Figure 2. Cross-sections of MOs making a contribution greater than 5% of the total density along the λ_2-eigenvectors with Rem as the sum total of the MOs making less than 5% contributions.

The methodology explored in the previous chapter revealed that the topology of each MO at a critical point can be used as an indication of its bonding contribution. Specifically, MOs that concentrate density at the CP(M,C) were seen to be of σ-bonding nature (due to single bell-shaped traces obtained from cross-sections). Moreover, MOs that deplete density at the CP(M,C) but concentrate density elsewhere on the λ_2-eigenvector were seen to be of π-bonding nature (double bell-shaped traces were obtained). The same methodology is used here. The λ_2-eigenvector (Figure 2) shows multiple σ-symmetric orbitals (having only a single peak) and in all structures only a single π-symmetric interaction (having a double peak with a node at the bond critical point). This shows a large degree of inductive (*"through-bond"*) effects influencing the bonding interaction for these complexes. Notably, inclusion of CH_3 groups on the carbene ligand resulted in a number of additional σ-symmetric MOs – an observation not noted for the other structures studied here.

In going from the Cl to Cp structures it is seen that peak maxima are lower indicating a more delocalised nature in the interaction. This is especially pronounced in the $TiCp_2CHCH_3$ structure (Figure 2d) where the major σ-symmetric orbital χ^{52} is not as far removed from the other orbitals as is observed with the other structures.

The results for the integrated cross-sections (Figure 3) show that the more complex carbene ligand led to a reduced contribution for the main σ-symmetric interaction while not having an influence on the contribution of the π-interaction (suggesting the π-interaction to be diatomic). For instance, χ^{31} contributes 36% to the ED at CP(M,C) when L = CH_2, (Figure 3a) whereas the equivalent MO (χ^{35}) contributes only 30% when L = $CHCH_3$. This is especially noted in the Cp structures where the contribution of the main σ-symmetric component is almost halved going from L = CH_2 to L = $CHCH_3$. The amount of delocalisation per MO increased when the more complex carbene ligand (L = $CHCH_3$) is present with the increased delocalisation being mostly of σ-symmetry. This suggests that the inductive "*through-bond*" effects dominate when determining the nature of the carbene bond.

Changes in the other ligands present on the metal did not drastically alter the trends for the relative contributions of the MOs for non-major orbitals. The majority of the density in the bonding region between the metal and carbene carbon atoms is comprised of electrons from the carbene ligand interacting with the other parts of the structure. The nature of the carbene bond is greatly determined by the carbene ligand. Other ligands present on the metal can also have quite significant influences in the observed character of the bond, such as the degree of σ- and π-bonding. It is hypothesised that this indicates an interaction between the ligands

present on the metal through the bonds already in place.

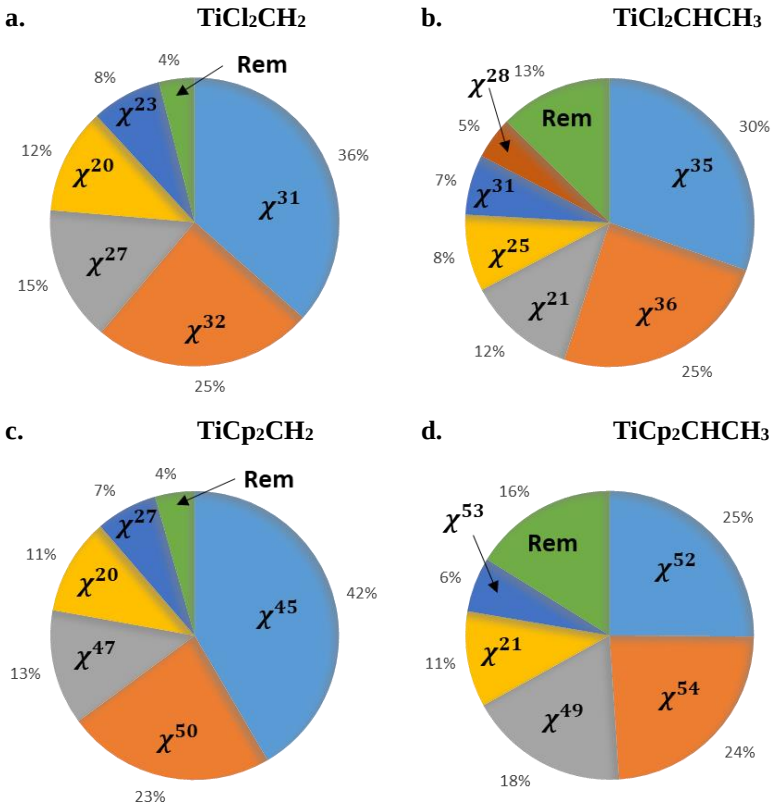

Figure 3. Relative contributions of MOs to the total density, integrated along the λ_2-eigenvector. Individual MOs with a contribution greater than 5% are shown with the other MOs collected in the Rem fraction.

NBO Cross-Section Analysis

The NBO approach imposes Lewis structures on molecules using quantum mechanical wavefunctions. This provides a localised description (natural orbitals) of the electrons in the bonding regions which mimics the classical understanding of chemical bonding. For the structures studied here (with the exception of $TiCl_2CHCH_3$) the NBO approach generates more than two NBOs to describe the interaction (Figure 4). The large number of NBOs generated for $TiCp_2CH_2$ exhibits the multicentric nature of the carbene bond in this complex, furthermore, many of these NBOs have π-symmetry which shows that this complex relies on interactions with the other ligands present on the metal through metal p- and d-orbitals. The orbital isosurfaces presented in Figure B11 show that a number of Rydberg states are involved, which is not the case for the other structures.

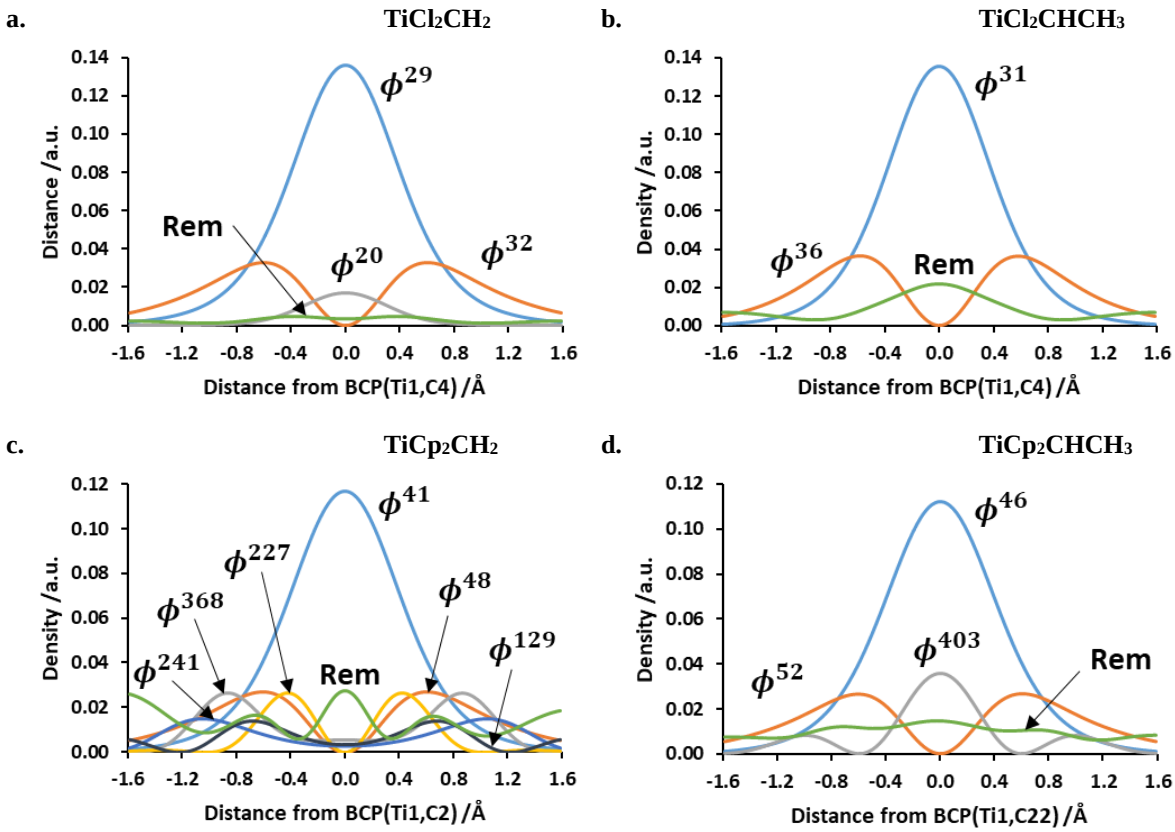

Figure 4. Cross-sections of NBOs making a contribution greater than 5% of the total density along the λ_2-eigenvectors with Rem as the sum total of the NBOs making less than 5% contributions.

Considering the number of NBOs predicted by the cross-section method to make significant contributions it stands in contrast to the *"classical"* way in which NBOs are analysed – only the bonding σ- and π-symmetric NBOs have non-negligible occupation – suggesting a large degree of multicentric character to the bonding in organometallic carbene complexes.

The asymmetric structures ($TiCl_2CHCH_3$ and $TiCp_2CHCH_3$) were better localised by the NBO algorithm, indicating the destabilisation of asymmetric carbene bonds due to the lack of degeneracy and multicentric nature which stabilised the symmetric structures. The localisation of the carbene bond to the M—C interatomic region means that breaking the bond associated with this interaction only depends on the interaction between the metal and the carbene carbon, whereas for the symmetric system the interactions between the carbene carbon and the other ligands added additional factors which had to be considered when investigating bond breaking and formation. Polarisation of orbitals could also lead to destabilisation of the asymmetric structures. It is seen in Figure B7 that the π-symmetric orbitals for asymmetric carbenes (ϕ^{27} in Figure B7b and ϕ^{340} in Figure B7d) are polarised and there is an indication of the formation of a node taking place in only one lobe of the orbital (ϕ^{340} in Figure B7d).

The integration of the NBO densities along the λ_2-eigenvectors shows that the major σ-symmetric NBO (light blue, Figure 5) makes up about twice as much density as the major π-symmetric NBO (orange, Figure 5). This again strengthens the argument proposed from the MO analysis that there is a large degree of inductive "*through-bond*" effects regulating the bonding nature of the metal-carbene carbon interaction.

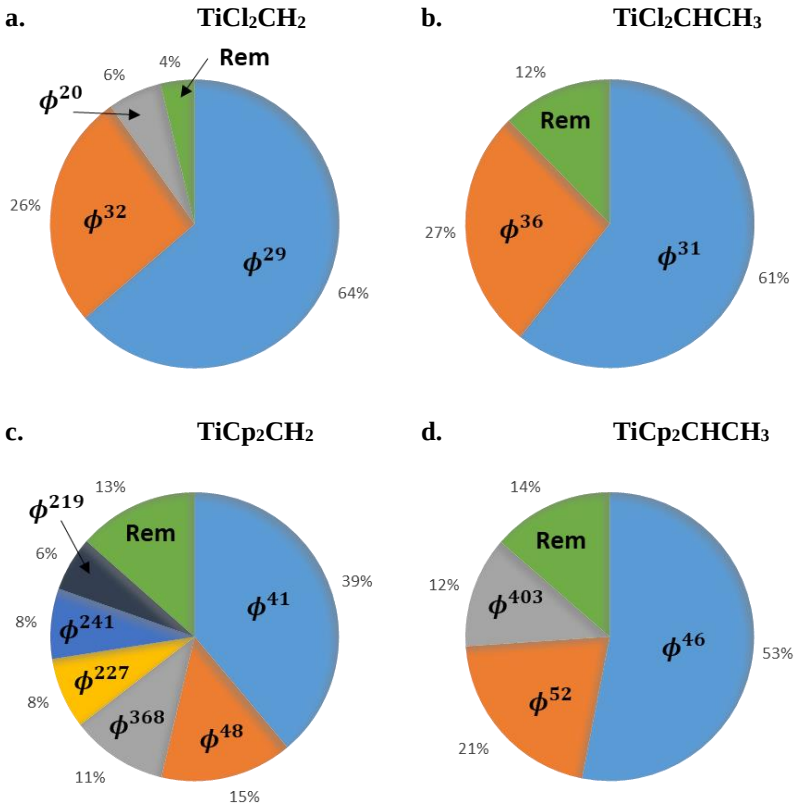

Figure 5. Relative contributions of NBOs to the total density, integrated along the λ_2-eigenvector. Individual NBOs with a contribution greater than 5% are shown with the other NBOs collected in the Rem fraction.

Comparable percentages are obtained for the remaining orbitals (green, Figure 5) of the asymmetric structures. These asymmetric structures (with L = $CHCH_3$) obtained stability from collectively more, albeit smaller, interactions.

It is noted that for the Cp structures the major σ-symmetric NBOs (ϕ^{48} Figure 5c and ϕ^{52} Figure 5d) make a smaller contribution compared to the major σ-symmetric NBOs (ϕ^{32} Figure 5a and ϕ^{36} Figure 5b) of the Cl structures. This fact suggests that the Cp structure has a more covalent character as hypothesised for Schrock carbene complexes. This puts forward that the Cl structure shows some degree of donor-acceptor type character, more typical of the nature of Fischer carbene complexes, although the carbene ligand contains no heteroatom, nor

aromaticity, and is a typical Schrock carbene ligand. This supports works in previous publications.[17]

FALDI Cross-Section Analysis

The FALDI *deloc*-ED cross-sections (Figure 6) show all interactions to be σ-symmetric dominated with the metal-carbene carbon interaction making up the majority of the bonding interaction. This does not mean that there are no π-symmetric interactions, but rather that such interactions are not dominating for the atoms of interest over the λ-eigenvectors (see Figure 8).

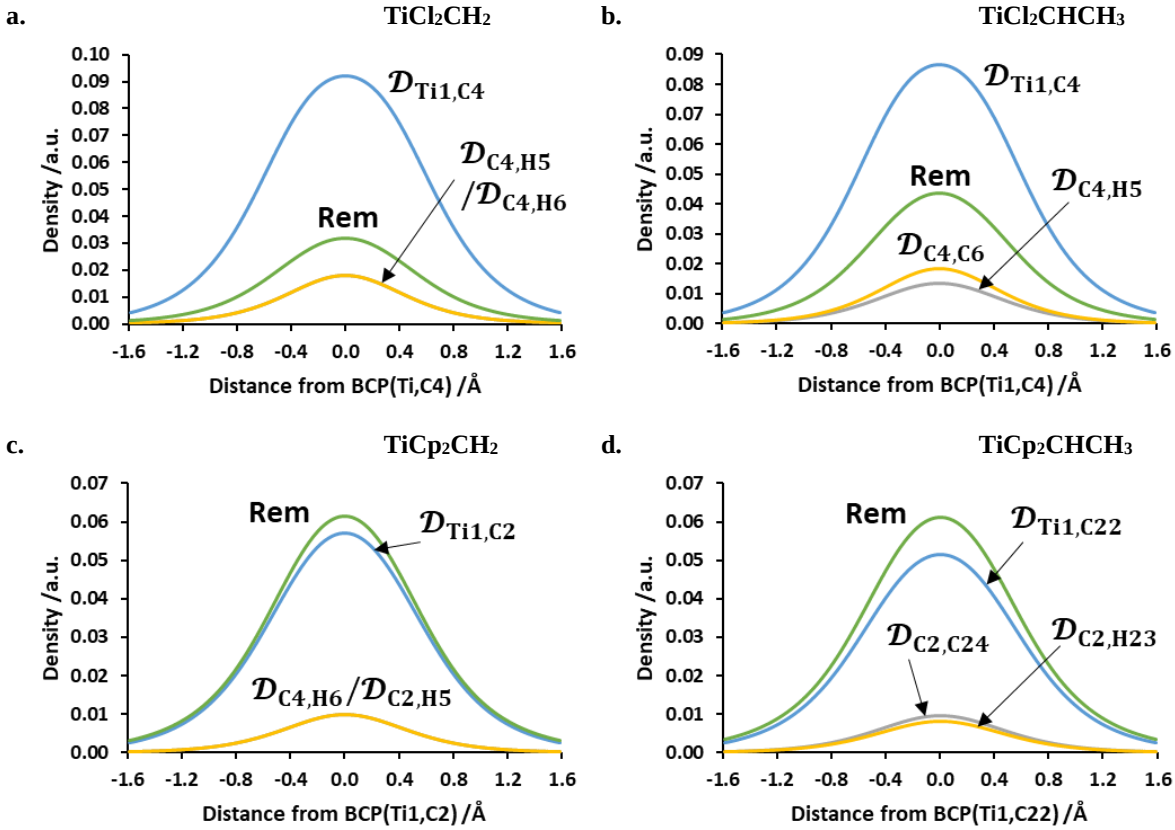

Figure 6. Cross-sections of FALDI deloc-ED making a contribution greater than 5% of the total density along the λ_2-eigenvectors with Rem as the sum total of the deloc-ED making less than 5% contributions.

An interesting observation on the FALDI *deloc*-ED is that the Cl structures show a predominantly diatomic interaction while the Cp structures show the M—C carbene interaction to be less than the remaining (Rem) fraction. This undoubtedly illustrates the multicentric nature of the carbene bond and illustrates the dependence of the bond character on the overall structure of the complex by the presence of a long-range ligand-ligand interaction.

The integration along the λ_2-eigenvector shows the large degree of diatomic nature for the Cl structures (Figure 7a and b), evidenced by the large contributions of the Ti—C atom-pair, while highlighting the multicentric nature of the Cp structures (Figure 7c and d). This adds to the argument of when which classification (Fischer or Schrock) is appropriate to use for which carbene structure (see reference[17]). The Cl structures seem to show some degree of donor-acceptor type character whereas the Cp structures appear more covalent in character, but no clear division can be made without further investigation.

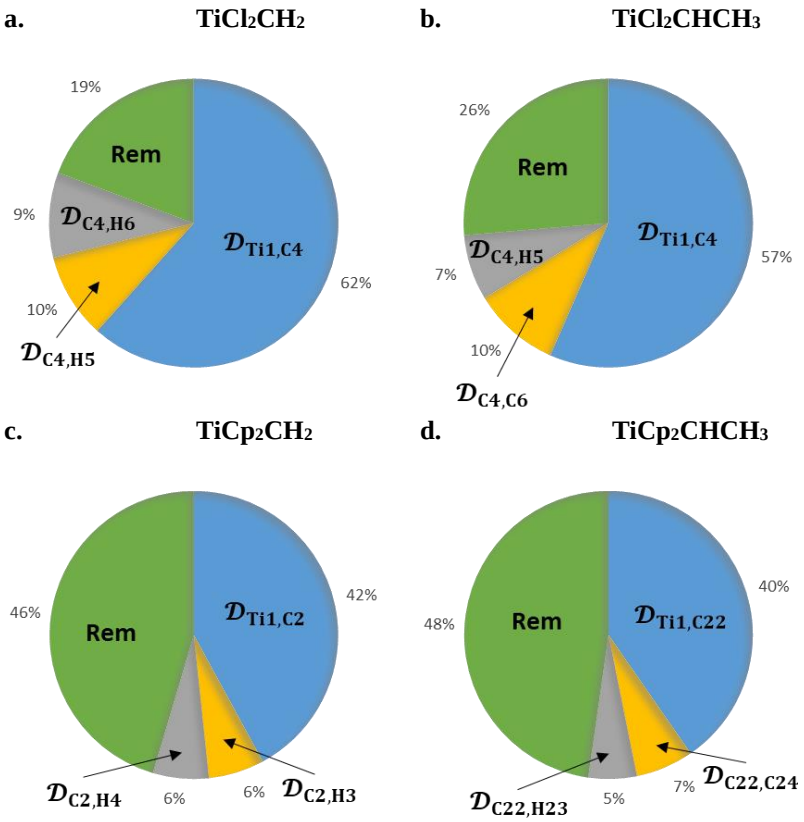

Figure 7. Relative contributions of FALDI deloc-EDs to the total density, integrated along the λ_2-eigenvector. Individual deloc-EDs with a contribution greater than 5% are shown with the other deloc-EDs collected in the Rem fraction.

These results put forward that the ligand-ligand interaction dominates in determining the nature of the interaction. The ligands present on the metal determine whether a Schrock carbene structure truly has a Schrock carbene bonding nature or if it possibly shows a Fischer carbene bonding nature. The approach which only considers the spin state of the carbene ligand to determine the bonding nature does not take ligand-ligand interactions into account. The ligand-ligand interaction becomes more relevant with larger, more complex ligands on the metal atom as is often the case with carbene complexes of interest in active research.[8,9]

NDF Cross-Section Analysis

The NDF decomposition of the *deloc*-ED on the M—C carbene interaction (Figure 8) shows a simplistic description of the bonding that correlates well with the NBO results. It is clear that the electrons used in the bonding interaction are composed of a σ-symmetric NDF and a π-symmetric NDF (Figure B21 – B24). These were near perfectly localised as seen when comparing the λ_1- and λ_2-eigenvectors which shows a single σ-symmetric interaction on both eigenvectors and a single π-symmetric interaction only along the λ_2-eigenvector.

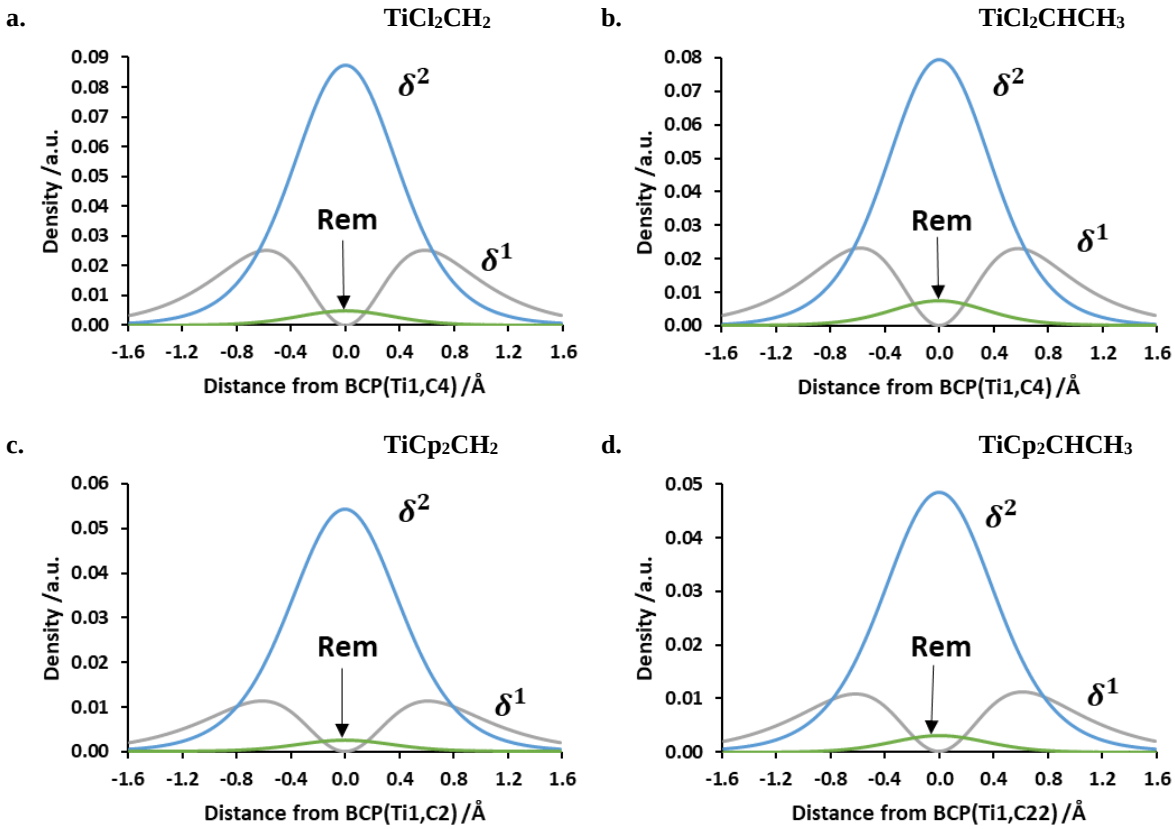

Figure 8. Cross-sections of FALDI deloc-ED NDFs for the Ti—C interaction making a contribution greater than 5% of the total density along the λ_2-eigenvectors with Rem as the sum total of the NDFs making less than 5% contributions.

This isolated interaction of the metal and carbene carbon atoms restores some faith in the classical description of carbene bonding. For this interaction the covalent model appears to hold well with the observation of the bonding. The accepted descriptions of carbene bonding hold for diatomic descriptions, but this work shows that long-range ligand-ligand interactions, which are themselves not classical interactions a chemist would be expected to consider, are important factors to consider when investigating the bonding in organometallic carbene

complexes and possibly also in other transition metal chemistry examples.

Integration of the NDF along the λ_2-eigenvectors (Figure 9) shows that changes to the carbene fragment do not greatly influence the ratio of σ- to π-symmetry for the NDFs. However, changes to the ligands from Cl to Cp increase the contribution from the σ-symmetric component. This confirms the presence of a long-range ligand-ligand interaction in a fashion acting inductively through the bonds that are already present in the system.

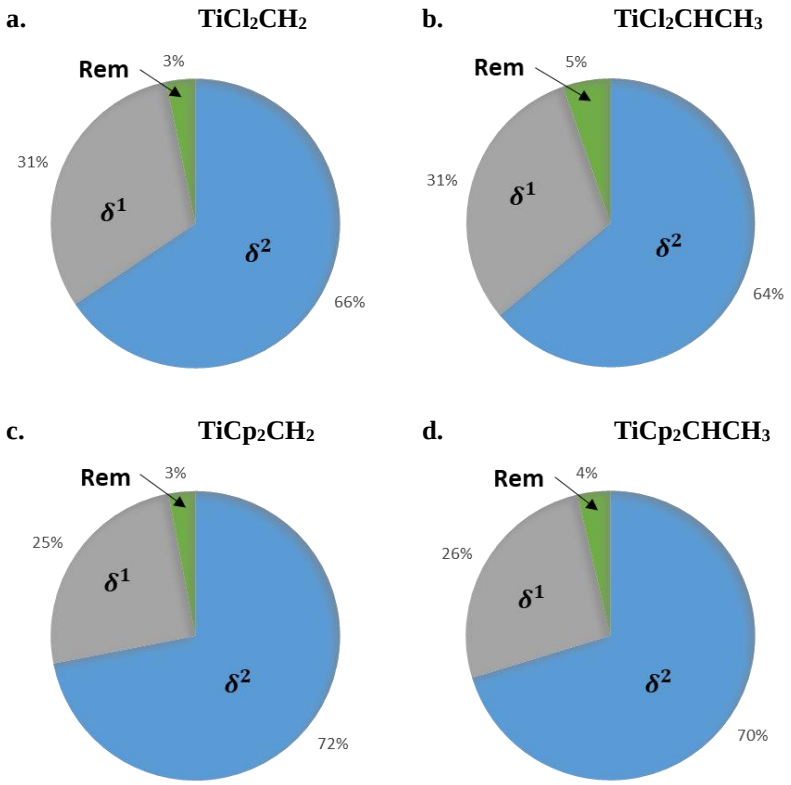

Figure 9. Relative contributions of FALDI deloc-ED NDFs for Ti—C interaction to the total density, integrated along the λ_2-eigenvector. Individual NDFs with a contribution greater than 5% are shown with the other NDFs collected in the Rem fraction.

The results clearly showed the presence of a ligand-ligand interaction which dominated in determining the nature of the carbene bond. Fischer and Schrock descriptions of organometallic carbene bonding do not seem to be sufficient to completely and accurately describe the bonding observed.

Conclusion

The MO analysis revealed that a more complex carbene ligand (R = CH_3 as opposed to R = H) led to significantly more MOs contributing electron density in the M—C internuclear region, and, consequently, increased delocalisation between the metal cluster and the carbene ligand. Similarly, the more complex ligands present on the metal (L = Cp as opposed to L = Cl) also led to more MOs involved in the metal-carbon interaction and a more molecular wide distribution of the delocalisation. The π-symmetric orbitals were observed to be diatomic and did not change significantly with variations to the structure. The extent of σ-symmetric orbitals indicated a great inductive *"through-bond"* effect to determine the nature of the carbene bond.

The asymmetric structures were well localised by the NBO algorithm. Degeneracies in the orbitals complicated the naturalisation which indicated the extent of multicentric character in these structures, highlighting long-range ligand-ligand interactions. The larger ligands led to more equal σ- and π-symmetric orbitals indicative of increased covalent character in the bonding.

The increased multicentric nature of the metal carbene bond of the substituted carbene ligands, as well as the Cp-containing metal complexes, was particularly clear when investigated using FALDI. However, FALDI also highlighted the importance of long-range ligand-ligand interactions and showed that these interactions delocalise electrons in a predominantly σ-fashion in the M—C internuclear region. This observation corroborates the inductive and "through-bond" delocalisation observed using MO and NBO decompositions.

The integrated cross-section method proved useful but needs improvement to detect δ-symmetric interactions. This can be achieved by a surface integral over the interatomic space defined by the λ-eigenvectors of the Hessian matrix.

Insights from the FALDI and NDF results illustrate the value in analysing the electron density to investigate the bonding nature in compounds. These results give representations of the quantum mechanical descriptions of the electrons in a chemically intuitive manner based on atomic descriptions and can also be decomposed into NDFs which give a more detailed description based on symmetries.

References

1. de Beer, S.; Cukrowski, I.; de Lange, J. H. *J. Comp. Chem.* **2020**, 1-12.

2. Santamaría, J.; Aguilar, E. *Org. Chem. Front.* **2016**, 3(11), 1561-1588.

3. Beckhaus, R.; Santamaría, C. *J. Organomet. Chem.* **2001**, 617, 81-97.

4. Frenking, G.; Pidun, U. *J. Chem. Soc.*, Dalton Transactions **1997**(10), 1653-1662.

5. Vyboishchikov, S. F.; Frenking, G. *Chem. Eur. J.* **1998**, 4(8), 1428-1438.

6. Fröhlich, N.; Pidun, U.; Stahl, M.; Frenking, G. *Organometallics* **1997**, 16(3), 442-448.

7. Zatsepin, P.; Lee, E.; Gu, J.; Gau, M. R.; Carroll, P. J.; Baik, M.-H.; Mindiola, D. J. *J. Am. Chem. Soc.* **2020**, 142(22), 10143-10152.

8. Frenking, G.; Solà, M.; Vyboishchikov, S. F. *J. Organomet. Chem.* **2005**, 690(24-25), 6178-6204.

9. de Fremont, P.; Marion, N.; Nolan, S. P. *Coord. Chem. Rev.* **2009**, 253(7-8), 862-892.

10. Cukrowski, I.; de Lange, J. H.; Adeyinka, A. S.; Mangondo, P. *Comput. Theor. Chem.* **2015**, 1053, 60-76.

11. Frisch, M. J.; Trucks, G. W.; Schlegel, H. B.; Scuseria, G. E.; Robb, M. A.; Cheeseman, J. R.; Scalmani, G.; Barone, V.; Mennucci, B.; Petersson, G. A.; Nakatsuji, H.; Caricato, M.; Li, X.; Hratchian, H. P.; Izmaylov, A. F.; Bloino, J.; Zheng, G.; Sonnenberg, J. L.; Hada, M.; Ehara, M.; Toyota, K.; Fukuda, R.; Hasegawa, J.; Ishida, M.; Nakajima, T.; Honda, Y.; Kitao, O.; Nakai, H.; Vreven, T.; Montgomery, J. A. J.; Peralta, J. E.; Ogliaro, F.; Bearpark, M.; Heyd, J. J.; Brothers, E.; Kudin, K. N.; Staroverov, V. N.; Keith, T.; Kobayashi, R.; Normand, J.; Raghavachari, K.; Rendell, A.; Burant, J. C.; Iyengar, S. S.; Tomasi, J.; Cossi, M.; Rega, N.; M. Millam, J. M.; Klene, M.; Knox, J. E.; Cross, J. B.; Bakken, V.; Adamo, C.; Jaramillo, J.; Gomperts, R.; Stratmann, R. E.; Yazyev, O.; Austin, A. J.; Cammi, R.; Pomelli, C.; Ochterski, J. W.; Martin, R. L.; Morokuma, K.; Zakrzewski, V. G.; Voth, G. A.; Salvador, P.; Dannenberg, J. J.; Dapprich, S.; Daniels, A. D.; Farkas, O.; Foresman, J. B.; Ortiz, J. V.; Cioslowski, J.; Fox, D. J. In Gaussian09, Revision D01: Wallingford CT, **2009**.

12. Reed, A. E.; Curtiss, L. A.; Weinhold, F. *Chem. Rev.* **1988**, 88(6), 899-926.

13. Keith, T. A.; TK Gristmill Software: Overland Park KS, USA, **2016**.

14. Tebbe, F.; Parshall, G.; Reddy, G. d. *J. Am. Chem. Soc.* **1978**, 100(11), 3611-3613.

15. Petasis, N. A.; Bzowej, E. I. *J. Am. Chem. Soc.* **1990**, 112(17), 6392-6394.

16. Cecchin, G.; Morini, G.; Piemontesi, F. *Kirk-Othmer Encyclopedia of Chemical Technology* **2000**.

17. Mindiola, D. J.; Scott, J. *Nat. Chem.* **2011**, 3(1), 15-17.

Chapter Five

FALDI Fragment-Based Decomposition of Electron Density

Introduction

As is often the case in chemistry it is of interest to study a specific bond or bonding interaction. This has been approached by various different methods over time, ranging from the hook-and-eye model,[1] Lewis theory,[2] valence shell electron pair repulsion theory,[3] valence bond theory,[4-6] molecular orbital[7,8] theory to modern day case by case studies utilising quantum chemical software packages.

Prior to the incorporation of quantum mechanics into chemistry it was well established that the study of chemical bonding required some formalism by which atoms could be combined to form chemical functionalities and these consequently combined to form molecules.[2] With the introduction of quantum mechanics into chemistry the definition of the atom was lost when considering a molecular system. It required significant work to develop theories, such as the Quantum Theory of Atoms in Molecules (QTAIM), which allowed atoms to be reintroduced in the field of quantum chemistry.[9,10]

Many fragment-based analysis techniques, such as the Extended Transition State coupled with Natural Orbitals for Chemical Valence (ETS-NOCV),[11] requires breaking up the system and performing the study on dynamically changing states of subsystems while monitoring changes that occur in particular energy terms during the process. This does yield invaluable insights, but such a fragmentation may not always be possible or chemically justified.[12,13] This is emphasized when studying intramolecular interactions, which may at times be long-range interactions, such as is the case when studying the N···H interaction present in protonated ethylenediamine.[14]

The Fragment, Atomic, Localised, Delocalised and Interatomic (FALDI) density decomposition scheme allows the study of the electron density without the need to fragment or partition the system.[14] Furthermore, the FALDI scheme makes use of the definitions of atoms from QTAIM which leads to a depiction of the bonding that is representative of the quantum mechanics while still maintaining chemical intuition. The FALDI scheme makes extensive use of localised electron densities (*loc*-ED) as well as delocalised electron densities (*deloc*-ED).[15]

In the early days of chemistry it was supposed that a chemical bond exists when an electron pair is shared between two atoms, with two or three electron pairs being shared for double and triple bonds respectively.[2] More recently, the interatomic exchange-correlation energies have been identified as the “glue” that holds atoms together[16] and have been linked to delocalisation indices (DIs) as derived in the QTAIM formalism.[17,18] Even though the “glue” is known it is

still not well defined when an interaction is to be classified as a bond. This often leads to uncertainties on what the accepted molecular structure of a chemical system is.[19] It is becoming more customary to rather define an interaction based on its DI instead of stating that a bond is present, although this generally applies to diatomic interactions whereas it is often the case that chemical "bonds" are multicentric in nature.[20,21]

In the previous chapters of this dissertation, it has been noted that the long-range, ligand-ligand interactions in Schrock carbene metal complexes are particularly important for the description of organometallic bonds. The work presented here looks to combine a fragment-based analysis (which is chemically intuitive and easier to interpret) with the concept of DIs, in order to provide a quantitative insight to the exchange correlation effects describing the various interactions in Schrock carbene metal complexes. Previous works on the FALDI scheme have looked at improving the descriptions of localised and delocalised indices (LIs and DIs) such that the LI only describes truly localised electrons.[15] The aim is then to describe the number of electrons used to form the bonding interaction which leads to the stabilisation of the complexes as well as give useful insights into which parts of the structures have a greater influence on the bonding nature of the M—C carbene bond.

The titanium cyclopentadienyl structures studied play roles as active intermediates during parts of the catalytic processes in olefin metathesis and the chloride structures are part of the production of the catalyst or act as by-products produced during the process.[22-27] Cyclopentadienyl ligands have also never been studied using full FALDI analysis before, and a FALDI-based interpretation should provide interesting insights on the hapticity of the ligand.

In this work the organometallic carbene systems have the general formula of TiL_2CHR with L = Cl, Cp with Cp = C_5H_5 and R = H, CH_3. The fragments are set up as TiL_2 which is referred to as the metal fragment and CHR which is referred to as the carbene fragment. The first part of the study looks at the fragment-based FALDI data produced. This provides insights on the interaction between the fragments. Thereafter, the inter-fragment *deloc*-ED (a measure of the bonding between the fragments) is contrasted to the diatomic Ti—C *deloc*-ED (a measure of the bonding between the titanium and carbon atoms) in order to refine the description of the bonding as observed in the systems.

Theoretical Background

The FALDI scheme

The FALDI scheme was described in Chapter Two; hence, this section will only provide a brief review.

The *loc*-ED $\mathcal{L}_A(\mathbf{r})$ and *deloc*-ED $\mathcal{D}_{A,B}(\mathbf{r})$ used here are calculated using the localised-delocalised overlap (LDO) algorithm. The core of the FALDI scheme starts with the diagonalization of the atomic overlap matrices obtained from QTAIM calculations giving the eigenfunction describing the natural density functions (NDFs) and their respective occupations.

$$\mathbf{S}^{\mathrm{A}}\mathbf{S}^{\mathrm{X}}\mathbf{U}^{\mathrm{AX}} = n^{\mathrm{AX}}\mathbf{U}^{\mathrm{AX}} \tag{1}$$

This allows for the description of NDFs $\phi_i^{AX}(\mathbf{r})$ by the equation,

$$\phi_i^{AX}(\mathbf{r}) = \sum_j^{N_{MO}} \chi_j(\mathbf{r}) U_{ji}^{AX} \tag{2}$$

Using the NDFs as a new basis it is then possible to define the *loc*-ED as

$$\mathcal{L}_A(\mathbf{r}) = \sum_i^{N_{MO}} n_i^{AA}[\phi_i^{AA}(\mathbf{r})]^2 \tag{3}$$

and the *deloc*-ED is defined as

$$\mathcal{D}_{A,B}(\mathbf{r}) = \sum_i^{N_{MO}} n_i^{AB}[\phi_i^{AB}(\mathbf{r})]^2 \tag{4}$$

The LDO algorithm calculates the overlap of the *loc*-ED with all other *loc*-ED and *deloc*-ED to ensure that the LDO-free *loc*-ED only represents electrons which are truly localised to the atomic basin under question. The LDO-free *deloc*-ED then represents the maximum possible delocalisation.

The overlap of the *loc*-ED with another *loc*-ED is given by

$$\boldsymbol{s}\left(\mathcal{L}_A^i; \mathcal{L}_B^j\right) = \sqrt{n_i^{AA} n_j^{BB}}[(\mathbf{U}^{\mathrm{AA}})^{\dagger}\mathbf{U}^{\mathrm{BB}}]_{ij} \tag{5}$$

and the overlap of the *loc*-ED with *deloc*-ED is given by

$$\boldsymbol{s}\left(\mathcal{L}_A^i;\mathcal{D}_{X,Y}^j\right)=\sqrt{n_i^{AA}n_j^{XY}}[(\mathbf{U}^{\mathrm{AA}})^{\dagger}\mathbf{U}^{\boldsymbol{XY}}]_{ij} \tag{6}$$

The total LDO on atomic basin A is then determined by

$$\mathrm{LDO}\left(\mathcal{L}_A^i\right)=\sum_{X\neq A}^{M_{Atoms}}\sum_{j}^{N_{MO}}\boldsymbol{s}\left(\mathcal{L}_A^i;\mathcal{L}_X^j\right)+\sum_{X}^{M_{Atoms}}\sum_{Y\neq A}^{M_{Atoms}}\sum_{j}^{N_{MO}}\boldsymbol{s}(\mathcal{L}_A^i;\mathcal{D}_{X,Y}^j) \tag{7}$$

The total LDO is used to adjust the occupations of the NDFs for the *loc*-ED after which the LDO-free *loc*-ED can be calculated using the adjusted occupations

$$\mathcal{L}_A''(\mathbf{r})=\sum_{i}^{N_{MO}}n_i''^{AA}[\phi_i^{AA}(\mathbf{r})]^2 \tag{8}$$

To adjust the occupations of the NDFs for the *deloc*-ED a weighting function is used to determine how much the overlap of *loc*-ED from one atomic basin contributes to respective *deloc*-EDs from all other atomic basin. This weighting function is defined as

$$w''\left(\mathcal{L}_A^i;\mathcal{D}_{A,B}^j\right)=\frac{\boldsymbol{s}(\mathcal{L}_A^i;\mathcal{D}_{A,B}^j)}{\sum_j\boldsymbol{s}(\mathcal{L}_A^i;\mathcal{D}_{A,B}^j)}\cdot\frac{\sum_k\boldsymbol{s}(\mathcal{L}_A^i;\mathcal{L}_B^k)}{\mathrm{LDO}(\mathcal{L}_A^i)} \tag{9}$$

It is then possible to calculate the LDO-free *deloc*-ED by the equation

$$\begin{aligned}\mathcal{D}_{A,B}''(\mathbf{r})=&\sum_{j}^{N_{MO}}n_j^{AB}\left[\phi_j^{AB}(\mathbf{r})\right]^2\\&+\sum_{j}^{N_{MO}}\sum_{i}^{N_{MO}}\left(n''\left(\mathcal{L}_A^i\rightarrow\mathcal{D}_{A,B}^j\right)[\phi_i^{AA}(\mathbf{r})]^2+n''\left(\mathcal{L}_B^i\rightarrow\mathcal{D}_{A,B}^j\right)\left[\phi_j^{BB}(\mathbf{r})\right]^2\right)\end{aligned} \tag{10}$$

Finally, it is then possible to determine the LDO-free localised and delocalised indices as

$$\lambda_{\mathrm{LDO-free}}(A)=\int_{-\infty}^{\infty}\mathcal{L}_A''(\mathbf{r})d\mathbf{r} \tag{11}$$

for the localised index, and

$$\delta_{\mathrm{LDO-free}}(A,B) = \int_{-\infty}^{\infty} \mathcal{D}''_{A,B}(\mathbf{r})d\mathbf{r} \tag{12}$$

for the delocalised index.

The LDO-free localised and delocalised indices with the grouping of fragment atomic basins described, allows for a description of the bonding in the system. This approach would be intuitive to the chemist's understanding while still maintaining foundations in the quantum mechanics used to describe chemical phenomena. Such an approach allows chemists access to the power of quantum mechanics in a familiar language.

Defining fragments in FALDI scheme

Fragments were arbitrarily defined by selecting the atoms (defined by their atomic basins as per QTAIM) which made up chemically meaningful groups. Atoms only occur within a single fragment such that the fragments combined make up the entire system. The *atom*-ED for a fragment $\mathcal{F}1$ can be expressed as

$$g_{\mathcal{F}1}^{total}(\mathbf{r}) = \sum_{\mathrm{A}}^{M_{\mathcal{F}1}} g_{\mathrm{A}}(\mathbf{r}) \tag{13}$$

where $M_{\mathcal{F}1}$ is the number of atoms in the fragment $\mathcal{F}1$. The total electron population on a fragment $\mathcal{F}1$ can be found by integrating the *atom*-ED over all space. Further, a 3D-isosurface can be generated from $g_{\mathcal{F}1}^{total}(\mathbf{r})$ to aid in interpretation of the total electron population of fragment $\mathcal{F}1$.

Similar to the FALDI scheme above, the *loc*-ED for the fragment can be calculated for each atom in the fragment $\mathcal{F}1$. Subsequently these *loc*-EDs can be summed to obtain the intra-fragment localised electron population (eq. 14)

$$\mathcal{L}_{\mathcal{F}1}(\mathbf{r}) = \sum_{\mathrm{A}}^{M_{\mathcal{F}1}} \mathcal{L}_{\mathrm{A}}(\mathbf{r}) \tag{14}$$

The intra-fragment *deloc*-ED for the fragment $\mathcal{F}1$ can be calculated in a similar manner by calculating the *deloc*-ED for each atom pair in the fragment $\mathcal{F}1$ and summing these.

$$\mathcal{D}_{\mathcal{F}1}^{intra}(\mathbf{r}) = \sum_{\mathrm{A}}^{M_{\mathcal{F}1}-1} \sum_{\mathrm{B=A+1}}^{M_{\mathcal{F}1}} \mathcal{D}_{\mathrm{A,B}}(\mathbf{r}) \tag{15}$$

The total intra-fragment ED can then be expressed (eq. 16) to find the electron density on a single fragment.

$$g_{\mathcal{F}1}^{intra}(\mathbf{r}) = \mathcal{L}_{\mathcal{F}1}(\mathbf{r}) + \mathcal{D}_{\mathcal{F}1}^{intra}(\mathbf{r}) \tag{16}$$

In order to obtain populations of electrons the intra-fragment-ED $g_{\mathcal{F}1}^{intra}(\mathbf{r})$ must be integrated over all space. This yields the total intra-fragment electron population as the sum of LIs and DIs of the atoms within the fragment $\mathcal{F}1$, $N^{intra}(\mathcal{F}1) = \int g_{\mathcal{F}1}^{intra}(\mathbf{r})d\mathbf{r} = \sum_{\mathrm{A}} \mathrm{LI(A)} + \sum_{\mathrm{A,B}} \mathrm{DI(A,B)}$, where $\mathrm{A,B} \in \mathcal{F}1$.

To obtain the *deloc*-ED that is representative of the bonding interaction between two fragments $\mathcal{F}1$ and $\mathcal{F}2$ a similar logic is applied to the intra-fragment *deloc*-ED but using atoms that are not contained in the same fragment. This is defined as the inter-fragment *deloc*-ED.

$$\mathcal{D}_{\mathcal{F}1,\mathcal{F}2}^{inter}(\mathbf{r}) = \sum_{\mathrm{A}}^{M_{\mathcal{F}1}} \sum_{\mathrm{B}}^{M_{\mathcal{F}2}} \mathcal{D}_{\mathrm{A,B}}(\mathbf{r}) \tag{17}$$

Similar to the above, the inter-fragment electron population of fragments $\mathcal{F}1$ and $\mathcal{F}2$ can be obtained by integrating $\mathrm{D}_{\mathcal{F}1,\mathcal{F}2}^{inter}(\mathbf{r})$ over all space, $\mathrm{DI}(\mathcal{F}1,\mathcal{F}2) = \int \mathrm{D}_{\mathcal{F}1,\mathcal{F}2}^{inter}(\mathbf{r})\, d\mathbf{r} = \sum_{\mathrm{A,B}} \mathrm{DI(A,B)}$, where $\mathrm{A} \in \mathcal{F}1$ and $B \in \mathcal{F}2$.

The total ED, consequently also the total population, can then be expressed by summing the intra- and inter-fragment parts (eq. 16 and eq. 17).

$$g_{\mathcal{F}1}^{total}(\mathbf{r}) = g_{\mathcal{F}1}^{intra}(\mathbf{r}) + \sum_{\mathrm{X}}^{\mathcal{M}} \frac{1}{2} \mathcal{D}_{\mathcal{F}1,\mathcal{F}\mathrm{X}}^{inter}(\mathbf{r}) \tag{18}$$

where $\mathcal{M}$ is the number of fragments in the molecule. For the LDO algorithm $\mathcal{D}_{\mathcal{F}2,\mathcal{F}1}^{inter} \neq \mathcal{D}_{\mathcal{F}1,\mathcal{F}2}^{inter}$ and these need to be accounted for individually.

Computational Details

All structures were optimised in Gaussian 09,[28] using DFT with the B3LYP functional while

utilising the 6-311++G(d,p) basis set in the gas phase. QTAIM atomic overlap matrices were calculated using AIMAll version 17.11.14.[29] FALDI data was calculated using in-house software, incorporating the LDO algorithm.[15] All FALDI isosurfaces were visualised using VMD version 1.9.3.[30]

FALDI densities were calculated on diatomic interactions and fragment data was generated by post processing of the diatomic data.

Results and Discussion

The work looks at the fragment analysis of the FALDI delocalisation indices with the diatomic interactions to produce a refined model on carbene bonding. Each system studied had the general formula of TiL_2CHR where L = Cl, Cp with Cp = C_5H_5 and R = H, CH_3 (see Figure 1).

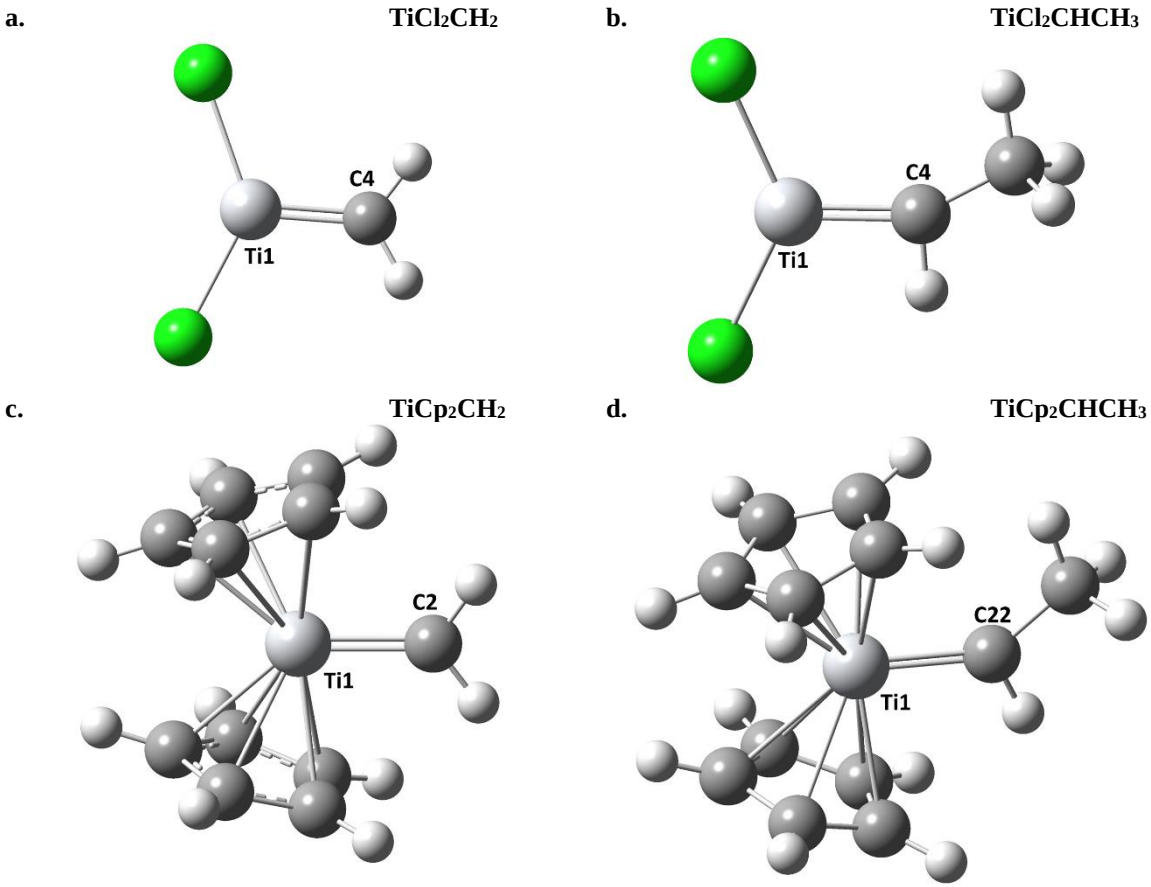

Figure 1. Structures studied in this chapter with the labelling on the atoms of interest.

The systems were analysed as two separate fragments with the metal fragments being TiL_2 and the carbene fragment CHR (see Figure 2).

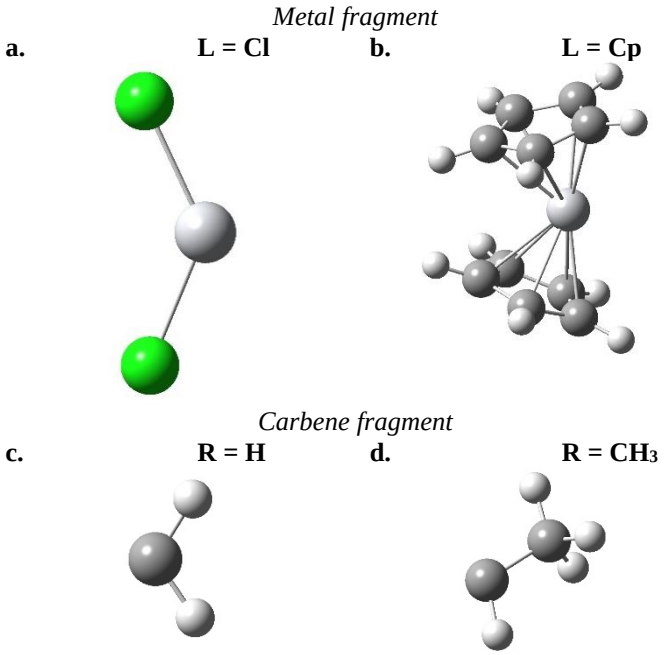

Figure 2. Fragments used in this chapter to study the titanium-carbon carbene bond.

Using $TiCl_2CH_2$ as an example, the meaning and impact of the parameters given in Table 1 are illustrated before it is used to investigate the trends with varying structures. The total electron count of both fragments has to recover the classically expected number of electrons on the system, i.e. 64 electrons for $TiCl_2CH_2$. For the carbene fragment there are 1.978 intra-fragment localised electrons, signifying the carbon 2s electrons. There are also 3.880 intra-fragment delocalised electrons which represents the two C—H bonds. The metal fragment has 38.724 intra-fragment localised electrons, correlating to the expected 38 core electrons of the chlorine and titanium atoms with slightly more electrons to account for non-bonded electrons. The intra-fragment delocalised electron count (10.815e^-) is higher than would be expected if there were only two Ti—Cl single bonds. This value is rationalised by considering the various resonance structures possible for the Ti—Cl bond. The inter-fragment delocalised electrons for both fragments added together make up the difference in order to recover the 64 total electrons. The 8.603 inter-fragment delocalised electrons are again much higher than the expected four electrons for the Ti—C double bond. However, similar to the Ti—Cl interaction there are various resonance structures to be considered which leads to the larger than expected value.

Table 1. Summary of population analysis on TiL_2CHR systems with L = Cl, Cp and R = H, CH_3. All values are given in a.u. and were calculated using the FALDI LDO algorithm.

Structure	Total Electron Population	Total Intra-Fragment†	Intra-Fragment Localised	Intra-Fragment Delocalised††	Inter-Fragment Delocalised†††
			Metal fragment		
$TiCl_2CH_2$	55.466	49.539	38.724	10.815	5.927
$TiCl_2CHCH_3$	55.529	47.420	37.314	10.107	8.109
$TiCp_2CH_2$	91.347	87.964	29.538	58.426	3.382
$TiCp_2CHCH_3$	91.397	86.962	29.396	57.565	4.433
			Carbene fragment		
$TiCl_2CH_2$	8.534	5.858	1.978	3.880	2.676
$TiCl_2CHCH_3$	16.471	13.676	3.921	9.755	2.796
$TiCp_2CH_2$	8.652	5.242	1.923	3.319	3.409
$TiCp_2CHCH_3$	16.601	12.638	3.846	8.792	3.962

† the total intra-fragment gives the sum of the localised and the delocalised electrons within the fragment.
†† the intra-fragment delocalised component describes electrons delocalised over the atoms comprising the fragment
††† the inter-fragment delocalised component describes electrons which are fully delocalised between atoms in separate fragments

Inspection of the total electron population in Table 1 suggests that the metal fragment gains a small degree of electron density when the methyl R-group is added (+0.063 and +0.050e^- for L = Cl and L = Cp, respectively) – in line with a classical inductive effect. However, these changes are relatively small in comparison to other changes throughout the complexes. On the metal fragment it is seen that the intra-fragment localised and delocalised electrons decrease when the methyl group is present on the carbene, while the inter-fragment delocalisation increases. For instance, with L = Cl, 1.141 localised electrons and 0.708 intra-fragment delocalised electrons are lost upon addition of the methyl group, whereas 2.182e^- are gained on the metal fragment as a result of delocalisation over both fragments. A decrease of the localised electrons upon addition of the methyl group suggests that these localised electrons become delocalised between the fragments to stabilise the carbene bond when the bulkier carbene is present. Clearly, the addition of the methyl group has a profound effect on the electronic structure of the molecule – an observation that is not apparent from investigating only the electron populations on atoms/fragments.

There was a greater change in localised electrons upon addition of the methyl group (R = CH_3) when L = Cl. There was also a greater change in the intra-fragment delocalised electrons for R = CH_3 when L = Cp. This can be understood when considering that the chloride ligands contain just the chlorine atoms and thus mostly consists of localised (or "core") electrons. In contrast, the cyclopentadienyl ligands consist of aromatic rings and the electrons are thus

already highly delocalised; hence, most of the electrons would originate from these intra-fragment delocalised electrons. The combined contributions of localised and intra-delocalised electrons are captured in Table 1 as total intra-fragment population, which, upon addition of the methyl group, decreased by 2.119e^- when L = Cl (49.539e^- when R = H and 47.420e^- when R = CH_3) and 1.002e^- when L = Cp (87.964e^- when R = H and 86.962e^- when R = CH_3). This difference, in which electrons are used to adjust the inter-fragment delocalised electrons, suggests that the metal plays a lesser role in the stabilisation of the carbene bond. Although the values of the various components change, the isosurfaces of these intra-fragment components (Figure 3) do not show any significant major changes. This shows that the density removed from the intra-fragment densities is taken uniformly throughout the space when added to the inter-fragment density.

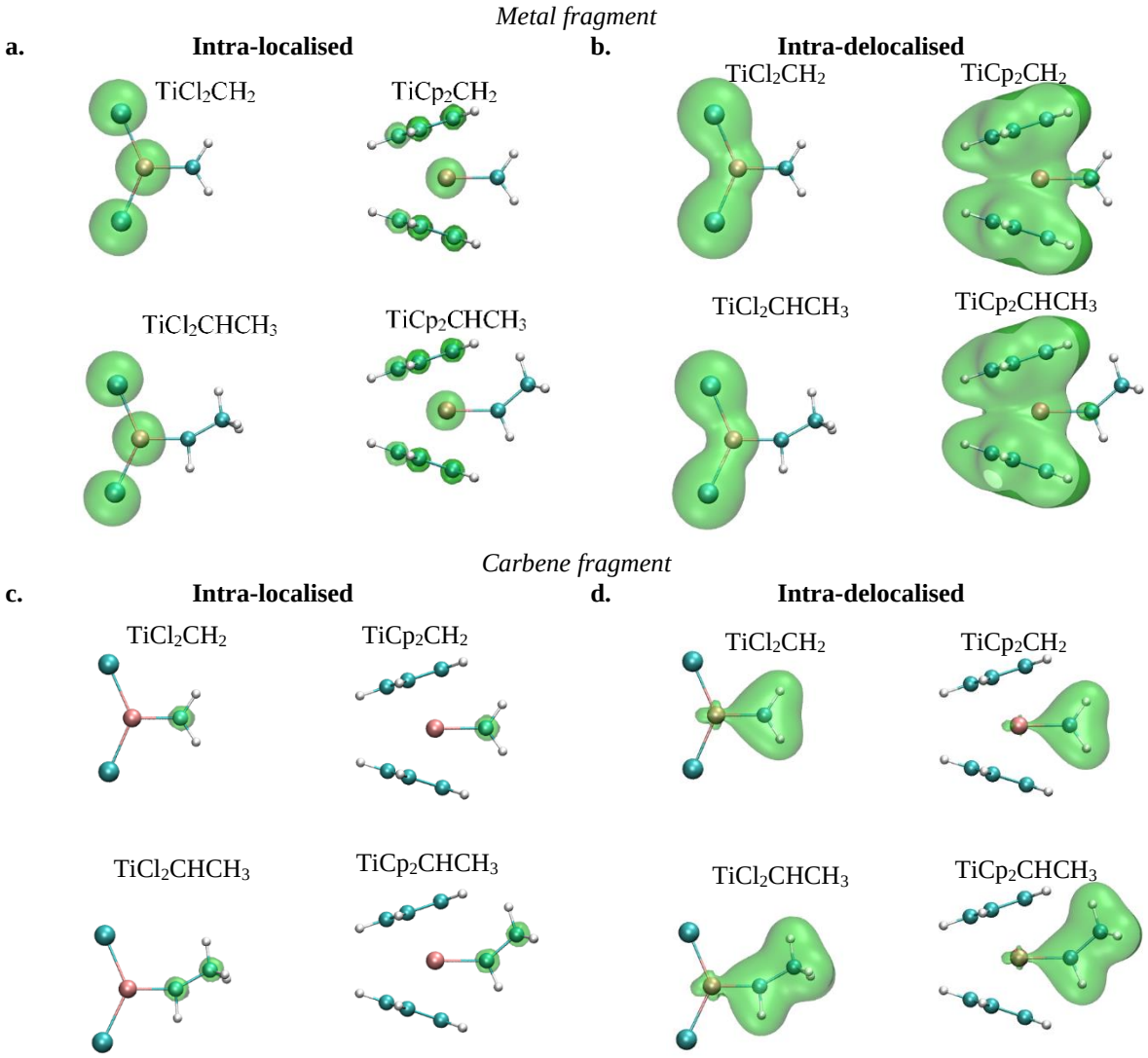

Figure 3. Localised and delocalised electron densities on metal and carbene fragments at iso-value of 0.01 a.u.

Interestingly, the inter-fragment delocalisation (Table 1) shows that the chloride ligands share more electrons than the cyclopentadienyl when structures have the same carbene fragment. To this effect the following was found: 5.927e^- when L = Cl, R = H as opposed to 3.382e^- when L = Cp, R = H. It is expected that the increased electron sharing would reduce the strain from the high number of localised electrons present on the chloride ligands. The opposite is true, however, for the inter-fragment delocalisation contribution to the carbene fragments. The carbene fragments share more electrons in the presence of the cyclopentadienyl ligands (2.676e^- when L = Cl, R = H and 3.409e^- when L = Cp, R = H) owing to the already delocalised nature of the cyclopentadienyl ligands. Changes to the carbene fragment do not have as pronounced an influence on the inter-fragment delocalisation of the carbene fragment as changes to the other ligands had on the inter-fragment delocalisation of the metal fragments. Comparing the values of inter-fragment delocalisation from the metal and carbene fragments on the same complex shows that the chloride structures share more electrons from the metal fragment whereas the cyclopentadienyl structures show a balanced sharing between the fragments. This observation indicates that the cyclopentadienyl structures have a more covalent character compared to the chloride structures. The latter show more donor-acceptor type character with the metal fragment acting as the donor and the carbene fragment as the acceptor. This mimics Fischer carbene bonding character where metal-to-ligand back bonding is observed when the metal fragment contains ligands with highly localised electrons or carbene fragments that are able to accommodate excess electron density from the metal fragment (low lying unfilled orbitals). This observation agrees with work on non-heteroatom stabilised Fischer carbenes.[31]

For similar carbene fragments, the number of intra-fragment localised electrons remains the same when the ligands on the metal are changed. However, going from the chloride to the cyclopentadienyl ligand, there is a decrease in the number of intra-fragment delocalised electrons showing the intra-fragment bonds for the carbene ligand to be stronger with the chloride ligands present. This suggests a strong interaction between the various ligands present on the metal.

To further prove the ligand-ligand interaction, the diatomic interaction of the titanium atom with the carbene carbon atom (classically expected to represent the carbene *bond*) was subtracted from the inter-fragment delocalisation in order to obtain the ligand-ligand interaction population (Table 2). In all four systems this interaction (‘Difference’ column in Table 2) had a larger number of electrons being shared than the diatomic interaction of the

metal and the carbene carbon. This indicates that the ligands present collectively have the greater influence on the bonding nature. For instance, when L = Cl, R = CH_3, the Ti atom and carbene carbon share 3.725e^-, indicating a bond order of close to two (i.e. almost two electron pairs are shared). On the other hand, the total inter-fragment delocalisation between the metal cluster and the entire carbene ligand is 10.904e^-. Subtracting the number of diatomic delocalised electrons from the number of inter-fragment delocalised electrons (the long-range ligand-ligand interaction) gives 7.180e^- – which is a very significant number and considerably larger than the diatomic interaction. This would indicate that the ligands present, collectively, have the greater influence on the bonding nature. As mentioned above, however, the density is not equally shared by the Cl and the carbene ligands: of the 7.180e^- shared by the ligand-ligand interaction when L = Cl, R = CH_3, 6.025e^- contributes to the Cl atoms whereas only 1.154e^- contributes to the carbene ligand. The situation is considerably different for L = Cp structures, however. For instance, when L = Cp and R = CH_3, 5.858e^- are shared amongst the long-range ligand-ligand interaction, where 3.000e^- is contributed to the Cp ligands and 2.858e^- is contributed to the carbene ligand.

Table 2. Population analysis of the metal-carbene inter-fragment delocalisation and the Ti—C diatomic delocalisation along with the difference between the fragment-based and diatomic delocalisation.

	Inter-Fragment Delocalisation			Diatomic Delocalisation			Difference		
Structure	Total	Metal	Carbene	Ti—C	Ti	C	Total	Metal†	Carbene†
$TiCl_2CH_2$	8.603	5.927	2.676	3.725	1.903	1.822	4.878	4.024	0.854
$TiCl_2CHCH_3$	10.904	8.109	2.796	3.725	2.083	1.641	7.180	6.025	1.154
$TiCp_2CH_2$	6.791	3.382	3.409	2.535	1.372	1.163	4.256	2.010	2.246
$TiCp_2CHCH_3$	8.395	4.433	3.962	2.537	1.432	1.104	5.858	3.000	2.858

† the difference on the metal is determined by subtracting the contribution of titanium to the diatomic delocalisation from the metal fragment contribution to the inter-fragment delocalisation index $\Delta\mathcal{D}(Metal) = \mathcal{D}(TiL_2) - \mathcal{D}(Ti)$.
†† the difference on the carbene is determined by subtracting the contribution of carbene carbon to the diatomic delocalisation from the carbene fragment contribution to the inter-fragment delocalisation index $\Delta\mathcal{D}(Carbene) = \mathcal{D}(CHR) - \mathcal{D}(C)$.

To gain a holistic description of the bonding in these carbene complexes, the major contributors to the difference in inter-fragment and diatomic delocalisation must be identified. (A full list of the diatomic contributions to the inter-fragment delocalisation can be found in Table C5.) A large portion of these remaining electrons, once the delocalised electrons of the titanium and carbene carbon are removed, can be described by the interactions of the carbene

carbon with the other ligands, chloride or cyclopentadienyl. The densities in Figure 4 show that the inter-fragment delocalised density persists over large portions if not all of the structure whereas the diatomic Ti—C interaction only covers the titanium and carbon regions, the diatomic delocalised density in $TiCp_2CHCH_3$ is seen to be quite delocalised itself, extending into much of the methyl group.

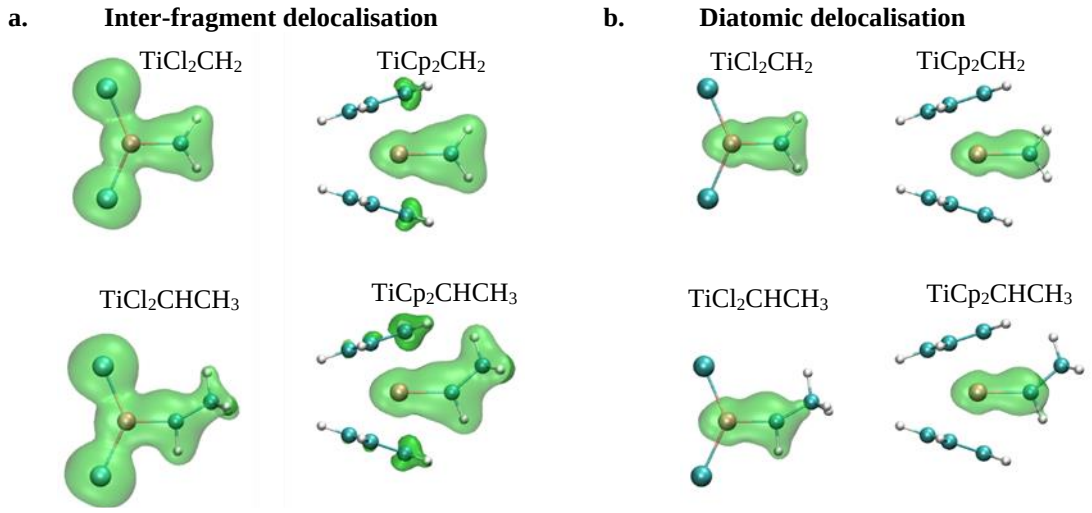

Figure 4. Delocalised electron densities for the fragments (a) and the diatomic interaction (b)associated with the titanium-carbon carbene bond at iso-value of 0.01 a.u.

In $TiCl_2CH_2$, 8.603e^- are shared in total between the metal cluster and the carbene ligand. 2.591e^- (30%) of the total constitute the interaction between the carbene carbon and chloride ligands, 1.565e^- (18%) is the interaction of hydrogen atoms with the chloride ligands and 0.723e^- (8%) is the titanium metal with the hydrogen atoms. It is noted in general that the delocalised electrons between the carbene carbon and the other ligands or the other ligands with the rest of the carbene ligand make up large portions of the inter-fragment delocalised density. At an extreme it is noted that for $TiCp_2CHCH_3$ there are three interactions (Ti1 with C22, C22 with the ancillary ligands and ancillary ligands with the remainder of the carbene ligand) collectively making up nearly the same number of electrons (about 2.45e^- or 30%) which shows the equal importance of these components. This hints at a large overall delocalisation and a multicentric nature of the bonding in the complex.

The multicentric bonding nature of the carbene complex is emphasized in the $TiCp_2CH_2$ structure, which acts as the active intermediate for the catalysts in many olefin metathesis reactions. In this complex the electrons shared between the carbene carbon and other ligands are 2.700e^- which is more than the 2.535e^- shared between the titanium and carbene carbon.

The interaction of the carbene carbon with the other ligands present on the metal has occupations ranging from 2.403e^- to 2.700e^-. Another important aspect supporting the multicentric bonding nature is the interaction between the titanium metal atom and the remainder of the carbene fragment (excluding the carbene carbon which is directly bonded to the metal) where the electrons shared ranges between 0.520e^- and 1.653e^-. The interaction here is especially sensitive to the carbene structure as the titanium interaction with the methyl group is 1.197e^- and 0.808e^- for chloride and cyclopentadienyl, respectively.

Conclusion

It was shown that bonding in organometallic carbene complexes is quite complex and highly depends on the environment in which the system is placed. Here it was noted that ligands with highly localised electron density favour donor-acceptor type characters whereas those ligands with highly delocalised electrons favour covalent bonding. Furthermore, carbene ligands with more flexible electronic structures allow for better acceptance of electrons from the metal fragment. Thus, bulky carbene ligands will favour donor-acceptor type bonding whereas rigid or small carbenes will favour covalent bonding. This once again blurs the line between what can be classified as a Fischer or a Schrock carbene and what criteria should be used to determine this.

Although the diatomic Ti—C interaction is the major diatomic contributor to the electrons forming the carbene bond, it has been shown that a large amount of electron sharing is taking place between other parts of the system which can have a great influence on the bonding. The carbene carbon shows a great interaction with the other ligands present on the metal, while the metal shows a great interaction with the remainder of the carbene ligand. In particular, when a smaller ionic ligand was used (L = Cl), the long-range interaction between the carbene carbon and the Cl ligands was observed to be very unbalanced, with most of the shared electrons residing on the Cl atoms. On the other hand, with the Cp ligands, the long-range ligand-ligand interaction was much more balanced on both fragments.

Ligand-ligand interactions are identified as major stabilising components for the systems studied. This ligand-ligand interaction is seen to be weaker when a larger carbene fragment is used, thus providing insights on the mechanisms where these systems are used as catalysts. With the presence of the larger carbene ligands much of the interaction appears to become more metal-centric. A larger set of applicable systems, where the ancillary ligands as well as the

carbene ligand are varied, should be studied via this method to provide more insights on the nature of the ligand-ligand interactions and how to utilise these interactions.

With theoretical tools, such as the FALDI scheme, available to chemists which provides an intuitive view to the electron density and with the possibility of fragment-based analysis it can only be expected that such practices will soon become commonplace for the analysis of organometallic bonding and other applications in transition metal chemistry, especially considering the computationally inexpensive manner in which this tool can be implemented.

References

1. Hill, J. W. *J. Chem. Educ.* **1986**, 63(6), 503.
2. Lewis, G. N. *J. Am. Chem. Soc.***1916**, 38(4), 762-785.
3. Gillespie, a. R.; Nyholm, R. *Q. Rev. Chem. Soc.* **1957**, 11(4), 339-380.
4. Heitler, W.; London, F. *Z. Phys.* **1927**, 44(6-7), 455-472.
5. Shaik, S.; Hiberty, P. C. *Rev. Comput. Chem.* **2004**, 20, 1.
6. Pauling, L. *J. Am. Chem. Soc.* **1931**, 53(4), 1367-1400.
7. Mulliken, R. S. *Phys. Rev.* **1932**, 40(1), 55.
8. Hückel, E. *J. Chem. Soc. Faraday Trans.* **1934**, 30, 40-52.
9. Hirshfeld, F. L. *Theor. Chim. Acta* **1977**, 44(2), 129-138.
10. Bader, R.; Nguyen-Dang, T. T.; Tal, Y. *Rep. Prog. Phys.* **1981**, 44(8), 893.
11. Mitoraj, M. P.; Michalak, A.; Ziegler, T. *J. Chem. Theor. Comput.* **2009**, 5(4), 962-975.
12. Bader, R. F. *Chem. Eur. J.* **2006**, 12(10), 2896-2901.
13. Poater, J.; Solà, M.; Bickelhaupt, F. M. *Chem. Eur. J.* **2006**, 12(10), 2902-2905.
14. De Lange, J. H.; Cukrowski, I. *J. Comput. Chem.* **2017**, 38(13), 981-997.
15. de Lange, J. H.; Cukrowski, I. *J. Comput. Chem.* **2018**, 39(20), 1517-1530.
16. Kurth, S.; Perdew, J. P. *Int. J. Quantum Chem.* **2000**, 77(5), 814-818.
17. Francisco, E.; Menéndez Crespo, D.; Costales, A.; Martín Pendás, Á. *J. Comput. Chem.* **2017**, 38(11), 816-829.

18. Bader, R. F.; Stephens, M. E. *J. Am. Chem. Soc.* **1975**, 97(26), 7391-7399.

19. García-Revilla, M.; Francisco, E.; Popelier, P. L.; Martín Pendás, A. *ChemPhysChem* **2013**, 14(6), 1211-1218.

20. de Lange, J. H.; van Niekerk, D. M.; Cukrowski, I. *J. Comput. Chem.* **2018**, 39(16), 973-985.

21. de Lange, J. H.; van Niekerk, D. M.; Cukrowski, I. *J. Comput. Chem.* **2018**, 39(27), 2283-2299.

22. Tebbe, F.; Parshall, G.; Reddy, G. S. *J. Am. Chem. Soc.***1978**, 100(11), 3611-3613.

23. Cannizzo, L. F.; Grubbs, R. H. *J. Org. Chem.* **1985**, 50(13), 2316-2323.

24. Breit, B. *Angew. Chem. Int.* **1998**, 37(4), 453-456.

25. Petasis, N. A.; Bzowej, E. I. *J. Am. Chem. Soc.* **1990**, 112(17), 6392-6394.

26. Cecchin, G.; Morini, G.; Piemontesi, F. *Kirk-Othmer Encyclopedia of Chemical Technology* **2000**.

27. Trnka, T. M.; Grubbs, R. H. *Acc. Chem. Res.* **2001**, 34(1), 18-29.

28. Frisch, M. J.; Trucks, G. W.; Schlegel, H. B.; Scuseria, G. E.; Robb, M. A.; Cheeseman, J. R.; Scalmani, G.; Barone, V.; Mennucci, B.; Petersson, G. A.; Nakatsuji, H.; Caricato, M.; Li, X.; Hratchian, H. P.; Izmaylov, A. F.; Bloino, J.; Zheng, G.; Sonnenberg, J. L.; Hada, M.; Ehara, M.; Toyota, K.; Fukuda, R.; Hasegawa, J.; Ishida, M.; Nakajima, T.; Honda, Y.; Kitao, O.; Nakai, H.; Vreven, T.; Montgomery, J. A. J.; Peralta, J. E.; Ogliaro, F.; Bearpark, M.; Heyd, J. J.; Brothers, E.; Kudin, K. N.; Staroverov, V. N.; Keith, T.; Kobayashi, R.; Normand, J.; Raghavachari, K.; Rendell, A.; Burant, J. C.; Iyengar, S. S.; Tomasi, J.; Cossi, M.; Rega, N.; M. Millam, J. M.; Klene, M.; Knox, J. E.; Cross, J. B.; Bakken, V.; Adamo, C.; Jaramillo, J.; Gomperts, R.; Stratmann, R. E.; Yazyev, O.; Austin, A. J.; Cammi, R.; Pomelli, C.; Ochterski, J. W.; Martin, R. L.; Morokuma, K.; Zakrzewski, V. G.; Voth, G. A.; Salvador, P.; Dannenberg, J. J.; Dapprich, S.; Daniels, A. D.; Farkas, O.; Foresman, J. B.; Ortiz, J. V.; Cioslowski, J.; Fox, D. J. In Gaussian09, Revision D01: Wallingford CT, **2009**.

29. Keith, T. A. In AIMAll (Version 171114); TK Gristmill Software: Overland Park KS, USA, **2016**.

30. Humphrey, W.; Dalke, A.; Schulten, K. *J. Mol. Graph.* **1996**, 14(1), 33-38.

31. Santamaría, J.; Aguilar, E. *Org. Chem. Front.* **2016**, 3(11), 1561-1588.

Chapter Six

Orbital-Based Decomposition of Atomistic Electron Delocalisation Index

Introduction

Since the establishment of atomic subspaces within the molecular space[1] various modes of analysis have been put forth[2-6] to study chemical bonding in terms of atoms-in-molecules. As the decomposition of molecular space gained a foothold with the development of the quantum theory of atoms in molecules (QTAIM)[7] the analysis of molecular wavefunctions, such as through molecular orbital (MO) theory, have lost some popularity. The rising popularity of QTAIM and other density-based methods is partially due to the complexity of wavefunctions and partially to the ease of understanding chemical bonding in terms of electrons shared between atoms – as is taught in most introductory chemistry courses.[8]

However, each theory or model provides its own unique perspective on the chemical bonding phenomena. Where QTAIM provides insights on which atoms partake in bonding interactions and how many electrons are involved,[1,9] MO theory provides insights on how these electrons are distributed over the system as a whole and which parts of the system are linked by quantum mechanical correlation effects. By the combined application of both of these models one can obtain an analysis which provides insights on the atoms involved in specific interactions. Quantitative measures of the extent of these interactions are obtained while maintaining the quantum mechanical links between different parts of the system.

Demanding multiconfigurational studies suggested that the bonding in Schrock carbene complexes does not adhere to the proposed models of covalent bonding between the metal and carbon atoms.[10] Further studies also revealed the dependence of the nature of the carbene bond on its chemical environment, such that the other ligands on the metal and the substituents on the carbon can influence the nature of the carbene bond.[11] These insights were then applied to the study of olefin metathesis catalysts.[12] Important research questions arose from this work regarding the nature of the carbene bond and factors which influence it.[13] These research questions relate to the development of a computational scheme to predict the properties of organometallic carbene complexes, the influence that ancillary ligands have on the carbene bond and the influence of other main group elements in the carbene ligand.

The nature of the carbene bond in titanium Schrock carbene complexes with main group atoms was investigated for a subset of main group elements utilizing multiconfigurational methods.[14] This revealed the importance of ligand-to-metal back bonding in the stabilization of complexes of this type, i.e. transition metal Schrock carbene complexes.

The dependence of the bonding nature on (i) the structure of the carbene ligand, (ii) the

identity of the central metal atom and (iii) the nature of ancillary ligands suggests that the system should be studied as a whole in order to gain an accurate description of the metal-carbon carbene bonding interaction. This would apply to both Schrock and Fischer carbene complexes as the bonding models for these complexes (covalent and donor-acceptor, respectively) are shown to exist in various resonance states of Schrock carbene complexes.[10,11] Unfortunately, a holistic approach to the study of bonding is often not followed, given the difficulty of interpreting delocalised, molecular-wide MOs.

QTAIM provides an atomistic and localised description of the bonding that simplifies the study of bonding in polyatomic systems. Other localisation procedures, purely based on MO overlap exist[15] but, unlike QTAIM, are sensitive to the choice of basis set and incorporation of virtual orbitals.[2] Since QTAIM does not employ any arbitrary condition for localisation (such as adherence to Lewis structures,[16] dependence on basis set definition[17] or use of non-chemical reference states[18]) the full details of the delocalisation of the electrons as provided by MO theory is maintained. In this way, QTAIM provides a chemically intuitive, atomistic description of bonding.

In this chapter, the relationship between molecular wide MOs and an atomistic QTAIM-based framework is explored in a series of Schrock carbene complexes. The method of analysis described here gives insights similar to those from the study of different resonance structures.[10,11] Moreover, without the need of multiconfigurational calculations, it provides electron counts that are representative of the mixed hybrid resonance state.

Theoretical Background

This work presents a method of decomposing the orbital densities (canonical MOs) into localised and delocalised atomistic contributions, in accordance with the previously reported MO-DI method.[19] Atomic basins Ω are defined using the descriptors from QTAIM[2,7] where an atomic basin is described by the zero-flux surface of the electron density

$$\nabla\rho(\mathbf{r}) \cdot \mathbf{n}(\mathbf{r}) = 0 \qquad (1)$$

where $\mathbf{r}$ is a coordinate on the surface, and $\mathbf{n}(\mathbf{r})$ describes the normal vector of the surface.

Atomic overlap matrices can then be calculated for each atomic basin by

$$S_{ij}^{\Omega} = \int_{\Omega} \chi_i(\mathbf{r})\chi_j(\mathbf{r})d\mathbf{r} = \langle \chi_i | \chi_j \rangle_{\Omega} \quad (2)$$

where χ_i and χ_j are the MOs which are integrated over the volume of the atomic basin to obtain the contribution of those orbitals to the atom described by the particular atomic basin in question.

In order to calculate the atomistic MO occupations correctly it was required sum of all the occupations add up to the total number of electrons in the molecule. Thus, the occupations for each orbital had to add up to 2 for the restricted, closed-shell orbitals used in this work. This work only used double occupied closed shell and single determinant wavefunctions within the Hartree-Fock approximated and thus the Kronecker delta function could be used to factor in the MO occupations.

$$\nu_{ij} = 2\delta_{ij} \quad (3)$$

Two sets of matrices were then calculated. The first matrix represents the localised occupations for a specific atomic basin A

$$LMAT_{ij}^{A} = \sum_{n}^{N} \sqrt{\nu_i \nu_j} S_{in}^{A} S_{nj}^{A} \quad (4)$$

where ν_i is the occupation number of the i^{th} MO, ν_j is the occupation number of the j^{th} MO and N is the number of MOs. The trace of the matrix $\mathbf{LMAT}^{\mathrm{A}}$ recovers the QTAIM defined $LI(\mathrm{A})$.

The second matrix was calculated in a similar manner and represents the delocalised occupations over two atomic basins.

$$DMAT_{ij}^{A,B} = \sum_{n}^{N} \sqrt{\nu_i \nu_j} (S_{in}^{A} S_{nj}^{B} + S_{in}^{B} S_{nj}^{A}) \quad (5)$$

where ν_i is the occupation on the i^{th} MO, ν_j is the occupation on the j^{th} MO and N is the number of MOs. The trace of the matrix $\mathbf{DMAT}^{\mathrm{A,B}}$ recovers the QTAIM defined $DI(\mathrm{A},\mathrm{B})$.

The elements on the main diagonal of these matrices ($\mathbf{LMAT}^{\mathrm{A}}$ and $\mathbf{DMAT}^{\mathrm{A,B}}$) for each atomic basin or atomic basin pair were collected together in a separate table to gain an overview of the occupations per atomic basin for each MO. This has the consequence that $LMAT_{ii}^{A}$ describes the localised contribution that atomic basin A makes to the i^{th} MO. Similarly,

$DMAT_{ii}^{A,B}$ describes the delocalised contribution that atomic basins A and B make to the i^{th} MO. Furthermore, the sum of $LMAT_{ii}^{A}$ and $DMAT_{ii}^{A,B}$ over all atomic basins recovers the total occupation of the i^{th} MO. Finally, the sum of $LMAT_{ii}^{A}$ over all MOs recovers the $LI(\mathrm{A})$ as defined in QTAIM, and, by the same reasoning, the sum of $DMAT_{ii}^{A,B}$ over all MOs recovers the $DI(\mathrm{A,B})$ as defined in QTAIM.

The constructed table gives an insight into the mode of bonding (covalent or donor-acceptor) while providing quantitative occupations for the contributions. Importantly, the sign of each element shows correlation with the bonding, antibonding or non-bonding nature of MOs with respect to the interaction described by such element.

Computational Details

All structures were optimised in Gaussian 09, Rev. D.01,[20] using B3LYP with the 6-311++G(d,p) basis set in the gas phase. QTAIM molecular graphs and atomic overlap matrices were calculated using AIMAll version 17.11.14.[21] All MO isosurfaces were visualised using VMD version 1.9.3.[22]

Calculations on MO decomposition were performed using in-house software.

Results and Discussion

This section was divided into two parts to aid in the understanding of the method applied. The first part studies $TiCl_2CH_2$ to establish the foundations of and develop an intuitive feeling for the approach followed in the second part. The second part considers various structures in order to identify general trends in the bonding nature of the carbene bond in Schrock carbene complexes.

Investigation of the carbene bond in $TiCl_2CH_2$

The MO diagram for $TiCl_2CH_2$ shown in Figure 1 shows how the carbene bond is constructed from non-bonding carbon 2p orbitals and non-bonding titanium 3d orbitals. This suggests that the carbene bond is a double bond with a σ and a π orbital. Furthermore, it proposes a diatomic nature for the carbene bond since it is formed from non-bonding orbitals on both the metal and carbon atoms.

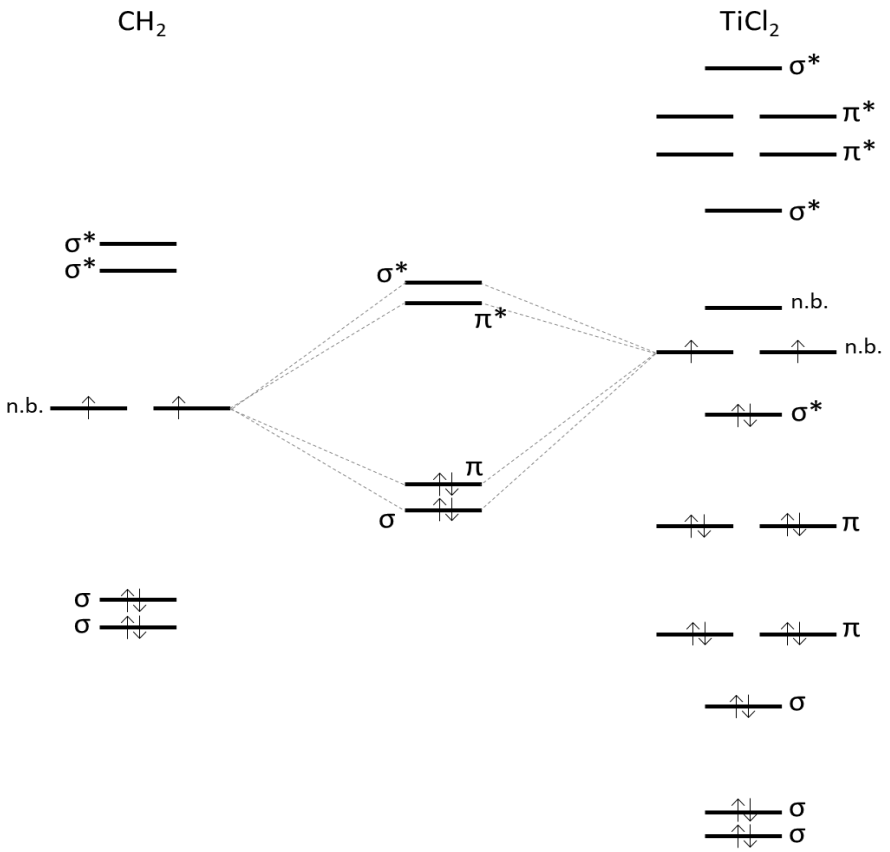

Figure 1. Approximate MO diagram for $TiCl_2CH_2$ showing the bonding between the $TiCl_2$ and CH_2. Simply put, the diagram shows the double bond nature of the carbene bond.

In MO theory the description of the bonding is based on orbital overlap. Thus, MOs are defined by the atomic orbitals that overlap to form the MOs. These orbitals are described as bonding, antibonding or non-bonding based on the relative phases of the overlapping orbitals. The full power of MO theory is revealed with the application of group theory. Symmetry labels can be derived for molecules of specific point group symmetries. This assignment requires some degree of symmetry in order to be useful. Furthermore, the symmetry labels are complex and only comparable under certain transformations. Therefore, these symmetries are often simplified to diatomic σ, π, δ and ϕ with their respective antibonding symmetries. This simplification works well for diatomic interactions and does not require any molecular symmetries to be present.

For the $TiCl_2CH_2$ molecule studied, examples of various orbitals with their respective symmetries can be collected (Figure 2). The non-bonding orbital χ^{22} does not share any electron density between the metal and the carbon. It does not strengthen, nor weaken the

carbene bond. The bonding orbitals $\chi^{31}$and χ^{32} share electron density between the metal and carbon atoms in a way that the carbene bond is strengthened. Contrary to this, the antibonding orbitals χ^{25} and χ^{30} weaken the carbene bond with nodes being present in the bonding region of the carbene bond.

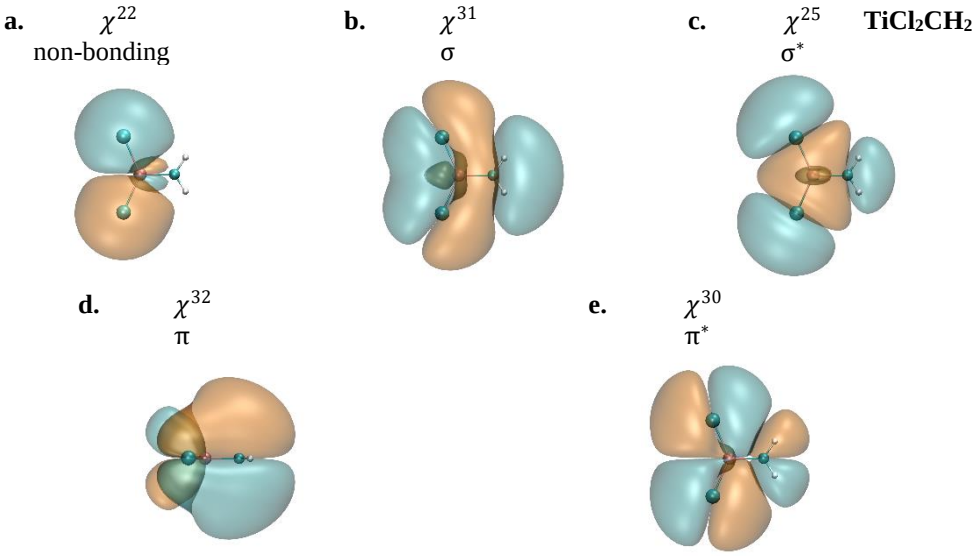

Figure 2. Examples of a non-bonding (a), σ-bonding (b), σ-antibonding (c), π-bonding (d) and π-antibonding (e) orbitals of $TiCl_2CH_2$ at isovalue 0.001a.u.

MO theory proposed a double bond character, thus a sharing of four electrons. Modern quantum chemical computations provide a more detailed insight into this number. Localisation (LI) and delocalisation (DI) indices can be obtained from QTAIM (Figure 3) in order to obtain insights to the bonding. The LI(Ti1) = 18.515e^- indicates the number of electrons localised to the Ti1 atomic basin. Similarly, LI(C2) = 4.707e^- indicates the number of electrons localised to the C2 atomic basin. The DI(Ti1,C2) = 1.720e^- indicates the number of electrons delocalised between the Ti1 and C2 atomic basins. This gives a measure of the covalent bond order,[23] indicating a double bond for the Ti—C bond in the case of $TiCl_2CH_2$.

Although accurate numbers of localised or delocalised electrons are obtained per atomic basin with the application of QTAIM, the molecular wide insights provided by MO theory is lost. Restricted, closed-shell MOs have an occupation of either 2 or 0 electrons per MO, but these electrons could originate from anywhere in the molecule. The method of analysis developed in this chapter aims to combine aspects of QTAIM and MO theory.

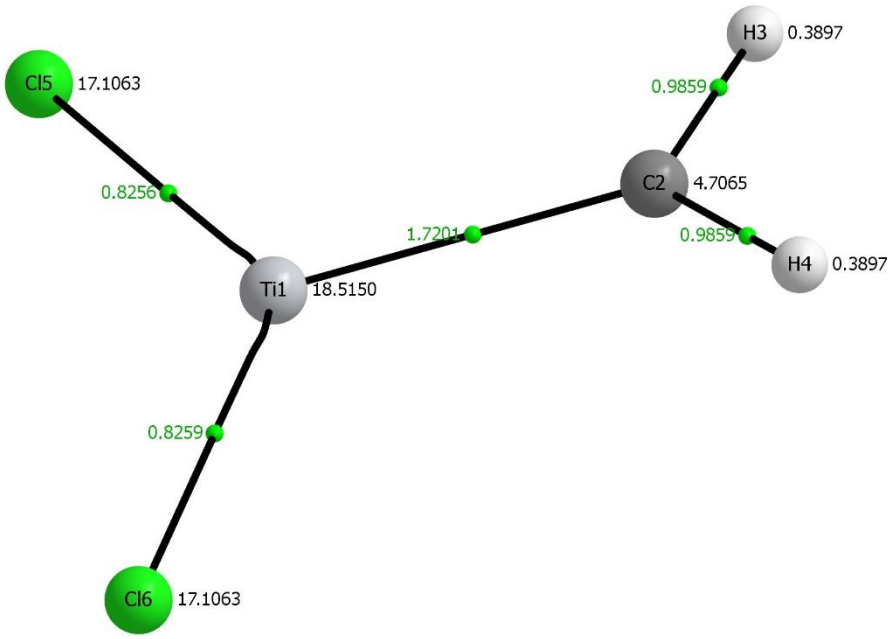

Figure 3. Molecular graph with QTAIM LI (black) and DI (green) values for the main interactions.

The localisation and delocalisation indices can be decomposed into the MOs that contribute to the LI or DI (Table 1). This decomposition provides a unique understanding on the contributions that each atom makes towards the orbital density of each individual MO. The LI and DI values in Table 1 give an indication for the interaction between the titanium and carbene carbon atom. The bonding orbitals χ^{31} and χ^{32} (Figure 2.b and d) were earlier described as strengthening the bond. Here it is seen that the DI of these orbitals have positive values showing that they increase the sharing of the electrons across these atomic basins. On the other hand, the antibonding orbitals χ^{25} and χ^{30} (Figure 2.c and e) were said to weaken the bond. These orbitals have negative DI values, indicating that the delocalisation is decreased and less sharing of electrons is taking place. The non-bonding orbital χ^{22} (Figure 2.a) was said to not participate and here has a DI of 0.000 a.u. which confirms that it has no influence on the covalent bond order.

This approach also enables the determination of the dominant mode of bonding as either exchange dominated (covalent model) or Coulomb dominated (donor-acceptor model). A high DI (near 1 electron or 50% occupation of the MO) is indicative of a covalent interaction. The polarity of the bond can be identified by the LI on each atomic basin per MO. Equal LIs for each atomic basin with a high DI suggests a non-polar covalent bond. If one atomic basin has a higher LI the electrons will tend towards that atomic basin. Coulomb dominated interactions

are seen to have low DI values with high LI values on either of the atomic basins. A perfect non-polar covalent bond would thus have $LI(\mathrm{A}) = LI(\mathrm{B})$ and $DI(\mathrm{A},\mathrm{B}) = 2 \times LI(\mathrm{A})$.

Table 1. Localised index of MOs for Ti1, C2 and delocalised index of Ti1—C2 interaction given for $TiCl_2CH_2$.

Orbital	LI(Ti1)	LI(C2)	DI(Ti1,C2)
$\chi^1 - \chi^{20}$	17.804	2.025	0.058
χ^{21}	0.008	0.001	0.001
χ^{22}	0.014	0.000	0.000
χ^{23}	0.023	0.944	0.096
χ^{24}	0.006	0.465	0.054
χ^{25}	0.042	0.005	-0.001
χ^{26}	0.035	0.055	-0.004
χ^{27}	0.089	0.141	0.200
χ^{28}	0.012	0.000	0.001
χ^{29}	0.015	0.000	0.003
χ^{30}	0.002	0.007	-0.003
χ^{31}	0.130	0.522	0.444
χ^{32}	0.334	0.591	0.872
Total	18.515	4.707	1.720

The titanium and carbon occupations make up most of the orbital χ^{32} occupation (0.334e^- for electrons localised on titanium, 0.591e^- for electrons localised on carbon and 0.872e^- for electrons delocalised between titanium and carbon giving 89.9% of the total orbital occupation, Table 1). Therefore, this orbital can be described as a predominantly covalent bonding orbital for the carbene bond with additional polarisation of the density towards the carbon atom.

The chloride ligands make up about two thirds of the electron occupation for χ^{27} (with 0.657 localised electrons per chloride ligand, Table D5). The carbon atom also has a larger part of the occupation (0.141e^-, Table D5). There is an exchange interaction between the titanium atom and the carbon atom (0.200e^-, Table D5), but since this interaction makes up much less than one electron (or 50% of the total orbital occupation) this interaction is not dominated by the covalent contribution (nature). This is further illustrated by the total localised occupation (1.568e^- computed for χ^{27}) far outweighing the total delocalised occupation (0.432e^-) computed for this orbital.

The $TiCl_2CH_2$ complex is classified as a Schrock carbene with the assumption that the carbene bond will be made up by a covalent σ-bond and a covalent π-bond. This suggests that there should be two Ti—C interactions with delocalised occupations near one, but it is observed that there is only one such MO (χ^{32} with π-symmetry, Figure 2.d). There are, however, two

additional MOs with delocalised occupations that are higher than the rest, χ^{27} and χ^{31} (Figure 4 and Figure 2.b). Inspection of the orbital isosurfaces shows these orbitals to be σ-symmetric with respect to the titanium-carbon bond, but the occupations of these orbitals for this specific interaction does not indicate a high degree of covalency for either of these orbitals. Instead, χ^{31} has a much greater occupation for the electrons localised to the carbon atom, along with this is a high occupation of electrons localised to the chloride ligands for this orbital. The exchange interaction of the Ti—Cl interaction for χ^{31} is antibonding, but the high localised occupations for the ligand atoms suggest that this orbital takes part in ligand-to-metal electron donation to form a dative σ-bonding orbital. A similar trend exists for χ^{27}, but it is more localised to the chloride ligands, whereas χ^{31} has more electrons localised to the carbon atom.

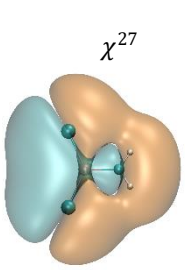

Figure 4. Isosurface of χ^{27} showing σ-symmetric bonding nature for the Ti-C interaction at isovalue of 0.001a.u.

Trends in major orbitals for titanium Schrock carbenes with structural changes

This section looks at the four structures given in Figure 5 by applying the decomposition of MOs into localised and delocalised densities. Each structure studied had the general formula of TiL_2CHR where L = Cl, Cp with Cp = C_5H_5 and R = H, CH_3 (see Figure 5).

The delocalisation index of the titanium-carbon interaction for each compound (Table 2) shows that changing the carbene ligand (R = H or R = CH_3) has only a small effect on the carbene interaction. The larger carbene ligand (R = CH_3) has a lower DI, with electrons being more delocalised within the ligand itself. However, a large decrease in the titanium-carbene carbon DI is obtained when changing the ligands on the metal atom (L = Cl to L = Cp). For L = Cl, the carbene interaction has around 1.7 electrons being shared between the titanium and carbon in an exchange fashion (covalent bonding). Considering that this is representative of the resonance structures of the systems, a DI value near two is indicative of a covalent double bond character. For L = Cp, the carbene interaction has a much lower DI value near 1.3. This

indicates a large decrease in the covalent nature of the bonding.

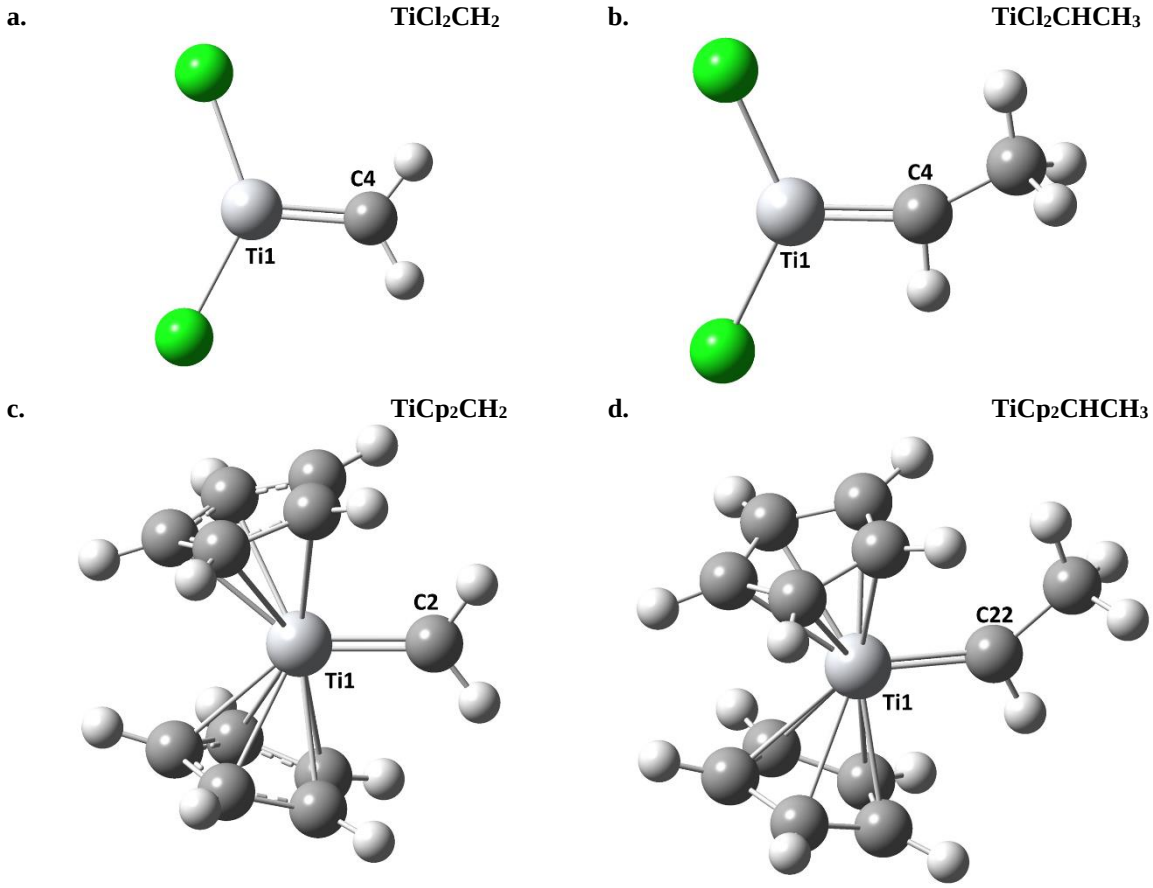

Figure 5. Structures studied in this chapter with the labelling on the atoms of interest.

These titanium-carbon interactions can be decomposed (Table D7). The three major orbitals which make up the carbene interaction for each structure are given in Table 3. This allows one to study the interaction in greater depth and obtain more representative descriptions of the mode of bonding which plays the dominate role in Schrock carbene complexes. For each system the orbital with the highest occupation of the delocalised component is a π-symmetric orbital (first row in Figure 6) with respect to the carbene bond with the other two orbitals being σ-symmetric orbitals with respect to the carbene bond (Figure 6). For all the orbitals the LI(C) is greater than LI(Ti), indicating that the electrons of the carbene bond are polarised towards the carbon.

For L = Cl the DI(Ti,C) of the highest occupied molecular orbital (HOMO) approach 1 electron, suggesting that the π-orbitals have covalent natures. For L = Cp, the DI(Ti,C) is lower, which suggests a less covalent nature for this ligand. When R = H there is an additional orbital with a DI(Ti,C) of 0.444e^- which, although still donor-acceptor dominated with a large LI(C),

shows a high degree of covalent nature. A similar observation can be made when R = CH_3, with the values being lower for this more complex ligand.

Table 2. Delocalisation index of titanium-carbon interaction for the carbene bond.

Compound	DI(Ti,C)
$TiCl_2CH_2$	1.720
$TiCl_2CHCH_3$	1.672
$TiCp_2CH_2$	1.377
$TiCp_2CHCH_3$	1.325

For each of the systems studied one of the σ-orbitals has a remarkably low LI(Ti) with a much higher LI(C). This suggests that the σ-bond rather forms from a donor-acceptor model view with the orbital being polarised towards the carbon atom.

Table 3. LIs of Ti and C atoms and DI of Ti-C interaction of the major orbitals for the various structures studied with L = Cl, Cp and R = H, CH_3.

Compound	Orbital	LI(Ti)	LI(C)	DI(Ti,C)
$TiCl_2CH_2$	χ^{32}	0.334	0.591	0.872
	χ^{31}	0.130	0.522	0.444
	χ^{27}	0.089	0.141	0.200
$TiCl_2CHCH_3$	χ^{36}	0.367	0.480	0.795
	χ^{35}	0.112	0.450	0.378
	χ^{25}	0.026	0.549	0.104
$TiCp_2CH_2$	χ^{50}	0.243	0.542	0.687
	χ^{47}	0.025	0.274	0.102
	χ^{45}	0.162	0.447	0.444
$TiCp_2CHCH_3$	χ^{54}	0.286	0.433	0.648
	χ^{52}	0.055	0.409	0.233
	χ^{49}	0.100	0.143	0.186

Visually, the orbital isosurfaces (Figure 6) compare well between the various structures. The HOMOs are all π-symmetric and the other two identified orbitals are of σ-symmetry. It can be seen that the isosurfaces show the orbitals to extend to the ancillary ligands. For each orbital the sum of all LI and DI values should equal 2, since a restricted, closed-shell wavefunction is being used. The majority of the unaccounted electrons for the σ-orbitals come from the ancillary ligands (Table D8).

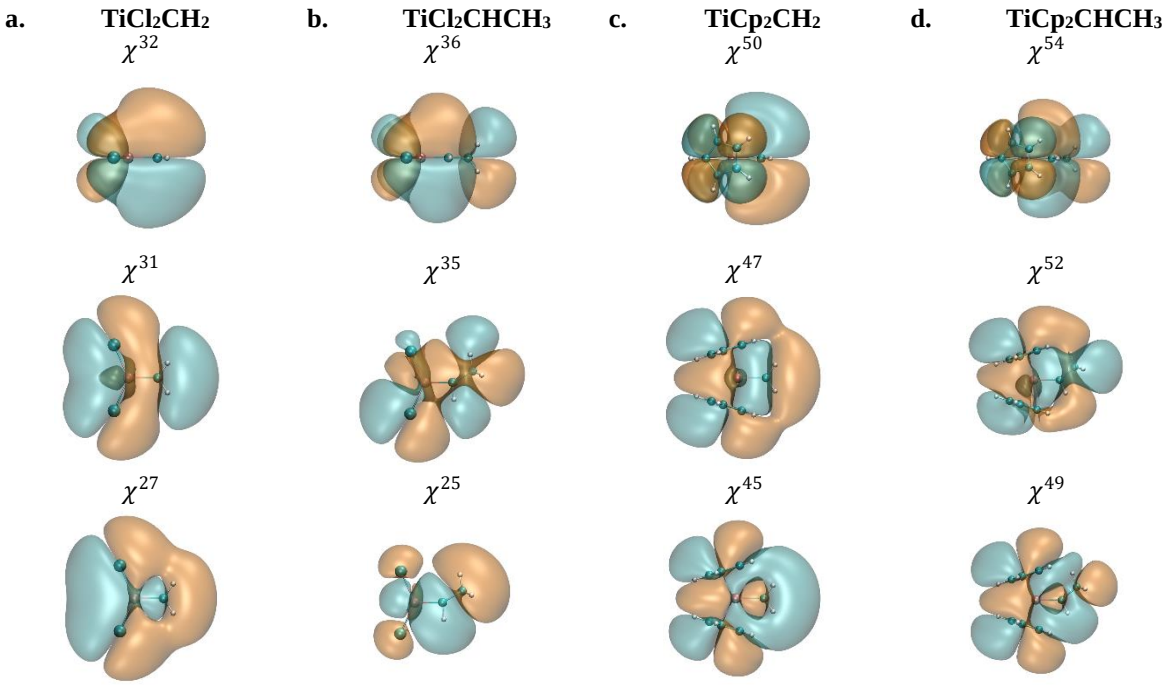

Figure 6. The isosurfaces of the major orbitals identified for the carbene bond at isovalue of 0.001a.u. for each of the compounds studied.

Although the greatest occupations occur for the orbitals represented in Figure 6, it is noted that all the orbitals show similar structures across the range of systems with the exception of χ^{25} on the $TiCl_2CHCH_3$ system. There is however another orbital (χ^{31}, Figure 7) which appears visually similar to the orbital χ^{27} on $TiCl_2CH_2$, but was not identified as having one of the highest DI(Ti,C) values. Although, this orbital conforms with the other trends identified in the various structures. Seemingly polarisation from the lack of symmetry skewed the generalised description of the bonding for $TiCl_2CHCH_3$. This highlights the importance of maintaining a holistic view of the bonding, especially in asymmetric systems.

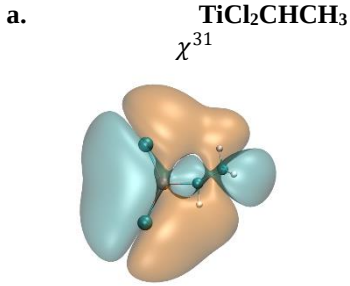

Figure 7. Isosurface for MO on $TiCl_2CHCH_3$ that shows great similarity to that on $TiCl_2CH_2$.

Conclusion

This work has shown that the $TiCl_2CH_2$ system consists of a covalent π-orbital and two separate σ-orbitals both of a donor-acceptor nature. This result is similar to the results obtained by Cundari and Gordon,[10] with the extension of identifying more orbitals that are contributing to the nature of the bond. This is possible since the method applied here did not include multiconfigurational studies and could thus be performed on the full occupation matrix.

Quantitative measures were produced for the bond order of specific interactions allowing the identification of bonding, antibonding and non-bonding interactions which stabilise a chemical bond. This shows potential use in catalyst design where specific interactions are to be favoured and others disfavoured. For instance, specific case studies should reveal which interactions lead to catalyst poisoning and thus allows one to identify the orbitals involved as well as the atoms involved. The chemist would therefore have access to information that can guide the improved design of catalysts by altering specific atoms and consequently know which MOs would be influenced by doing so.

The studies on the various carbene complexes presented in the last section show the importance of the other ligands on the metal and how these can have a significant impact on the nature of the carbene bond. This shows the presence of a long-range ligand-ligand interaction which plays a major role in stabilising the system similar to the results presented by Cundari and Gordon.[11]

The point is brought forward regarding the difference between transition metal Schrock and Fischer carbene complexes in terms of the bonding patterns observed for each. It is suggested that bonding in these two classes of organometallic carbene complexes can be better classified according to the environment that the atoms are in. Simply considering what atoms are bonded to the metal and carbon atoms is clearly not sufficient to accurately describe the bonding in these complexes.

References

1. Bader, R. F.; Stephens, M. E. *J. Am. Chem. Soc.* **1975**, 97(26), 7391-7399.

2. Matta, C. F.; Boyd, R. J.; Becke, A. The Quantum Theory of Atoms in Molecules: From Solid State to DNA and Drug Design; Wiley, **2007**.

3. Ponec, R. *J. Math. Chem.* **1997**, 21(3), 323-333.

4. Ponec, R. *J. Math. Chem.* **1998**, 23(1-2), 85-103.

5. De Lange, J. H.; Cukrowski, I. *J. Comput. Chem.* **2017**, 38(13), 981-997.

6. de Lange, J. H.; Cukrowski, I. *J. Comput. Chem.* **2018**, 39(20), 1517-1530.

7. Bader, R. F. W. Atoms in Molecules : a Quantum Theory; Clarendon Press: Oxford, **1990**.

8. Levy Nahum, T.; Mamlok-Naaman, R.; Hofstein, A.; Taber, K. S. *Sci. Educ.* **2010**, 46(2), 179-207.

9. Bader, R.; Nguyen-Dang, T. T.; Tal, Y. *Rep. Prog. Phys.* **1981**, 44(8), 893.

10. Cundari, T. R.; Gordon, M. S. *J. Am. Chem. Soc.* **1991**, 113(14), 5231-5243.

11. Cundari, T. R.; Gordon, M. S. *J. Am. Chem. Soc.* **1992**, 114(2), 539-548.

12. Cundari, T. R.; Gordon, M. S. *Organometallics* **1992**, 11(1), 55-63.

13. Gordon, M. S.; Cundari, T. R. *Coord. Chem. Rev.* **1996**, 147, 87-115.

14. Chung, G.; Gordon, M. S. *Organometallics* **2003**, 22(1), 42-46.

15. Sax, A. F. *J. Comput. Chem.* **2012**, 33(17), 1495-1510.

16. Weinhold, F.; Landis, C. R.; Press, C. U. Valency and Bonding: A Natural Bond Orbital Donor-Acceptor Perspective; Cambridge University Press, **2005**.

17. Mulliken, R. S. *Science* **1967**, 157, 13.

18. Hirshfeld, F. L. *Theor. Chim. Acta* **1977**, 44(2), 129-138.

19. de Lange, J. H.; van Niekerk, D. M.; Cukrowski, I. *Phys. Chem. Chem. Phys.* **2019**, 21(37), 20988-20998.

20. Frisch, M. J.; Trucks, G. W.; Schlegel, H. B.; Scuseria, G. E.; Robb, M. A.; Cheeseman, J. R.; Scalmani, G.; Barone, V.; Mennucci, B.; Petersson, G. A.; Nakatsuji, H.; Caricato, M.; Li, X.; Hratchian, H. P.; Izmaylov, A. F.; Bloino, J.; Zheng, G.; Sonnenberg, J. L.; Hada, M.; Ehara, M.; Toyota, K.; Fukuda, R.; Hasegawa, J.; Ishida, M.; Nakajima, T.; Honda, Y.; Kitao, O.; Nakai, H.; Vreven, T.; Montgomery, J. A. J.; Peralta, J. E.; Ogliaro, F.; Bearpark, M.; Heyd, J. J.; Brothers, E.; Kudin, K. N.; Staroverov, V. N.; Keith, T.; Kobayashi, R.; Normand, J.; Raghavachari, K.; Rendell, A.; Burant, J. C.; Iyengar, S. S.; Tomasi, J.; Cossi, M.; Rega, N.; M. Millam, J. M.; Klene, M.; Knox, J. E.; Cross, J. B.; Bakken, V.; Adamo, C.; Jaramillo, J.; Gomperts, R.; Stratmann, R. E.; Yazyev, O.; Austin, A. J.; Cammi, R.; Pomelli, C.; Ochterski,

J. W.; Martin, R. L.; Morokuma, K.; Zakrzewski, V. G.; Voth, G. A.; Salvador, P.; Dannenberg, J. J.; Dapprich, S.; Daniels, A. D.; Farkas, O.; Foresman, J. B.; Ortiz, J. V.; Cioslowski, J.; Fox, D. J. In Gaussian09, Revision D01: Wallingford CT, **2009**.

21. Keith, T. A.; TK Gristmill Software: Overland Park KS, USA, **2016**.

22. Humphrey, W.; Dalke, A.; Schulten, K. *J. Mol. Graph.* **1996**, 14(1), 33-38.

23. Outeiral, C.; Vincent, M. A.; Pendás, Á. M.; Popelier, P. L. *Chem. Sci.* **2018**, 9(25), 5517-5529.

Chapter Seven

Conclusions

Introduction

In the preceding chapters various quantum chemical tools were utilized in the study of four titanium Schrock carbene complexes. This work studied the metal-carbon bonding in order to gain insights which can be generalised to develop notions suggested on the nature of carbene bonding suggested since the 1990's.[1-3] This work suggested that transition metal Schrock and Fischer carbene complexes are not completely different in terms of the bonding patterns observed for each. The classification of complexes as Fischer- or Schrock-type in terms of the presence of heteroatoms on the carbene carbon was shown to be insufficient. This classification should rather be made according to the environment that the atoms are in.

In final conclusion, this work highlighted three aspects of carbene bonding, (i) the degree of σ- and π-bonding in the complexes, (ii) the effects of delocalisation on the complexes and the bonding, (iii) the role of metal core densities on the electronic structure, and also suggested a novel approach to determine bond orders in organometallic carbene complexes.

The goal of this research was to lay the theoretical groundwork for future developments in the field of chemistry, both theoretically and experimentally. It is hoped that the insights gained from this work will guide the development of not only organometallic carbene chemistry, but also the wider fields of inorganic and organic chemistry. It is the author's wishes to extend these approaches in the future, with a focus on catalyst design for the vital role that catalysis plays in all of chemistry and life.

The degree of σ- and π-bonding in the complexes

Group theory provides a means to determine the symmetry of the bonding in complexes, but insightful analysis is restricted to systems where the point group is of higher symmetries. Contrary to this, the analysis of the orbital isosurfaces by inspection can provide insights without the mathematical difficulties. However, interpretations of the orbital isosurfaces can be easily misinterpreted as the quantum nature of the electron is unintuitive.

The cross-section analysis provided in chapters three and four could characterise the orbital and electron densities in terms of σ- and π-symmetry. Furthermore, it could give the relative contribution of each orbital or electron density to the overall interaction which reduced complex quantum mechanical descriptions to simple σ- and π-symmetric interactions that chemists know well.

The effects of delocalisation on the complexes and the bonding

There is clear evidence of the existence of a long-range ligand-ligand interaction which contributed a significant portion of the stabilisation of the carbene interaction. This is due in part to a σ-delocalisation through the bonds (*inductive effect*) already established in the complex and is noted to be largely dependent on the structures present in the complex. This interaction had been noted in previous literature[1-4] and was further studied in this work. The methods employed in the previous studies were too computationally expensive to study the interaction extensively whereas the methods presented in this work allowed for a computationally inexpensive manner to gain equivalent insights.

This long-range ligand-ligand interaction and the role that it plays in the stabilisation of the carbene interaction can be utilised in the design of catalysts,[4] such as those presented in chapter one. Since these methods allow for a quantitative characterisation of this interaction it can be used to fine-tune catalyst specific requirements.

The role of metal core densities on the electronic structure

In various parts of this work it was noted that core densities made noteworthy contributions to the carbene bond. Although a full study of this effect is outside the scope of the current work it deserves to be mentioned. The influence of core density on the electronic structures of transition metal complexes was studied and reported on in previous literature,[3] but was dependent on multiconfigurational studies which impeded the progress and extent of complexes that could be studied. The tools provided by the current work can be used to further investigate the influence that core densities have on the carbene bond as well as on the bonding in other transition metal complexes.

A novel approach to determine bond orders in carbene complexes

Various approaches to determine bond orders were presented in this work, each with different aspects of bonding being highlighted, either symmetry, fragment-based interactions, atomistic-orbital-based descriptions or electron delocalisation. Each approach provided unique insights and the author strongly suggests their use in conjunction with each other, rather than debating which is regarded as the best.

The approach suggested in chapters three and four highlighted the symmetry of interactions and was able to provide relative quantification of the symmetries. Although it did not provide an absolute bond order, it was used to gain insights of the important factors to consider when studying a specific interaction or bond.

Chapter five presented an approach based on fragments which can be arbitrarily defined. This provided a bond order based on the delocalised density between fragments. Fragment-based descriptions are especially useful to the chemist investigating the influence of ligands or clusters on bonding without the need to look into each interaction for every atom in the molecule under investigation.

The final approach suggested in chapter six attempted to retain information from various different methods and combine them into a single presentation. This approach gave the orbitals associated with an interaction and the electrons shared in order to obtain localisation and delocalisation indices per atom per molecular orbital. The widespread distribution of the orbitals between various atoms shows the chemist which parts of the structure are correlated while the decomposed delocalised index provided a quantitative measure of the extent to which the atoms are interacting.

Suggestions for future work

The nature of carbene interactions should not be classified into general groups, but rather according to the collective structure of the complex as a whole. This work illustrated that the bonding nature of the M—C interaction can vary for structures classically considered to be very similar. When studied these interactions revealed colourful natures based on the overall effects of each ligand and the metal. This should be further studied on a wider variety of carbene structures, ancillary ligands and metal species to gain a descriptive picture of the electronic structure changes associated with these groups, especially cases where Schrock-type and Fischer-type carbene complexes can be contrasted.

A useful development on this work would be to implement a surface integral on the cross-sections presented in chapter three and four such that the entire interatomic surface can be studied as this would reveal δ-symmetric interactions. In general, this might seem redundant to a chemist, but complex ligands could form symmetry adapted orbitals with a δ-symmetry and hence could pose an additional mode of bonding which have hereto not been investigated

extensively nor reported on much in the literature.

It should be noted that mathematically there seems no fault in constructing fragment-based atomic overlap matrices by adding together the atomic overlap matrices of atomic basins constituting the fragments. Further computations can be performed on these fragment overlap matrices. However, the software utilized in this work did not follow this logic, therefore this logic was not reported here. In theory all properties calculated from the integration of atomic basins should be additive. There seems to be no logical fault in the approach taken in this work, but setting up fragment overlap matrices could provide algorithmic optimization for large structures where computation of each diatomic interaction becomes resource intensive. The alternative method proposed will be investigated in future work as it does hold further conceivable value in the interpretation of the NDFs that would be produced for these fragments.

On the method presented in chapter six additional developments could be implemented as a calculation of the correlation between different orbitals or interactions. Preliminary calculations had been performed at the time of writing this work which suggested value in such an approach toward quantifying the correlation between various parts of the structure.

Lastly, developments in fragment-based analyses are encouraged as these make the interpretation of the related chemistry more intuitive and also allows the generalisation of bonding models developed.

References

1. Cundari, T. R.; Gordon, M. S. *J. Am. Chem. Soc.* **1991**, 113(14), 5231-5243.
2. Cundari, T. R.; Gordon, M. S. *J. Am. Chem. Soc.* **1992**, 114(2), 539-548.
3. Gordon, M. S.; Cundari, T. R. *Coord. Chem. Rev.* **1996**, 147, 87-115.
4. Cundari, T. R.; Gordon, M. S. *Organometallics* **1992**, 11(1), 55-63.

Appendix A

Supplementary information for chapter three

Characterization of bonding modes in metal complexes through electron density cross-sections

Shane de Beer, Ignacy Cukrowski, Jurgens H. de Lange*

Department of Chemistry, Faculty of Natural and Agricultural Sciences, University of Pretoria, Lynnwood Road, Hatfield, Pretoria 0002, South Africa

* Correspondence to Jurgens H. de Lange

E-mail: jurgens.delange@up.ac.za

Supplementary information

Table of Contents **Page**

Part 1 – XYZ Coordinates of optimized geometries

Table S1. Molecule specification of $TiCl_3^+$

Atom	X	Y	Z
Ti1	0.000000	0.000000	0.000000
Cl2	0.000000	2.124531	0.000000
Cl3	1.839897	–1.062265	0.000000
Cl4	–1.839897	–1.062265	0.000000

Molecular energy: –2 230.010 924 a.u.

Table S2. Molecule specifications for $TiCl_2CHCH_3$

Atom	X	Y	Z
Ti1	0.000000	0.000000	0.000000
Cl2	0.000000	0.000000	2.260269
Cl3	1.666685	0.000000	–1.485007
C4	–1.653807	0.000460	–0.770724
H5	–2.190643	0.000070	0.204580
C6	–2.524076	0.002542	–1.983932
H7	–3.175511	–0.880065	–2.003707
H8	–3.179885	0.881978	–1.997676
H9	–1.933308	0.006993	–2.902276

Molecular energy: –1 848.652 391 a.u.

Part 2 – Supplementary Data for $TiCl_3^+$

The titanium valence atomic orbitals are given in Figure S1.

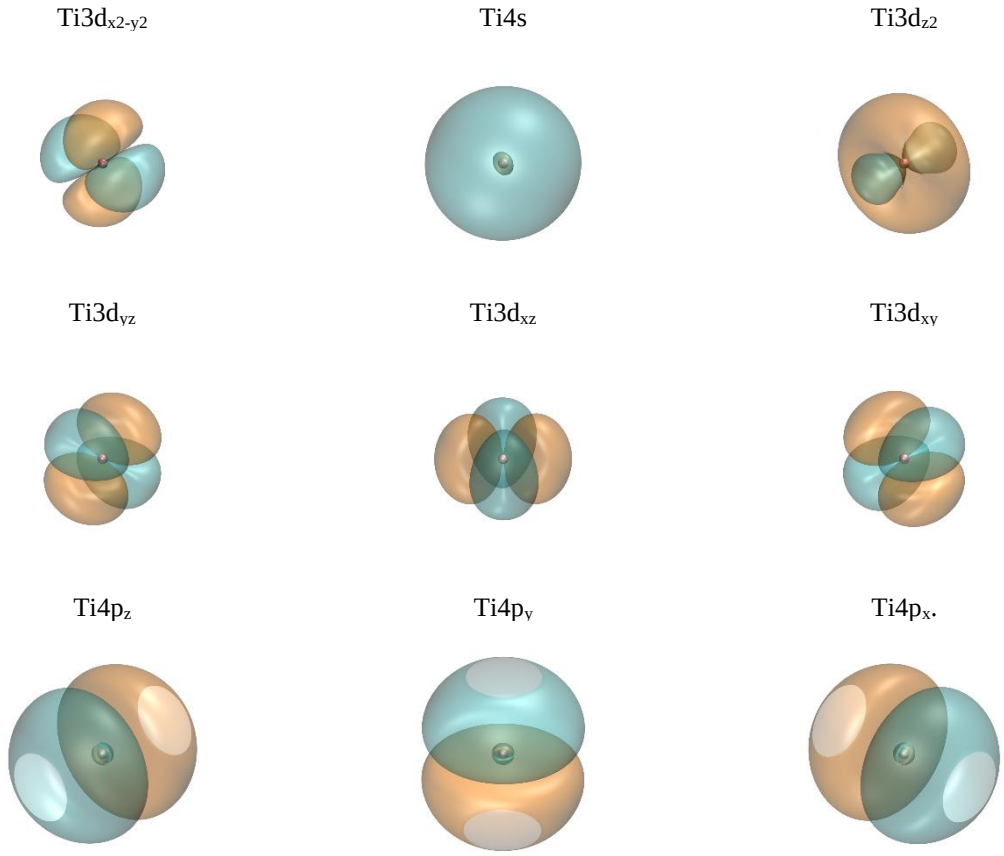

Figure S1. Atomic orbitals on central titanium atom in D_{3h} point group symmetry system. a.

The ligand orbitals are combined as a linear combination of symmetry adapter (SALC) orbitals from which the symmetries are relabelled according to the D_{3h} point group symmetry. The valence Cl_3-ligand SALCs are given in Figure S2. with their symmetry labels and calculated energies according to DFT-B3LYP level of theory using a 6–311++G(d,p) basis set in gas phase. The coordinates of the atoms were the same as the chlorine atoms in Table S1

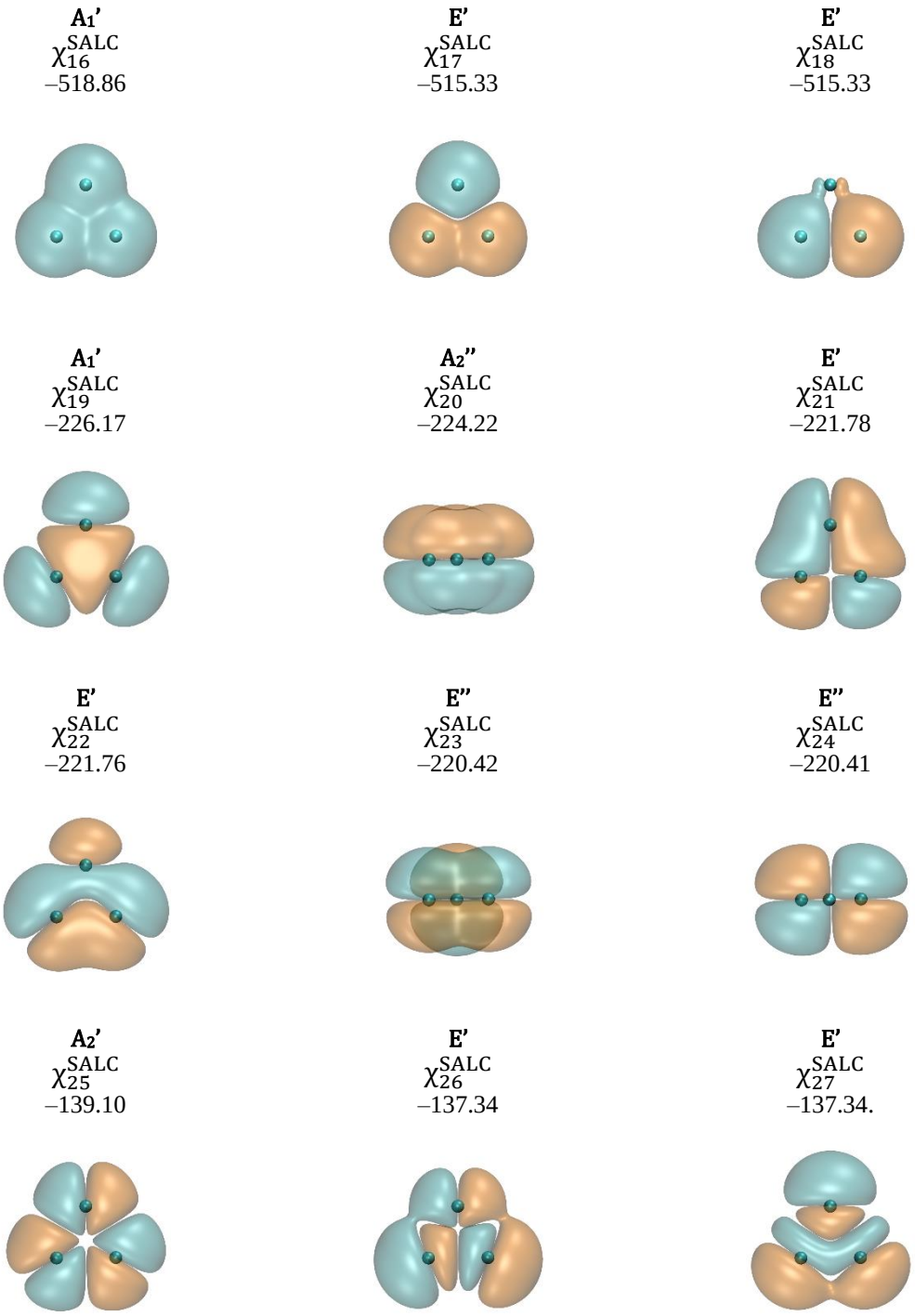

Figure S2. Symmetry adapted orbitals for Cl_3 ligands in D_{3h} point group symmetry. The orbitals are labelled as follows with orbital label, symmetry label and orbital energy (in kcal/mol).

The valence molecular orbital isosurfaces for the $TiCl_3^+$ system is given in Figure S3. with their symmetry labels and orbital energies.

A₁'
χ_{25}^{MO}
–659.62

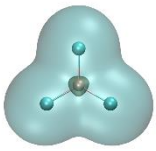

E'
χ_{26}^{MO}
–652.39

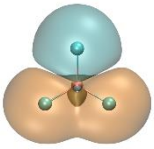

E'
χ_{27}^{MO}
–652.39

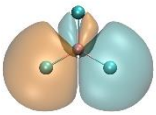

A₁'
χ_{28}^{MO}
–392.90

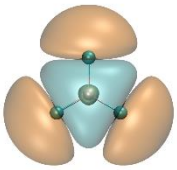

E'
χ_{29}^{MO}
–387.22

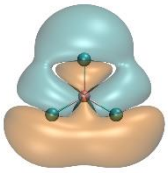

E'
χ_{30}^{MO}
–387.22

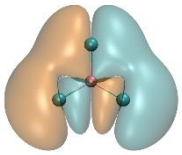

E''
χ_{31}^{MO}
–366.19

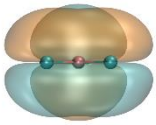

E''
χ_{32}^{MO}
–366.19

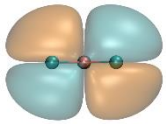

E'
χ_{33}^{MO}
–359.98

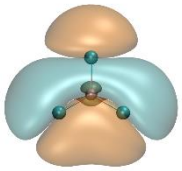

E'
χ_{34}^{MO}
–359.98

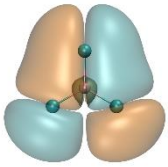

A₂''
χ_{35}^{MO}
–356.88

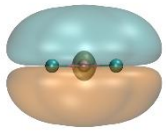

A₂'
χ_{36}^{MO} (HOMO)
–342.51

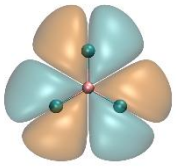

A₁'
χ_{37}^{MO} (LUMO)
–248.90

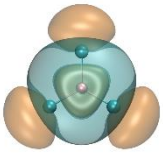

E''
χ_{38}^{MO}
–238.94

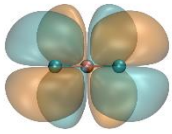

E''
χ_{39}^{MO}
–238.94

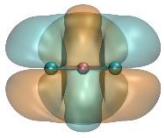

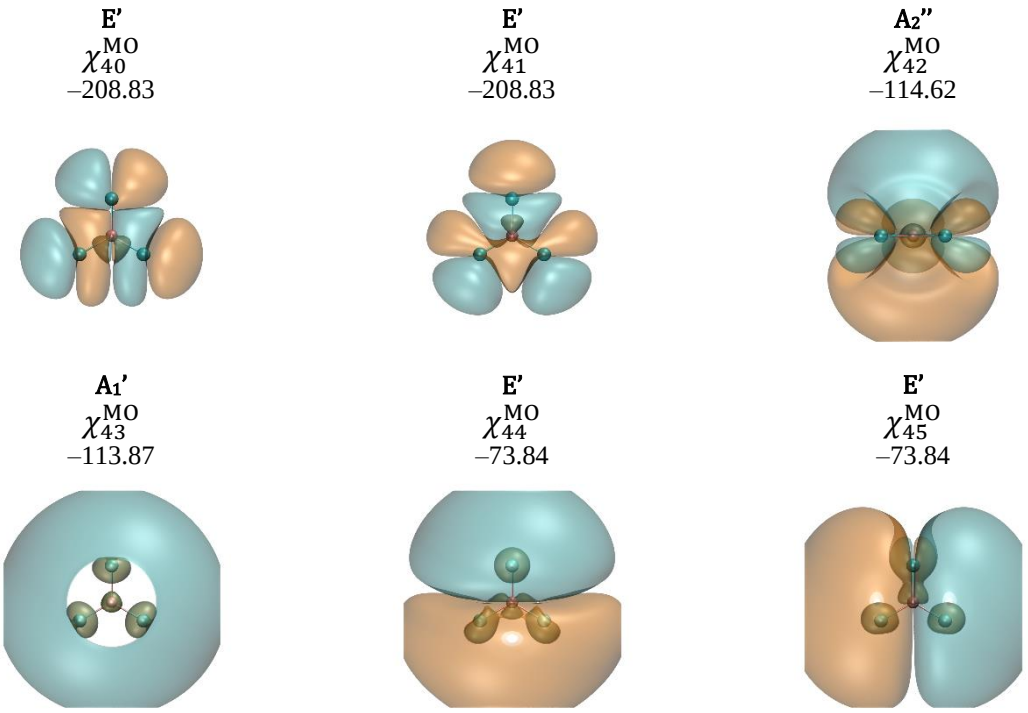

Figure S3. Canonical molecular orbitals for $TiCl_3^+$ in D_{3h} point group symmetry. The orbitals are labelled as follows with orbital label, symmetry label and orbital energy (in kcal/mol)

The cross section for $TiCl_3^+$ for the major MO contributions is given in Figure S4.

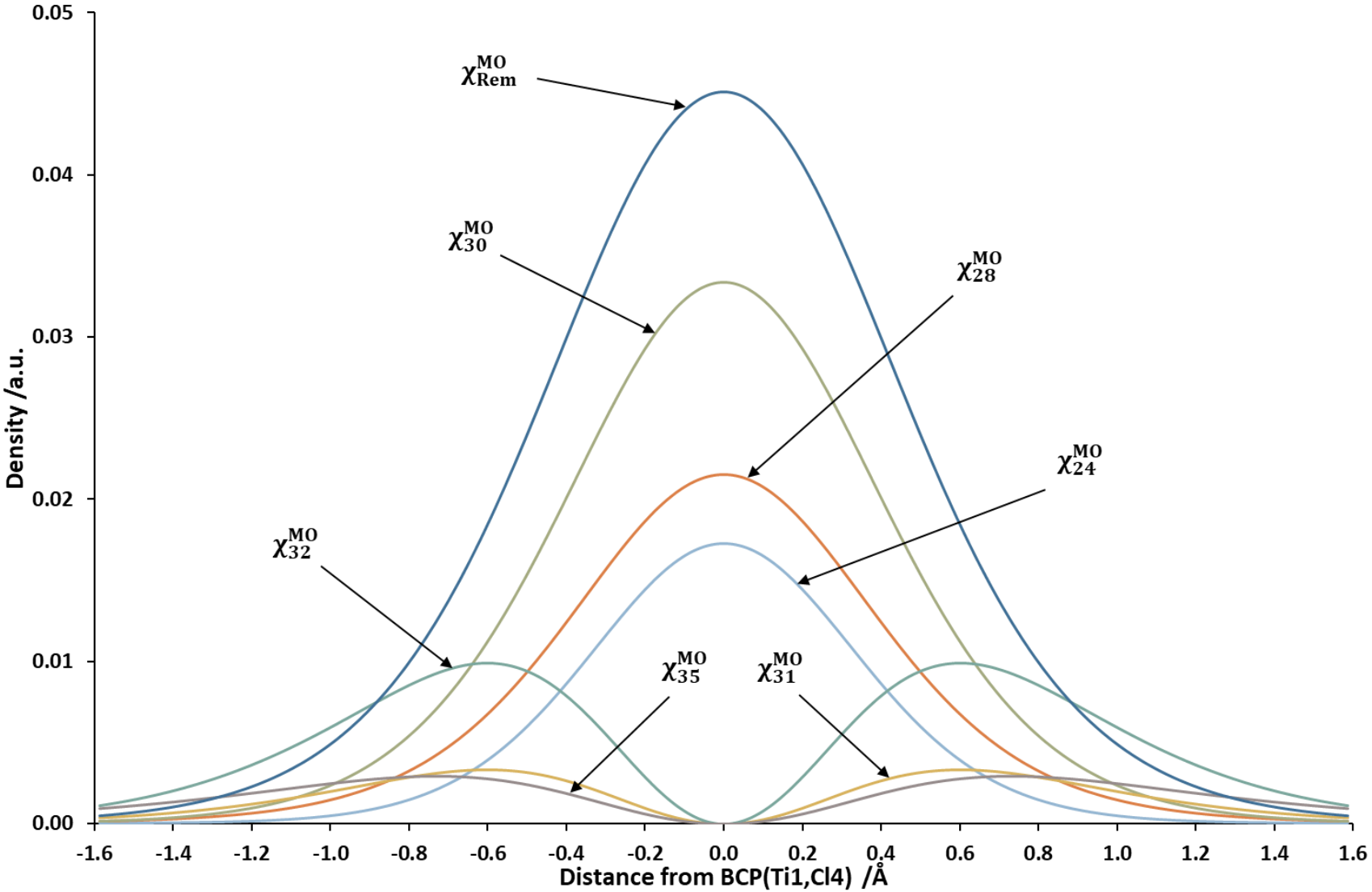

Figure S4. MO cross-section for $TiCl_3^+$ showing relative contributions from major MOs.

The electron densities and their relative percentage contributions to the total electron density of the $TiCl_3^+$ system along the λ_1– and λ_2–eigenvectors are given in Table S3. as is per molecular orbital.

Table S3. MO integrated cross section dataset

Molecular Orbital	Symmetry label	$\rho_{\lambda 1}^{sum}(\boldsymbol{r})$	$\%\rho_{\lambda 1}^{sum}(\boldsymbol{r})$	$\rho_{\lambda 2}^{sum}(\boldsymbol{r})$	$\%\rho_{\lambda 2}^{sum}(\boldsymbol{r})$
MO10	E'	0.000001	0.00%	0.000001	0.00%
MO11	A_1'	0.000001	0.00%	0.000001	0.00%
MO12	E'	0.000003	0.00%	0.000003	0.00%
MO13	E'	0.000001	0.00%	0.000001	0.00%
MO14	A_1'	0.000002	0.00%	0.000002	0.00%
MO21	A_1'	0.007386	2.56%	0.007457	2.61%
MO22	A_2"	0.000000	0.00%	0.004171	1.46%
MO23	E'	0.012537	4.35%	0.009500	3.32%
MO24	E'	0.029412	10.20%	0.028500	9.97%
MO25	A_1'	0.018454	6.40%	0.016428	5.74%
MO26	E'	0.006513	2.26%	0.006671	2.33%
MO27	E'	0.018825	6.53%	0.020014	7.00%
MO28	A_1'	0.053970	18.72%	0.041099	14.37%
MO29	E'	0.035784	12.42%	0.021822	7.63%
MO30	E'	0.060594	21.02%	0.065465	22.89%
MO31	E"	0.000000	0.00%	0.010440	3.65%
MO32	E"	0.000000	0.00%	0.031319	10.95%
MO33	E'	0.021446	7.44%	0.003053	1.07%
MO34	E'	0.017660	6.13%	0.009159	3.20%
MO35	A_2"	0.000000	0.00%	0.010880	3.80%
MO36	A_2'	0.005634	1.95%	0.000000	0.00%

The electron densities and their relative percentage contributions to the total electron density of the $TiCl_3^+$ system along the λ_1– and λ_2–eigenvectors are given in Table S4. as is after grouping together all molecular orbital densities of the same symmetry.

Table S4. grouped data set for MO integrated cross section

Symmetry	$\rho_{\lambda 1}^{sum}(\boldsymbol{r})$	$\%\rho_{\lambda 1}^{sum}(\boldsymbol{r})$	$\rho_{\lambda 2}^{sum}(\boldsymbol{r})$	$\%\rho_{\lambda 2}^{sum}(\boldsymbol{r})$
A_1'	0.079814	27.69%	0.064987	22.72%
A_2'	0.005634	1.95%	0.000000	0.00%
A_2"	0.000000	0.00%	0.015051	5.26%
E'	0.202779	70.35%	0.164190	57.41%
E"	0.000000	0.00%	0.041759	14.60%

The electron densities and their relative percentage contributions to the total electron density of the $TiCl_3^+$ system along the λ_1– and λ_2–eigenvectors are given in Table S5. as is per natural bond orbital.

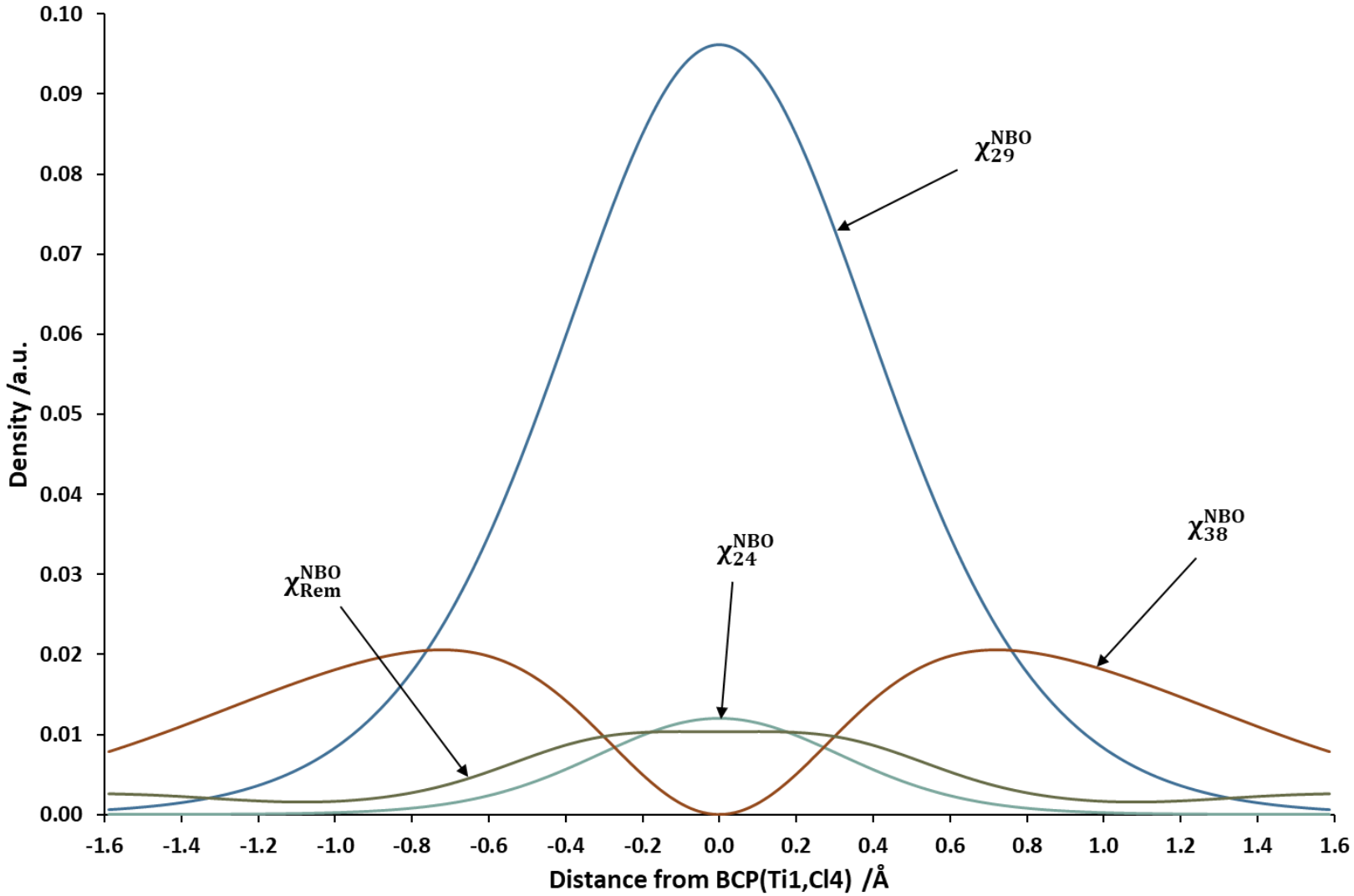

Figure S5. NBO Cross section for $TiCl_3^+$

Table S5. NBO dataset for integrated cross section

NBO	$\rho_{\lambda 1}^{sum}(\boldsymbol{r})$	$\%\rho_{\lambda 1}^{sum}(\boldsymbol{r})$	$\rho_{\lambda 2}^{sum}(\boldsymbol{r})$	$\%\rho_{\lambda 2}^{sum}(\boldsymbol{r})$
NBO5	0.000022	0.01%	0.000022	0.01%
NBO6	0.000000	0.00%	0.000006	0.00%
NBO7	0.000034	0.01%	0.000033	0.01%
NBO8	0.000015	0.01%	0.000011	0.00%
NBO9	0.001406	0.56%	0.001424	0.44%
NBO10	0.000004	0.00%	0.000002	0.00%
NBO11	0.000004	0.00%	0.000002	0.00%
NBO13	0.000000	0.00%	0.000019	0.01%
NBO15	0.000005	0.00%	0.000000	0.00%
NBO16	0.000006	0.00%	0.000000	0.00%
NBO17	0.000062	0.02%	0.000058	0.02%
NBO18	0.000034	0.01%	0.000019	0.01%
NBO19	0.000003	0.00%	0.000000	0.00%
NBO20	0.000003	0.00%	0.000001	0.00%
NBO21	0.003153	1.25%	0.003065	0.94%
NBO22	0.000000	0.00%	0.003383	1.04%
NBO23	0.008613	3.40%	0.006319	1.94%
NBO24	0.019560	7.73%	0.018956	5.83%
NBO25	0.004332	1.71%	0.004796	1.48%
NBO26	0.000335	0.13%	0.000216	0.07%
NBO27	0.000334	0.13%	0.000215	0.07%
NBO28	0.003434	1.36%	0.000006	0.00%
NBO29	0.195581	77.27%	0.195827	60.24%
NBO30	0.003428	1.35%	0.000006	0.00%
NBO31	0.000000	0.00%	0.000003	0.00%
NBO32	0.000000	0.00%	0.000388	0.12%
NBO34	0.000449	0.18%	0.000399	0.12%
NBO35	0.008576	3.39%	0.000000	0.00%
NBO36	0.000449	0.18%	0.000399	0.12%
NBO37	0.000000	0.00%	0.002925	0.90%
NBO38	0.000000	0.00%	0.080852	24.87%
NBO39	0.000000	0.00%	0.002629	0.81%
NBO42	0.000002	0.00%	0.000002	0.00%
NBO54	0.000001	0.00%	0.000000	0.00%
NBO57	0.000001	0.00%	0.000000	0.00%
NBO59	0.000006	0.00%	0.000003	0.00%
NBO62	0.000000	0.00%	0.000009	0.00%
NBO73	0.000010	0.00%	0.000003	0.00%
NBO76	0.000015	0.01%	0.000094	0.03%
NBO78	0.000000	0.00%	0.000003	0.00%
NBO82	0.000000	0.00%	0.000001	0.00%
NBO90	0.000001	0.00%	0.000000	0.00%
NBO96	0.001095	0.43%	0.000943	0.29%
NBO97	0.000001	0.00%	0.000000	0.00%

NBO98	0.000004	0.00%	0.000004	0.00%
NBO100	0.000751	0.30%	0.000750	0.23%
NBO107	0.000001	0.00%	0.000000	0.00%
NBO119	0.000059	0.02%	0.000008	0.00%
NBO128	0.000000	0.00%	0.000001	0.00%
NBO129	0.000051	0.02%	0.000030	0.01%
NBO137	0.000001	0.00%	0.000001	0.00%
NBO141	0.000001	0.00%	0.000001	0.00%
NBO153	0.000018	0.01%	0.000001	0.00%
NBO155	0.000032	0.01%	0.000032	0.01%
NBO157	0.001210	0.48%	0.001194	0.37%

The electron densities and their relative percentage contributions to the total electron density of the $TiCl_3^+$ system along the λ_1– and λ_2–eigenvectors are given in Table S6. as is per FALDI component.

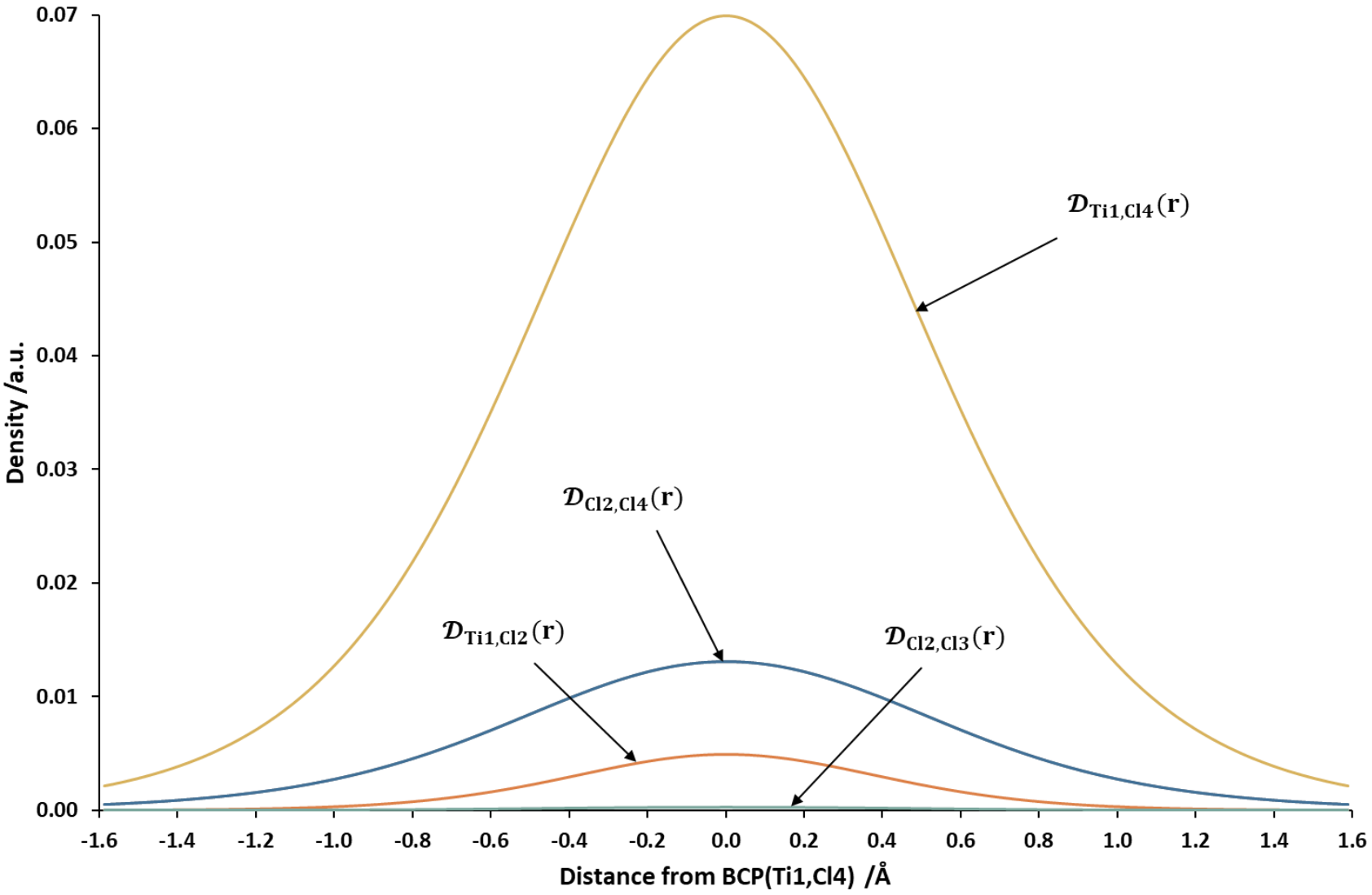

Figure S6. FALDI cross section of $TiCl_3^+$

Table S6. Delocalised FALDI data for integrated cross section

Component	$\rho_{\lambda 1}^{sum}(\boldsymbol{r})$	$\%\rho_{\lambda 1}^{sum}(\boldsymbol{r})$	$\rho_{\lambda 2}^{sum}(\boldsymbol{r})$	$\%\rho_{\lambda 2}^{sum}(\boldsymbol{r})$
$\mathcal{D}_{\mathrm{Ti1,Cl2}}$	0.012798	4.84%	0.009457	3.61%
$\mathcal{D}_{\mathrm{Ti1,Cl3}}$	0.010867	4.11%	0.007340	2.81%
$\mathcal{D}_{\mathrm{Ti1,Cl4}}$	0.161353	61.05%	0.175416	67.05%
$\mathcal{D}_{\mathrm{Cl2,Cl3}}$	0.002044	0.77%	0.000550	0.21%
$\mathcal{D}_{\mathrm{Cl2,Cl4}}$	0.038597	14.60%	0.034432	13.16%
$\mathcal{D}_{\mathrm{Cl3,Cl4}}$	0.038633	14.62%	0.034440	13.16%

The electron densities and their relative percentage contributions to the total electron density of Ti1–Cl4 interaction in the $TiCl_3^+$ system along the λ_1– and λ_2–eigenvectors are given in Table S7. as is per natural density function.

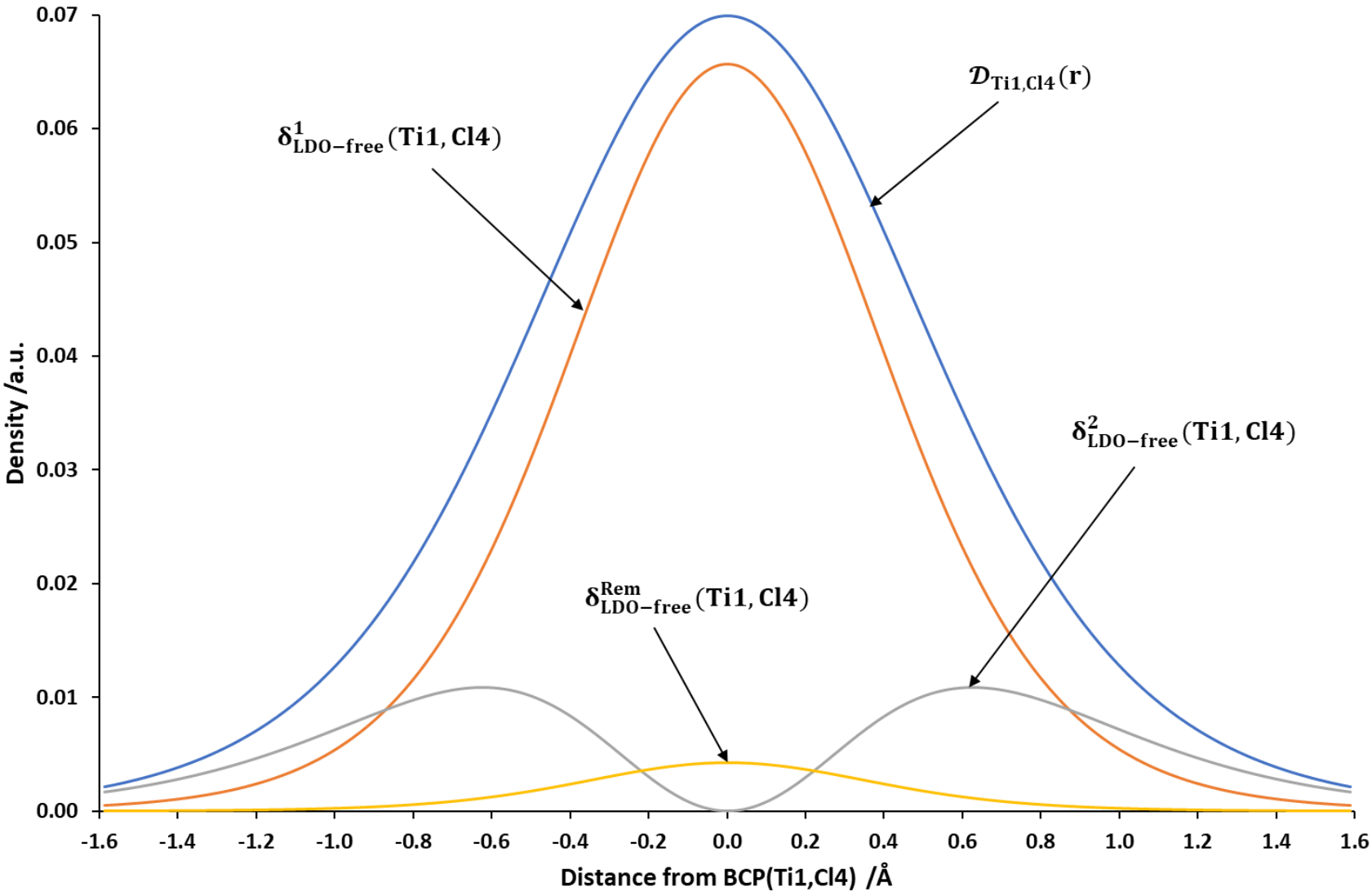

Figure S7. FALDI NDF cross section on $TiCl_3^+$

Table S7. Ti1–Cl4 FALDI-NDF decomposition data for integrated cross section

NDF	$\rho_{\lambda 1}^{sum}(\boldsymbol{r})$	$\%\rho_{\lambda 1}^{sum}(\boldsymbol{r})$	$\rho_{\lambda 2}^{sum}(\boldsymbol{r})$	$\%\rho_{\lambda 2}^{sum}(\boldsymbol{r})$
NDF1	0.130411	80.82%	0.131844	75.16%
NDF2	0.000005	0.00%	0.035694	20.35%
NDF3	0.023478	14.55%	0.000777	0.44%
NDF4	0.004013	2.49%	0.003811	2.17%
NDF5	0.002386	1.48%	0.002286	1.30%
NDF6	0.000891	0.55%	0.000495	0.28%
NDF7	0.000000	0.00%	0.000283	0.16%
NDF8	0.000000	0.00%	0.000011	0.01%
NDF9	0.000225	0.14%	0.000218	0.12%
NDF10	0.000003	0.00%	0.000003	0.00%
NDF11	0.000002	0.00%	0.000002	0.00%
NDF21	0.000000	0.00%	–0.000007	0.00%
NDF22	–0.000043	–0.03%	–0.000001	0.00%
NDF23	–0.000020	–0.01%	0.000000	0.00%

Part 3 – Supplementary Data for $TiCl_2CHCH_3$

The valence molecular orbital isosurfaces for the $TiCl_2CHCH_3$ system is given in Figure S8. with their symmetry labels and orbital energies.

χ_{22}^{MO}
–506.60
σ

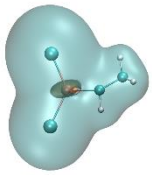

χ_{23}^{MO}
–500.97
π in plane

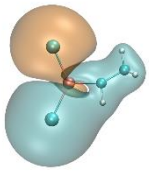

χ_{24}^{MO}
–480.41
σ*

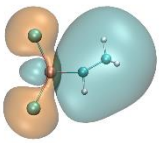

χ_{25}^{MO}
–379.01
σ*

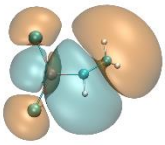

χ_{26}^{MO}
–281.71
π in plane

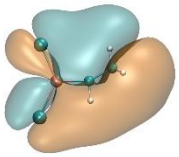

χ_{27}^{MO}
–270.35
π out of plane

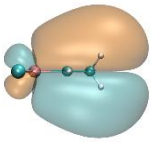

χ_{28}^{MO}
–257.05
σ

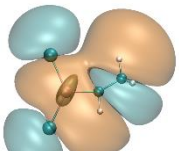

χ_{29}^{MO}
–239.58
σ

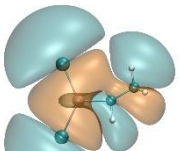

χ_{30}^{MO}
–226.94
σ

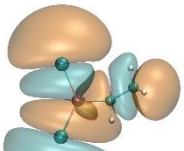

χ_{31}^{MO}
–215.67
σ

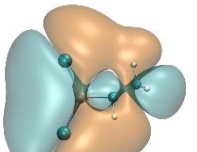

χ_{32}^{MO}
–215.47
δ

χ_{33}^{MO}
–210.16
π

χ_{34}^{MO}
–207.80
σ

χ_{35}^{MO}
–185.87
σ

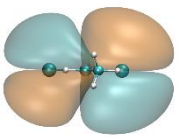

χ_{36}^{MO} (HOMO)
–155.47
π

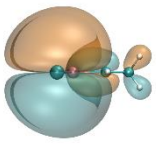

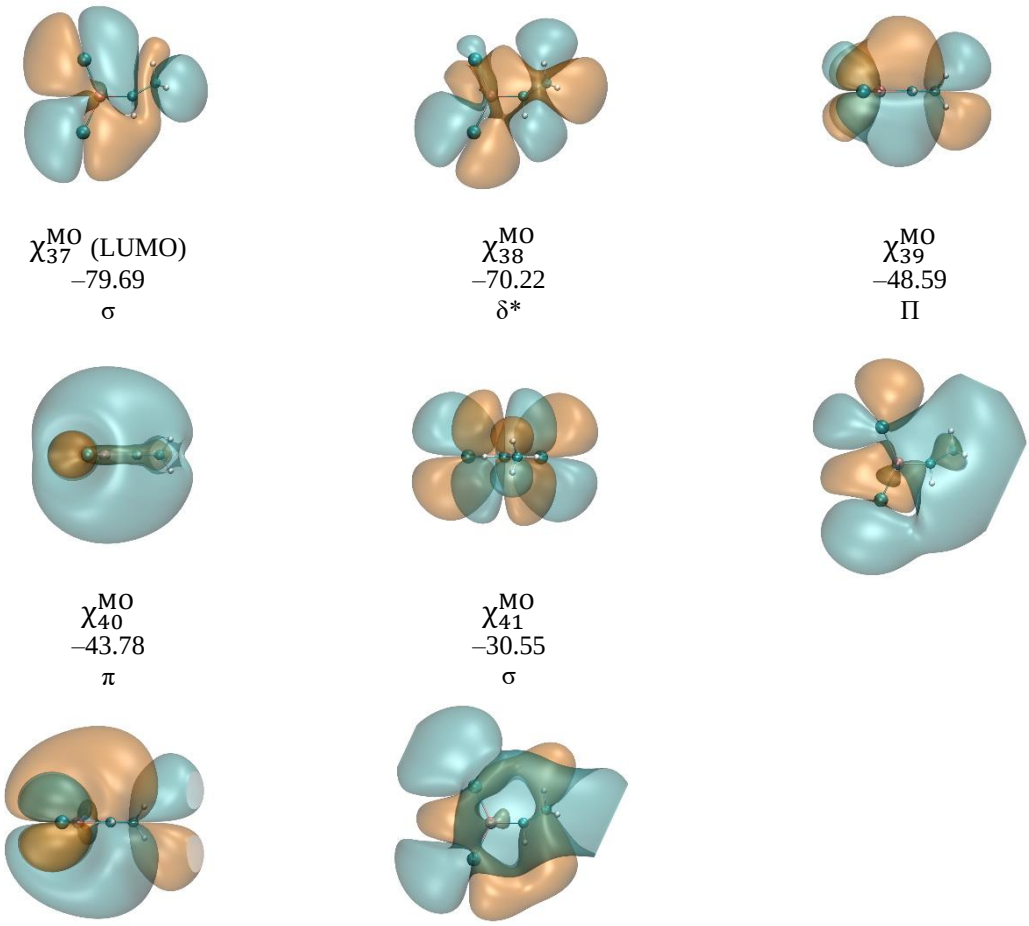

Figure S8. The occupied valence molecular orbital isosurfaces of the $TiCl_2CHCH_3$ system as well as the first five lowest energy unoccupied orbitals as an isovalue of 0.001 a.u.

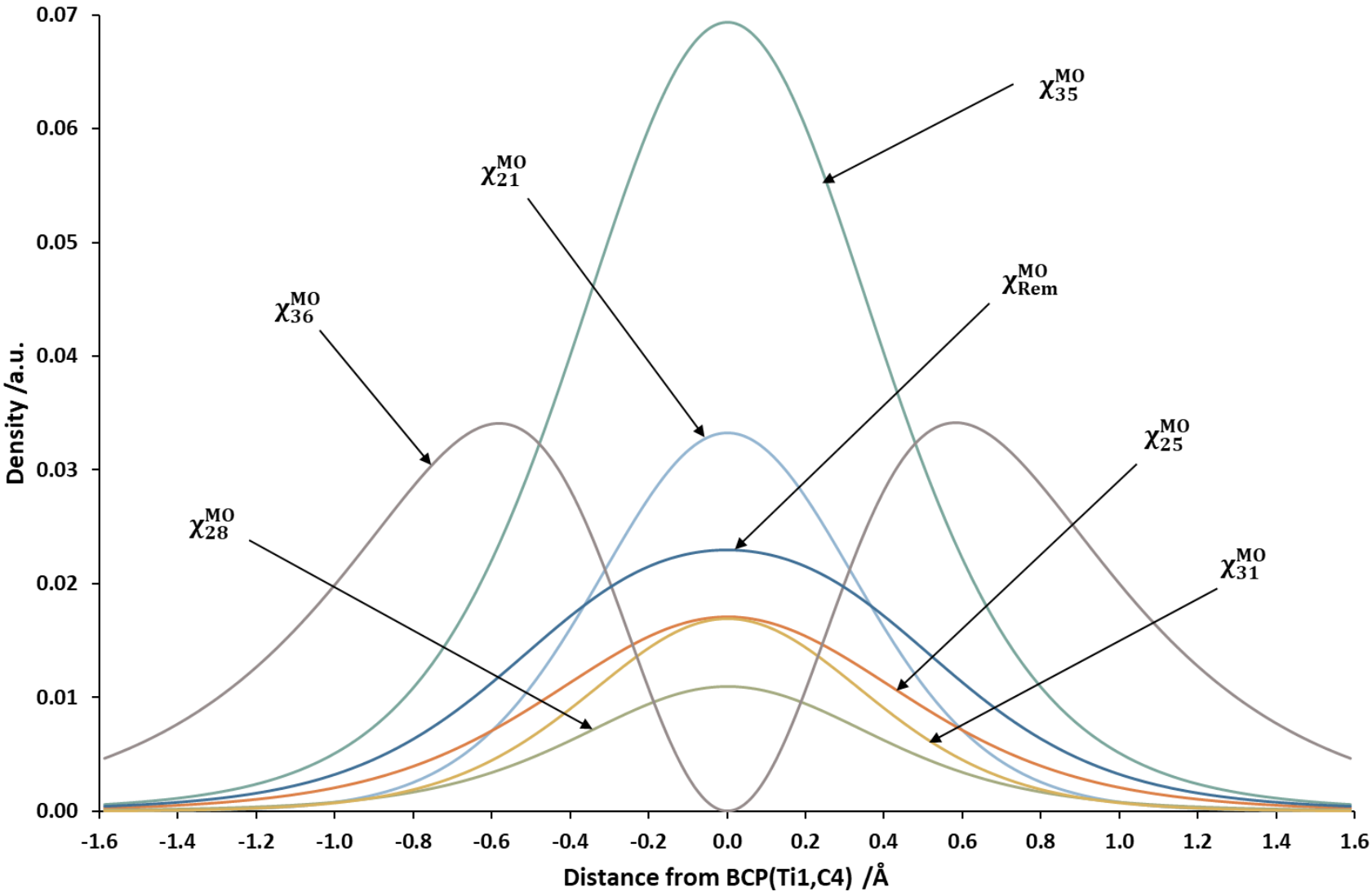

Figure S9. MO cross section on $TiCl_2CHCH_3$.

The electron densities and their relative percentage contributions to the total electron density of the $TiCl_2CHCH_3$ system along the λ_1– and λ_2–eigenvectors are given in Table S8. as is per molecular orbital.

Table S8. MO integrated cross section dataset

Molecular Orbital	$\rho_{\lambda 1}^{sum}(\boldsymbol{r})$	$\%\rho_{\lambda 1}^{sum}(\boldsymbol{r})$	$\rho_{\lambda 2}^{sum}(\boldsymbol{r})$	$\%\rho_{\lambda 2}^{sum}(\boldsymbol{r})$
MO9	0.000007	0.00%	0.000006	0.00%
MO18	0.011009	2.91%	0.010887	2.47%
MO19	0.006192	1.64%	0.000006	0.00%
MO20	0.000000	0.00%	0.006217	1.41%
MO21	0.053910	14.26%	0.053611	12.19%
MO22	0.001036	0.27%	0.000161	0.04%
MO23	0.000343	0.09%	0.000092	0.02%
MO24	0.007775	2.06%	0.006627	1.51%
MO25	0.054186	14.33%	0.037883	8.61%
MO26	0.018324	4.85%	0.004821	1.10%
MO27	0.000000	0.00%	0.003406	0.77%
MO28	0.044145	11.68%	0.020754	4.72%
MO29	0.005409	1.43%	0.004126	0.94%
MO30	0.006345	1.68%	0.004117	0.94%
MO31	0.025734	6.81%	0.029705	6.75%
MO32	0.000001	0.00%	0.000109	0.02%
MO33	0.000000	0.00%	0.000889	0.20%
MO34	0.017884	4.73%	0.014149	3.22%
MO35	0.125729	33.26%	0.133519	30.35%
MO36	0.000000	0.00%	0.108834	24.74%

The NBO isosurfaces of the four orbitals which are predicted by the NBO Gaussian 09 software to contribute to the Ti1–C4 interaction with their symmetries and orbital occupations are given in Figure S10.

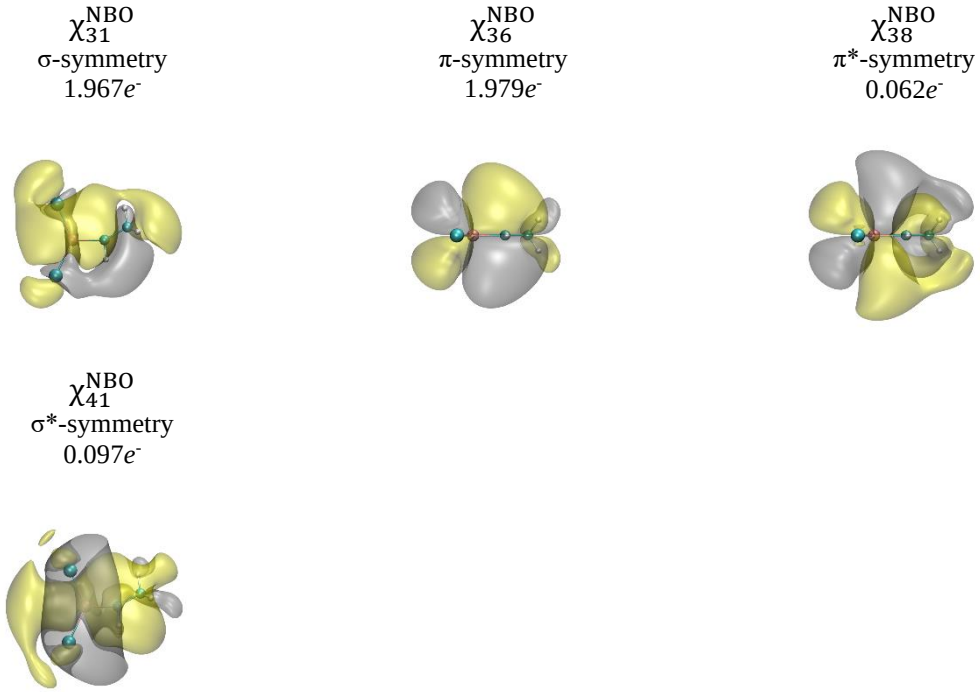

Figure S10. Orbital isosurfaces of $TiCl_2CHCH_3$ system for NBOs of the Ti1–C4 interaction at an isovalue of 0.001 a.u.

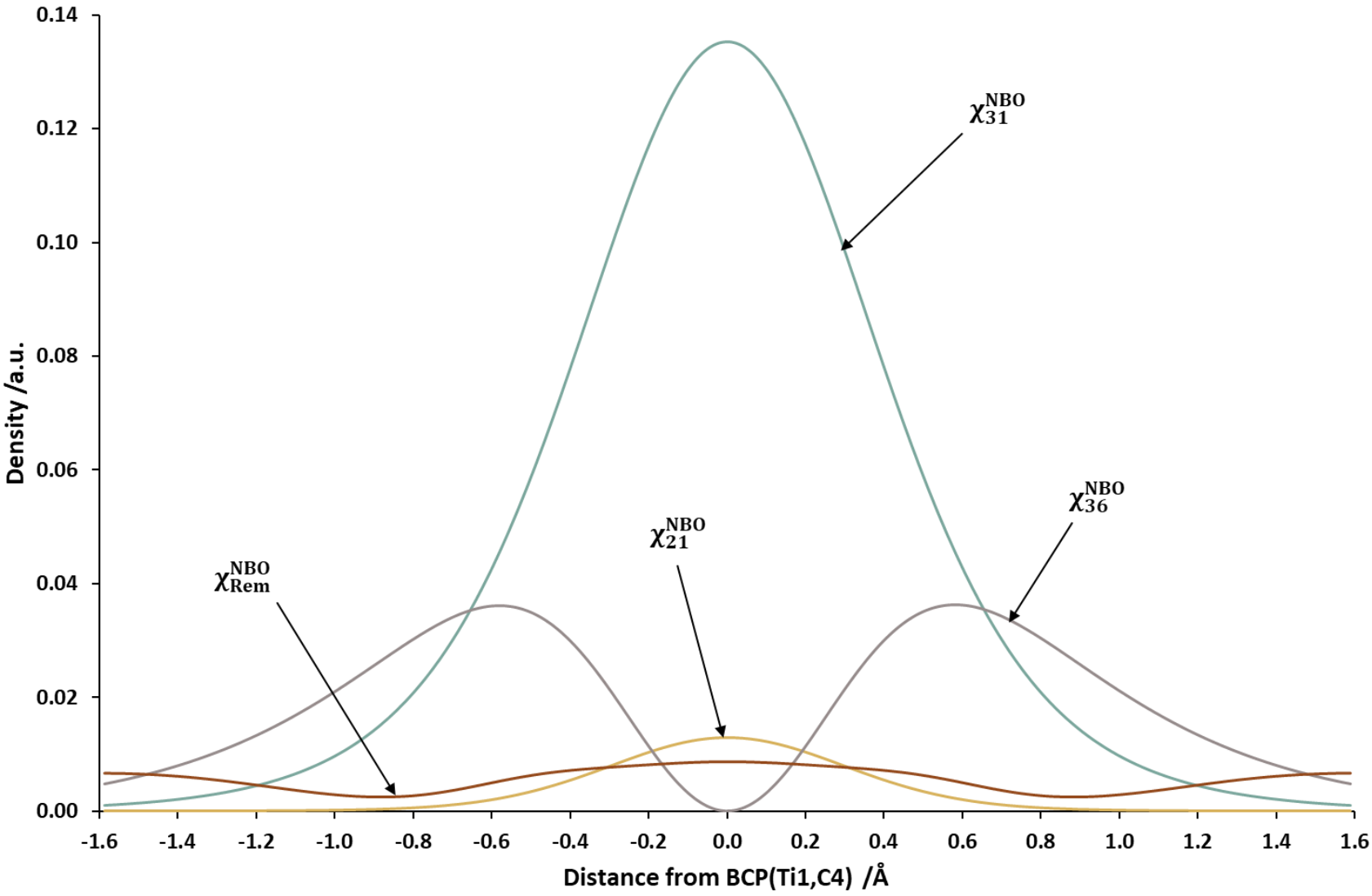

Figure S11. NBO cross section on $TiCl_2CHCH_3$.

The electron densities and their relative percentage contributions to the total electron density of the $TiCl_2CHCH_3$ system along the λ_1– and λ_2–eigenvectors are given in Table SI.B.3. as is per natural bond orbital.

Table S9. NBO dataset of integrated cross section on TiCl2CHCH3

NBO	$\rho_{\lambda 1}^{sum}(\boldsymbol{r})$	$\%\rho_{\lambda 1}^{sum}(\boldsymbol{r})$	$\rho_{\lambda 2}^{sum}(\boldsymbol{r})$	$\%\rho_{\lambda 2}^{sum}(\boldsymbol{r})$
NBO4	0.000436	0.13%	0.000430	0.10%
NBO5	0.000032	0.01%	0.000025	0.01%
NBO6	0.000000	0.00%	0.000013	0.00%
NBO7	0.000093	0.03%	0.000085	0.02%
NBO8	0.000012	0.00%	0.000003	0.00%
NBO9	0.000004	0.00%	0.000003	0.00%
NBO10	0.001038	0.31%	0.001024	0.24%
NBO11	0.000044	0.01%	0.000028	0.01%
NBO13	0.000001	0.00%	0.000000	0.00%
NBO14	0.000008	0.00%	0.000001	0.00%
NBO15	0.000003	0.00%	0.000000	0.00%
NBO17	0.000002	0.00%	0.000000	0.00%
NBO18	0.001243	0.37%	0.001221	0.29%
NBO19	0.000000	0.00%	0.004707	1.10%
NBO20	0.008634	2.58%	0.006207	1.45%
NBO21	0.020799	6.22%	0.018945	4.44%
NBO22	0.000386	0.12%	0.000131	0.03%
NBO23	0.000282	0.08%	0.000129	0.03%
NBO24	0.002566	0.77%	0.000172	0.04%
NBO25	0.002334	0.70%	0.000281	0.07%
NBO26	0.004986	1.49%	0.001824	0.43%
NBO27	0.026582	7.95%	0.001760	0.41%
NBO28	0.000440	0.13%	0.000006	0.00%
NBO29	0.000333	0.10%	0.000437	0.10%
NBO30	0.000332	0.10%	0.000435	0.10%
NBO31	0.255744	76.53%	0.258958	60.65%
NBO32	0.000000	0.00%	0.000036	0.01%
NBO33	0.000002	0.00%	0.000001	0.00%
NBO34	0.000391	0.12%	0.000251	0.06%
NBO36	0.000000	0.00%	0.115384	27.03%
NBO37	0.000000	0.00%	0.000058	0.01%
NBO38	0.000000	0.00%	0.000028	0.01%
NBO39	0.000000	0.00%	0.011359	2.66%
NBO40	0.003998	1.20%	0.000088	0.02%
NBO41	0.000316	0.09%	0.000180	0.04%
NBO62	0.000001	0.00%	0.000004	0.00%
NBO65	0.000000	0.00%	0.000127	0.03%
NBO68	0.000135	0.04%	0.000041	0.01%
NBO69	0.000005	0.00%	0.000003	0.00%
NBO78	0.000005	0.00%	0.000002	0.00%
NBO79	0.000003	0.00%	0.000001	0.00%

NBO83	0.000000	0.00%	0.000003	0.00%
NBO86	0.000008	0.00%	0.000002	0.00%
NBO98	0.000052	0.02%	0.000031	0.01%
NBO103	0.000028	0.01%	0.000006	0.00%
NBO104	0.000010	0.00%	0.000011	0.00%
NBO106	0.000000	0.00%	0.000002	0.00%
NBO107	0.000000	0.00%	0.000008	0.00%
NBO110	0.000003	0.00%	0.000001	0.00%
NBO120	0.000078	0.02%	0.000070	0.02%
NBO123	0.000000	0.00%	0.000001	0.00%
NBO126	0.000001	0.00%	0.000000	0.00%
NBO127	0.000000	0.00%	0.000004	0.00%
NBO129	0.000022	0.01%	0.000009	0.00%
NBO141	0.000001	0.00%	0.000000	0.00%
NBO143	0.000013	0.00%	0.000041	0.01%
NBO144	0.000104	0.03%	0.000091	0.02%
NBO150	0.000362	0.11%	0.000153	0.04%
NBO155	0.000052	0.02%	0.000015	0.00%
NBO156	0.000020	0.01%	0.000023	0.01%
NBO157	0.000000	0.00%	0.000002	0.00%
NBO168	0.000265	0.08%	0.000169	0.04%
NBO176	0.000032	0.01%	0.000032	0.01%
NBO182	0.000009	0.00%	0.000006	0.00%
NBO194	0.000002	0.00%	0.000002	0.00%
NBO195	0.001934	0.58%	0.001853	0.43%
NBO196	0.000001	0.00%	0.000001	0.00%

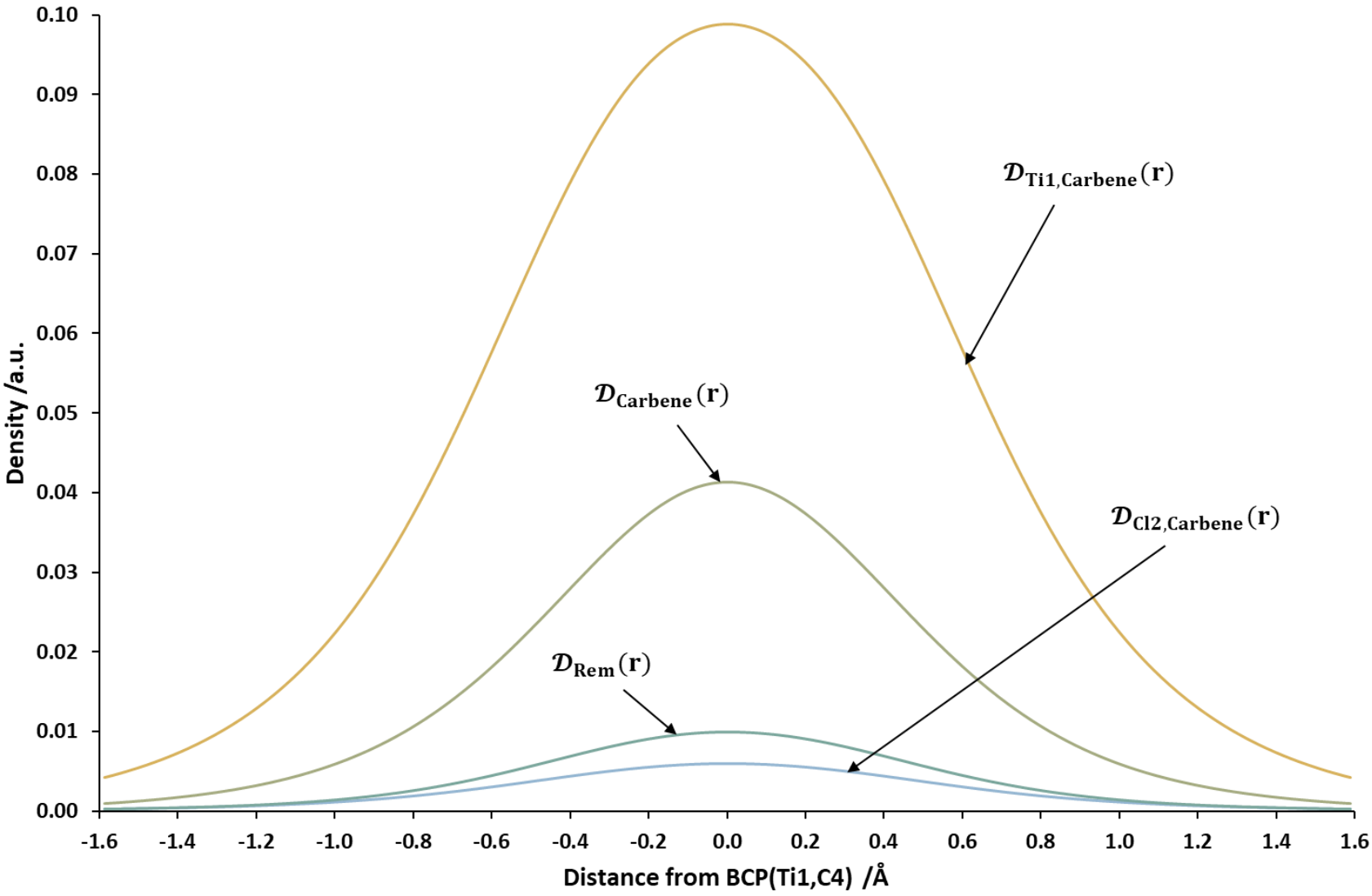

Figure S12. FALDI cross section on $TiCl_2CHCH_3$.

The electron densities and their relative percentage contributions to the total electron density of the $TiCl_2CHCH_3$ system along the λ_1– and λ_2–eigenvectors are given in Table S10. as is per FALDI component.

Table S10. Delocalised FALDI data for integrated cross section

Component	$\rho_{\lambda 1}^{sum}(\boldsymbol{r})$	$\%\rho_{\lambda 1}^{sum}(\boldsymbol{r})$	$\rho_{\lambda 2}^{sum}(\boldsymbol{r})$	$\%\rho_{\lambda 2}^{sum}(\boldsymbol{r})$
$\mathcal{D}_{Ti1,Cl2}$	0.011111	3.06%	0.011029	2.60%
$\mathcal{D}_{Ti1,Cl3}$	0.012276	3.38%	0.011973	2.82%
$\mathcal{D}_{Ti1,C4}$	0.163211	45.00%	0.239967	56.57%
$\mathcal{D}_{Ti1,H5}$	0.007451	2.05%	0.007818	1.84%
$\mathcal{D}_{Ti1,C6}$	0.009569	2.64%	0.012242	2.89%
$\mathcal{D}_{Ti1,H7}$	0.002328	0.64%	0.005622	1.33%
$\mathcal{D}_{Ti1,H8}$	0.002345	0.65%	0.005626	1.33%
$\mathcal{D}_{Ti1,H9}$	0.002189	0.60%	0.002524	0.59%
$\mathcal{D}_{Cl2,Cl3}$	0.001581	0.44%	0.000138	0.03%
$\mathcal{D}_{Cl2,C4}$	0.012721	3.51%	0.014746	3.48%
$\mathcal{D}_{Cl2,H5}$	0.001372	0.38%	0.000082	0.02%
$\mathcal{D}_{Cl2,C6}$	0.000309	0.09%	0.000121	0.03%
$\mathcal{D}_{Cl2,H7}$	0.000132	0.04%	0.000052	0.01%
$\mathcal{D}_{Cl2,H8}$	0.000132	0.04%	0.000052	0.01%
$\mathcal{D}_{Cl2,H9}$	0.000148	0.04%	0.000031	0.01%
$\mathcal{D}_{Cl3,C4}$	0.014935	4.12%	0.016508	3.89%
$\mathcal{D}_{Cl3,H5}$	0.000855	0.24%	0.000091	0.02%
$\mathcal{D}_{Cl3,C6}$	0.000573	0.16%	0.000133	0.03%
$\mathcal{D}_{Cl3,H7}$	0.000246	0.07%	0.000062	0.01%
$\mathcal{D}_{Cl3,H8}$	0.000247	0.07%	0.000062	0.01%
$\mathcal{D}_{Cl3,H9}$	0.000362	0.10%	0.000022	0.01%
$\mathcal{D}_{C4,H5}$	0.053841	14.85%	0.031134	7.34%
$\mathcal{D}_{C4,C6}$	0.041580	11.46%	0.041382	9.76%
$\mathcal{D}_{C4,H7}$	0.005072	1.40%	0.006531	1.54%
$\mathcal{D}_{C4,H8}$	0.005060	1.40%	0.006515	1.54%
$\mathcal{D}_{C4,H9}$	0.006852	1.89%	0.006881	1.62%
$\mathcal{D}_{H5,C6}$	0.002009	0.55%	0.000433	0.10%
$\mathcal{D}_{H5,H7}$	0.000309	0.09%	0.000043	0.01%
$\mathcal{D}_{H5,H8}$	0.000312	0.09%	0.000043	0.01%
$\mathcal{D}_{H5,H9}$	0.000893	0.25%	0.000009	0.00%
$\mathcal{D}_{C6,H7}$	0.000816	0.23%	0.000820	0.19%
$\mathcal{D}_{C6,H8}$	0.000817	0.23%	0.000822	0.19%
$\mathcal{D}_{C6,H9}$	0.000851	0.23%	0.000420	0.10%
$\mathcal{D}_{H7,H8}$	0.000040	0.01%	0.000098	0.02%
$\mathcal{D}_{H7,H9}$	0.000062	0.02%	0.000075	0.02%
$\mathcal{D}_{H8,H9}$	0.000062	0.02%	0.000075	0.02%

$\mathcal{D}_{\mathrm{Ti,C}}(\mathbf{r})$
DI = 3.72e^-

$\mathcal{D}_{\mathrm{Ti,\{Carbene\}}}(\mathbf{r})$
DI = 5.38e^-

$\mathcal{D}_{\mathrm{Cl,\{Carbene\}}}(\mathbf{r})$
DI = 2.67e^-

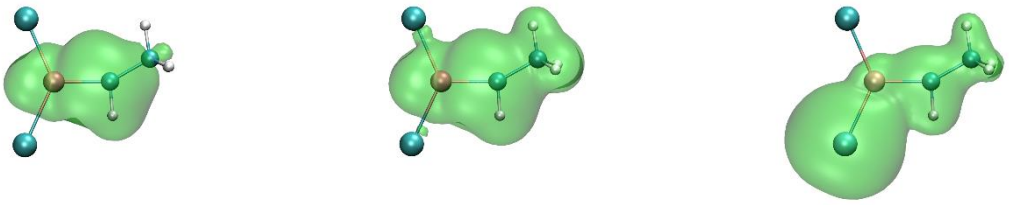

Figure S13. Isosurfaces of the dominant FALDI components that contribute to the ED of a Ti–C bond in $TiCl_2CHCH_3$. The FALDI-defined delocalization indices of each component is also shown. All isosurfaces are displayed at an isovalue of 0.001 au.

$\delta^1_{\mathrm{LDO-free}}(\mathrm{Ti1,C4}) = 1.318e^-$
π-symmetry

$\delta^2_{\mathrm{LDO-free}}(\mathrm{Ti1,C4}) = 1.285e^-$
σ-symmetry

Figure S14. Major NDFs of $TiCl_2CHCH_3$ with their contributions to the λ_2– eigenvector.

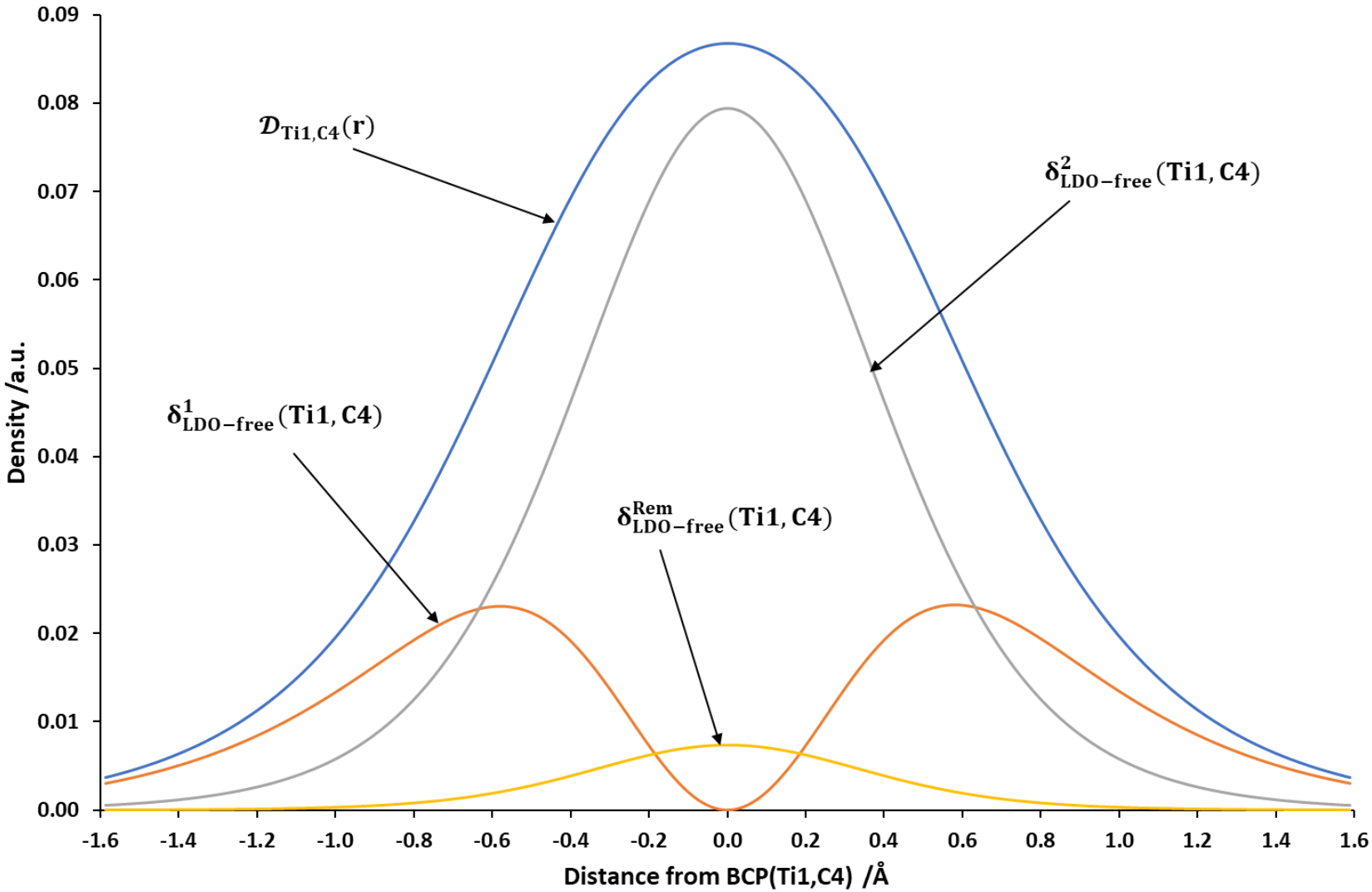

Figure S15. FALDI NDF cross section on $TiCl_2CHCH_3$. Composition of $\mathcal{D}_{Ti1,C2}(\mathbf{r})$ interaction showing that the σ-component makes up about two thirds of the interaction and the π-component makes up much of the rest.

The electron densities and their relative percentage contributions to the total electron density of the Ti1–C4 interaction in the $TiCl_2CHCH_3$ system along the λ_1- and λ_2-eigenvectors are given in Table S11. as is per natural density function.

Table S11. Ti1–C4 FALDI-NDF decomposition data for integrated cross section

NDF	$\rho_{\lambda1}^{sum}(\boldsymbol{r})$	$\%\rho_{\lambda1}^{sum}(\boldsymbol{r})$	$\rho_{\lambda2}^{sum}(\boldsymbol{r})$	$\%\rho_{\lambda2}^{sum}(\boldsymbol{r})$
NDF1	0.000038	0.02%	0.073665	30.70%
NDF2	0.146335	89.66%	0.153447	63.94%
NDF3	0.007677	4.70%	0.003969	1.65%
NDF4	0.006963	4.27%	0.006784	2.83%
NDF5	0.001330	0.81%	0.000944	0.39%
NDF6	0.000002	0.00%	0.000329	0.14%
NDF7	0.000649	0.40%	0.000573	0.24%
NDF8	0.000001	0.00%	0.000005	0.00%
NDF9	0.000203	0.12%	0.000194	0.08%
NDF10	0.000082	0.05%	0.000079	0.03%
NDF11	0.000003	0.00%	0.000002	0.00%
NDF12	0.000001	0.00%	0.000001	0.00%
NDF20	–0.000001	0.00%	0.000000	0.00%
NDF21	–0.000019	–0.01%	–0.000002	0.00%
NDF22	–0.000018	–0.01%	–0.000011	0.00%
NDF23	0.000000	0.00%	–0.000001	0.00%
NDF24	–0.000036	–0.02%	–0.000014	–0.01%

Appendix B

Supplementary information for chapter four

XYZ Coordinates of optimized geometries

Table B1. Molecule specification of $TiCl_2CH_2$

Atom	X	Y	Z
Ti1	0.000000	0.000000	0.424465
Cl2	0.000000	3.870382	-1.258442
Cl3	0.000000	-3.870382	-1.258442
C4	0.000000	0.000000	3.900398
H5	0.000000	1.733819	5.023219
H6	0.000000	-1.733819	5.023219

Molecular energy: -1809.32683885628 a.u.

Table B2. Molecule specifications for $TiCl_2CHCH_3$

Atom	X	Y	Z
Ti1	0.000000	0.000000	0.000000
Cl2	0.000000	0.000000	4.271290
Cl3	3.149579	0.000000	-2.806256
C4	-3.125242	0.000869	-1.456458
H5	-4.139716	0.000131	0.386601
C6	-4.769813	0.004805	-3.749088
H7	-6.000847	-1.663082	-3.786457
H8	-6.009112	1.666698	-3.775061
H9	-3.653423	0.013214	-5.484506

Molecular energy: -1848.65239122118 a.u.

Table B3. Molecule specification of $TiCp_2CH_2$

Atom	X	Y	Z
Ti1	-0.000003	0.565569	-0.000299
C2	-0.000036	4.220883	-0.000493
H3	1.686211	5.414210	-0.000125
H4	-1.686297	5.414190	-0.001172
C5	-3.030267	-2.871537	0.000395
H6	-2.403337	-4.811871	0.001061
C7	-3.480636	-1.364578	2.162769
C8	-3.480026	-1.365848	-2.162992
H9	-3.280417	-1.967174	4.104362
C10	-4.265328	1.067120	1.339974
H11	-3.279304	-1.969601	-4.104175
C12	-4.264953	1.066346	-1.341827
H13	-4.777794	2.631073	2.540402
H14	-4.777109	2.629609	-2.543293
C15	4.264530	1.066334	1.342409
H16	4.776322	2.629541	2.544102
C17	3.479368	-1.365919	2.163201
C18	4.265725	1.067243	-1.339392
H19	3.278090	-1.969799	4.104284
C20	3.030308	-2.871498	-0.000421
H21	4.778516	2.631264	-2.539592
C22	3.481331	-1.364416	-2.162559
H23	2.403406	-4.811842	-0.001394
H24	3.281680	-1.966891	-4.104252

Molecular energy: -1275.95754082820 a.u.

Table B4. Molecule specification of $TiCp_2CHCH_3$

Atom	X	Y	Z
Ti1	-1.791120	0.182128	-0.974712
C2	-4.119874	4.052647	-0.880865
H3	-3.201584	5.806000	-1.364407
C4	-5.382558	2.404015	-2.577763
C5	-4.303281	2.995804	1.580606
H6	-5.597966	2.675497	-4.585567
C7	-6.339617	0.337438	-1.155027
H8	-3.528015	3.799770	3.291301
C9	-5.709973	0.730000	1.412210
H10	-7.394509	-1.244969	-1.900786
H11	-6.162325	-0.516420	2.960861
C12	-1.255094	-4.291016	-0.466104
H13	-2.620821	-5.588209	-1.256786
C14	0.905897	-3.321258	-1.722862
C15	-1.308541	-3.277085	2.006299
H16	1.490084	-3.776334	-3.620106
C17	2.176309	-1.676347	-0.019474
H18	-2.725123	-3.650761	3.424056
C19	0.790190	-1.644198	2.275484
H20	3.900353	-0.656808	-0.388846
H21	1.259136	-0.563975	3.944731
C22	-0.004247	1.735844	-3.812374
H23	-0.989945	3.351818	-4.649796
C24	2.418283	1.382814	-5.281476
H25	2.018402	1.058988	-7.295617
H26	3.579913	3.105345	-5.214365
H27	3.606400	-0.177815	-4.638484

Molecular energy: -1315.27979917587 a.u.

MO Data for λ_1-Cross Sections

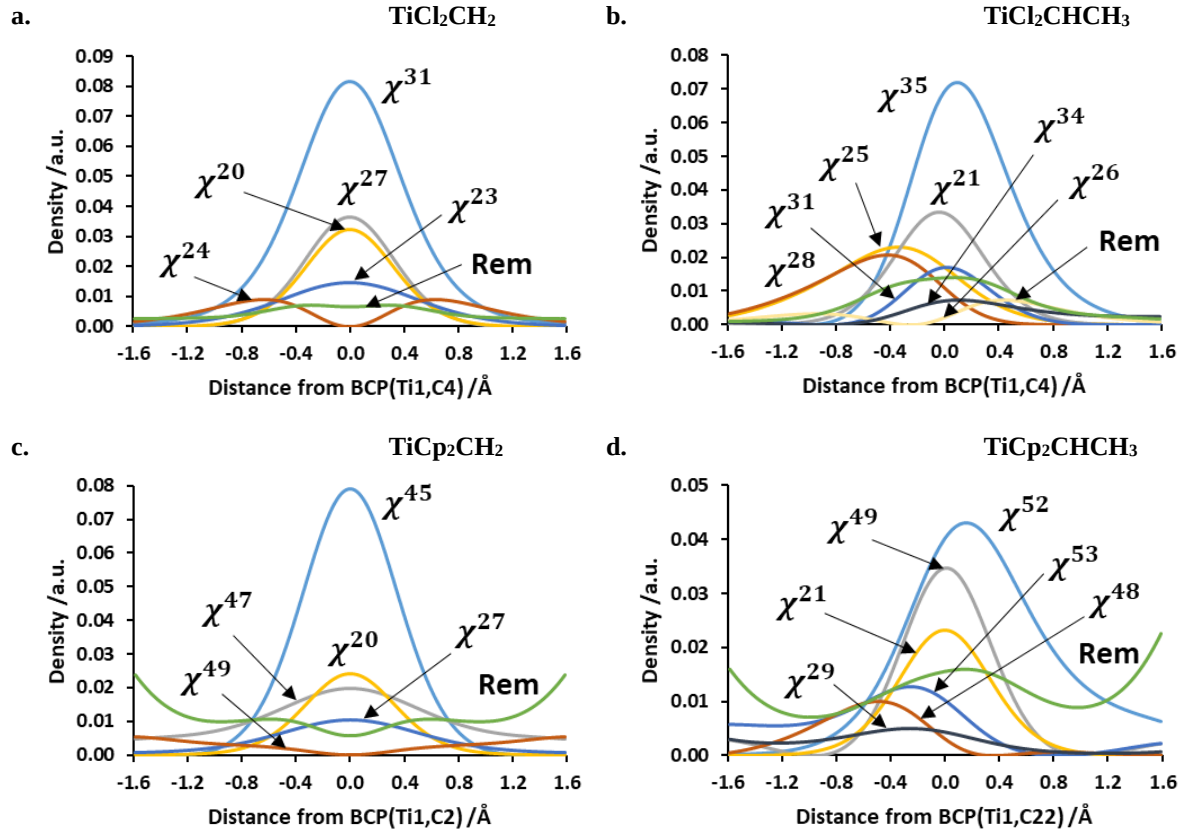

Figure B1. Cross-sections of MOs making a contribution greater than 5% of the total density along the λ_1-eigenvectors with Rem as the sum total of the MOs making less than 5% contributions.

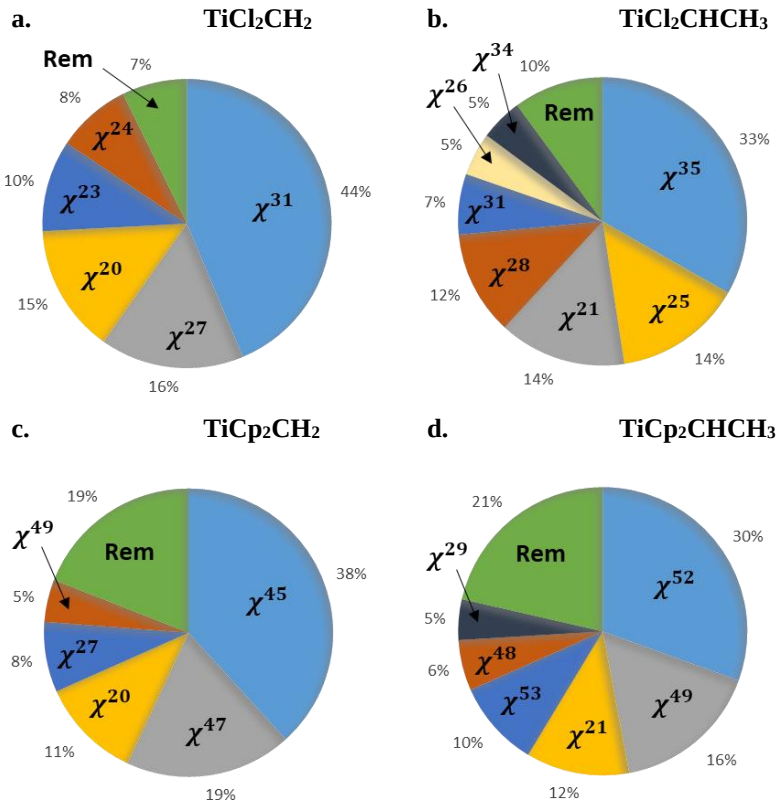

Figure B2. Relative contributions of MOs to the total density, integrated along the λ_1-eigenvector.

Individual MOs with a contribution greater than 5% are shown with the other MOs collected in the Rem fraction.

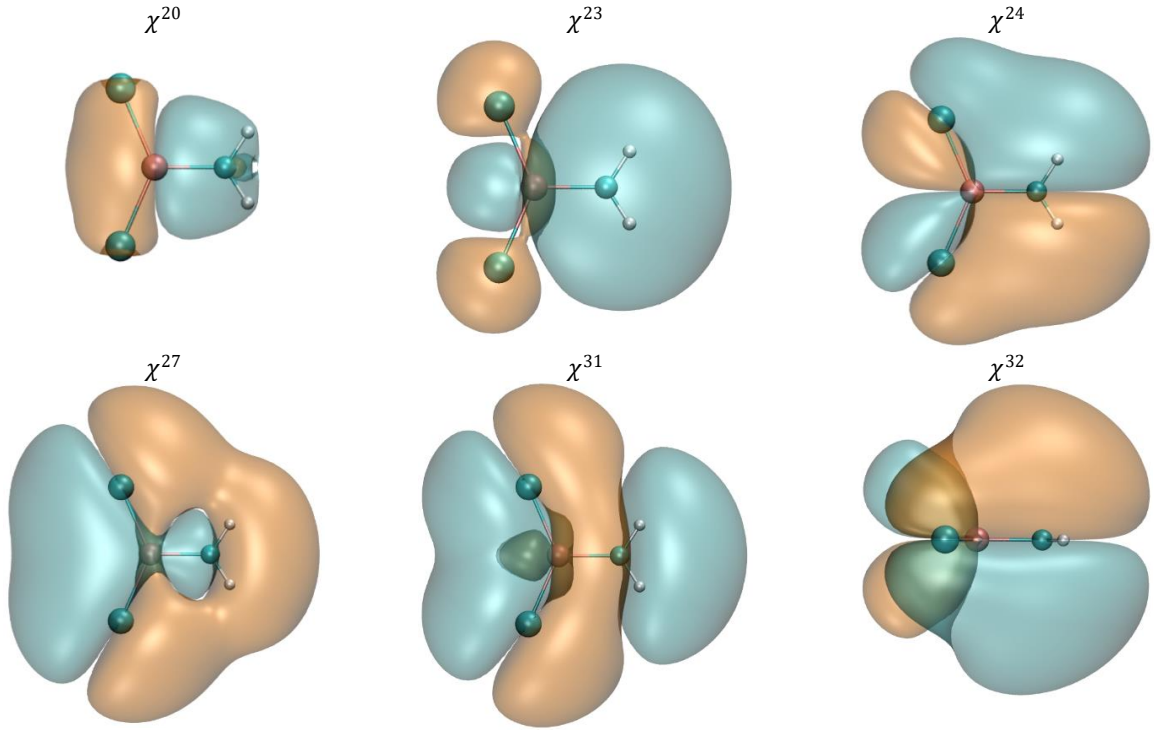

Figure B3. Isosurfaces of significant MOs for $TiCl_2CH_2$ at isovalue 0.001a.u.

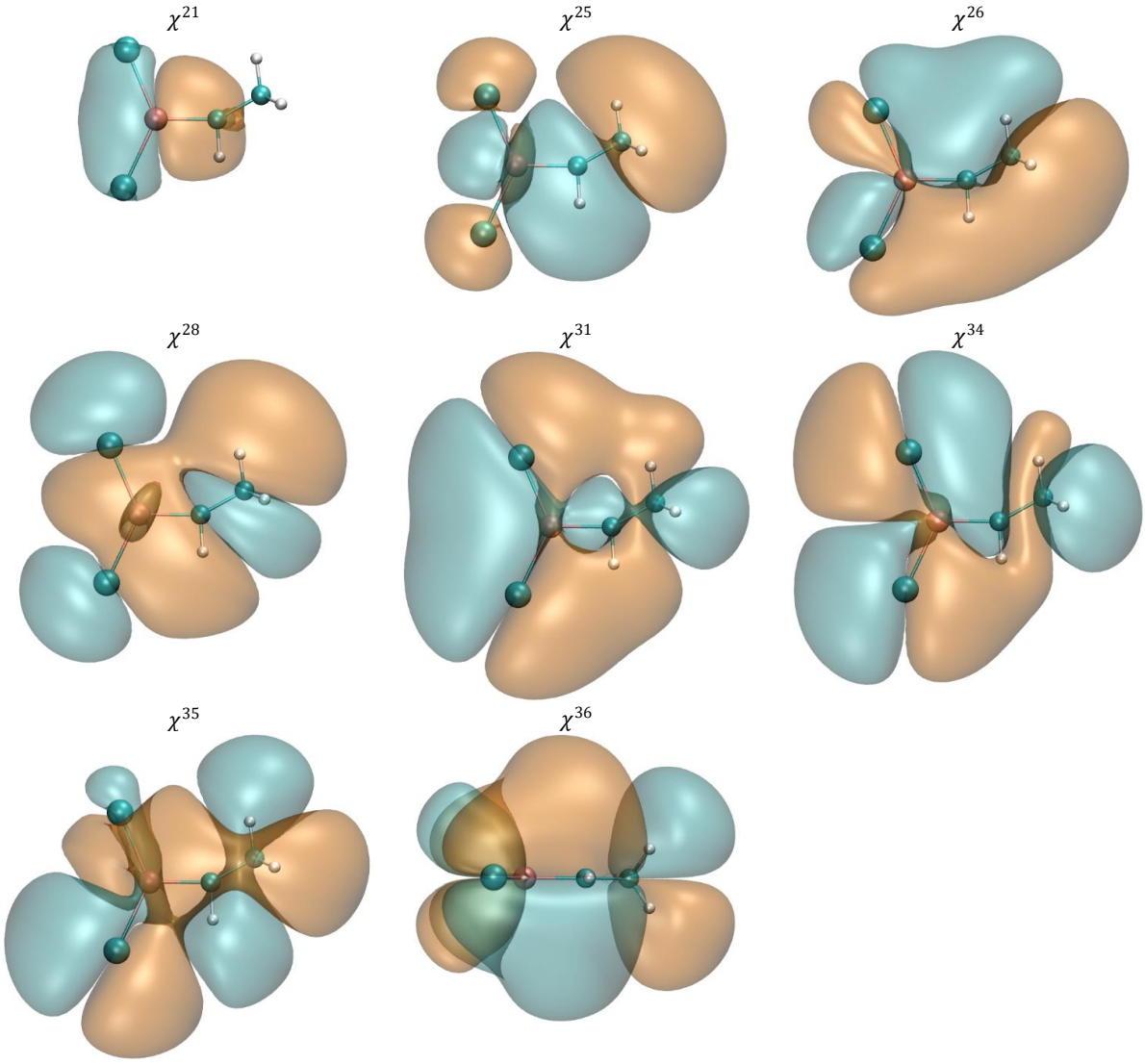

Figure B4. Isosurfaces of significant MOs for $TiCl_2CHCH_3$ at isovalue 0.001a.u.

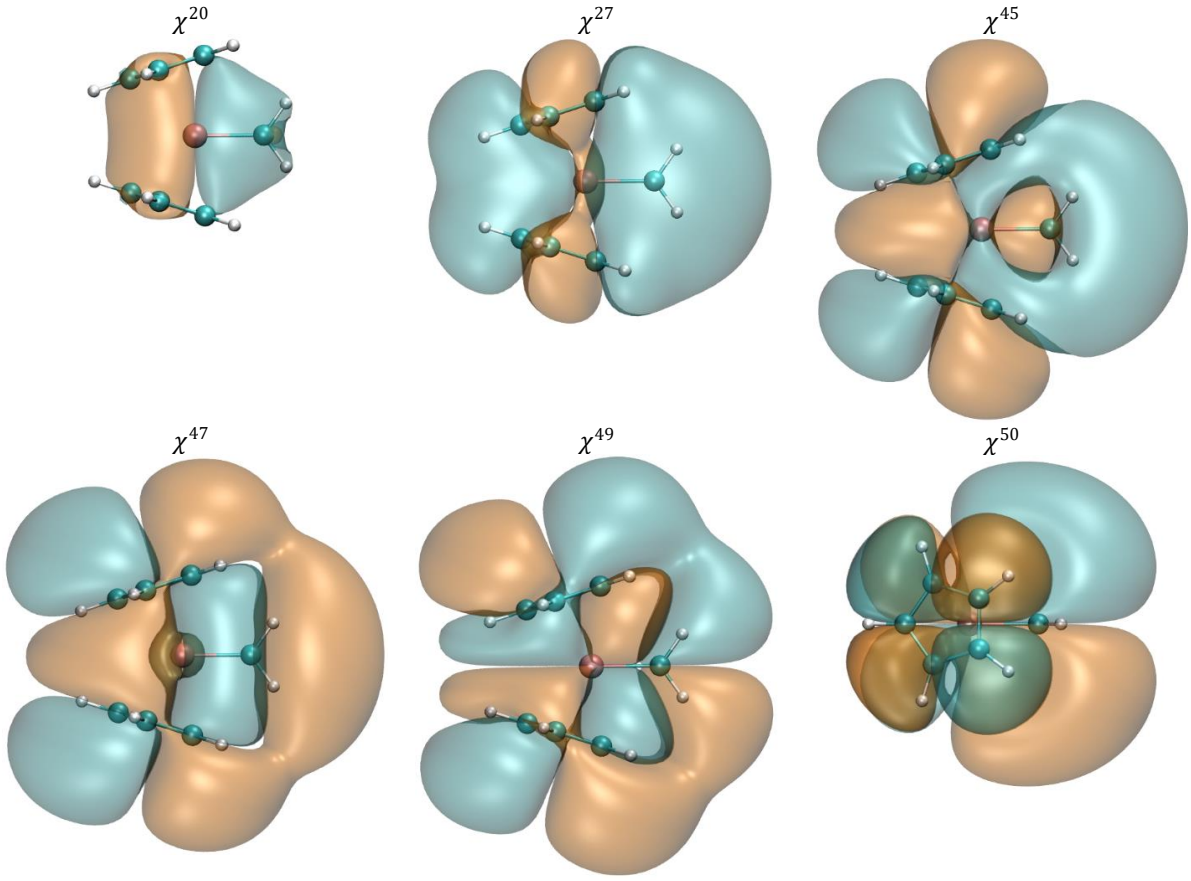

Figure B5. Isosurfaces of significant MOs for $TiCp_2CH_2$ at isovalue 0.001a.u.

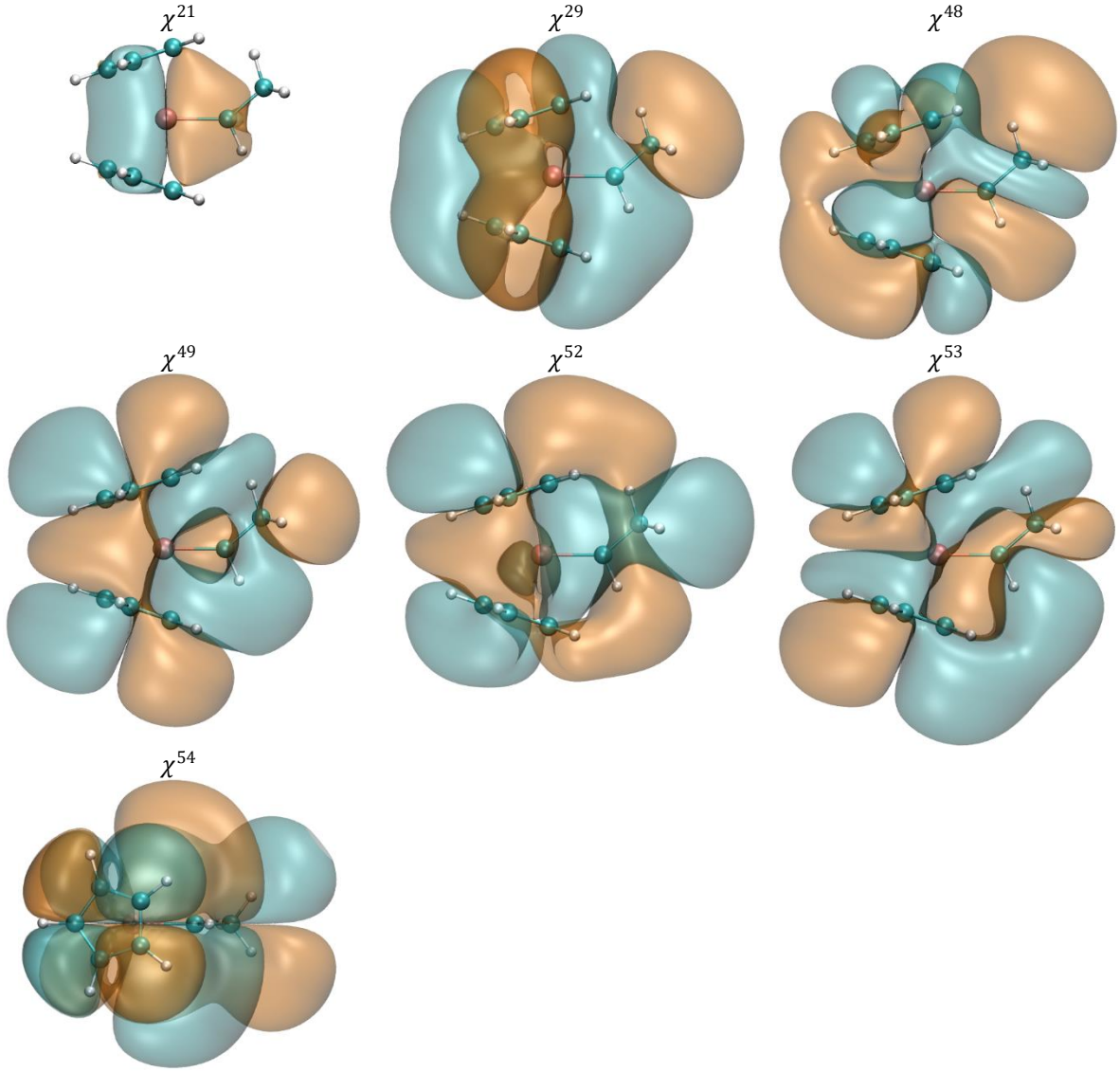

Figure B6. Isosurfaces of significant MOs for $TiCp_2CHCH_3$ at isovalue 0.001a.u.

NBO Data for λ_1-Cross Sections

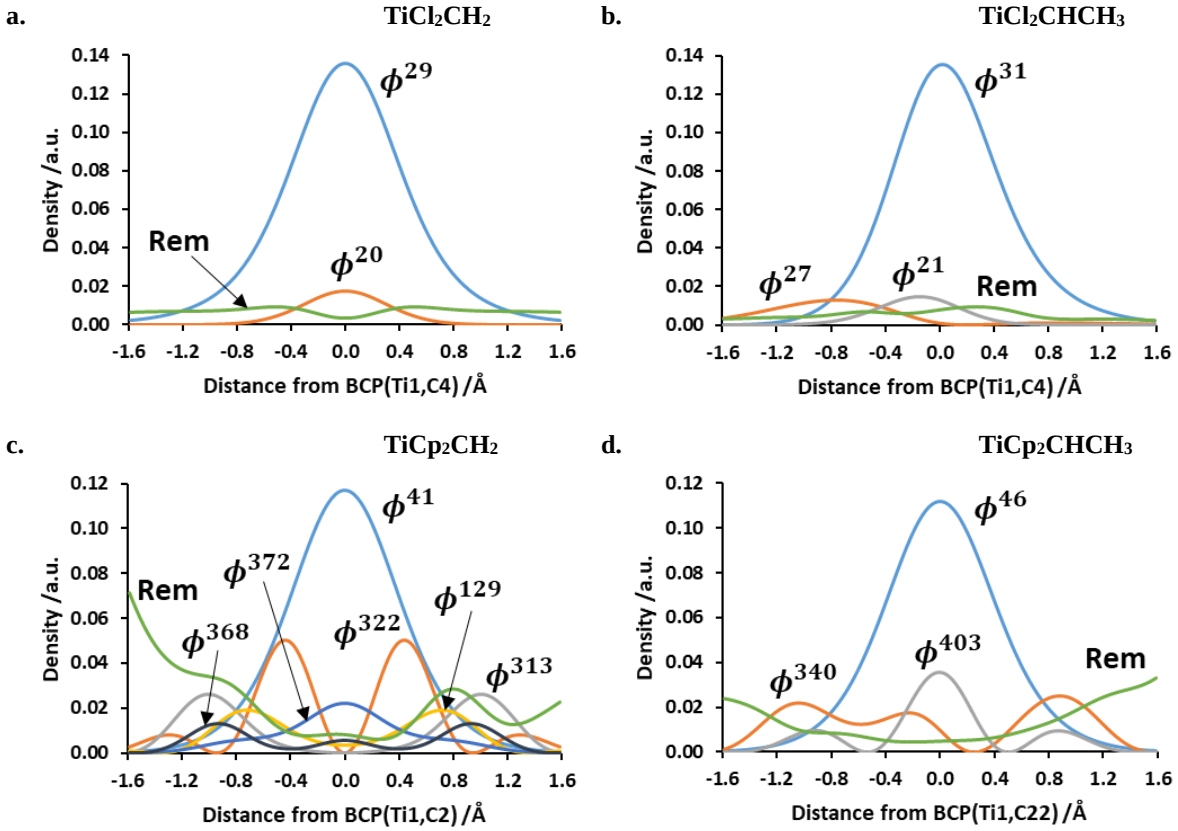

Figure B7. Cross-sections of NBOs making a contribution greater than 5% of the total density along the λ_1-eigenvectors with Rem as the sum total of the NBOs making less than 5% contributions.

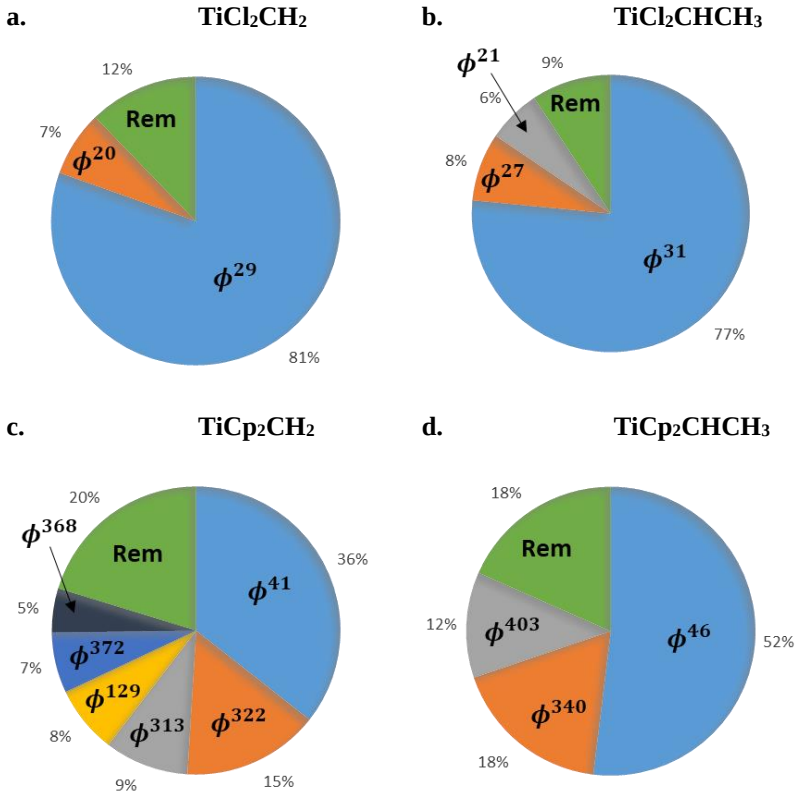

Figure B8. Relative contributions of NBOs to the total density, integrated along the λ_1-eigenvector.

Individual NBOs with a contribution greater than 5% are shown with the other NBOs collected in the Rem fraction.

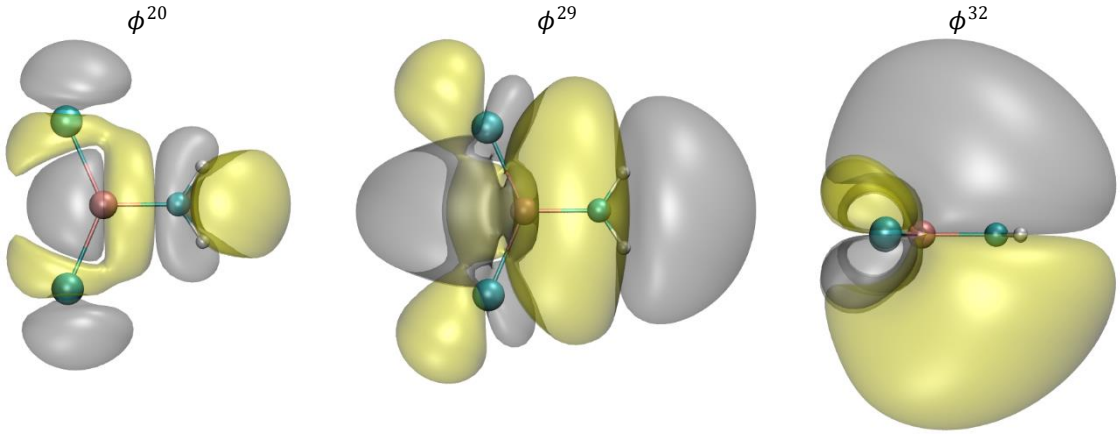

Figure B9. Isosurfaces of significant NBOs for $TiCl_2CH_2$ at isovalue 0.001a.u.

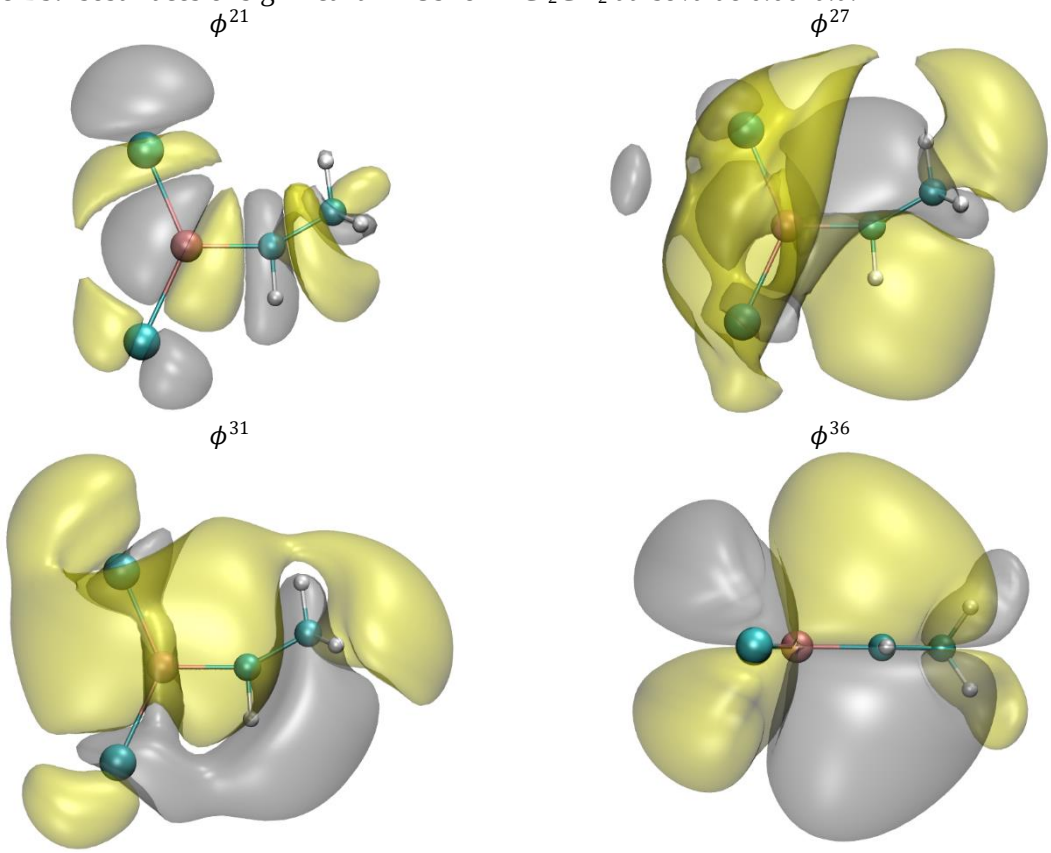

Figure B10. Isosurfaces of significant NBOs for $TiCl_2CHCH_3$ at isovalue 0.001a.u.

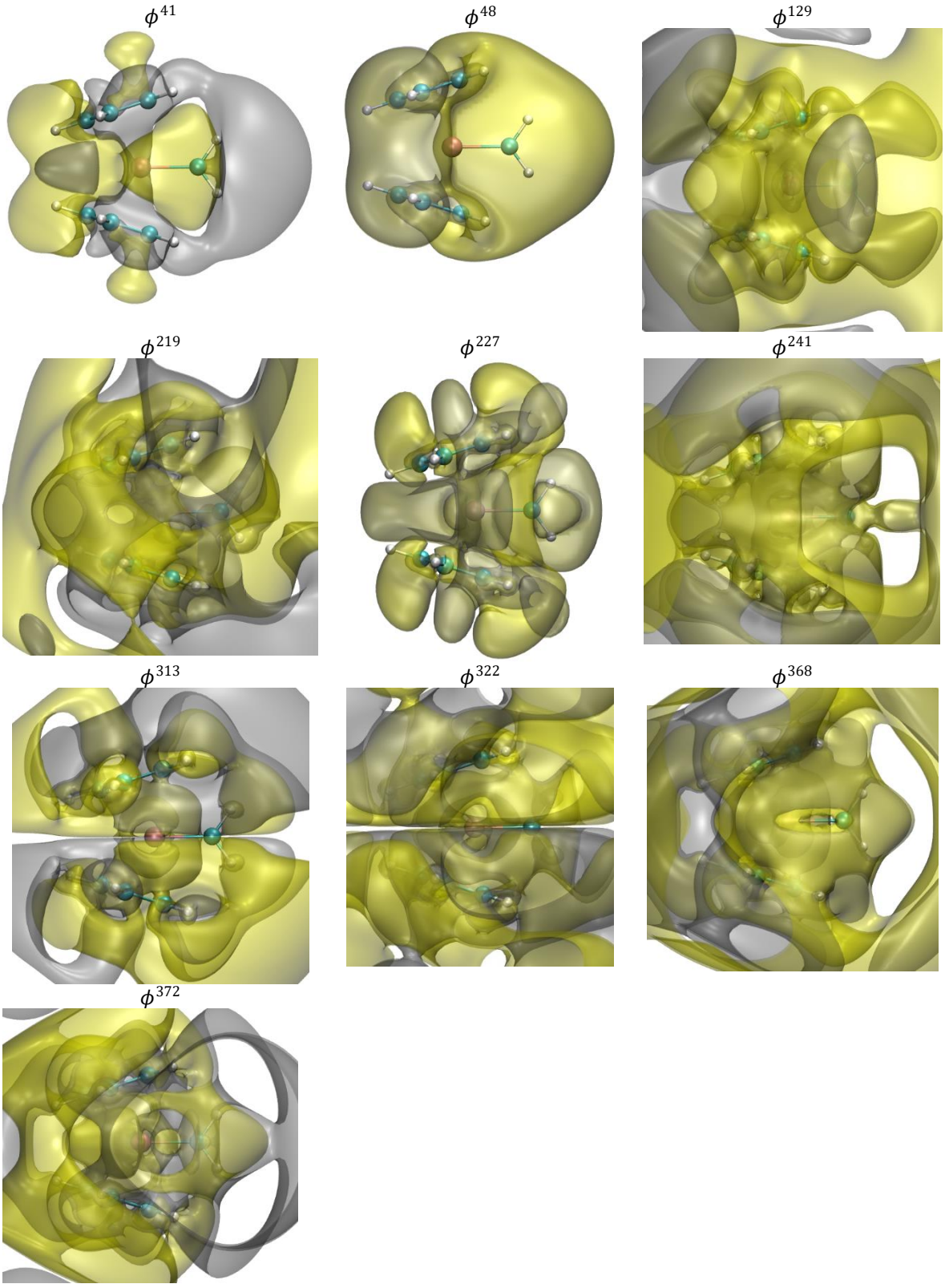

Figure B11. Isosurfaces of significant NBOs for $TiCp_2CH_2$ at isovalue 0.001a.u.

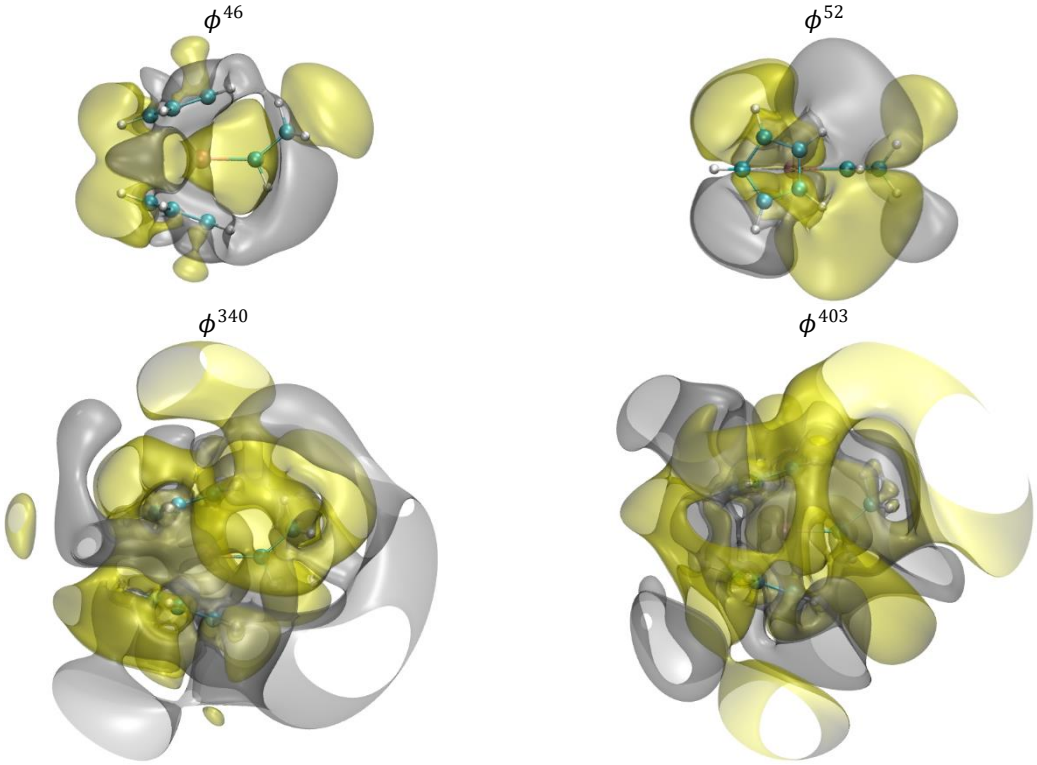

Figure B12. Isosurfaces of significant NBOs for $TiCp_2CHCH_3$ at isovalue 0.001a.u.

FALDI Data for λ_1-Cross Sections

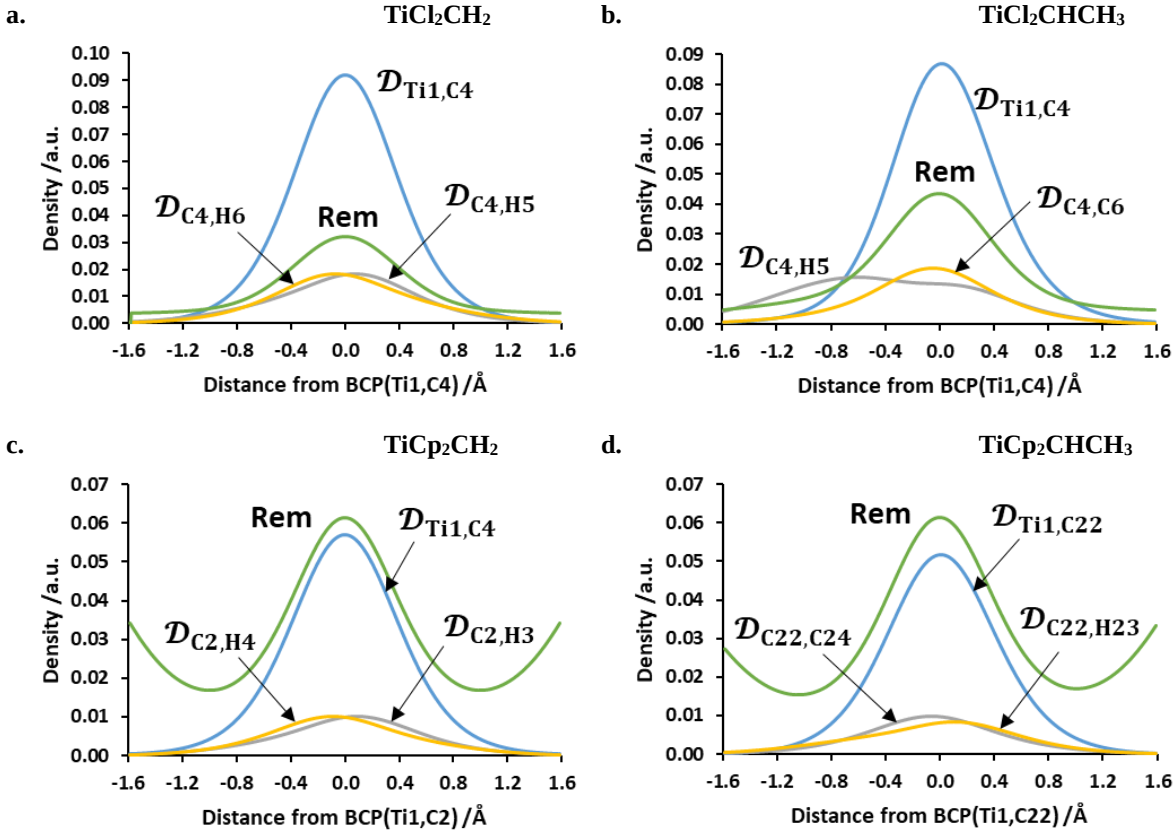

Figure B13. Cross-sections of FALDI deloc-ED making a contribution greater than 5% of the total density along the λ_1-eigenvectors with Rem as the sum total of the deloc-ED making less than 5% contributions.

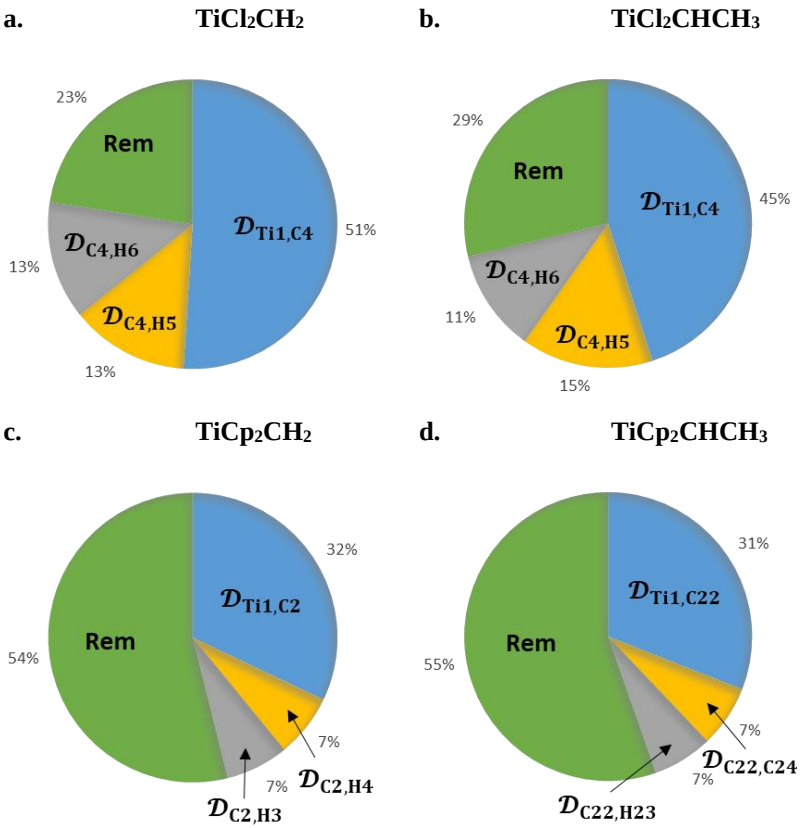

Figure B14. Relative contributions of FALDI deloc-EDs to the total density, integrated along the λ_1-eigenvector. Individual deloc-EDs with a contribution greater than 5% are shown with the other deloc-EDs collected in the Rem fraction.

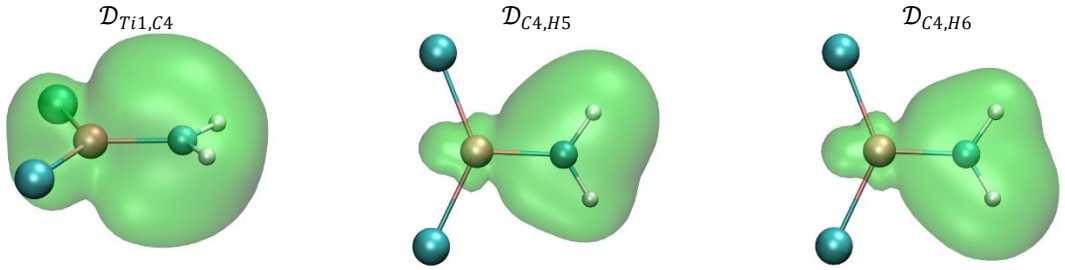

Figure B15. Isosurfaces of significant FALDI deloc-EDs for $TiCl_2CH_2$ at isovalue 0.001a.u.

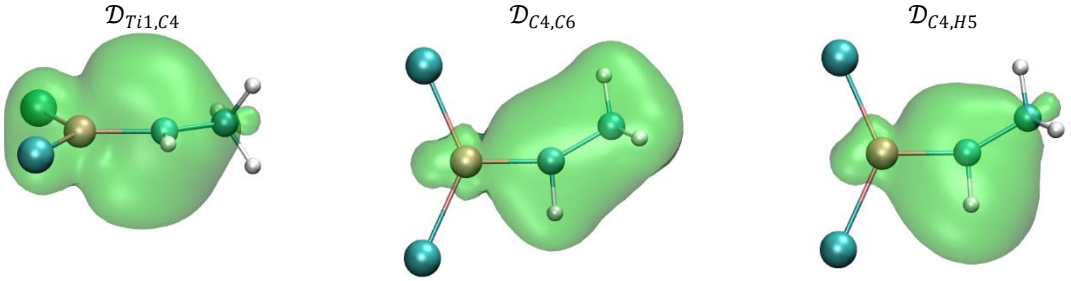

Figure B16. Isosurfaces of significant FALDI deloc-EDs for $TiCl_2CHCH_3$ at isovalue 0.001a.u.

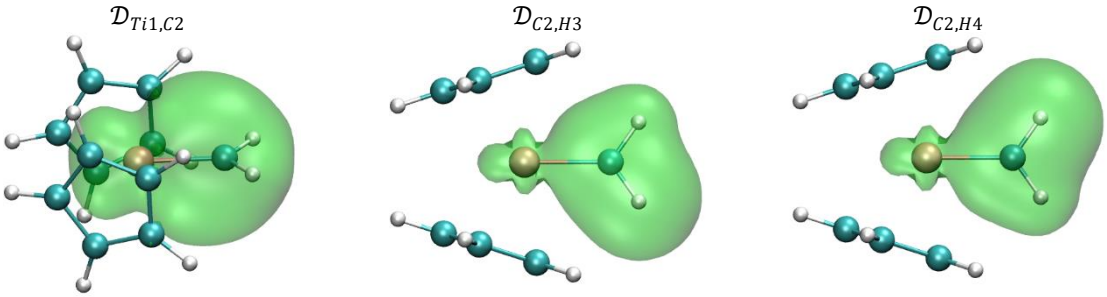

Figure B17. Isosurfaces of significant FALDI deloc-EDs for $TiCp_2CH_2$ at isovalue 0.001a.u.

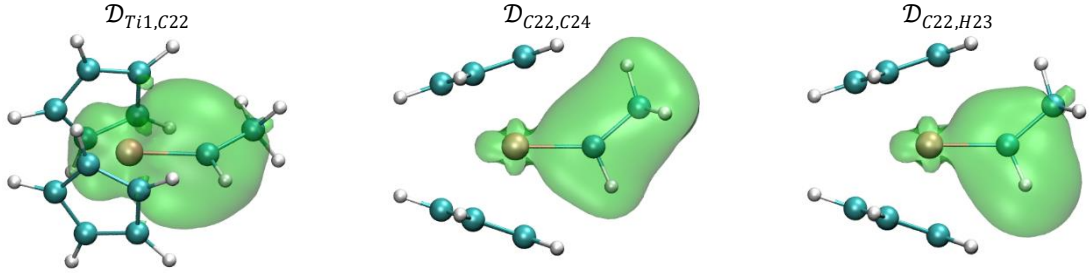

Figure B18. Isosurfaces of significant FALDI deloc-EDs for $TiCp_2CHCH_3$ at isovalue 0.001a.u.

FALDI NDF Data for λ_1-Cross Sections

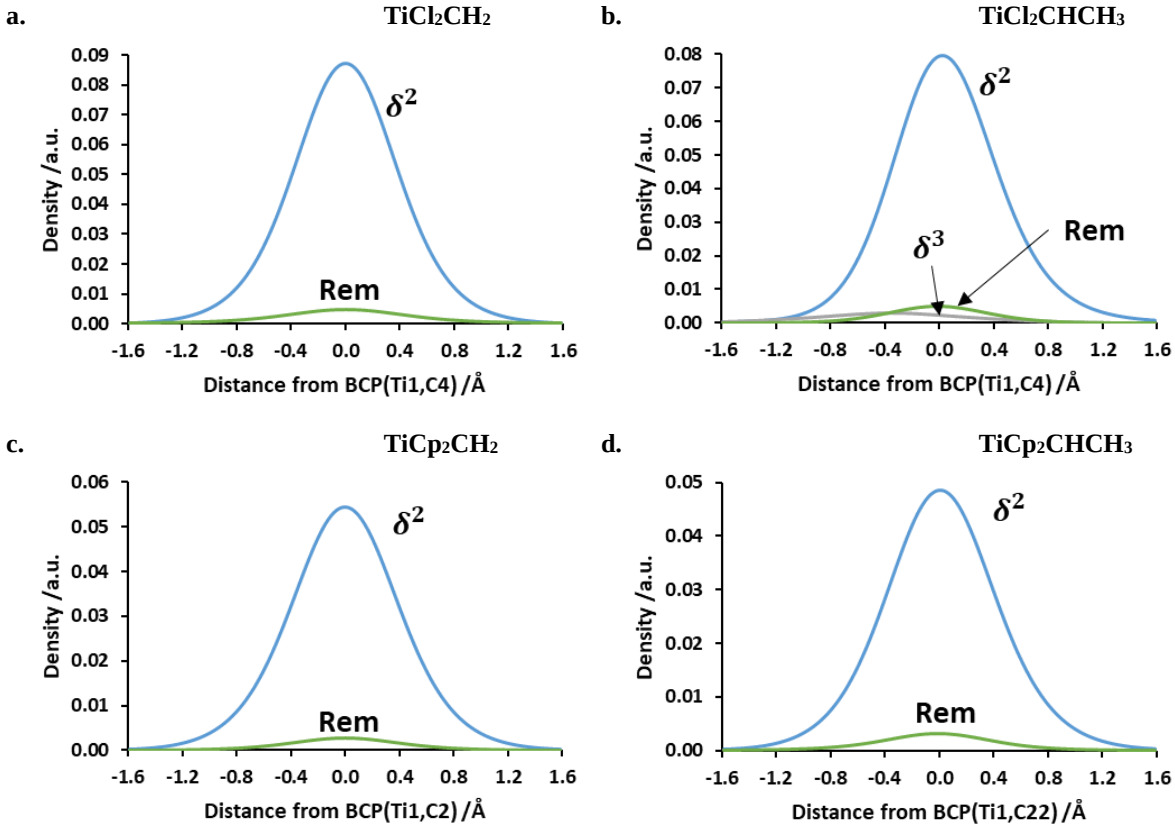

Figure B19. Cross-sections of FALDI deloc-ED NDFs making a contribution greater than 5% of the total density along the λ_2-eigenvectors with Rem as the sum total of the NDFs making less than 5% contributions.

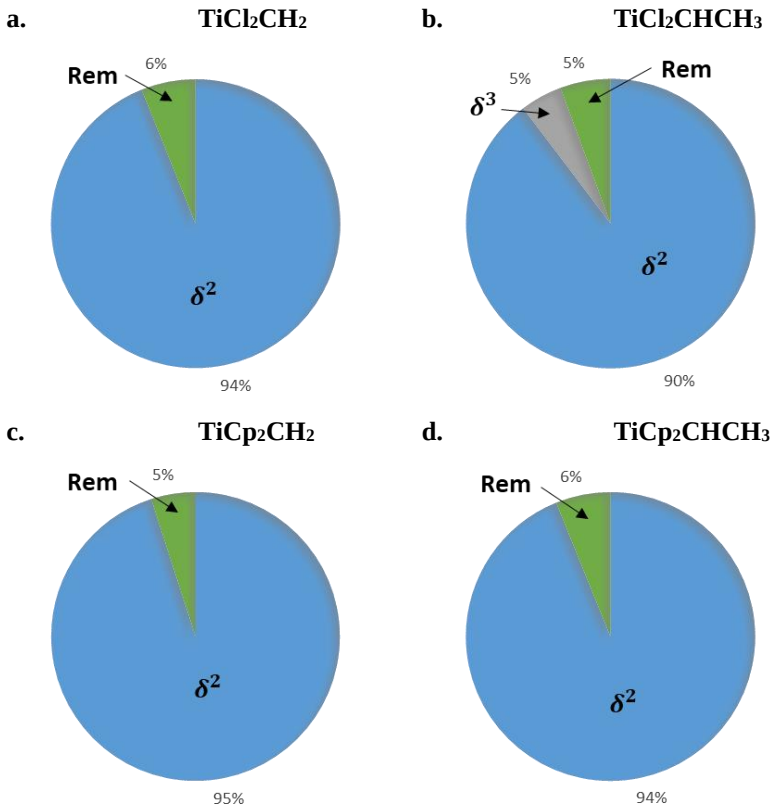

Figure B20. Relative contributions of FALDI deloc-ED NDFs for Ti—C interaction to the total density, integrated along the λ1-eigenvector. Individual NDFs with a contribution greater than 5% are shown with the other NDFs collected in the Rem fraction.

Figure B21. Isosurfaces of significant FALDI deloc-ED NDFs for Ti—C interaction for $TiCl_2CH_2$ at isovalue 0.001a.u.

Figure B22. Isosurfaces of significant FALDI deloc-ED NDFs for Ti—C interaction for $TiCl_2CHCH_3$ at isovalue 0.001a.u.

Figure B23. Isosurfaces of significant FALDI deloc-ED NDFs for Ti—C interaction for $TiCp_2CH_2$ at isovalue 0.001a.u.

Figure B24. Isosurfaces of significant FALDI deloc-ED NDFs for Ti—C interaction for $TiCp_2CHCH_3$ at isovalue 0.001a.u.

Appendix C

Supplementary information for chapter five

XYZ Coordinates of optimized geometries

Table C1. Molecule specification of $TiCl_2CH_2$

Atom	X	Y	Z
Ti1	0.000000	0.000000	0.426717
C2	0.000000	-0.000000	3.902732
H3	0.000000	1.733403	5.026014
H4	0.000000	-1.733403	5.026014
Cl5	-0.000000	3.868428	-1.260476
Cl6	-0.000000	-3.868428	-1.260476

Molecular energy: -1809.3268391 a.u.

Table C2. Molecule specifications for $TiCl_2CHCH_3$

Atom	X	Y	Z
Ti1	0.000000	0.000000	0.000000
Cl2	0.000000	0.000000	4.271290
Cl3	3.149579	0.000000	-2.806256
C4	-3.125242	0.000869	-1.456458
H5	-4.139716	0.000131	0.386601
C6	-4.769813	0.004805	-3.749088
H7	-6.000847	-1.663082	-3.786457
H8	-6.009112	1.666698	-3.775061
H9	-3.653423	0.013214	-5.484506

Molecular energy: -1848.6523912 a.u.

Table C3. Molecule specification of $TiCp_2CH_2$

Atom	X	Y	Z
Ti1	-0.000003	0.565569	-0.000299
C2	-0.000036	4.220883	-0.000493
H3	1.686211	5.414210	-0.000125
H4	-1.686297	5.414190	-0.001172
C5	-3.030267	-2.871537	0.000395
H6	-2.403337	-4.811871	0.001061
C7	-3.480636	-1.364578	2.162769
C8	-3.480026	-1.365848	-2.162992
H9	-3.280417	-1.967174	4.104362
C10	-4.265328	1.067120	1.339974
H11	-3.279304	-1.969601	-4.104175
C12	-4.264953	1.066346	-1.341827
H13	-4.777794	2.631073	2.540402
H14	-4.777109	2.629609	-2.543293
C15	4.264530	1.066334	1.342409
H16	4.776322	2.629541	2.544102
C17	3.479368	-1.365919	2.163201
C18	4.265725	1.067243	-1.339392
H19	3.278090	-1.969799	4.104284
C20	3.030308	-2.871498	-0.000421
H21	4.778516	2.631264	-2.539592
C22	3.481331	-1.364416	-2.162559
H23	2.403406	-4.811842	-0.001394
H24	3.281680	-1.966891	-4.104252

Molecular energy: -1275.9575408 a.u.

Table C4. Molecule specification of $TiCp_2CHCH_3$

Atom	X	Y	Z
Ti1	-1.791120	0.182128	-0.974712
C2	-4.119874	4.052647	-0.880865
H3	-3.201584	5.806000	-1.364407
C4	-5.382558	2.404015	-2.577763
C5	-4.303281	2.995804	1.580606
H6	-5.597966	2.675497	-4.585567
C7	-6.339617	0.337438	-1.155027
H8	-3.528015	3.799770	3.291301
C9	-5.709973	0.730000	1.412210
H10	-7.394509	-1.244969	-1.900786
H11	-6.162325	-0.516420	2.960861
C12	-1.255094	-4.291016	-0.466104
H13	-2.620821	-5.588209	-1.256786
C14	0.905897	-3.321258	-1.722862
C15	-1.308541	-3.277085	2.006299
H16	1.490084	-3.776334	-3.620106
C17	2.176309	-1.676347	-0.019474
H18	-2.725123	-3.650761	3.424056
C19	0.790190	-1.644198	2.275484
H20	3.900353	-0.656808	-0.388846
H21	1.259136	-0.563975	3.944731
C22	-0.004247	1.735844	-3.812374
H23	-0.989945	3.351818	-4.649796
C24	2.418283	1.382814	-5.281476
H25	2.018402	1.058988	-7.295617
H26	3.579913	3.105345	-5.214365
H27	3.606400	-0.177815	-4.638484

Molecular energy: -1315.2797992 a.u.

Diatomic delocalised densities

Table C5. Diatomic contributions to inter-fragment delocalised density.

$TiCl_2CH_2$		$TiCl_2CHCH_3$		$TiCp_2CH_2$		$TiCp_2CHCH_3$	
Ti1,C2	3.725	Ti1,C4	3.725	Ti1,C2	2.535	Ti1,C22	2.537
C2,Cl6	1.296	Cl3,C4	1.291	C2,C18	0.343	Ti1,C24	0.380
C2,Cl5	1.295	Cl2,C4	1.126	C2,C10	0.343	C4,C22	0.309
H4,Cl6	0.432	Cl2,H5	0.599	C2,C15	0.343	C2,C22	0.309
H3,Cl5	0.432	Ti1,C6	0.593	C2,C12	0.343	C14,C22	0.305
Ti1,H4	0.361	Ti1,H5	0.455	Ti1,H4	0.260	C17,C22	0.304
Ti1,H3	0.361	Cl3,C6	0.410	Ti1,H3	0.260	Ti1,H23	0.227
H3,Cl6	0.351	Cl3,H5	0.364	C2,C22	0.144	Ti1,H25	0.158
H4,Cl5	0.350	Cl2,C6	0.322	C2,C8	0.144	Ti1,H26	0.158
		Cl3,H8	0.268	C2,C17	0.144	C17,C24	0.135
		Cl3,H7	0.268	C2,C7	0.144	C14,C24	0.135
		Cl3,H9	0.258	C2,C20	0.111	C7,C22	0.134
		Ti1,H8	0.234	C2,C5	0.111	C5,C22	0.133
		Ti1,H7	0.234	C2,H13	0.089	C12,C22	0.123
		Cl2,H8	0.217	C2,H21	0.089	C19,C22	0.123
		Cl2,H7	0.217	C2,H14	0.089	Ti1,H27	0.112
		Cl2,H9	0.185	C2,H16	0.089	C9,C22	0.108
		Ti1,H9	0.136	H3,C18	0.075	C15,C22	0.098
				H4,C10	0.075	C4,H23	0.083
				H3,C15	0.075	C2,H23	0.083
				H4,C12	0.075	H3,C22	0.080
				H4,C15	0.042	H6,C22	0.080
				H3,C12	0.042	C15,C24	0.071
				H3,C10	0.042	C19,C24	0.069
				H4,C18	0.041	H20,C22	0.069
				H3,C20	0.041	H16,C22	0.069
				H4,C5	0.041	C12,C24	0.069
				H3,C5	0.032	C17,H27	0.068
				H4,C20	0.032	C14,H27	0.067
				C2,H23	0.032	C2,C24	0.065
				C2,H6	0.032	C4,C24	0.065
				H4,C8	0.030	H16,C24	0.053
				H3,C17	0.030	H20,C24	0.052
				H4,C7	0.030	C14,H26	0.046
				H3,C22	0.030	C17,H25	0.046
				C2,H19	0.028	C9,C24	0.046
				C2,H11	0.028	C9,H23	0.042
				C2,H9	0.028	H20,H27	0.042
				C2,H24	0.028	H16,H27	0.041
				H3,C8	0.027	C5,C24	0.041
				H4,C17	0.027	C7,C24	0.041
				H3,C7	0.027	C15,H23	0.033
				H4,C22	0.027	C17,H23	0.032
				H3,H21	0.021	C14,H23	0.032
				H4,H13	0.021	C7,H23	0.032
				H4,H14	0.021	C5,H23	0.032
				H3,H16	0.021	C2,H25	0.029
				H4,H21	0.013	C4,H26	0.029
				H3,H13	0.013	H18,C22	0.029
				H3,H14	0.013	H11,C22	0.028

H4,H16	0.013	C12,H27	0.026
H3,H23	0.007	C19,H27	0.026
H4,H6	0.007	H21,C22	0.025
H4,H23	0.005	H10,C22	0.025
H3,H6	0.005	H13,C22	0.025
H4,H19	0.005	H8,C22	0.025
H3,H11	0.005	H6,H23	0.025
H4,H24	0.005	H3,H23	0.025
H3,H9	0.005	C2,H27	0.025
H3,H19	0.003	C4,H27	0.025
H4,H11	0.003	C4,H25	0.024
H4,H9	0.003	C2,H26	0.024
H3,H24	0.003	C15,H26	0.023
		C15,H25	0.023
		C12,H26	0.022
		C19,H25	0.022
		H3,C24	0.021
		H6,C24	0.021
		C14,H25	0.020
		C17,H26	0.020
		C9,H27	0.019
		H18,C24	0.019
		C19,H23	0.018
		C12,H23	0.018
		C15,H27	0.018
		C7,H26	0.017
		C5,H25	0.017
		C12,H25	0.017
		C19,H26	0.017
		C5,H27	0.015
		C7,H27	0.015
		C9,H26	0.014
		C9,H25	0.014
		H20,H23	0.013
		H16,H23	0.013
		C5,H26	0.010
		C7,H25	0.010
		H10,C24	0.009
		H8,C24	0.009
		H21,C24	0.009
		H13,C24	0.009
		H11,C24	0.008
		H16,H26	0.008
		H20,H25	0.008
		H3,H25	0.008
		H6,H26	0.008
		H18,H23	0.007
		H11,H23	0.007
		H18,H26	0.007
		H18,H25	0.006
		H16,H25	0.006
		H20,H26	0.006
		H18,H27	0.006
		H11,H27	0.005
		H21,H23	0.005

H13,H23	0.005
H6,H25	0.005
H3,H26	0.005
H6,H27	0.004
H3,H27	0.004
H10,H25	0.004
H8,H26	0.004
H11,H26	0.004
H11,H25	0.004
H21,H26	0.004
H13,H25	0.004
H13,H27	0.004
H21,H27	0.004
H10,H26	0.003
H8,H25	0.003
H10,H23	0.003
H8,H23	0.003
H21,H25	0.003
H13,H26	0.003
H8,H27	0.002
H10,H27	0.002

Appendix D

Supplementary information for chapter six

XYZ Coordinates of optimized geometries

Table D1. Molecule specification of $TiCl_2CH_2$

Atom	X	Y	Z
Ti1	0.000000	0.000000	0.426717
C2	0.000000	-0.000000	3.902732
H3	0.000000	1.733403	5.026014
H4	0.000000	-1.733403	5.026014
Cl5	-0.000000	3.868428	-1.260476
Cl6	-0.000000	-3.868428	-1.260476

Molecular energy: -1809.3268391 a.u.

Table D2. Molecule specification of $TiCl_2CHCH_3$

Atom	X	Y	Z
Ti1	0.000000	0.000000	0.000000
Cl2	0.000000	0.000000	4.271290
Cl3	3.149579	0.000000	-2.806256
C4	-3.125242	0.000869	-1.456458
H5	-4.139716	0.000131	0.386601
C6	-4.769813	0.004805	-3.749088
H7	-6.000847	-1.663082	-3.786457
H8	-6.009112	1.666698	-3.775061
H9	-3.653423	0.013214	-5.484506

Molecular energy: -1848.6523912 a.u.

Table D3. Molecule specification of $TiCp_2CH_2$

Atom	X	Y	Z
Ti1	-0.000003	0.565569	-0.000299
C2	-0.000036	4.220883	-0.000493
H3	1.686211	5.414210	-0.000125
H4	-1.686297	5.414190	-0.001172
C5	-3.030267	-2.871537	0.000395
H6	-2.403337	-4.811871	0.001061
C7	-3.480636	-1.364578	2.162769
C8	-3.480026	-1.365848	-2.162992
H9	-3.280417	-1.967174	4.104362
C10	-4.265328	1.067120	1.339974
H11	-3.279304	-1.969601	-4.104175
C12	-4.264953	1.066346	-1.341827
H13	-4.777794	2.631073	2.540402
H14	-4.777109	2.629609	-2.543293
C15	4.264530	1.066334	1.342409
H16	4.776322	2.629541	2.544102
C17	3.479368	-1.365919	2.163201
C18	4.265725	1.067243	-1.339392
H19	3.278090	-1.969799	4.104284
C20	3.030308	-2.871498	-0.000421
H21	4.778516	2.631264	-2.539592
C22	3.481331	-1.364416	-2.162559
H23	2.403406	-4.811842	-0.001394
H24	3.281680	-1.966891	-4.104252

Molecular energy: -1275.9575408 a.u.

Table D4. Molecule specification of $TiCp_2CHCH_3$

Atom	X	Y	Z
Ti1	-1.791120	0.182128	-0.974712
C2	-4.119874	4.052647	-0.880865
H3	-3.201584	5.806000	-1.364407
C4	-5.382558	2.404015	-2.577763
C5	-4.303281	2.995804	1.580606
H6	-5.597966	2.675497	-4.585567
C7	-6.339617	0.337438	-1.155027
H8	-3.528015	3.799770	3.291301
C9	-5.709973	0.730000	1.412210
H10	-7.394509	-1.244969	-1.900786
H11	-6.162325	-0.516420	2.960861
C12	-1.255094	-4.291016	-0.466104
H13	-2.620821	-5.588209	-1.256786
C14	0.905897	-3.321258	-1.722862
C15	-1.308541	-3.277085	2.006299
H16	1.490084	-3.776334	-3.620106
C17	2.176309	-1.676347	-0.019474
H18	-2.725123	-3.650761	3.424056
C19	0.790190	-1.644198	2.275484
H20	3.900353	-0.656808	-0.388846
H21	1.259136	-0.563975	3.944731
C22	-0.004247	1.735844	-3.812374
H23	-0.989945	3.351818	-4.649796
C24	2.418283	1.382814	-5.281476
H25	2.018402	1.058988	-7.295617
H26	3.579913	3.105345	-5.214365
H27	3.606400	-0.177815	-4.638484

Molecular energy: -1315.2797992 a.u.

Distributions of Electrons for $TiCl_2CH_2$

Table D5. Distribution of localised electrons for $TiCl_2CH_2$.

Orbital	Ti1	C2	H3	H4	Cl5	Cl6	Total
χ^1-χ^{20}	17.804	2.025	0.000	0.000	10.015	10.015	39.858
χ^{21}	0.008	0.001	0.000	0.000	0.963	0.963	1.936
χ^{22}	0.014	0.000	0.000	0.000	0.968	0.968	1.950
χ^{23}	0.023	0.944	0.127	0.127	0.002	0.002	1.225
χ^{24}	0.006	0.465	0.200	0.200	0.021	0.021	0.913
χ^{25}	0.042	0.005	0.001	0.001	0.768	0.768	1.585
χ^{26}	0.035	0.005	0.004	0.004	0.786	0.786	1.620
χ^{27}	0.089	0.141	0.012	0.012	0.657	0.657	1.568
χ^{28}	0.012	0.000	0.000	0.000	0.864	0.864	1.740
χ^{29}	0.015	0.000	0.000	0.000	0.899	0.899	1.813
χ^{30}	0.002	0.007	0.006	0.006	0.906	0.906	1.835
χ^{31}	0.130	0.522	0.039	0.039	0.250	0.250	1.230
χ^{32}	0.334	0.591	0.001	0.001	0.008	0.008	0.941
Total	18.515	4.707	0.390	0.390	17.106	17.106	58.214

Table D6. Distribution of delocalised electrons for $TiCl_2CH_2$.

Orbital	Ti1-C2	Ti1-H3	Ti1-H4	Ti1-Cl5	Ti1-Cl6	C2-H3	C2-H4	C2-Cl5	C2-Cl6	H3-H4	H3-Cl5	H3-Cl6	H4-Cl5	H4-Cl6	Cl5-Cl6	Total
χ^{1}-χ^{20}	0.058	0.000	0.000	0.042	0.042	0.000	0.000	0.000	0.000	0.000	0.000	0.000	0.000	0.000	0.000	0.142
χ^{21}	0.001	0.000	0.000	0.033	0.033	0.000	0.000	0.001	0.001	0.000	0.000	0.000	0.000	0.000	-0.004	0.064
χ^{22}	0.000	0.000	0.000	0.023	0.023	0.000	0.000	0.000	0.000	0.000	0.000	0.000	0.000	0.000	0.004	0.050
χ^{23}	0.096	-0.014	-0.014	0.000	0.000	0.359	0.359	0.003	0.003	-0.017	0.001	-0.001	-0.001	0.001	0.000	0.775
χ^{24}	0.054	0.025	0.025	0.012	0.012	0.454	0.454	0.006	0.006	0.045	-0.001	-0.001	-0.001	-0.001	0.000	1.088
χ^{25}	-0.001	-0.001	-0.001	0.214	0.214	0.002	0.002	0.011	0.011	0.000	0.000	0.001	0.001	0.000	-0.039	0.415
χ^{26}	-0.004	-0.003	-0.003	0.172	0.172	0.006	0.006	0.003	0.003	0.001	0.002	0.003	0.003	0.002	0.016	0.380
χ^{27}	0.200	0.016	0.016	0.096	0.096	0.026	0.026	-0.023	-0.023	0.000	-0.008	0.003	0.003	-0.008	0.010	0.432
χ^{28}	0.001	0.000	0.000	0.143	0.143	0.000	0.000	0.006	0.006	0.000	0.000	0.000	0.000	0.000	-0.038	0.260
χ^{29}	0.003	0.000	0.000	0.067	0.067	0.000	0.000	0.001	0.001	0.000	0.000	0.000	0.000	0.000	0.048	0.187
χ^{30}	-0.003	-0.002	-0.002	0.033	0.034	0.010	0.010	0.010	0.010	0.001	0.007	0.002	0.002	0.007	0.047	0.165
χ^{31}	0.444	0.033	0.033	-0.015	-0.014	0.092	0.092	0.043	0.043	0.002	0.011	-0.003	-0.003	0.011	0.001	0.770
χ^{32}	0.872	0.027	0.027	0.006	0.006	0.036	0.036	0.023	0.023	0.001	0.001	0.001	0.001	0.001	0.000	1.059
Total	1.720	0.081	0.081	0.826	0.826	0.986	0.986	0.083	0.083	0.034	0.014	0.005	0.005	0.014	0.045	5.787

Distribution of Electrons for All Structures

Table D7. Localised and delocalised electrons for the titanium and carbon atoms given for all the systems studied.

Orbital	$TiCl_2CH_2$			$TiCl_2CHCH_3$			$TiCp_2CH_2$			$TiCp_2CHCH_3$		
	Ti1	C2	Ti1-C2	Ti1	C2	Ti1-C2	Ti1	C2	Ti1-C2	Ti1	C2	Ti1-C2
χ^1-χ^{20}	17.804	2.025	0.058	15.876	2.025	2.004	2.017	2.002	0.058	0.022	0.043	0.014
χ^{21}	0.008	0.001	0.001	1.915	0.022	0.040	0.004	0.001	0.000	1.931	0.014	0.027
χ^{22}	0.014	0.000	0.000	0.009	0.003	0.001	0.014	0.000	0.000	0.005	0.001	0.000
χ^{23}	0.023	0.944	0.096	0.012	0.001	0.000	0.003	0.004	0.000	0.013	0.000	0.000
χ^{24}	0.006	0.465	0.054	0.005	0.387	0.020	0.003	0.000	0.000	0.004	0.188	0.006
χ^{25}	0.042	0.005	-0.001	0.026	0.549	0.104	0.003	0.000	0.000	0.003	0.000	0.000
χ^{26}	0.035	0.005	-0.004	0.007	0.244	0.051	0.002	0.001	0.001	0.003	0.000	0.000
χ^{27}	0.089	0.141	0.200	0.004	0.080	0.033	0.014	0.858	0.075	0.002	0.038	0.003
χ^{28}	0.012	0.000	0.001	0.017	0.227	0.070	0.000	0.020	0.000	0.002	0.098	0.005
χ^{29}	0.015	0.000	0.003	0.048	0.014	0.009	0.002	0.001	0.003	0.007	0.227	0.034
χ^{30}	0.002	0.007	-0.003	0.042	0.010	0.014	0.000	0.001	0.000	0.002	0.132	0.011
χ^{31}	0.130	0.522	0.444	0.049	0.052	0.088	0.000	0.000	0.000	0.002	0.001	0.003
χ^{32}	0.334	0.591	0.872	0.014	0.000	0.002	0.001	0.014	0.000	0.000	0.000	0.000
χ^{33}				0.014	0.000	0.002	0.001	0.003	0.001	0.003	0.130	0.015
χ^{34}				0.017	0.047	0.042	0.009	0.007	0.001	0.001	0.008	0.000
χ^{35}				0.112	0.450	0.378	0.004	0.000	0.000	0.002	0.072	0.008
χ^{36}				0.367	0.480	0.795	0.001	0.001	0.001	0.009	0.070	0.025
χ^{37}							0.005	0.010	0.006	0.006	0.007	0.003
χ^{38}							0.001	0.011	-0.001	0.003	0.003	0.003
χ^{39}							0.008	0.090	0.005	0.002	0.001	0.001
χ^{40}							0.000	0.001	-0.001	0.002	0.011	-0.001
χ^{41}							0.000	0.000	0.000	0.005	0.085	0.008
χ^{42}							0.000	0.000	0.000	0.000	0.030	0.004
χ^{43}							0.003	0.003	0.000	0.001	0.005	0.000
χ^{44}							0.008	0.295	0.022	0.000	0.000	0.000
χ^{45}							0.162	0.447	0.444	0.001	0.024	0.008
χ^{46}							0.059	0.000	0.003	0.002	0.002	0.000
χ^{47}							0.025	0.274	0.102	0.008	0.017	0.005
χ^{48}							0.024	0.005	-0.013	0.008	0.258	0.031
χ^{49}							0.027	0.017	-0.003	0.100	0.143	0.186
χ^{50}							0.243	0.542	0.687	0.056	0.000	0.003
χ^{51}										0.028	0.002	-0.008
χ^{52}										0.055	0.409	0.233
χ^{53}										0.032	0.113	0.052
χ^{54}										0.286	0.433	0.648
Total	18.515	4.707	1.720	18.534	4.590	3.653	2.645	4.609	1.392	2.604	2.567	1.325

Table D8. Localisation and delocalisation indices for the fragments of the various structures.

Interaction	$TiCl_2CH_2$			$TiCl_2CHCH_3$			$TiCp_2CH_2$				$TiCp_2CHCH_3$		
	χ^{27}	χ^{31}	χ^{32}	χ^{25}	χ^{31}	χ^{35}	χ^{36}	χ^{45}	χ^{47}	χ^{50}	χ^{49}	χ^{52}	χ^{54}
Localisation index													
Metal	0.089	0.130	0.334	0.026	0.049	0.112	0.367	0.162	0.025	0.243	0.100	0.055	0.286
Carbene	0.217	0.787	0.665	1.861	0.128	0.893	0.628	0.650	0.426	0.623	0.225	0.777	0.556
Ancillary	1.324	0.501	0.016	0.004	1.552	0.454	0.018	0.493	1.152	0.035	1.158	0.665	0.038
Delocalisation index													
Metal, Carbene	0.232	0.509	0.925	0.101	0.114	0.464	0.927	0.513	0.117	0.736	0.222	0.285	0.751
Metal, Ancillary	0.192	-0.029	0.011	0.002	0.179	-0.034	0.011	0.237	0.102	0.131	0.350	0.066	0.139
Carbene, Ancillary	-0.054	0.103	0.050	0.006	-0.022	0.111	0.049	-0.056	0.177	0.232	-0.057	0.150	0.229